The TAM receptor family in multiple myeloma

Justine Clark

Myeloma Research Laboratory

School of Biomedicine

Faculty of Health and Medical Sciences

University of Adelaide

&

Precision Cancer Medicine Theme

South Australian Health and Medical Research Institute

(SAHMRI)

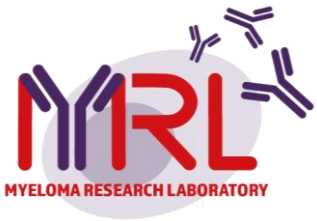

A thesis submitted to the University of Adelaide

for the degree of Doctor of Philosophy

February 2023

TABLE OF CONTENTS

ABSTRACT

Multiple myeloma (MM) is a haematological malignancy of antibody secreting monoclonal plasma cells (PCs) in the bone marrow (BM). MM PC growth and survival is supported by other cells within the BM microenvironment including osteoblasts, osteoclasts, bone marrow stromal cells and immune cells. Paracrine signalling between MM PCs and these other cell types is mediated by an array of cytokines, receptors and adhesion molecules. The TAM receptor family, Tyro3, Axl and Mer represent a distinct family of tyrosine kinase cell surface receptors, which have been implicated in the pathogenesis of cancers including MM. The studies presented in this thesis utilised single TAM receptor expressing 5TGM1 murine myeloma cell lines to further elucidate the roles of Axl and Mer in MM. The CRISPR Cas9 system and retroviral transduction were used to generate a 5TGM1 cell line expressing no TAM receptors (5TGM1 EV), a 5TGM1 cell line expressing only Axl (5TGM1 Axl) and a 5TGM1 cell line expressing only Mer (5TGM1 Mer).

Dormant MM PCs that reside long term in the bone marrow of patients can be reactivated following therapy, giving rise to disease relapse. Given that Axl was highly expressed by dormant 5TGM1 MM cells in previous studies, the present study sought to determine whether high Axl expression alone was sufficient to initiate and maintain 5TGM1 MM cell dormancy. Features of dormancy in 5TGM1 Axl compared to 5TGM1 EV cells were assessed *in vitro* using cell cycle analysis and labelling with the heritable dye, DiD. 5TGM1 Axl and 5TGM1 EV cells were also inoculated into the C57BL/KaLwRij murine model of MM, and tumour burden was assessed. These studies provided no evidence that high Axl expression in 5TGM1 cells promote features of dormancy *in vitro* or *in vivo* when compared to the 5TGM1 EV cell line that does not express Axl.

Studies in this thesis revealed that 5TGM1 Mer cells produce significantly greater myeloma tumour burden *in vivo* in comparison to 5TGM1 EV cells following intravenous inoculation into the C57BL/KaLwRij mouse model. However, following inoculation of cells directly into the bone marrow, Mer expression did not produce an increase in tumour burden. Additionally, when 5TGM1 Mer cells and 5TGM1 EV

cells were inoculated into the immune compromised NSG mouse model, Mer expression had no effect on tumour burden. Immune checkpoint proteins PD-L1, Galectin 9 and PVR were upregulated in 5TGM1 Mer cells compared to 5TGM1 EV cells at the mRNA level. These findings indicate that the mechanism of action of Mer in potentiating MM tumour burden may be through increased 5TGM1 BM homing and regulating expression levels of immune checkpoint molecules in myeloma cells.

Future studies should aim to fully characterise the possible role of Mer in MM immune suppression. Given that Mer and its ligand Gas6 are widely expressed by MM PCs of myeloma patients, Mer represents an attractive therapeutic target to limit MM disease progression.

DECLARATION

I certify that this work contains no material which has been accepted for the award of any other degree or diploma in my name, in any university or other tertiary institution and, to the best of my knowledge and belief, contains no material previously published or written by another person, except where due reference has been made in the text. In addition, I certify that no part of this work will, in the future, be used in a submission in my name, for any other degree or diploma in any university or other tertiary institution without the prior approval of the University of Adelaide and where applicable, any partner institution responsible for the joint award of this degree.

I give permission for the digital version of my thesis to be made available on the web, via the University's digital research repository, the Library Search and also through web search engines, unless permission has been granted by the University to restrict access for a period of time.

I acknowledge the support I have received for my research through the provision of an Australian Government Research Training Program Scholarship.

Signed **Date: 16-02-23**

X

Justine Clark

ACKNOWLEDGMENTS

Firstly, I would like to acknowledge Dr. Duncan Hewett and Prof. Andrew Zannettino, who believed in me from day one, when I was a psychology undergrad who didn't know the first thing about cell surface receptors. I want to extend an especially heartfelt thank you to Duncan for being an epic supervisor, mentor, and friend throughout my years at MRL. Your constant support, guidance and honesty have made me into the scientist I am today. My entire supervisory panel, Duncan, Bill and Andrew, should be very proud of what we have accomplished together and all the hard work we have put into this thesis.

Thank you to the entire team within the MRL and MSC groups, it has been my privilege to learn from all of you throughout my PhD and to be a part of such an amazing group of people. To anyone who helped me work through experimental problems, taught me things in the lab, or helped with my animal work despite your own busy schedules – thank you so much for your constant patience with me. Some of you (Alanah especially) have gone out of your way to help me on numerous occasions and that will always be much appreciated.

One of the best things about my PhD experience has been sharing it with the students of MRL and MSC. Kim, Mara, Khatora, Clara, Alanah, Natalya, Saoirse, Laura, Emma, Hayley, Nick, Connor and Jvaughn – most of you support me and antagonise me in equal parts, and I miss you already. Special mention to Natalya, who was by my side every day for 3.5 years literally at our big shared desk. We have been through it all together and came out the other side with matching tattoos!

Finally, thank you to my immediate family – Mum, Hayley, Nanna and Pop – and friends outside of academia, for listening to me complain over the years. Thank you especially to my Mum, who has had the pleasure of living with me through my entire post-graduate studies.

Thank you all!

ABBREVIATIONS

MM	multiple myeloma
PC	plasma cell
BM	bone marrow
PCL	plasma cell leukemia
SRE	skeletal related event
MDE	myeloma defining event
NK	natural killer
MGUS	monoclonal gammopathy of undetermined significance
CRAB	hypercalcaemia, renal insufficiency, anaemia, bone lesions
SMM	smouldering multiple myeloma
IgA	immunoglobulin A
IgG	immunoglobulin G
IgH	immunoglobulin heavy chain
MRI	magnetic resonance imaging
RISS	Revised International Staging System
mSMART	Mayo Stratification of Myeloma and Risk-Adapted Therapy
EMD	extra-medullary disease
CPC	circulating plasma cell
F-FDG	fluorodeoxyglucose
PET-CT	positron emission tomography/computed tomography
IMiD	immunomodulatory imide drug
CRBN	cereblon
ASCT	autologous stem cell transplant
MRD	minimal residual disease
FLC	free light chain
IgL	immunoglobulin light chain
IgM	immunoglobulin M
IgE	immunoglobulin E
CSR	class switch recombination
SHM	somatic hypermutation

AID	activation induced deaminase
DSB	double stranded break
NHEJ	non-homologous end joining
CNA	copy number abnormalities
SNV	single nucleotide variant
In/dels	insertion/deletion mutations
HSC	hematopoietic stem cell
BMSC	bone marrow stromal cell
Th17	T-helper 17 cells
RPE	retinal pigment epithelial
PR	photoreceptor
AML	acute myeloid leukemia
ADT	androgen deprivation therapy
Treg	regulatory T cell
shRNA	short hairpin RNA
siRNA	short interfering RNA
TAM	Tyro3, Axl, Mer
NF	nuclease free
NTC	no template control
EDTA	ethylenediamine tetraacetic acid
sgRNA	single guide RNA
GFP	green fluorescent protein
FBS	foetal bovine serum
IMDM	Iscove’s modified Dulbecco’s media
DMEM	Dulbecco’s modified eagle media
SDS-PAGE	Sodium dodecyl-sulfate polyacrylamide gel electrophoresis
TBST	tris-buffered saline, tween
FACS	fluorescence activated cell sorting
PBS	phosphate buffered saline
SPEP	serum paraprotein electrophoresis
PFE	PBS, FBS, EDTA
i.p.	intraperitoneal

FPKM	fragments per kilobase of exon per million mapped reads
HDR	homology directed repair
NMD	nonsense mediated decay
PTC	premature termination codon
CM	conditioned media
i.v.	intravenous
i.t.	intratibial
DiD^{hi}	DiD high
DiD^{neg}	DiD negative
BLI	bioluminescence imaging
MFI	mean fluorescence intensity
ALL	acute lymphoblastic leukemia
KaLwRij	KaLwRijHsd
NSG	NOD/SCID/IL2rγnull
PD-1	Programmed cell death protein 1
PD-L1	Programmed cell death ligand 1

PUBLICATIONS

Scientific Manuscripts

1. Khoo WH, Ledergor G, Weiner A, Roden DL, Terry RL, McDonald MM, Chai RC, De Veirman K, Owen KL, Opperman KS, Vandyke K, **Clark JR**, Seckinger A, Kovacic N, Nguyen A, Mohanty ST, Pettitt JA, Xiao Y, Corr AP, Seeliger C, Novotny M, Lasken RS, Nguyen TV, Oyajobi BO, Aftab D, Swarbrick A, Parker B, Hewett DR, Hose D, Vanderkerken K, Zannettino ACW, Amit I, Phan TG & Croucher PI (2019). A niche-dependent myeloid transcriptome signature defines dormant myeloma cells. *Blood* 134, 30-43.

Conference Proceedings

1. Clark, J.R., Hewett, D.R., Panagopoulos, V., Zannettino A.C.W. (2019). The TAM receptor family in multiple myeloma. *EMBL Australia Postgraduate Symposium*. Poster Presentation.
2. Clark, J.R., Hewett, D.R., Panagopoulos, V., Zannettino A.C.W. (2019). Do TAMs hold the key to dormancy? *Florey Postgraduate Research Conference*. Poster Presentation.
3. Clark, J.R., Hewett, D.R., Panagopoulos, V., Zannettino A.C.W. (2020). The TAM receptor family in multiple myeloma. *Florey Postgraduate Research Conference*. Poster Presentation.
4. Clark, J.R., Hewett, D.R., Panagopoulos, V., Zannettino A.C.W. (2021). Mer expression is associated with increased tumour burden in multiple myeloma. *Australian Society for Medical Research Scientific Meeting*. Poster Presentation.
5. Clark, J.R., Hewett, D.R., Panagopoulos, V., Zannettino A.C.W. (2021). Investigating the functions of the TAM receptor family in multiple myeloma. *Cancer in SA Translational Meeting.* Invited speaker.
6. Clark, J.R., Hewett, D.R., Panagopoulos, V., Zannettino A.C.W. (2021). Mer expression is associated with increased tumour burden in multiple myeloma. *Florey Postgraduate Research Conference.* Poster Presentation.
7. Clark, J.R., Hewett, D.R., Panagopoulos, V., Zannettino A.C.W. (2021). Mer expression is associated with increased tumour burden in multiple myeloma. *ANZSCDB SA Meeting*. Poster Presentation.
8. Clark, J.R., Hewett, D.R., Panagopoulos, V., Zannettino A.C.W. (2022). Mer receptor expression promotes multiple myeloma tumour development. *New Directions in Leukaemia Research Meeting*. Poster Presentation.
9. Clark, J.R., Hewett, D.R., Panagopoulos, V., Zannettino A.C.W. (2022). Mer receptor expression promotes multiple myeloma tumour development. *Florey Postgraduate Research Conference.* Poster Presentation.

1. Introduction

1.1 Multiple myeloma

Multiple myeloma (MM) is a haematological malignancy characterised by the uncontrolled proliferation of plasma cells (PCs) in the bone marrow (BM). PCs are terminally differentiated B cells that secrete non-functional monoclonal immunoglobulins known as paraprotein, or M-protein, which can be detected in blood serum[1]. In most instances, MM is preceded by premalignant PC proliferative disorders, and in its later stages, MM can undergo a leukemic progression leading to development of plasma cell leukaemia (PCL), which displays an inferior prognosis[2]. MM exhibits significant inter-patient genetic heterogeneity, which can impact treatment response[3]. Despite the development of new therapeutic options, most patients relapse and do not achieve long term treatment-free remission[4]. The discovery of novel precision medicine targets is necessary to achieve durable treatment response and better patient outcomes.

1.1.1 Epidemiology

MM is the second most common haematological malignancy, accounting for ~10% of all haematological malignancies and ~1% of all cancers[5]. In Australia, 2,515 new cases of MM were diagnosed in 2021, with an age standardised incidence rate of 7.9 cases per 100,000 people[6]. The highest incidence rates of MM have been identified in New Zealand, Australia, the UK, Israel and Norway[7]. MM is diagnosed primarily in older adults, with the median age at diagnosis being 71.1 years[6]. The prevalence of MM is higher in males (9.8 cases per 100,000) compared to females (6.2 cases per 100,000). In addition to older age and male gender, ethnicity is a risk factor for developing MM. To this end, the incidence is increased in people of African American[8], Hispanic[9] and Māori[10] descent compared to those of European descent. MM contributes to the global burden of disease, being responsible for over 2.1 million disability adjusted life years globally[11]. In Australia, the current 5-year survival rate from date of MM diagnosis is 54.9%, which remains lower than other common cancers such as colorectal, breast and prostate cancers[6].

1.1.2 Clinical features

MM patients face significant diagnostic delays compared to other cancers[12], and at the time of diagnosis, end organ damage is already evident in most patients. One

of the most significant causes of morbidity in MM patients arises from skeletal related events (SREs) such as bone pain, pathological fractures, vertebral collapse, and spinal cord compression[13, 14]. SREs develop due to osteolytic lesions, which are present in up to 90% of patients at some point during the course of disease[15]. Osteolysis occurs in MM due to PC production of factors that both activate bone-resorbing osteoclasts, including RANKL[16,17], and inhibit bone-forming osteoblasts, including Dickkopf1 (DKK1) and interleukin 7 (IL-7)[18, 19]. Osteolytic bone resorption can result in excess released calcium, or hypercalcaemia, defined as corrected serum calcium ≥11 mg/dL, which is observed in ~15-20% of MM patients[20]. Hypercalcemia and excess nephrotoxic serum free light chain production by PCs can result in renal insufficiency, observed in 25-75% of MM patients[21]. Anaemia is seen in almost all MM patients and is caused by cancerous PC infiltration in the bone marrow leading to inhibition of erythropoietic differentiation of haematopoietic stem and progenitor cells[22]. Together these clinical manifestations are known as the CRAB features (hypercalcaemia, renal insufficiency, anaemia, and bone lesions), which are recognised as key myeloma defining events (MDEs) leading to diagnosis[5]. Another clinical feature of MM contributing greatly to morbidity is a high frequency of viral and bacterial infections owing to global immune suppression, including immunoparesis (the suppression of polyclonal immunoglobulins), reduced T cell diversity, and dysfunction of B cells, dendritic cells and NK (natural killer) cells[23].

1.1.3 Disease stages

1.1.3.1 Monoclonal gammopathy of undetermined significance

MM is preceded by the premalignant PC proliferative disorder known as monoclonal gammopathy of undetermined significance (MGUS). Three criteria must be met for a diagnosis of MGUS: (1) Detectable serum monoclonal protein <3gm/dL, (2) Detectable clonal BM PC <10%, and (3) No evidence of end-organ damage such as CRAB features[5]. It is estimated that approximately 3% of the population aged over 50 has MGUS[24], with a risk of progression to MM of 1% per year[25]. The size and type of M protein, number of BM PCs and serum free light chain ratio can help to identify patients at risk of progression[26, 27]. The current standard of care for MGUS patients is clinical monitoring for progression. Although treatment for MGUS is not warranted, close monitoring can enable early detection of progression to MM[28].

1.1.3.2 Smouldering multiple myeloma

Smouldering multiple myeloma (SMM) is an intermediate stage of disease between MGUS and MM that is observed in some patients. For diagnosis with SMM, both of the following criteria must be met: (1) Serum monoclonal protein (IgG or IgA) ≥3gm/dL, or urinary monoclonal protein ≥500 mg per 24h and/or clonal bone marrow plasma cells 10-60%, and (2) absence of MDEs[5]. Progression from SMM to MM occurs at a rate of approximately 10% per year over the first 5 years following diagnosis, 3% per year over the next 5 years, and 1.5% per year thereafter. The time to progression is influenced by cytogenetic subtype, and patients with immunoglobulin heavy chain (IgH) translocation t(4;14) or deletions involving chromosome 17p (del(17p)) are classed as high-risk and are likely to progress within 2 years[29]. Recent studies have shown that treatment for high risk SMM patients can significantly increase both progression free survival and overall survival[30-32]. However, a consensus decision on an approved treatment for SMM requires further clinical studies. New recommendations suggest that high-risk patients should participate in Phase III randomised clinical trials to identify treatments that offer the best overall survival advantage[33-35].

1.1.3.3 Multiple myeloma

For a diagnosis of MM, both of the following criteria must be met: (1) Clonal bone marrow plasma cells ≥10% or biopsy-proven bony or extramedullary plasmacytoma and (2) Any one or more of the following MDEs: (a) Evidence of CRAB features, (b) clonal bone marrow plasma cell percentage ≥60%, (c) involved: uninvolved serum free light chain (FLC) ratio ≥100 (involved free light chain level must be ≥100 mg/L), or (d) >1 focal lesions on magnetic resonance imaging (MRI) studies (at least 5mm in size)[5]. MM patients at diagnosis are risk stratified according to the Revised International Staging System (RISS), which combines tumour burden and disease biology (cytogenetic abnormalities, lactate dehydrogenase levels and serum β2 microglobulin levels) to construct a unified prognostic staging system for clinical decision making[36]. In addition to the RISS, the Mayo Stratification of Myeloma and Risk-Adapted Therapy (mSMART) staging system (www.msmart.org) can be used to stratify patients into high, intermediate and low risk groups to determine therapeutic approach[37]. The mSMART staging system utilises cytogenetic

abnormalities, RISS stage, plasma cell S-phase proportion and gene expression profiling to define risk groups.

1.1.3.4 Plasma cell leukaemia and extramedullary disease

MM continues to evolve over both its disease course and in response to treatment. In later stages of disease, malignant PCs can lose dependency on bone marrow residency for growth and survival[38]. MM PCs become detectable in blood, known as plasma cell leukaemia (PCL), or in other soft tissues, known as extramedullary disease (EMD). PCL was previously diagnosed based on the following diagnostic criteria: ≥ 20% circulating plasma cells (CPCs) on peripheral blood smear and plasma cell count ≥ 2×10^9/L[39]. However, a recent study indicated no differences in survival outcomes in patients with 5-19% CPCs compared to those with ≥20% CPCs[40]. This has led to the revision of diagnostic criteria to ≥5% CPCs in peripheral blood smears in patients otherwise diagnosed with symptomatic MM[41]. When EMD is suspected, a diagnosis can be achieved through whole-body X-ray or MRI, or ^{18}fluorodeoxyglucose (^{18}F-FDG) PET/CT[42]. EMD can be either paraskeletal, where tumours protrude through cortical bone, or can have organ involvement, where tumours develop at a distant soft tissue or organ site[43]. A diagnosis of PCL and/or EMD results in significantly worse prognosis for MM patients, and as such can affect treatment decisions according to mSMART[40, 43].

1.1.4 Treatment modalities

Over the past 20 years, the 5-year survival rate of MM patients has markedly increased owing to the availability of novel therapeutic options[44]. The two main categories of drugs used to treat MM encompass immunomodulatory imide drugs (IMiDs; thalidomide, lenalidomide and pomalidomide) and proteasome inhibitors (bortezomib, carfilzomib and ixazomib)[45]. Thalidomide and its derivatives bind to cereblon (CRBN), resulting in degradation of transcription factors Ikaros family zinc finger proteins, Ikaros and Aoilos[46]. This drives the anti-myeloma effects of IMiDs, namely inducing MM PC apoptosis,[47] as well as promoting interleukin (IL)-2 and interferon (IFN)-γ secretion, which enhances T cell and NK cell activation[48]. Proteasome inhibitors work by inhibiting NF-κB signalling, the accumulation of unfolded proteins, endoplasmic reticulum stress, and the unfolded protein response, resulting in apoptosis[49]. Other drugs used for the treatment of MM include DNA

alkylating agents (melphalan and cyclophosphamide) and corticosteroids (dexamethasone and prednisone)[45]. Autologous stem cell transplant (ASCT) is also part of MM standard of care, and its use has been expanded to encompass not only younger patients but also elderly patients without significant co-morbidities[50]. Numerous treatment strategies have been developed combining these novel drugs and ASCT to form induction, consolidation and maintenance regimens.

Treatment decisions for MM patients vary geographically and are constantly evolving, but typical decisions for patients in the US are provided here. For newly diagnosed MM patients, initial treatment decisions are based on eligibility for ASCT and risk stratification[45]. Transplant-eligible patients typically undergo 3-4 cycles of induction therapy with bortezomib, lenalidomide and dexamethasone followed by stem cell harvest[45, 51]. Patients can either then undergo ASCT or delay until first relapse, however upfront ASCT is favoured in high-risk patients and patients with advanced age, other co-morbidities and frailty[50]. Fit older patients >65 years or younger patients with co-morbidities can opt to undergo a reduced intensity autologous transplantation using low dose melphalan prior to transplant[52]. In patients who are not candidates for ASCT, initial therapy typically involves 8-12 cycles of bortezomib, lenalidomide and dexamethasone[53]. Following this, patients typically undergo lenalidomide maintenance therapy, which results in significant improvements in progression free survival[54]. Due to the optimisation of these front-line therapies, patients typically achieve a complete response and minimal residual disease (MRD) negativity[55, 56].

Despite these improvements in MM patient response to treatment and survival rates using modern combination therapies, almost all patients will inevitably relapse. A panel of six expert physicians have defined the following criteria for biochemical relapse: (1) increase of at least 25% in serum paraprotein, (2) increase of at least 25% in urine paraprotein, (3) increase of > 25% in the difference between involved and uninvolved FLC, or (4) increase in BM PCs by ≥ 10%, in patients affected by non-secretory MM[57]. Alternatively, relapse can be clinical, with evidence of at least one CRAB feature. At the time of relapse, treatment choice is affected by many patient-specific factors including patient age, cytogenetic profile, comorbidities, aggressiveness of the relapse and most importantly, response to frontline

therapies[58]. One of the most important considerations for the second line of therapy is whether the patient is refractory to lenalidomide[59]. At this point in the disease history, that the use of emerging agents may be considered. These include the second generation IMiD pomalidomide[60], and monoclonal antibodies targeting SLAMF7 (elotuzumab)[61] and CD38 (daratumumab and isatuximab)[59, 62]. For patients not refractory to lenalidomide, preferred treatment is either daratumumab or carfilzomib, plus lenalidomide and dexamethasone. For patient's refractory to lenalidomide, preferred treatments are pomalidomide, bortezomib and dexamethasone or alternatively daratumumab or isatuximab, carfilzomib and dexamethasone[59]. At the time of first relapse, salvage ASCT should be considered in combination with the use of multiple agents, particularly for patients who did not receive ASCT as part of frontline therapy[63]. Throughout the course of disease, MM patients acquire resistance to treatments necessitating a third line, or more, of therapy. Patients refractory to IMiDs, proteasome inhibitors and CD38 targeted monoclonal antibody therapy have been shown to have a very poor prognosis[64].

In addition to therapy to treat MM itself, supportive care is also offered to treat the clinical manifestations of the CRAB features as well as frequent infections. Osteolytic bone lesions represent one of the most common complications of MM, resulting in SREs. Bisphosphonates work by inhibiting osteoclast activity and are used to limit osteolysis and minimise SREs[65]. Hypercalcemia resulting from osteolytic lesions can be treated by aggressive hydration, corticosteroids, bisphosphonates and calcitonin[66]. Renal disease presents in many MM patients due to light chains being filtered through the glomerulus, causing nephropathy. Early reduction in FLC burden is associated with improved renal function, and therefore the treatment for renal disease in MM is rapid initiation of chemotherapy, or in severe cases, removal of FLCs through plasma exchange[67]. MM patients experience anaemia caused by BM PC expansion and chemotherapy, which disrupts erythropoiesis[66]. Anaemia is treated through the use of iron replacement, red blood cell transfusions, and in some cases, erythropoietin-stimulating agents, although these present an increased risk of thromboembolism[68]. MM patients suffer frequent life-threatening infections, particularly during the first 3 months post-diagnosis and upon relapse[69]. To mitigate the risks of infection, recommendations suggest that MM patients should undergo vaccinations against common pathogens (e.g.,

influenza) either while in the MGUS stage or prior to therapy, as well as 6-12 months after ASCT[23]. Risk-adopted antimicrobial prophylaxis should also be considered. At the first sign of infection, such as fever, a broad-spectrum antibiotic should be administered while diagnostic tests are being performed.

1.1.5 Genetic aetiology

Myeloma is a genetic disease in which each patient displays a unique combination of primary and secondary genetic events[70]. These events drive the initiation of MM and disease progression.

1.1.5.1 Primary genetic events

The initiation and progression of MM occurs due to genetic events that result in changes to the intrinsic biology of PCs. PCs are terminally differentiated B-cells that originate as pre-B-cells in the bone marrow, where their immunoglobulin heavy chain (IgH) and light chain (IgL) genes are rearranged to generate a functional B-cell precursor receptor[70]. Following this, PCs migrate to the germinal centre of the peripheral lymphoid organs, where they undergo affinity maturation in response to antigens expressed by antigen presenting cells. After the initial contact of a B-cell with its antigen, low affinity IgM is produced, and class switch recombination (CSR) changes that isotype to IgG, IgA or IgE generating specific antibodies[71]. Together with CSR, somatic hypermutation (SHM) induces point mutations in the rearranged Ig genes of the B-cell precursor receptor, producing high affinity antibodies that bind to specific antigens. CSR and SHM require activation induced deaminase (AID) and are mediated by the introduction of double stranded breaks (DSBs) at the Ig loci[72]. In normal B-cells, DSBs are repaired locally through non-homologous end joining (NHEJ). However, they can sometimes be joined to other DSBs occurring elsewhere in the genome. MM PCs display heavily mutated Ig loci and aberrant chromosomal translocations of IgH genes located at chromosome 14q32[73, 74]. Some of these translocations result in the juxtaposition of oncogenes and strong IgH promoters, resulting in oncogene upregulation[73]. The most common translocations, which occur in more than 80% of MM patients and are used for risk stratification, are t(11;14)(q13;q32), t(4;14)(p15;q32), t(14;16)(q32;q23) and t(14;20)(q32;q11)[45]. The translocation t(11;14), occurs in 15-21% of newly diagnosed MM patients and

involves IgH and the proto-oncogene cyclin D1 (CCND1) on chromosome 11[75, 76]. This results in cyclin D1 upregulation, cell cycle progression from G1 to S phase, and increased proliferation[77]. t(11;14) MM has other unique biological features such as an increased dependency on BCL-2 for survival, making MM PCs harbouring a t(11;14) translocation more susceptible to targeting with the BCL-2 inhibitor Venetoclax[78]. The second most common translocation, t(4;14), results in aggressive disease, and as such, the 11-15% of newly diagnosed MM patients harbouring this translocation are stratified as high-risk[2]. The t(4;14) translocation results in overexpression of nuclear SET domain–containing 2 (NSD2, also known as WHSC1/MMSET) genes and fibroblast growth factor receptor 3 (FGFR3)[79]. NSD2 overexpression results in epigenetic reprogramming of t(4;14) MM PCs and alters cellular adhesion, proliferation and survival[80]. Furthermore, a recent study suggests that epigenetic reprogramming conferred by NSG2 overexpression contributes to bortezomib resistance mechanisms in MM PCs harbouring the t(4;14) translocation[79]. Two common translocations present in <5% of newly diagnosed MM patients, t(14;16) and t(14;20) result in upregulation of the MAF transcription factors (*MAF* or *MAFB*)[81]. This in turn drives the overexpression of cyclin D2 (CCND2) and APOBEC cytidine deaminases[82].

Hyperdiploidy is another early genetic event affecting 50% of MM patients, characterised by trisomies in one or more of the odd numbered chromosomes 3, 5, 7, 9, 11, 13, 15, 19, and 21[81]. Previous studies report that patients with hyperdiploidy have better outcomes compared to those without[83, 84]. However, patients typically present with overlapping cytogenetic abnormalities[85], and hyperdiploidy does not abrogate the poor prognosis associated with other high risk cytogenetics[86]. IgH translocations and hyperdiploidy are present from the stage of MGUS in most cases, indicating that they are disease initiating events that are not sufficient on their own to drive progression to MM[87].

1.1.5.2 Secondary genetic events

MM patients also display several secondary genetic events, including *MYC* translocations, copy number abnormalities (CNAs) and genetic mutations. While translocations involving IgH are considered to be initiating genetic events, MYC translocations are considered secondary owing to their presence in only 3% of

MGUS compared to 15% of MM patients[88]. MYC translocations lead to overexpression of MYC, resulting in poor patient outcomes[82]. CNAs are characterised by the gains and losses of genomic regions, and gain of the odd numbered chromosomes is characteristic of hyperdiploidy[81]. Although numerous CNAs can be observed in MM patients at diagnosis not all are of prognostic importance, with del(8p), del(11q), del(12p) and del(16q) being prognostically neutral[89]. CNAs that confer adverse overall survival are del(1p), gain 1q, and del(17p)[90]. At diagnosis, approximately 10% of MM patients present with del(17p)[91], which commonly confers mutations in the tumour suppressor gene p53 and results in poor prognosis and extramedullary disease[90, 92]. Gain 1q occurs in 30-40% of MM patients at diagnosis, and numerous oncogenes map to this genomic loci, however no single gene has been implicated in 1q myeloma pathogenesis[93]. Although gain 1q is not currently considered a cytogenetic risk factor, a recent study suggests that patients stratified at RISS stage 3 with gain 1q21 have a very poor prognosis[94].

Malignant changes to PC biology also arise due to the acquisition of single nucleotide variants (SNVs) and insertion deletion mutations (in/dels). MM patients have a high mutational load with over 400 somatic mutations documented on average per patient[95]. Whole exome and whole genome sequencing studies have identified significant inter-patient heterogeneity in mutated genes and a lack of unifying driver mutations[96, 97]. RAS/MAP kinase pathway is the most frequently mutated pathway in MM, as 21.2% of patients have mutations of *KRAS*, 19.4% of *NRAS* and 6.7% of *BRAF*. *KRAS* and *NRAS* mutations are usually mutually exclusive and do not influence prognosis[97]. Other genes are mutated at lower frequencies such as *TP53* (3%), *DIS3* (8.6%) and *FAM46C* (5.6%), and numerous other genes are mutated at frequencies of <5% of MM patients.

Over the course of disease, MM PCs rapidly proliferate and continue to mutate, giving rise to multiple generations of genetically distinct cellular populations, or subclones[98]. Next generation sequencing studies of MM tumour samples provide evidence of this, showing the existence of multiple genetically heterogeneous subclones within each tumour[99, 100]. Individual PC subclones harbour primary and secondary genetic events as well as mutations in oncogenic driver genes, which are believed to confer subclonal fitness, contributing to the subclones survival and

outgrowth[101]. Genetic changes also deregulate many aspects of PC biology, including expression of cell surface receptors and adhesion molecules, which facilitate communication with the BM microenvironment[70]. Clonal evolution is thought to occur in a 'Darwinian' manner, with selection pressures from the BM microenvironment driving subclonal competition for survival and resources[102]. This highlights the importance of the bone marrow microenvironment in supporting MM disease progression.

1.2 The bone marrow microenvironment

MM PCs reside almost exclusively in the bone marrow, where they rely on extrinsic factors within their microenvironment to support PC proliferation and survival[103]. The bone marrow is a complex microenvironment composed of cellular and non-cellular components including endothelial cells, stromal cells, adipocytes, haematopoietic cells, osteoblasts, osteoclasts, immune cells and extracellular matrix proteins[104]. The interaction of MM PCs with these different cell types is mediated by cell surface receptors and ligands as well as cytokine signalling (Figure 1.1)[105-107]. MM PCs are believed to reside within specialised niches in the bone marrow, where they take advantage of the specific niche microenvironment to support disease progression[108].

1.2.1 Bone marrow niches

The bone marrow microenvironment contains distinct regions termed "niches" that differentially support the growth and differentiation of numerous cell types[109, 110]. The two main bone marrow niches are the vascular niche, located close to the BM vasculature, and the endosteal niche, located close to the endosteal bone surface[108, 111]. The vascular niche is a site with rich blood supply, where hematopoietic stem cell (HSC) growth, differentiation and mobilisation to the blood stream occurs[112]. The endosteal niche is an extremely hypoxic environment, populated by osteoblasts on the bone surface, which are able to maintain HSCs in a quiescent or dormant state[113]. Results of a previous study found that when U266 human MM PCs were inoculated into immunodeficient mice, they preferentially engrafted at the metaphyseal region of the endosteal bone surface, where they

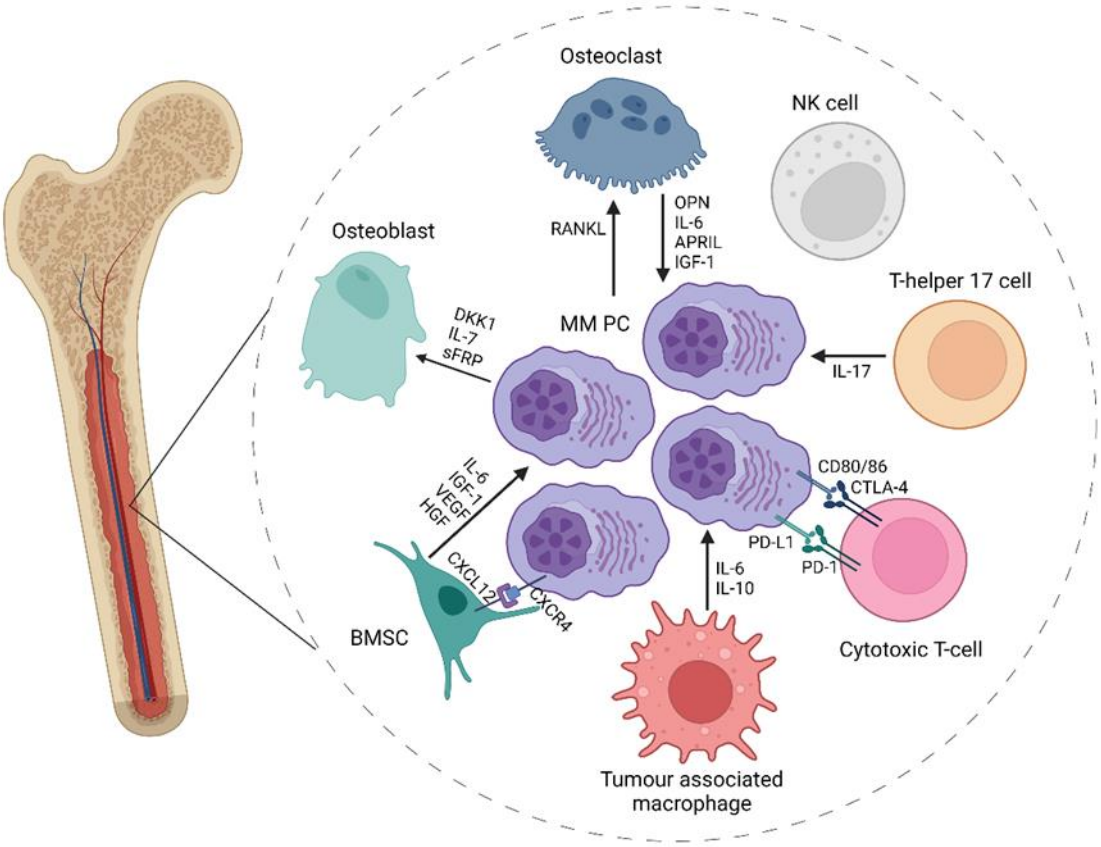

Figure 1.1: Interaction of MM PCs with other cell types in their bone marrow niche. MM PC interacts with cellular and non-cellular components of the BM. Arrows indicate secretion and/or effect on target cell. Key cell types, signalling cascades and transmembrane proteins are represented. MM PC adhesion to BMSCs is facilitated by the CXCL12/CXCR4 axis. Adhesion stimulates BMSC secretion of IL-6, IGF-1, VEGF and HGF, which support MM PC growth. MM PCs inhibit osteoblast differentiation through secretion of DKK1, IL-7 and sFRP. MM PCs also stimulate osteoclastogenesis resulting in excess bone resorption and the formation of osteolytic lesions. Osteoclasts secrete OPN, IL-6, APRIL and IGF-1, which promote MM PC proliferation. Tumour associated macrophages also support MM PC growth through secretion of IL-6 and IL-10. T-helper 17 cells are stimulated in the tumour microenvironment to produce IL-17, which promotes MM PC proliferation. NK cell and cytotoxic T-cell function is suppressed by MM PCs. MM PCs promote cytotoxic T-cell exhaustion through immune checkpoint inhibitory pathways PD-L1/PD-1 and CD80/CTLA-4.

initiated cell-cell interactions with osteoclasts and osteoblasts[114]. In addition to osteoclasts and osteoblasts, other cell types such as bone marrow stromal cells (BMSCs) and immune cells as well as extracellular matrix proteins form a MM permissive microenvironment termed the "MM niche"[103]. Paracrine signalling between MM PCs and these other cell types is mediated by an array of cytokines, receptors and adhesion molecules[115]. However, further study is required to fully elucidate the cell-cell signalling mechanisms that contribute to the initiation and progression of MM.

1.2.2 Bone marrow stromal cells MM PCs interactions

Bone marrow stromal cells (BMSCs) are multipotent progenitors of skeletal tissue components such as bone, cartilage, the haematopoiesis-supporting stroma, and adipocytes[116]. BMSCs play an important role in the bone marrow homing and retention of HSCs via upregulation of the chemoattractant CXCL12[117]. Notably, evidence suggests that malignant PCs hijack this mechanism to support their own BM homing, adhesion, and therapeutic resistance[118]. Expression of CXCL12 is upregulated in MM patient BMSCs compared to healthy control cells, and its corresponding receptor, CXCR4, is expressed by PCs of MM patients and human MM cell lines[119, 120]. Previous studies indicate that use of a CXCL12 inhibitor *in vivo* reduced MM PC dissemination and engraftment at bone marrow sites[121], and that use of a CXCR4 inhibitor *in vivo* increased circulating MM PCs[122].

MM remains incurable owing to acquired resistance to therapy, which is, in part, thought to be mediated by PC adhesion to BMSCs[123]. Studies have shown that inhibition of either CXCR4 or CXCL12 can sensitise MM PCs to multiple chemotherapeutic agents *in vitro*[120, 122, 124]. MM PCs are also known to express other adhesion molecules that support their contact with BMSCs including ICAM-1, LFA-1, VLA-4, LAM-1, and CD44[125, 126]. Importantly, adhesion of MM PCs to BMSCs triggers NF-κB-dependent stromal cell secretion of interleukin-6 (IL-6), a potent myeloma cell growth factor, resulting in MM PC proliferation[105]. When co-cultured with MM PCs, BMSCs also produce other growth and anti-apoptotic factors for MM cells such as IGF-1, VEGF and HGF[103].

1.2.3 Osteoblast MM PC interactions

In normal physiology, osteoblasts and osteoclasts maintain homeostasis of bone resorption and new bone formation. This process is dysregulated in MM, where MM PCs suppress osteoblast function whilst simultaneously enhancing osteoclast function, resulting in osteolysis[15]. MM PCs inhibit bone-forming osteoblasts through secretion of Dickkopf1 (DKK1), interleukin 7 (IL-7) and Frizzled-related protein (sFRP) [18, 19]. Additionally, transforming growth factor-β (TGF-β) is released from bone matrices when bone is resorbed during osteolysis, and thus high levels of TGF-β is present within MM osteolytic lesions[127]. TGF-β inhibits later phases of osteoblast differentiation, preventing bone formation by mature osteoblasts. Results from previous studies showed that inhibition of TGF-β resulted in the differentiation of mature osteoblasts, suppressed MM PC growth in a murine model of MM and suppressed bone destruction[128]. Another study showed that contact with osteoblasts can maintain murine MM PCs in a long term dormant state, and that osteoclast remodelling of the endosteal niche is able to 'release' MM PCs from dormancy *in vivo*[129].

1.2.4 Osteoclast MM PC interactions

Osteoclastogenesis and resultant osteolytic lesions occur in parallel to MM disease progression. MM PCs secrete the chemokines macrophage inflammatory protein (MIP) -1α and -1β, which stimulate osteoclastogenesis and bone resorption resulting in osteolysis[130, 131]. The MM bone marrow microenvironment displays a high level of receptor activator of NF-κB ligand (RANKL) expression, which is secreted by MM PCs themselves, as well as BMSCs and osteocytes. RANKL binds to RANK on osteoclasts, increasing osteoclastogenesis and osteoclast activity[132]. Yaccoby, *et al*., found that co-culture of osteoclast precursor cells with MM PCs from MM patient bone marrow resulted in osteoclastogenesis as well as enhanced MM PC proliferation and survival[107]. Osteoclasts secrete CCR2 chemokines and growth factors that directly support MM PC growth, including OPN, IL-6, APRIL and IGF-1[133, 134].

1.2.5 The immune microenvironment in MM

MM PC evasion of the host immune system enables their unchecked proliferation and survival within the bone marrow. The bone marrow immune microenvironment is composed of cytotoxic CD8+ T-cells, T-helper cells, regulatory T-cells, regulatory B-cells, NK cells, dendritic cells and tumour-associated macrophages[135, 136]. MM PCs nurture an MM permissive immune microenvironment characterised by widespread immune cell dysfunction, the progressive exhaustion and dysfunction of T-cells and NK cells, which prevents their anti-tumour cytotoxicity[137-139]. Other immune cell types, including T-helper cells and tumour associated macrophages, are reprogrammed by MM PCs to directly support tumourigenesis. Abundant IL-6 and TGF-β in the MM tumour microenvironment stimulate the production of T-helper 17 (Th17) cells, which produce the pro-inflammatory cytokine interleukin 17 (IL-17)[140]. IL-17 is expressed in the peripheral blood of MM patients and has been shown to promote the proliferation of human MM cell lines *in vitro,* as well as promote osteoclastogenesis and osteolysis[140, 141]. Tumour-associated macrophages support MM PC growth through secretion of the pro-tumourigenic cytokines IL-6 and IL-10 and are also able to promote MM angiogenesis when exposed to VEGF[142, 143]. Importantly, CD4+ regulatory T-cells (Tregs) and CD8+ cytotoxic T-cells have been identified as cell types that play a significant role in MM immune suppression[137, 144].

1.2.6 T-cells in MM

Results from a previous study indicate that immune cell populations are heterogeneous between MM patients and dynamic across disease stages, with greater proportions of Tregs and cytotoxic CD8+ T-cells identified during MM disease progression[135]. Furthermore, the ratio of Th17 cells to Tregs has been shown to impact patient survival. To this end, newly diagnosed patients with a higher frequency of Tregs showed reduced progression free survival[145, 146]. Although the function of Tregs in MM requires further elucidation, studies have shown that a skewed Th17/Treg ratio, defined by increased Treg populations, resulted in CD8+ T cell suppression, particularly in response to an IMiD treatment regime[147]. In addition, a recent study showed that Treg depletion, prior to MM PC administration, prevented tumour engraftment[148]. Immune checkpoint proteins, expressed by cancer cells, are commonly upregulated as a mechanism of immune subversion, enabling cancer cells to escape detection by the host immune system[149]. PD-1 is an

immune checkpoint receptor expressed by CD4+ and CD8+ T cells, and its ligand PD-L1 is expressed by macrophages, dendritic cells and many types of cancer cells [150]. The PD-1/PD-L1 interaction inhibits T cell proliferation, promotes T cell apoptosis and thereby prevents the cytotoxic ability of T cells [151]. PD-L1 and another immune checkpoint protein, cytotoxic lymphocyte antigen 4 (CTLA-4), have been identified as attractive therapeutic targets to stimulate an anti-myeloma immune response[152, 153].

1.2.7 Cellular dormancy in MM

Dormancy in cancer can be defined either by overall tumour growth arrest, called tumour dormancy, or by the growth arrest of a single cancer cell, called cellular dormancy[154]. Cellular dormancy in myeloma occurs when MM PCs do not progress through the cell cycle, do not divide and reside long term within specialised bone marrow niches. Dormant MM PCs are thought to reside at the endosteal niche where they are maintained in a dormant state whilst in contact with osteoblasts[129]. Populations of dormant MM PCs residing in the bone marrow following a therapeutic response is clinically recognised as minimal residual disease (MRD), which is monitored to evaluate remission status[155]. Cancer cell dormancy enables MM PCs to evade targeting by the immune system and chemotherapy, and subsequently become reactivated, resulting in the frequent incidence of clinical disease relapse in myeloma patients[156]. Therapeutic targeting of dormant MM PCs may be an effective way to control MM patient relapse. This could be achieved by understanding the mechanisms of dormancy to either maintain dormancy long term or reactivate cells prior to conventional therapy to target actively dividing cells.

1.3 The TAM receptors

1.3.1 TAM receptor biology

The TAM receptors, Tyro3, Axl and Mer represent a distinct tyrosine kinase cell surface receptor family[157]. The extracellular domains of the TAM receptors are composed of two structural modules that are configured in a defining two-plus-two combination (Figure 1.2)[158]. The amino-terminus regions of these domains carry tandem immunoglobulin-related domains that mediate ligand binding, followed by tandem fibronectin type III repeats[159]. TAM receptors have a single pass trans-

membrane domain and carry a catalytically competent tyrosine kinase domain, which is activated following ligand binding[158, 160]. The TAM receptors have multiple known ligands, including growth arrest specific-6 (Gas6), Protein S (Pros1) [158], Tubby, Tubby-like protein (TULP1) and Galectin-3[161, 162]. The most well characterised TAM receptor ligands are Gas6 and Pros1. As these ligands are both secreted by osteoblasts, an important component of the MM niche [163, 164], and are both implicated in cancer [165-168], they will be the focus of this study. Gas6 and Pros1 are structurally homologous proteins that bind phosphatidylserine on the external membrane of apoptotic cells[169]. The glutamate-rich Gla domains of Gas6 and Pros1 are post-translationally γ-carboxylated in a vitamin K dependent reaction, which enables them to bind phosphatidylserine and subsequently bind and activate TAM receptors. Of note, phosphatidylserine is expressed on the surface of cancer cells including MM PCs due to uncontrolled cell division, dysregulated membrane trafficking pathways and increased cell death pathway signalling[170, 171]. Activation of a TAM receptor is coupled with activation of a downstream signalling pathway, commonly the phosphoinositide 3 kinase (PI3K)/Akt pathway or alternatively the JAK/STAT pathway[158, 172]. TAM receptor activation results in binding and phosphorylation of growth factor receptor bound protein 2 (Grb2), which acts as an adaptor protein, coupling the activated receptor to other signalling proteins[173]. TAM receptors can also directly bind to the p85 subunit of PI3K or recruit the p85 subunit of PI3K through an SH3 (Grb2)-proline-rich domain (p85) interaction[174]. Mobilization of the p85/p110 PI3K complex then results in the downstream phosphorylation and activation of Akt[158]. These pathways are required for TAM receptor-mediated regulation of cell survival and proliferation, and engulfment of apoptotic cells by phagocytes[173, 175, 176].

1.3.2 TAM receptors in normal physiology

Early knowledge about TAM receptor function in normal physiology can be attributed to studies on TAM receptor knockout mice. TAM receptor triple knockout mice develop broad spectrum autoimmune disease in the first 3 weeks of life, which is thought to be the result of an uncontrolled inflammatory response and a build-up of apoptotic cells resulting in tissue necrosis[177]. This is thought to be due to the necessity of TAM receptor expression by dendritic cells and macrophages for phagocytic clearance of apoptotic cells [178, 179].

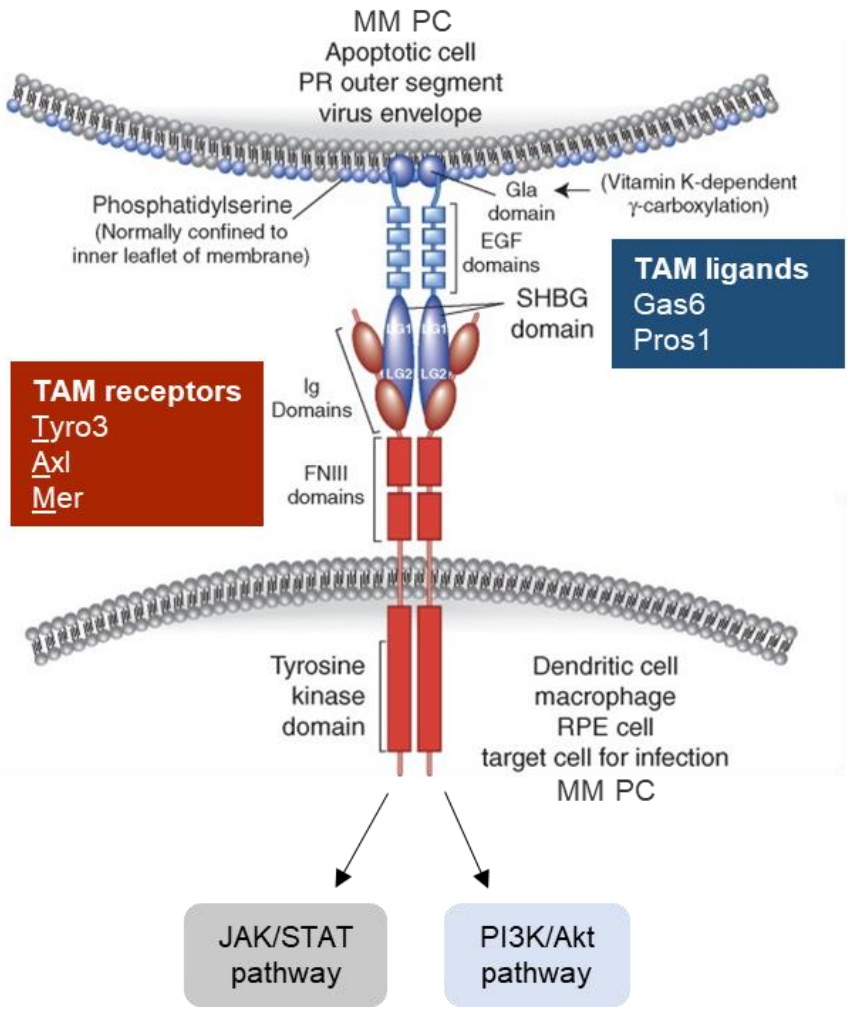

Figure 1.2. TAM receptor and ligand structure. The N-terminal Gla domain of Gas6/Pros1 (blue) is γ-carboxylated and binds phosphatidylserine on the surface of an apoptotic cell, photoreceptor (PR), virus or MM cancer cell. Gas6/Pros1 binds the TAM receptor (red) through its C-terminal sex-hormone binding globulin (SHBG) domain, inducing dimerization of the TAM receptor immunoglobulin (Ig) domain followed by tandem fibronectin type III repeats (FNIII repeats). Activation of the tyrosine kinase domain of the TAM receptor is coupled with activation of downstream signalling pathways (modified from Lemke, G., 2013[158]).

These triple TAM knockout mice also developed male infertility resulting from the loss of TAM receptor function in Sertoli cells. Male infertility is thought to be the result of the progressive death of differentiating germ cells in the testes, which are normally supported by Sertoli cells, as well as an inability of Sertoli cells to clear apoptotic germ cells generated during meiosis[180]. Mer knockout mice develop blindness in the first few months of life as most of their photoreceptors are lost due to cell death[181]. Mer expressed by retinal pigment epithelial (RPE) cells is essential for the maintenance of photoreceptors by facilitating the phagocytosis of photoreceptor outer segments by RPEs. A recent study of skeletal muscle regeneration, following injury, in Mer knockout mice revealed a reduced capacity for phagocytic clearance of apoptotic cells by infiltrating macrophages, resulting in delayed tissue repair[182]. Together, these studies indicate that the main functions of TAM receptors expressed by a number of different cell types is to facilitate phagocytosis and inhibit inflammation as part of the innate immune system[183]. Phagocytic clearance, mediated by TAM receptors, is facilitated by Gas6 or Pros1, which serve as bridging molecules that physically link a TAM receptor to phosphatidylserine, simultaneously activating the TAM receptor[158]. PI3K/AKT pathway signalling is then initiated, which is involved in mitogenic signalling, intracellular vesicle trafficking and cytoskeleton remodelling, essential for phagocytosis of apoptotic cells by macrophages[172]. Although TAM receptor functions are essential for normal physiology, TAM receptors and ligands are also expressed by many types of cancer cells[166, 184-187], where their functions are exploited by the tumour to support cancer development and disease progression.

1.3.3 Gas6 and Pros1 signalling in cancer

Gas6 has been shown to regulate cancer cell proliferation and enhance cancer cell survival in many cancers, including myeloma, acute myeloid leukaemia (AML) and prostate cancer [164, 166, 188, 189]. Cancer cells within the bone marrow can secrete and utilise their own Gas6 through autocrine signalling mechanisms as well as respond in a paracrine manner to Gas6 produced from accessory cells such as bone marrow stromal cells and osteoblasts. Co-culture of AML cells with bone marrow stromal OP-9 cells promoted the upregulation of Gas6 in the stromal cell line. This stromal cell-derived Gas6 was found to contribute to the chemoprotective and proliferative effects of bone marrow stromal cells on AML cells [190]. Elevated Gas6 expression in

whole patient blood or bone marrow samples is also a marker of poor clinical outcomes in adult AML patients, with most patients ≥ 60 years of age, which display elevated Gas6 expression being unable to achieve complete remission[191]. Exogenous Gas6 induced G_1 cell cycle arrest, reduced cell proliferation and enhanced survival of human prostate cancer cell lines treated with a chemotherapeutic agent[189]. Interestingly, knockdown of Gas6 in human myeloma cell lines RPMI-8226 and U266 resulted in rapid cell death, showing that these myeloma cell lines are reliant on Gas6 for survival[166]. Exogenous Gas6 increased the proliferation of RPMI-8226 cells *in vitro*[188], and transgene-mediated overexpression of Gas6 in U266 cells also significantly increased growth of the cell line *in vivo*[166]. As Gas6 mRNA expression is upregulated in bone marrow PCs of both MGUS and MM patients, compared to healthy controls, Gas6 may be an attractive therapeutic target to limit PC growth and improve outcomes for the majority of MM patients [166, 188].

Pros1 is overexpressed in human papillary thyroid cancer cell lines and human lung cancer cell lines, compared to healthy control cell lines[192, 193]. In human lung cancer cell lines, Pros1 signals through Mer or Tyro3 to promote migration and colony formation *in vitro*[193]. Pros1 has not yet been studied in MM, and its expression by MM patient PCs is currently unknown. Further study is required to fully elucidate the functional roles of TAM receptor and ligand signalling in MM cells.

1.3.4 Role of Axl in cancer

Elevated Axl expression in several cancer types has been identified as a marker of poor prognosis. A recent study found that liver cancer patients with high Axl expressing-tumours have significantly reduced overall survival in comparison with those that have low Axl expression[194]. Analysis of Axl expression in tumours from head and neck cancer patients revealed an inferior prognosis for patients with high Axl expression who are treated with surgery alone[195]. Furthermore, high Axl expression in BM or peripheral blood from acute myeloid leukaemia patients was also associated with poor overall survival[190]. Given that Axl expression can confer poor prognosis in some cancers, numerous studies have made efforts to understand the functional role of Axl in cancer. Studies in several different cancer types indicate that Axl expression is associated with cancer cell metastasis, therapeutic resistance and dormancy.

Axl has been shown to promote the migration of prostate and breast cancer cells, both of which commonly metastasise from the primary site of tumour to secondary sites within the bone marrow [196-199]. Axl knockdown in human prostate cancer cell lines PC3 and Du145 significantly reduced cell migration across transwells *in vitro*[196, 197]. Similarly, recent studies have found that treatment with Axl monoclonal antibodies attenuated the *in vitro* migration of breast cancer[200], ovarian cancer and non-small-cell lung cancer cell lines[201]. Treatment with Axl inhibitors in murine models of triple negative breast cancer suppressed the metastasis of breast cancer cells, particularly to sites within the bone marrow[198, 199]. Metastasis of MM PCs to new bone marrow sites involves processes similar to the bone metastasis of solid tumour cells[202]. Therefore, investigating the role of Axl in MM PC migration, particularly to secondary sites *in vivo*, is warranted.

Numerous previous studies have identified that Axl expression, by cancer cells, confers resistance to therapy. A previous study found that Axl is phosphorylated in epidermal growth factor receptor (EGFR) mutant non-small-cell lung cancer cells when they are treated with an EGFR inhibitor[203]. Axl knockdown in these EGFR mutant non-small-cell lung cancer cells sensitised them to EGFR inhibitor treatment, indicating that Axl expression may be responsible for EGFR inhibitor resistance. Additionally, activation of Axl and the tyrosine kinase receptor, RON, promoted prostate cancer resistance to androgen deprivation therapy (ADT)[204]. Findings of this study indicated that RON was able to recruit Gas6-expressing macrophages to the tumour microenvironment, resulting in Gas6/Axl signalling and ADT resistance. Another recent study found that a dual Axl and FLT3 inhibitor was more effective than a FLT3 inhibitor alone to limit the growth of FLT3-mutant acute myeloid leukaemia (AML) cell lines *in vitro* and AML patient xenografts *in vivo*[205]. These studies suggest that the use of Axl inhibitors, in combination with other existing therapies, may offer clinical benefit to cancer patients and should be explored in further studies.

Axl expression has been shown to regulate dormancy in metastatic human prostate cancer and melanoma cell lines *in vitro* and *in vivo* [164, 185, 206, 207]. Prostate cancer

cells commonly disseminate from the primary site of tumour to the bone marrow, where they enter into a state of long term cellular dormancy [202]. The ability of the Gas6/Axl axis to regulate prostate cancer dormancy may be mediated by interactions with other ligands and receptors. Co-culture with osteoblasts induces prostate cancer cell dormancy and upregulation of both TGF-β ligands (TGF-β1 and TGF-β2) and their receptors (TGF-βR2 and TGF-βR3) in prostate cancer cells, and these effects were abrogated by shRNA mediated Axl knockdown[206]. Taken together, these data suggest that Axl expression may regulate TGF-β-induced dormancy in human metastatic prostate cancer. Interestingly, Axl overexpression in the PC3 human prostate cancer cell line was shown to significantly delay, but not prevent, tumorigenesis in an *in vivo* model of disseminated prostate cancer[185]. Melanoma cells commonly metastasise to the lungs in later stages of disease, where cells undergo short periods of dormancy prior to disease progression[208]. A recent study found that the non-canonical WNT5A signalling pathway is required for dissemination of melanoma cells and dormancy induction in the lungs of mice[209]. It was found that WNT5A and Axl are commonly co-expressed in melanoma cell lines, and that Axl expression may be regulated by WNT5A signalling. Furthermore, inducible overexpression of Axl in melanoma cells *in vivo* resulted in the formation of small non-proliferative micrometastases in the lungs compared to the control, which developed larger proliferative metastases. The first evidence of the association of Axl with myeloma dormancy was presented by Lawson, *et al.,*[129] who identified Axl as one of the most highly upregulated genes in a bone marrow resident dormant subpopulation of 5TGM1 murine MM cells.

1.3.5 Role of Axl in MM PC dormancy

Although novel therapeutic agents have improved outcomes for MM patients in the last two decades, MM remains an incurable malignancy and patients experience frequent disease relapse[210]. Relapse has been attributed, in part, to a subpopulation of dormant malignant PCs that do not divide and reside long term within specialised niches in the bone marrow[156 129]. As these cells do not undergo cell division, they evade conventional therapies, which target rapidly dividing cells, and their persistence results in MRD[211]. Dormant MM PCs can be selectively reactivated following stochastic changes within the bone marrow such as osteoclast mediated bone turnover [129, 212]. These cells then re-enter the cell cycle and undergo rapid cell

division, contributing to new tumours throughout the skeleton giving rise to what is clinically recognised as relapse. Factors that initiate and sustain myeloma dormancy, as well as regulate the molecular switch between cellular dormancy and reactivation, are not well characterised.

Axl has been identified as one of the most upregulated genes in dormant subpopulations of 5TGM1 murine myeloma cells *in vivo* [129, 213]. GFP+ 5TGM1 cells were labelled with DiD, a heritable dye that is shared between daughter cells, and cells were intravenously administered to C57BL/KaLwRijHsd (KaLwRij) mice[213]. The 5TGM1 cells subsequently home to the bone marrow where they form multiple myelomatous tumours, recapitulating many aspects of human MM disease. The bone marrow of mice was harvested after 21 days, cells were assessed by flow cytometry, and cells that had retained the DiD label and therefore had not divided were considered 5TGM1 GFP+ DiD^{hi} dormant cells. As well as Axl, the other genes that were highly upregulated in this dormant cell subset were the transcription factors *Irf7* and *Spic*, and the adhesion molecules and receptors *Fcer1g, Mpeg1, Sirpa and Vcam1*. Of note, Axl is expressed at low levels by human MM PCs, with an increased level of Axl expression identified in MM PCs of patients with MGUS compared to MM or relapsed MM[166, 213]. This is consistent with Axl being expressed by a subpopulation of dormant human MM PCs rather than by the proliferative PCs making up most of the tumour mass. From the panel of dormancy associated genes identified by Khoo, *et al.,*[213] Axl was chosen for targeting with a small molecule inhibitor, BMS-777607. However, BMS-777607 is not Axl specific, and also targets Met[214], Tyro3, Mer[215], and Ron[216]. Therefore, treatment with BMS-777607 *in vivo* has the ability to target Axl, Tyro3, Mer, Met and Ron on 5TGM1 cells, in addition to, for example, Axl expressed by macrophages[217], and Met expressed by osteoblasts[218], cells which form part of myeloma supportive niches in the bone marrow. Targeting Axl with BMS-777607 in the KaLwRij model of MM reduced the proportion of dormant 5TGM1 DiD^{hi} dormant cells and increased MM PC burden in the bone marrow. This observation is consistent with Axl expression by 5TGM1 cells being necessary for dormancy maintenance. However, these data have not yet been supported by a more Axl- specific genetic knockdown or knockout studies.

1.3.6 Role of Mer in cancer

Mer expression has been identified in numerous cancers[166, 186, 215, 219], and its expression is associated with poor prognosis in hepatocellular carcinoma[220]. Mer inhibition using either siRNA or a small molecule inhibitor, UNC2250, reduced cell proliferation of mantle cell lymphoma cell lines *in vitro*[221]. Treating mice with UNC2250 slowed disease progression in a xenograft model of mantle cell lymphoma. Furthermore, the use of UNC2250 sensitised mantle cell lymphoma cells to the chemotherapeutic agents, vincristine and doxorubicin *in vivo*, resulting in significant reductions in tumour size. In a xenograft model of acute myeloid leukaemia, treatment with a Mer inhibitor reduced leukemic burden and increased survival time[222]. When this treatment was combined with the chemotherapeutic agent methotrexate, the effects on tumour burden and survival were even more pronounced. Similarly, knockdown of Mer in non-small cell lung cancer xenografts promoted apoptosis and improved chemotherapeutic efficacy[223]. Other studies in hepatocellular carcinoma[220] and pancreatic cancer[224] have also noted reduced cell proliferation *in vitro* when cancer cells were treated with Mer small molecule inhibitors. These studies establish that Mer promotes cancer cell proliferation, survival and chemotherapy resistance. In addition, these studies demonstrate the efficacy of Mer small molecule inhibitors in limiting *in vivo* tumour burden both alone and in combination with chemotherapeutic agents.

1.3.7 Mer in cancer cell escape from immune surveillance

Recent studies implicate Mer in the promotion of an immune-suppressive tumour microenvironment by regulation of immune checkpoint signalling through the PD-1/PD-L1 axis [175, 186]. Immune checkpoint proteins are negative regulators of the immune system, which maintain self-tolerance and minimise damage to tissues during an immune response to pathogens [225, 226]. Immune checkpoint proteins are commonly upregulated in cancer as a mechanism of immune subversion, enabling cancer cells to escape detection by the host immune system [149]. PD-1 is expressed on T cells, and is the receptor for the ligand PD-L1, which is expressed by macrophages, dendritic cells and many types of cancer cells [150]. The PD-1/PD-L1 interaction inhibits T cell proliferation, promotes T cell apoptosis and thereby prevents the cytotoxic ability of T cells [151]. The PD-1/PD-L1 pathway is commonly upregulated in cancer, where it inhibits the activity of tumour reactive T cells,

preventing tumour rejection [225, 227, 228]. MM patients, stratified as high risk and patients with advanced disease, have high T cell expression of PD-1 [229]. Furthermore, human and murine MM PCs express high levels of PD-L1 [230]. PD-1/PD-L1 inhibitors have been successful in a number of cancers, but clinical trials involving these inhibitors have been put on hold in MM due to high toxicities of PD-1 and PD-L1 inhibitors in combination with other immunomodulatory IMiD drugs used for MM treatment, such as lenalidomide[231]. As there is evidence that the PD-1/PD-L1 axis may be facilitating MM PC escape from immune surveillance, the exploration of alternative strategies to exploit this pathway in MM may bypass the toxicities associated with direct PD-1/PD-L1 inhibitors.

Interestingly, Mer expression has been shown to upregulate PD-L1 on the cell surface of cancer cells themselves [175, 186, 232]. The combined use of a pan-TAM kinase inhibitor and an anti-PD-1 antibody in a murine model of breast cancer showed increased tumour infiltration of effector T cells and decreased tumour burden and lung metastasis compared to either monotherapy treatment [232]. Mer inhibition in a murine model of acute lymphoblastic leukaemia (ALL) decreased PD-L1 expression on the cell surface of bone marrow macrophages and monocytes[186]. Mer inhibition also decreased PD-1 expression on T cells and increased both CD4+ and CD8+ T cell activation. Mer inhibition *in vivo* in an immune competent C57BL/6 model of AML inoculated with Mer-negative ALL cells also significantly prolonged survival time, but had no effect in an immune compromised NSG model inoculated with the same Mer-negative cells [186]. These data demonstrate an immune-mediated therapeutic effect of Mer inhibition in ALL. Furthermore, results of a previous study indicated that in murine models of non-small cell lung cancer and pancreatic cancer, triple therapy, using radiation therapy, a Mer inhibitor and a PD-1 inhibitor produced the longest overall survival and reduced tumour burden[233]. Triple therapy increased cytotoxic T-cell and NK cell populations, and it was found that these cell types were essential for treatment efficacy.

1.3.8 Role of Mer in MM pathogenesis

The uncontrolled proliferation of clonal PCs is a process central to MM tumour development. Previous studies identified that the Gas6/Mer axis promotes the proliferation of human MM PCs[166, 188]. Malignant PCs from most MM patients

express both Gas6 and Mer at the mRNA level, with Gas6 expression increased compared to that seen in healthy control PCs [166, 188]. The RPMI-8226 human myeloma cell line, which expresses Gas6 and Mer, shows an increase in cell proliferation *in vitro* upon Gas6 overexpression[166], as well as when supplied with a source of exogenous Gas6 [188]. Mer knockdown in human myeloma cell lines RPMI-8226 and U266 reduced cell proliferation, even in the presence of stromal cell conditioned media rich in Gas6[166, 188]. Furthermore, in the orthotopic U266 *in vivo* model of MM, knockdown of Mer or therapeutic blockade of Gas6 using Warfarin significantly reduced tumour burden and increased survival time *in vivo*[166]. Taken together, these data suggest that both Gas6 and Mer are drivers of myeloma cell proliferation both *in vitro* and *in vivo.*

Recent studies identify a potential role for the Gas6/Mer axis in potentiating MM PC resistance to bortezomib. One study utilised scRNAseq analyses to evaluate the molecular features of an optimal vs. sub-optimal response to bortezomib[234]. Communication patterns analysis indicated that a source of Gas6 from MM PCs is predicted to signal through Mer expressed by macrophages in the tumour microenvironment. Of note, this signalling pathway was enriched in both the MM microenvironment compared to the healthy microenvironment, as well as in patients with a sub-optimal response to bortezomib. Another study found that heme-oxygenase 1 (HO-1) upregulates Gas6 expression in Gas6 and Mer expressing human MM cell lines RPMI8226 and U266[235]. HO-1 inhibition or siRNA knockdown in these human myeloma cell lines downregulated Gas6 expression. Furthermore, combined treatment of RPMI8226 cells or primary human MM PCs with a HO-1 inhibitor and bortezomib significantly reduced cell viability in comparison to bortezomib treatment alone.

Gas6 and TAM receptor signalling, mainly through Mer, has recently been implicated in regulating the immunosurveillance of MM. Natural killer (NK) cell function is commonly supressed in late stage MM, contributing to MM PC immune escape[236]. The NK cell stimulatory receptor NGKD2 is activated by binding of its ligand MICA, which is expressed by MM cells. Interestingly, Gas6/Mer signalling was found to downregulate MICA expression in human MM cell lines SKO-007(J3), U266 and ARP1, identifying a potential mechanism of NK cell suppression by MM

PCs[237]. Thus, Mer expressed by MM PCs may function not only as a pro-proliferative receptor stimulated by Gas6, but also as a regulator of MM immune evasion. Further characterisation of the potential role of Mer in facilitating MM PC immune evasion through regulation of T-cell or NK-cell inhibitory pathways is warranted.

1.4 Summary and aims

MM is a haematological malignancy characterised by the uncontrolled proliferation of antibody-secreting plasma cells in the bone marrow[2]. Although treatment options and overall survival of patients has improved over the past 20 years, almost all patients will inevitably relapse. Significant inter-patient genetic heterogeneity is observed in MM, with few unifying clinically actionable genetic events[91, 97, 102]. There is a pressing need to fully elucidate the molecular mechanisms underlying MM PC proliferation and dormancy to identify novel drug targets. Expression of the TAM tyrosine kinase receptors Axl and Mer by cancer cells has been implicated in the pathogenesis of lung cancer[223, 238], breast cancer[199, 200], prostate cancer[185, 239] and leukaemia[205, 240]. In the 5TGM1/ KaLwRij murine model of MM, Axl is expressed by a subpopulation of dormant 5TGM1 MM cells[129, 213]. When KaLwRij mice were treated with a small molecule inhibitor with targets including Axl, 5TGM1 cells were released from dormancy, resulting in increased BM tumour burden[213]. The role of Axl in initiating and maintaining MM PC dormancy will be investigated in this study using Axl-positive and Axl-negative 5TGM1 cell lines. The Mer/Gas6 axis has been shown to promote human MM PC proliferation *in vitro* and increased tumour burden *in vivo*[166]. In other cancers, Mer has been shown to play a role in immune checkpoint inhibition through modulation of PD-L1 expression[186]. This study will investigate the role of Mer in both MM PC proliferation and immune evasion using Mer-positive and Mer-negative 5TGM1 cell lines in immune competent and immune compromised mouse models.

The studies in this thesis were designed to address the following aims:

(1) To generate, using CRISPR Cas9 and retroviral transduction, single Axl and Mer receptor expressing 5TGM1 MM cell lines as well as a 'TAM null' cell line.

(2) To investigate the role of Axl expression by 5TGM1 MM cells in the induction of cellular dormancy.

(3) To investigate the role of Mer expression by 5TGM1 MM cells on cell proliferation and MM disease progression.

2. Materials and Methods

2.1 Molecular biology

2.1.1 RNA techniques

2.1.1.1 RNA isolation

For isolating total RNA from 5TGM1, OP9 and MC3T3-E1 cell lines, 5 x 10^6 cells were lysed in 0.5 mL of TRIzol™ Reagent (Invitrogen) and 0.1 mL of chloroform was added. Following vigorous shaking and a 3 minute incubation, the mixture was centrifuged at 12,000 x g and 4°C for 5 minutes, and the aqueous phase was collected. RNA was precipitated by adding 0.25 mL of isopropanol and incubating at room temperature for 10 minutes. The RNA was pelleted by centrifugation at 12,000 x g and 4°C for 15 minutes and then washed with 75% (v/v) ethanol. The RNA was resuspended in UltraPure™ DNase/RNase-Free Distilled Water (nuclease free (NF) water; Invitrogen). The concentration of RNA in solution was determined by measuring the absorbance at 260 nm on a NanoDrop™ 8000 Spectrophotometer (Thermo Fisher Scientific). RNA was stored at -80°C.

2.1.1.2. RNA isolation from bone marrow and compact bone

For isolating RNA from bone marrow and compact bone of C57BL/KaLwRij and NSG mice (section 2.3.1) femora and tibiae from both hind limbs were cleaned and crushed in PFE buffer (Phosphate Buffered Saline (PBS), 2% FCS, 2mM ethylenediamine tetraacetic acid (EDTA) pH 7.4) using a mortar and pestle. The bone marrow containing cell suspension was then passed through a 70µm filter and RNA was isolated as described in section 2.1.1.1. Bone fragments were transferred to a petri dish, covered with 4-5 drops of 3 mg/mL collagenase Type II (Gibco), 0.2% (w/v) DNase I (Sigma) in PFE buffer for 5 minutes. Bone fragments were manually chopped into smaller fragments with the use of a scalpel and then transferred to a 50 mL falcon tube and 2 mL collagenase/DnaseI was added. Bone fragments were then incubated for 45 minutes at 37°C with gentle shaking. 30 mL ice cold PFE buffer was added to bone fragments and released cells and centrifuged for 10 minutes at 400 x g. Bone fragments were resuspended in 1 mL TRIzol™ Reagent and incubated on ice for 15 minutes. RNA was isolated according to 2.1.1.1.

2.1.1.3. RNA DNase Treatment

RNA underwent DNase treatment with RQ1 DNase (Promega) as per manufacturer's instructions prior to cDNA manufacture.

2.1.1.4 cDNA synthesis and quantitative Reverse Transcription polymerase chain reaction

To quantitatively assess messenger RNA (mRNA) levels, quantitative reverse transcription polymerase chain reaction (q-RTPCR) was performed. Firstly, total RNA (2 µg) was reverse transcribed into single-stranded complementary DNA (cDNA) using SuperScript™ IV Reverse Transcriptase (Invitrogen). The RNA sample was resuspended in a total volume of 12 µL of NF water and 1 µL each of random hexamers (50µM), and deoxyribonucleotide triphosphate (dNTP) mix (10 mM) were added. The solution was incubated at 65°C for 5 minutes and immediately chilled on ice for at least 2 minutes. A mix containing 4 µL of 5x RT buffer, 1 µL of 0.1 M DTT and 1 µL of SuperScript™ IV enzyme (200 U) was then added to the denatured RNA. This reaction mixture was incubated for 10 minutes at 23°C, 10 minutes at 55°C and 10 minutes at 80°C. It was then diluted to a total volume of 0.1 mL with NF water and either used immediately for downstream applications or stored at –80°C. Negative control minus reverse transcriptase reactions were performed concurrently for all samples.

Secondly, qPCR was performed, with each 15 µL reaction containing 2 µL of cDNA, 1x RT^2 SYBR® Green qPCR Mastermix (QIAGEN), 0.5 µM forward primer, 0.5 µM reverse primer in NF water in a 96-well clear PCR plate (Bio-Rad). Primer sequences are listed in Table 2.1. All cDNA samples were analysed in triplicate. Minus reverse transcriptase and no template control (NTC) reactions were included for each sample and target gene, respectively. Reactions were performed on the QuantStudio™ 3 Real-Time PCR System (Thermo Fisher Scientific) using the following cycling parameters: 50°C for 2 minutes; 95°C for 15 minutes; 40 cycles of 95°C for 15 seconds, 60°C for 25 seconds and 72°C for 10 seconds; and 72°C for 3 minutes. A melt curve was then performed in which there was an incremental increase of 0.5°C/5 seconds from 65°C to 95°C. Relative changes in gene expression were assessed using the $2^{-\Delta\Delta Ct}$ method.[241]

Table 2.1: q-RTPCR primer sequences

Gene	Species	Forward/reverse primer sequences (*5' - 3'*)
Gas6	Mouse	AAGATGTGGACGAGTGCCAG/ GCGTAGTCTAATCACGGGGG
Pros1	Mouse	TCCAAAGAGCGTGCTTCACA/ TGGAATGAGCCAACACGGAA
Galectin-3	Mouse	GGAGCTTATCCTGGCCCAAC/ GGCATGACTCCTCCAGGCAA
GAPDH	Mouse	ACCCAGAAGACTGTGGATGG/ CAGTGAGCTTCCCGTTCAG
Hprt	Mouse	TGACACTGGCAAAACAATGCA/ GGTCCTTTTCACCAGCAAGCT
PD-L1	Mouse	TCCGTGGATCCAGCCACTTC/ TTGCCCTGGCTGTGATCTCC
PD-L2	Mouse	GAAGTGTACACCGTAGACGT/ ACTTGGACACTAGGGATGTG
Galectin-9	Mouse	GACTTCAGGTGACCCTCCAG/ ACTCTGACCTCTGCACCAGG
TNFSF-9	Mouse	TCCGTGGATCCAGCCACTTC/ TTGCCCTGGCTGTGATCTCC
ICOS-L	Mouse	CAGGCAGCCTGTTTGGAAGA/ TCCCTGGAGACTTGTAAGGC
PVR	Mouse	CTCTTGTGGCTGTCTTCCAC/ GCCTCTGCAGTGTTCTTAGG

2.1.2 DNA techniques

2.1.2.1 Genomic DNA extraction

Genomic DNA was extracted from clonal 5TGM1 Axl and Tyro3 knockout cell lines using the DNEasy Blood and Tissue Kit (QIAGEN) according to manufacturer's instructions. The concentration of DNA in solution was determined by measuring the absorbance at 260 nm on a NanoDrop™ 8000 Spectrophotometer (Thermo Fisher Scientific). DNA was stored at -20°C.

2.1.2.2 Polymerase chain reaction

PCR was performed using Phusion™ DNA Polymerase (New England Biolabs), with each 50 µL reaction containing 100-200 ng genomic DNA, 0.2 mM dNTPs, 0.5 µM forward primer, 0.5 µM reverse primer, 1x HF Buffer and 1.25 U DNA polymerase in NF water. NTC reactions were performed for each target gene and primer sequences are listed in table 2.2. Reactions were performed on a Veriti™ Thermal Cycler (Thermo Fisher Scientific) using the following cycling parameters: 98°C for 30 seconds; 35 cycles of 98°C for 10 seconds, 55°C for 30 seconds and 72°C for 30 seconds; and 72°C for 10 minutes. The PCR products were then visualised by agarose gel electrophoresis. A gel was cast containing 2 % (w/v) agarose in TAE buffer (40 mM Tris base, 20 mM acetic acid and 1 mM ethylenediamine tetraacetic acid (EDTA) pH 8.2) and 1:10,000 RedSafe™ (Intron Biotechnology) for DNA visualisation. The PCR products (10 µL) were mixed with 6x Gel Loading Dye (New England BioLabs), loaded into the gel, resolved by electrophoresis and visualised using a Gel Doc™ XR+ Imager (Bio-Rad).

Table 2.2 PCR primer sequences

Gene	**Forward/reverse primer sequences (*5' - 3'*)**	**Amplicon size**
Axl (mutation screening)	CGTACTCTTCACTCCTAGTT/ CTGAGTTGCTTTCCCTAACT	616bp
Tyro3 (mutation screening)	AACAGAATCCTGCCTCTTGC/ AGAAAGGGTGAGCTAGAAGC	560bp
Axl - 5' (cloning)	TGGTGAATTCAGGATGGGCAGGGTCCCGCT / CCTGGGCGCCAGGGCTCTAGGGGCACAGG A	1273bp
Axl - 3' (cloning)	GCCCTGGCGCCCAGGGCAAGGACAGCCAC T / GAAGCCGCGGTCAGGCTCCGTCCTCCTGCC	1424bp
Gas6 (cloning)	GCACGAATTCCACCATGCCGCCACCGCCCG GG/ GCTCCATATGGGGGGTGGCATGCTCCACAG	2046bp

Pros1 (cloning)	CATCGAATTCGCAATGAGGGTCCTGAGC/ GAGTCCGCGGATTCTTCTGGATCTTCCT	2045bp
mPlum (cloning)	GGCCACATGTTGAGCAAGGGCGAGGAGG/ GATCGCGGCCGCTCTAGGCGCCGGTGGAG T	700bp

2.1.2.3 Restriction enzyme digest

Restriction digests of DNA were routinely performed by digesting 1 µg of DNA with 10 units of restriction enzyme (New England BioLabs) in the supplied digestion buffer and in a total reaction volume of 50 µL. The reaction was incubated at the optimum temperature for 1 hour. The restriction enzyme was then inactivated by heat, where applicable, or the products were immediately resolved by agarose gel electrophoresis, as described in section 2.1.2.2, and gel purified using the UltraClean® 15 DNA Purification Kit (MO BIO Laboratories), according to the manufacturer's instructions.

2.1.2.4 Ligation

Ligations were routinely carried out in a total volume of 10 µL, containing insert and vector DNA at an insert:vector molar ratio of 3:1, 1x T4 DNA Ligase Reaction Buffer and 1 µL (400 U) of T4 DNA ligase (New England BioLabs). The ligation reaction mix was incubated at 4°C overnight. A negative control reaction containing no insert was also performed to assess the levels of vector re-ligation.

2.1.2.5 Preparation of chemically competent *E. coli* JM109 cells

Frozen *Escherichia coli* JM109 cells were streaked onto a LB agar plate, made using Difco LB Broth Lennox and Bacto™ Agar (BD Biosciences), and incubated at 37°C overnight. A single colony was inoculated into 2 mL of LB (Luria-Bertani) broth and grown in a 37°C shaking incubator overnight. This starter culture was used to inoculate 40 mL of LB broth and was grown in a 37°C shaking incubator until the culture reached OD_{600} = 0.6. The bacteria were incubated on ice for 15 minutes, then pelleted at 4,000 x g and 4°C for 5 minutes. The cell pellet was then resuspended in 40 mL of ice-cold TfbI buffer[242] (KOAc 30mM, KCl 100mM, $CaCl_2 2H_20$ 10mM, $MnCl_2 4H_20$, Glycerol 15%, pH 5.8), incubated on ice for 5 minutes and pelleted again. The bacteria were resuspended in 4 mL of ice-cold TfbII

buffer[242] (MOPS 10mM, $CaCl_2 2H_20$ 75 mM, KCl 10mM, Glycerol 15%, pH 6.5) and incubated on ice for 15 minutes. Aliquots were frozen and stored at -80°C until required.

2.1.2.6 Transformation of competent cells

A 100 µL frozen aliquot of chemically competent *E. coli* JM109 cells per ligation was thawed on ice for 5 minutes. The ligation reaction was added to a 100 µL aliquot of bacterial cells, mixed gently and incubated on ice for 30 minutes. The cells were then heat-shocked at 42°C for 90 seconds and placed back on ice for 5 minutes. Following this, 200 µL of LB broth was added to the cells and incubated for 30 minutes in a 37°C shaking incubator. The cells were then spread onto a LB agar plate containing 100 µg/mL ampicillin (Sigma-Aldrich) and incubated at 37°C overnight. Transformed colonies were picked and used to inoculate LB broth for subsequent plasmid purification.

2.1.2.7 Purification of plasmid DNA from bacteria

For small scale plasmid DNA extractions from bacteria, buffers P1, P2 and P3 (QIAGEN) were used to perform alkaline lysis-based mini-preps. Transformed colonies (section 2.1.2.6) were inoculated into 2 mL LB media and incubated overnight at 37°C in a shaking incubator. 1.5 mL bacteria was then centrifuged for 1 minute at 17,000 x g. The media was discarded and the bacterial pellet resuspended in 300 µl buffer P1. 300 µl buffer P2 was added and samples were incubated for 5 minutes at room temperature. 300 µl ice-cold buffer P3 was then added to each sample followed by a 5 minute incubation on ice. Samples were centrifuged for 10 minutes at 17,000 x g, 4°C and clear supernatant containing plasmid DNA was transferred to a fresh tube containing 700 µl isopropanol and samples were incubated for 10 minutes on ice. Samples were centrifuged at 17,000 x g for 10 minutes at 4°C, and supernatant was discarded. The plasmid DNA pellet was then washed with 70% (v/v) ethanol and resuspended in NF water. For medium scale plasmid DNA extractions from bacteria, the PureLink™ HiPure Plasmid Filter Midiprep Kit (Invitrogen) and PureLink™ HiPure Precipitator Modules (Invitrogen) were used to perform midi-preps, according to the manufacturer's instructions.

2.1.2.8 Sanger sequencing

Plasmids/linear DNA fragments, PCR products and appropriate primers were provided to the Australian Genome Research Facility (AGRF), which undertook the Sanger sequencing reactions and generated sequencing chromatograms. Analysis of the sequencing data was performed using the publicly available A plasmid Editor software (https://jorgensen.biology.utah.edu/wayned/ape/).

2.1.2.9 Generation of expression vectors

Axl and *Tyro3* sgRNA expression vectors

The MIT CRISPR design tool (http://crispr.mit.edu) was used to select Axl and Tyro3 single guide RNAs (sgRNAs). Two sgRNAs targeting exon 1 of *Axl* were designed and one sgRNA for exon 2 of Tyro3 was designed (Table 2.3). The top and bottom strands of sgRNA oligonucleotides were phosphorylated and reannealed in a mixture with a total volume of 10 µL containing 100 µM of each top and bottom sgRNA oligonucleotide, 1x T4 DNA Ligase Reaction Buffer and 1 µL (400 U) of T4 Polynucleotide Kinase (PNK; New England BioLabs). The reaction was performed in a Veriti™ Thermal Cycler (Thermo Fisher Scientific) using the following cycling parameters: 37°C for 30 minutes; 95°C for 5 minutes; ramp down to 25°C at 5°C per minute. Oligonucleotide duplexes with *BbsI* overhangs were diluted 1:200 in NF water and then ligated into the *BbsI* digested px458.SFFV.cer2 vector, a derivative of pSpCas9(BB)-2A-GFP[243]. Ligations were performed as described in section 2.1.2.4.

Table 2.3 Axl and Tyro3 sgRNA sequences

Gene	**Forward/reverse primer sequences (*5' - 3'*), sgRNA underlined**
Axl sgRNA #1	CACCGGTGGTTGGCGCTGTGCTGC/ AAACGCAGCACAGCGCCAACCACC
Axl sgRNA #2	CACCCTGGGGGTGTGCAGCCCATA/ AAACTATGGGCTGCACACCCCCAG
Tyro3 sgRNA	CACCTGGACACCTGGCTTGCATTC/ AAACGAATGCAAGCCAGGTGTCCA

HA-tagged *Gas6* pRufiG2 expression vector

The murine *Gas6* coding sequence was amplified from a 1:1 mixture of OP9 cell line-derived and MC3T3-E1 cell line-derived cDNA by PCR (Table 2.2) such that the product contained the *Gas6* open reading frame with the start codon forming part of an *EcoRI* site and the stop codon being replaced by an *NdeI* site. The *EcoRI* and *NdeI* flanked *Gas6* insert and the HA-tag-containing pRufiG2 retroviral vector[244] were then *EcoRI* and *NdeI* digested and ligated to generate the pRufiG2.Gas6-HA vector, which encodes *Gas6* with an in-frame C-terminal HA tag.

HA-tagged *Pros1* pRufiG2 expression vector

The murine *Pros1* coding sequence was amplified from a 1:1 mixture of OP9 cell line-derived and MC3T3-E1 cell line-derived cDNA by PCR (Table 2.2) such that the product contained the *Pros1* open reading frame with the start codon forming part of an *EcoRI* site and the stop codon being replaced by a *SacII* site. The *EcoRI* and *SacII* flanked *Pros1* insert and the HA-tag-containing pRufiG2 vector were then *EcoRI* and *SacII* digested and ligated to generate the pRufiG2.Pros1-HA vector, which encodes *Pros1* with an in-frame C-terminal HA tag.

Axl pRufimCh2 overexpression vector

The murine *Axl* coding sequence was amplified from 5TGM1 cell line-derived cDNA by PCR (Table 2.2) in two 5' and 3' segments overlapping at a natural *KasI* restriction site. The 5' product contained the *Axl* open reading frame with the start codon forming part of an *EcoRI* site and ending at the *KasI* restriction site. The 3' product contained the *Axl* open reading frame starting at the *KasI* restriction site and ending with a *SacII* site replacing the stop codon. The 5' segment of *Axl* was blunt ligated into the pGEM-T vector (Promega) according to manufacturer instructions. The 5' *Axl* containing pGEM-T vector and the 3' *Axl* segment were *KasI* and *SacII* digested and ligated to generate a pGEM-T vector encoding full length *Axl*. The *EcoRI* and *SacII* flanked full length *Axl* encoded in the pGEM-T vector and the pRufimCh2 vector were then *EcoRI* and *SacII* digested and ligated to generate the pRufimCh2.Axl vector.

Mer pRufimCh2 overexpression vector

A pRufimCh2.Mer vector previously generated by Dr. Duncan Hewett was provided for this study.

Gas6 pRufimPlum overexpression vector

GFP was removed from the pRufiG2.Gas6 vector by digestion with *NcoI* and *NotI* followed by gel purification of the vector away from the GFP insert using the PureLink™ Gel Extraction Kit (Invitrogen). mPlum was amplified using PCR (Table 2.2) from the FgH1tUTP vector (Addgene; #70183) such that the product contained the *mPlum* open reading frame with the start codon forming part of a *PciI* site and a natural *NotI* site following the stop codon. *PciI* and *NotI* digested *mPlum,* and *NcoI* and *NotI* digested pRufi.Gas6 were ligated to generate the pRufimPlum.Gas6 vector.

2.1.3 Protein Techniques

2.1.3.1 Western blotting

An appropriate amount of protein lysate was mixed with reducing buffer (50 mM Tris-HCl pH 7.4, 10% glycerol (v/v), 2% sodium dodecyl sulphate (SDS) (w/v), 0.02% bromophenol blue (w/v) and 5% β-mercaptoethanol (v/v)) and denatured by boiling for 4 minutes. Proteins were loaded into 10% SDS-polyacrylamide gel electrophoresis (PAGE) gels in Tris-Glycine-SDS running buffer (0.3% (w/v) Tris-HCl, 1.44% (w/v) glycine and 0.1% (w/v) SDS, pH 8.3). To resolve the proteins, gel electrophoresis was performed using the Mini-PROTEAN™ III System (Bio-Rad). Proteins were transferred from the gel to a nitrocellulose 0.45 µm membrane (Bio-Rad) using the Mini Trans-Blot® Electrophoretic Transfer Cell (Bio-Rad). The transfer was performed in transfer buffer (10% (v/v) Tris-Glycine Buffer (Biorad), 20% methanol (v/v) and 0.02% (w/v) SDS, pH 8.3) at 100 V and 4°C for 1 hour. Following the transfer, the membrane was incubated with membrane blocking buffer (5% (w/v) skim milk powder in 1x TBST buffer (50 mM Tris-HCl pH 7.5, 150 mM NaCl and 0.1% TWEEN 20) at room temperature for 1 hour. The blocked membrane was then probed with primary antibody (Table 2.4) at an optimised concentration in membrane blocking buffer with rocking and at 4°C overnight. For blots expected to have low signal intensity, the primary antibody was diluted in Solution 1 from the SignalBoost™ Immunoreaction Enhancer Kit (Merck). Following 4 washes in TBST, the blot was incubated with an appropriate DyLight-680/800-conjugated secondary antibody (Thermo Fisher Scientific) diluted 1:10,000 in TBST, or Solution 2 from the enhancer kit, with rocking and at room temperature in the dark for 1 hour. The blot

was again washed 4 times in TBST and then imaged using the Odyssey® CLx Imager (LI-COR).

Table 2.4 Primary antibodies used for western blotting

Target	Source	Concentration	Company	Catalogue no.
HA-tag	Monoclonal mouse	1:1,000	Merk Millipore	05-904
Tyro3	Monoclonal rabbit	1:500	Cell Signalling Technology	D38C6
β-Actin	Monoclonal mouse	1:2,500	Sigma-Aldrich	A1978

2.1.3.2 Immunoprecipitation

Conditioned media from NIH3T3 cells overexpressing HA-Gas6 or HA-Pros1 was collected as described in section 2.2.2. 10 mL of conditioned media was pre-cleared by adding 50 µL Protein G Sepharose™ 50% slurry (GE Healthcare) in PBS and incubated under rotation and at 4°C for 2 hours before being transferred to a new tube. 10 µL HA-tag antibody (Table 2.4) was added and the conditioned media was incubated under rotation overnight at 4°C. The antibody/antigen complex was then captured by adding 50 µL Protein G Sepharose™ 50% slurry in PBS and incubated under rotation for 2 hours at 4°C. The Sepharose was pelleted by centrifugation at 1000 x g for 2 minutes at 4°C, the depleted media was discarded and the pellet was washed twice in ice cold Hanks Buffered Salt Solution (HBSS; Sigma) 40 µL of 2x reducing buffer (section 2.1.3.1) was added and the mixture was denatured at 100°C for 3 minutes. The Sepharose was pelleted by centrifugation at 200 x g for 1 minute at 4°C and the eluates were resolved in a SDS-Page gel and subjected to western blotting using an anti-HA-tag primary antibody as described in section 2.1.3.1.

2.1.3.3 Enzyme linked immunosorbent assay (ELISA)

ELISAs to assess Gas6 secretion in NIH3T3 HA-Gas6 conditioned media and mouse serum were performed using a Mouse Gas6 ELISA Kit (Abcam; ab155447) according to manufacturer's instructions. Conditioned media was added to the ELISA plate undiluted. Mouse serum was collected as described in section 2.3.3 and was diluted 1:100 prior to use.

2.2 Cell culture techniques

2.2.1 Maintenance of cells in culture

All cell lines were maintained in a humidified environment at 37°C in the presence of 5% CO_2 and were manipulated within a class II biological safety cabinet. Unless otherwise specified, all cell culture reagents were sourced from Sigma-Aldrich and all media were supplemented with 2 mM L-glutamine, 100 U/mL penicillin, 100 µg/mL streptomycin, 1 mM sodium pyruvate, and 10 mM HEPES buffer. All cell lines were tested for mycoplasma infection using a MycoAlert™ Mycoplasma Detection Kit (Lonza) prior to use and were maintained in culture for a maximum of 3.5 weeks.

2.2.1.1 Mouse myeloma 5TGM1 cell line

The murine MM 5TGM1 PC line was originally kindly provided by Assoc Prof Claire Edwards (University of Oxford, UK). 5TGM1 cells expressing both GFP and luciferase were previously generated using the retroviral expression vector NES-TGL[245]. To generate a basal 5TGM1 cell line with enhanced BM tropism, 5TGM1 cells were previously injected i.v. into C57BL/KaLwRij (KaLwRij) mice (section 2.3.1.1) and those present 4 weeks later in the long bones of the hind limbs were purified by flow cytometry and expanded. 5TGM1 cells were maintained in Iscove's Modified Dulbecco's Medium (IMDM) with 20% fetal bovine serum (FBS, Thermo Fisher Scientific), which is termed complete IMDM. The cells were sub-cultured every 2-3 days to maintain a concentration of 0.2-2 x 10^6 cells/mL.

2.2.1.2 Mouse adherent cell lines

The mouse BM stromal cell (BMSC) line OP9 and the mouse fibroblastic cell line NIH3T3 were maintained in Dulbecco's Modified Eagle Medium (DMEM) with 10% FBS (complete DMEM). The pre-osteoblastic cell line MC3T3-E1 was maintained in Roswell Park Memorial Institute 1640 (RPMI) medium with 10% FBS. Medium was renewed every 2-3 days and confluent monolayers were split at a sub-cultivation ratio of 1:5. Briefly, cells were harvested by rinsing with sterile HBSS followed by addition of 0.05% (v/v) trypsin-EDTA. Cells were incubated at 37°C for 1-5 minutes, depending on the time taken to detach from the culture flask. Trypsin activity was then neutralised by the addition of FBS-containing medium and detached cells were

pelleted at 400 x g for 5 minutes. The cell pellet was resuspended in fresh complete DMEM and an appropriate aliquot of the cell suspension was added to a new culture flask.

2.2.1.3 Human embryonic kidney HEK293T cell line

HEK293T cells were cultured in complete DMEM and cells were sub-cultured every 2-3 days by trypsinisation, as described in section 2.2.1.2.

2.2.1.4 Co-culture of 5TGM1 cells with MC3T3-E1 cells

MC3T3-E1 cells were seeded into complete IMDM as described in section 2.2.1.2 and allowed to adhere to the flask. 5TGM1 cells were seeded onto the sub confluent MC3T3-E1 monolayer at a density of 2 x 10^5 cells/mL. Every 2 days 5TGM1 cells were harvested and placed onto a fresh subconfluent monolayer of MC3T3-E1 cells by repeated washing with complete IMDM and vigorous agitation of the flask until <5% of 5TGM1 cells remained adhered to the MC3T3-E1 monolayer by visual inspection under a microscope.

2.2.2 Generating NIH3T3 and MC3T3-E1 conditioned medium

NIH3T3 HA-EV, NIH3T3 HA-Gas6 or NIH3T3 HA-Pros1 cell lines were cultured in complete IMDM with the addition of 10 µM Vitamin K2 (V9378; Sigma Aldrich) and 1 mM Calcium Chloride (Merck) for 72 hours. When conditioned media was to be used in WST-1 assays (section 2.2.5.2) cells were cultured in phenol-red free IMDM. Media was collected and passed through a 0.22 µm filter before being aliquoted and stored at -80°C or used immediately. MC3T3-E1 cells were cultured in complete IMDM for 48 hours, and media was collected and passed through a 0.22 µm filter before being used immediately.

2.2.3 Generating apoptotic cells

Apoptotic cells were generated by resuspension of GFP negative parental 5TGM1 cells at a density of 1x10^6 cells/mL in serum free IMDM containing 20% DMSO followed by a 2 hour incubation at room temperature. Cells were centrifuged at

400 x g for 5 minutes and the cell pellet was washed once in serum free IMDM before being centrifuged again and resuspended in serum free IMDM. Cells were then stained for Annexin V as described in section (2.2.5.5).

2.2.4 Generating genetically modified cell lines

2.2.4.1 Generation of Axl and Tyro3 knockout 5TGM1 cell lines using CRISPR-Cas9

5TGM1 cells were seeded in 6-well plates at a density of 2 x 10^5 cells/mL in 4 mL complete IMDM. 4 µg of Axl- or Tyro3-sgRNA containing px458.SFFV.cer2, 100 µL IMDM and 20 µL Polyfect™ Transfection Reagent (QIAGEN) were mixed gently and incubated at room temperature for 10 minutes, followed by the addition of 600 µL IMDM. The mixture was added dropwise to 5TGM1 cells before the cells were incubated at 37°C with 5% CO_2 for 48 hours and then washed with complete IMDM. Successfully transduced GFP^+Cer^+ cells were isolated by FACS on a FACSAria™ Fusion (BD Biosciences) and single cells were deposited into 96-well plates. Clonal cell lines were propagated as described in section 2.2.1.1.

2.2.4.2 Generation of NIH3T3 cells overexpressing Gas6 or Pros1

HEK293T cells (2 x 10^6 cells/transfection) were seeded into 6 cm culture dishes in complete DMEM 24 hours prior to transfection. The cells were then transfected with 5 µg of either Gas6- or Pros1- encoding pRufiG2 vector or the empty vector and 5 µg each of the murine packaging plasmids pGP (Takata Bio Inc.) and pCMV-ECO-ENV[246] using Lipofectamine 3000 (Invitrogen), according to the manufacturer's instructions. After 48 hours, medium containing retrovirus was collected from the transfected HEK293T cells and filtered through a 0.45 µm surfactant-free cellulose acetate membrane filter (Thermo Scientific). NIH3T3 cells were seeded into T75 flasks at 1 x 10^4 cells/cm^2 and allowed to adhere to the flask before virus-containing media was added and cells were incubated at 37°C with 5% CO_2 overnight. The cells were washed with complete DMEM and expanded in culture. Following another wash, the NIH3T3 cells underwent fluorescence activated cell sorting (FACS) for GFP protein expression, which indicated successful transduction with the pRufiG2 viruses, on a FACSAria™ Fusion (BD Biosciences). Subsequent sorts were

conducted, where appropriate, until a pooled cell line consisting of > 90% GFP^+ NIH3T3 cells was obtained.

2.2.4.3 Generation of Axl and Mer expressing 5TGM1 cell lines

Infectious viral particles for either Axl- or Mer- encoding pRufimCh2 or the empty vector were generated according to section 2.2.4.2. 5TGM1 TAM null cells were seeded at a density of $2x10^5$ cells/mL in 2.5 mL in complete IMDM containing polybrene (16 µg/mL; Sigma Aldrich) into in a 6-well plate, and 2.5 mL virus-containing media was added dropwise. The 5TGM1 TAM null cell-virus mixtures were centrifuged in the 6-well plate at 1,000 x g at room temperature for 1 hour and then incubated at 37°C with 5% CO_2 overnight. The cells were washed with complete IMDM and expanded in culture. The 5TGM1 TAM null cells were sorted for GFP and mCherry expression as described in section 2.2.4.2.

2.2.4.4 Generation of differential Mer and Gas6 expressing 5TGM1 cell lines

Infectious viral particles for either Gas6 encoding pRufimPlum or the empty vector were generated according to section 2.2.4.2. Transfection of 5TGM1 Mer only or 5TGM1 EV cells with the pRufimPlum retroviruses was conducted as described in section 2.2.4.3. The modified 5TGM1 TAM null cells were sorted for GFP, mCherry and mPlum expression as described in section 2.2.4.2.

2.2.5 *In vitro* assays

2.2.5.1 Luciferase assay

Basal bioluminescence of cell lines was quantitated by assessing the luciferase activity of clonal 5TGM1 Axl-, Tyro3- or double- knock out cell lines. 100 µL of 5TGM1 cells were seeded at $5x10^7$ cells/mL in triplicate in complete IMDM in opaque black walled clear bottomed 96-well plates. Firefly D-Luciferin substrate (30 mg/mL in PBS, Biosynth) was diluted 1:100 in complete IMDM, and 100 µL per well was added 20 minutes prior to imaging the plates using the IVIS® Spectrum In Vivo Imaging System and Living Image® Software v4.5.5 (PerkinElmer). The background total flux (photons per second) of media only wells were subtracted from that of the wells containing 5TGM1 cells.

2.2.5.2 WST-1 proliferation assay

5TGM1 cell lines were plated at 1 x 10^5 cells/mL in triplicate in 100 µL of complete phenol-red free IMDM supplemented with 10mM Vitamin K and 1mM calcium, or 50% NIH3T3 ligand enriched conditioned IMDM (section 2.2.2) in 96-well plates and incubated at 37°C with 5% CO_2. Every 24 hours from 0 to 72 hours, 10 µL of WST-1 Reagent (Roche) was added to all the relevant wells of one plate, which was then returned to the incubator for 2 hours. Following the incubation, the absorbance of each well at 450 nm was measured using the iMark™ Microplate Absorbance Reader (Bio-Rad) and the plate discarded. The background was subtracted from the absorbance values and the fold-change in absorbance was calculated relative to day 0.

2.2.5.3 Migration assay

Transwell and migration assays were performed in 24-well plates with 8 µm pore transwells (Corning). For transwell assays, 5 x 10^5 5TGM1 cells in 1% FBS IMDM were seeded into the upper chamber of transwells in triplicate. The cells were allowed to migrate towards the lower chamber containing 20% IMDM only or 20% IMDM with the addition of 100 ng/mL recombinant mouse Gas6 (R&D Systems,8310-GS) or 100 ng/mL recombinant mouse Pros1 (R&D Systems, 9740-PS) for 24 hours. The contents of the bottom chamber were then transferred to FACS tubes and CountBright™ Absolute Counting Beads (ThermoFisher) were added. GFP+ events per 1000 bead events were measured for each sample on a BD FACS Symphony™ flow cytometer using FACSDiva™ software v8.0 (BD Biosciences), and absolute GFP+ cell number per well were calculated according to manufacturer's instructions.

2.2.5.4 5TGM1 single colour immunofluorescence staining and flow cytometry

5TGM1 cells were harvested from culture, washed and resuspended in ice-cold PFE buffer. 5TGM1 cells at 1 x 10^7 cells/mL were incubated with flow cytometry (FC) blocking buffer (1:100 mouse gamma globulin (Jackson ImmunoResearch) in PFE buffer) on ice for 30 minutes. Aliquots of 1 x 10^6 cells in 0.1 mL of FC blocking buffer were then incubated with the appropriate amount of primary antibody (Table 2.5) on ice for 30 minutes. Cells were washed twice with 2 mL of chilled PFE buffer and

then resuspended in 0.1 mL of 1:100 biotinylated rabbit anti-rat IgG (#BA-4001, Vector Laboratories) in PFE buffer. Following a 30 minute incubation cells were washed twice more with 2 mL of chilled PFE buffer and then resuspended in 0.1 mL of 1:100 Streptavidin-BV421 secondary antibody (#563259, BD Biosciences) in PFE buffer. Following a 15 minute incubation on ice and in the dark, cells were washed twice with 2 mL of chilled PFE and then resuspended in 0.2mL PFE. The percentage of BV421+ GFP+ cells were assessed for a minimum of 50,000 cells per sample on a BD FACS Symphony™ flow cytometer using FACSDiva™ software v8.0 (BD Biosciences) and the data was analysed using FlowJo v10.0.8 software (FlowJo, LLC).

Table 2.5 Primary antibodies used for 5TGM1 cell immunostaining

Target	Source	Conjugate	Concentration	Company	Cat no.
Axl	Monoclonal rat	Unconjugated	1:20	R&D Systems	MAB8541
Mer	Monoclonal rat	Unconjugated	1:20	R&D Systems	MAB5912
PD-L1	Monoclonal rat	Unconjugated	1:100	Biolegend	124301
Isotype control	Rat IgG2a (kappa)	Unconjugated	1:20	Thermo Fisher Scientific	13472485
Isotype control	Rat IgG2b	Unconjugated	1:20	Biolegend	400602

2.2.5.5 Annexin V and 7-AAD viability staining

5TGM1 cells were centrifuged at 400 x g for 5 minutes and resuspended in 200 µL Annexin V binding buffer (HBSS, 1% HEPES, 5mM $CaCl_2$ buffer). Annexin V-PE (BD Pharminogen) and 7-AAD Viability Dye (Beckman Coulter) both diluted 1:10 in Annexin V binding buffer were added to cells in suspension. Cells were incubated for 20 minutes on ice in the dark before being centrifuged and resuspended in 0.2 mL binding buffer. Unstained, single stained and double stained controls were prepared for gating cell populations. Cells were analysed on an LSRFortessa™ II flow cytometer using FACSDiva™ software v8.0 (BD Biosciences) and the data was analysed using FlowJo v10.0.8 software (FlowJo, LLC).

2.2.5.6 DiD labelling assay

5TGM1 cells were harvested from culture and resuspended at $1x10^6$ cells/mL in PBS. 5 µl Vybrant™ DiD Cell-Labeling Solution (Molecular Probes) per 1 mL of cell suspension was added and cells were incubated at 37°C with 5% CO_2 for 20 minutes. 5TGM1 cells were then washed in PBS and cultured as described in section 2.2.1.1. 5TGM1 cells were assessed for GFP+ DiDhi cell populations at day 0 and day 10 on a BD FACS Symphony™ flow cytometer using FACSDiva™ software v8.0 (BD Biosciences). For MC3T3-E1 co-culture assays, DiD labelled 5TGM1 cells were seeded at $2x10^5$ cells/mL onto a subconfluent monolayer of MC3T3-E1 cells. At day 0 and day 7 non-adherent 5TGM1 cells were removed by washing twice with IMDM and agitation, and GFP+ DiDhi cells were assessed. For assays using MC3T3-E1 conditioned media, media was collected as described in section 2.2.2. DiD-labelled 5TGM1 cells were then seeded at $2x10^5$ cells/mL into 50% conditioned media, and GFP+ DiDhi cells were assessed at day 0 and day 7.

2.2.5.7 Cell cycle analysis

5TGM1 cells were cultured overnight in normal media, or NIH3T3 conditioned media collected as described in section 2.2.2. 5TGM1 cells were harvested from culture and resuspended at $1x10^6$ cells/mL in complete IMDM. Hoescht and Pyronin Y double staining was used to identify cell cycle phases G0, G1, S, and G2/M by cellular DNA and RNA content.[247] Hoescht 33342 (Sigma) was added to a final concentration of 10 µg/mL and samples were incubated at 37°C for 45 minutes in the dark. Pyronin Y (Sigma) was then added directly to cells at a final concentration of 2µg/mL and samples were incubated at 37°C for 45 minutes in the dark. 5TGM1 cells were then washed with ice cold PFE and resuspended in 0.3 mL PFE. The proportion of cells in cell cycle phases G0, G1, G2 and M were then assessed according to cellular DNA and RNA content on a BD FACS Symphony™ flow cytometer using FACSDiva™ software v8.0 (BD Biosciences) and the data was analysed using FlowJo v10.0.8 software (FlowJo, LLC).

2.3 Animal techniques

2.3.1 *In vivo* models of MM tumour growth

C57BL/KaLwRij.Hsd ("KaLwRij") mice, originally kindly provided by Prof Andrew Spencer (Monash University, Australia) were rederived, bred and housed at the SAHMRI Bioresources Facility. NOD.CgPrkdc^{scid}Il2rg^{tm1Wjl}/SzJ ("NSG") mice were purchased from the SAHMRI Bioresources Facility. All procedures were performed with the approval of the SAHMRI Animal Ethics Committee. In all studies, the mice in different experimental groups were age- and sex-matched as far as was possible.

2.3.1.1 5TGM1 cells in KaLwRij and NSG mice intravenous and intratibial models

For intravenous (i.v.) delivery, 5TGM1 cells were washed and resuspended in sterile PBS at a concentration of 5 x 10^6 cells/mL. KaLwRij or NSG mice between 6 and 8 weeks old were injected with 0.1 mL of 5TGM1 cell suspension (5 × 10^5 cells) via the tail vein. The mice underwent *in vivo* bioluminescence imaging (BLI, section 2.3.2) 2, 3 and 4 weeks post-tumour cell injection and were humanely euthanised after 4 weeks. For intratibial (i.t.) delivery, 5TGM1 cells were washed and resuspended in sterile PBS at a concentration of 1 x 10^7 cells/mL. KaLwRij or NSG mice between 5 and 6 weeks old were anaesthetised by isoflurane inhalation for the duration of the procedure. A gas-sterilised 25 µL Hamilton syringe with a 27-gauge needle and containing 10 µL of cell suspension was inserted through the cortex of the anterior tuberosity of the left tibia. Once the bone cortex was traversed, the needle was inserted 3 to 5 mm down the diaphysis of the tibia, and the cell suspension (1 x 10^5 cells per inoculum) was injected into the marrow space. The injected mice underwent weekly *in vivo* BLI 1, 2 and 3 weeks after tumour cell injection and were humanely euthanised after 3.5 weeks. Mice with extensive extramedullary tumour growth in the injected leg, which indicated that the injection was misdirected, were excluded from the experimental analysis.

2.3.1.2 5TGM1 24 hour BM homing assay in KaLwRij mice

5TGM1 cells (5 x 10^6 in 0.1 mL of PBS) were injected i.v. into 6-8-week-old KaLwRij mice via the tail vein. After 24 hours the mice were humanely euthanised and GFP+ tumour cells were analysed by flow cytometry as described in section 2.3.4.

2.3.2 *In vivo* bioluminescence imaging

Mice injected with luciferase-expressing 5TGM1 cells were shaved under anaesthesia prior to *in vivo* BLI. To measure tumour burden, the mice were administered firefly D-Luciferin substrate (30 mg/mL in PBS, Biosynth) by intraperitoneal (i.p.) injection at a concentration of 150 mg/kg. After 10 minutes, during which time the mice were anaesthetised by isoflurane inhalation, the dorsal and ventral aspects of the mice were scanned using the IVIS® Spectrum In Vivo Imaging System and Living Image® Software v4.5.5 (PerkinElmer), which was also used to quantitate the bioluminescence signal in the mice.

2.3.3 Serum Paraprotein Electrophoresis (SPEP)

At the experimental endpoint, peripheral blood was collected from the 5TGM1-injected mice via tail vein bleed. The blood was allowed to clot at room temperature and then centrifuged at 2,000 x g and 4°C for 10 minutes. The serum supernatant was collected and stored at -20°C. Subsequently, the serum samples were thawed and the levels of M protein/paraprotein were assessed by performing serum protein electrophoresis (SPEP) using the Hydragel Protein(E) Kit (Sebia), according to the manufacturer's instructions. The stained SPEP gels were imaged on a Gel Doc™ XR+ Imager (Bio-Rad), and the intensity of the paraprotein band/M-spike was quantitated and normalised to the albumin band using Image Lab Software v6.0.1 (Bio-Rad).

2.3.4 Detection of GFP$^+$ tumour cells in mouse bone marrow by flow cytometry

At the experimental endpoint, mice were humanely euthanised and both femora and tibiae from each mouse were collected and cleaned. For i.t. injected mice only the tibia from the injected leg was used, and was kept separate from the femur and tibia of the non-injected leg. These bones were crushed in PFE buffer and the marrow was collected. All the cells were then filtered through a 70 µm cell strainer, pelleted (400 x g, 5 minutes) and resuspended in PFE buffer. Cells from a tumour naïve mouse were also analysed to act as a negative control for gating cell populations. The samples were immediately analysed for the presence of GFP$^+$ tumour cells by

flow cytometry on a LSRFortessa™ II (BD Biosciences) using FACSDiva™ software v8.0 (BD Biosciences), and a minimum of 1 million events were collected per sample. Bone marrow cells were subjected to red blood cell lysis (section 2.3.5) if they were to be analysed for mCherry expression or undergo immunofluorescence staining (section 2.2.5.4).

2.3.5 Red blood cell lysis

Mouse bone marrow cells in single cell suspension were centrifuged at 500 x g for 5 minutes and resuspended in 1 mL PFE. 7.5 mL red blood cell lysis buffer (308.8 mM ammonium chloride, 20 mM potassium bicarbonate, 2.2 mM disodium EDTA, pH 7.2) was added, mixed by inversion and incubated at room temperature for 10 minutes. Cells were then centrifuged at 500 x g for 5 minutes, washed in PFE, repelleted and then resuspended in 1mL PFE and stored on ice.

2.3.6 *In vivo* EdU incorporation assay

Mice were intravenously inoculated with 5TGM1 cells and allowed to develop tumours over 4 weeks. At this timepoint mice were i.p. injected with 50 mg/kg EdU (Invitrogen) in 0.1 mL PBS and 24 hours later were humanely euthanised. Mouse bone marrow cells were then harvested from the hind limbs as described in section (2.3.1.5). A ‘click’ chemistry reaction was performed to conjugate EdU to Alexa Fluor™ 350 using the Click-iT™ Plus EdU Flow Cytometry Kit (Invitrogen; C10645) according to manufacturer’s instructions. The percentage of EdU+ GFP+ cells were assessed for a minimum of 1 million events per sample on a LSRFortessa™ II flow cytometer using FACSDiva™ software v8.0 (BD Biosciences) and the data was analysed using FlowJo v10.0.8 software (FlowJo, LLC).

2.4 In silico analyses, scRNAseq analyses and statistics

2.4.1 Analysis of COMMPass dataset

RNA-sequencing data was obtained from the Multiple Myeloma Research Foundation (MMRF) CoMMpass (MMRF-COMMPASS) dataset, accessed via the NIH NCI GDC Data Portal (9 August 2019). Gene expression data (FPKM) for

CD138-selected BM PC was included from all MM patients (*n*=764) who had RNA-sequencing performed from a sample taken at diagnosis. Gene expression data was presented as fragments per kilobase of exon per million mapped reads (FPKM). Data analysis was performed by Dr. Kate Vandyke.

2.4.2 Statistics

Unless otherwise described, statistical analysis was performed using GraphPad Prism v9 (GraphPad Software). When two groups were being compared for a single variable, a parametric paired or unpaired t test were used. When three or more groups were being compared for a single variable, a parametric one-way ANOVA with Tukey's post-hoc multiple comparisons test was used. For time-course experiments, groups were compared using a two-way ANOVA with Sidak's or Tukey's multiple comparisons test. When two categorical variables were being compared, a Fisher's exact test was used. Differences were statistically significant when $P < 0.05$.

3. Generation of single TAM receptor expressing 5TGM1 murine multiple myeloma cell lines

3.1 Introduction

Multiple myeloma is the second most common haematological malignancy, with ~2000 patients diagnosed per year in Australia[6]. Myeloma progression is dependent on malignant plasma cell proliferation[166], migration to distal sites[248], escape from immune surveillance[249], and the ability to enter a reversible dormant state[129]. These processes are often driven by cell surface receptor signalling between MM PCs and other cells within the BM microenvironment such as stromal cells, osteoblasts, macrophages and immune cells[250]. Investigating the biological function and role of MM PC surface receptors in MM disease pathogenesis may identify novel therapeutic targets to limit MM disease progression. The study described herein, utilised CRISPR-Cas9 to genetically engineer 5TGM1 murine myeloma cell lines to uniquely express the TAM tyrosine kinase cell surface receptors, Axl and Mer.

The TAM receptor family of tyrosine kinase receptors, Tyro3, Axl and Mer, are expressed by cancer cells in prostate cancer[185, 207], breast cancer[215], and blood cancers including MM[166, 186, 188]. The TAM receptors have multiple known ligands, including growth arrest specific-6 (Gas6), Protein S (Pros1)[158], Tubby-like protein and Galectin-3[161, 162]. As Gas6 and Pros1 are both secreted by osteoblasts, an important component of the MM niche[163, 164], and are both implicated in cancer pathogenesis[165, 166, 191], they were used to stimulate TAM receptor signalling in this study. Gas6 and Pros1 are structurally homologous proteins that bind phosphatidylserine on the external membrane of apoptotic cells[169]. The Gla domains of Gas6 and Pros1 are post-translationally γ-carboxylated in a vitamin K-dependent reaction, which enables them to bind phosphatidylserine and subsequently bind and activate TAM receptors. Despite sharing common ligands, Tyro3, Axl and Mer are functionally distinct and play diverse, context-dependent roles in many different cancers.

Previous studies have shown that Axl expression is associated with MM PC dormancy[129, 213], while Mer expression has been shown to promote MM PC proliferation[166, 188]. Axl was shown to be one of the genes most highly expressed by dormant murine 5TGM1 cells in previous studies[129, 213]. Blockade of Axl using a small molecule inhibitor ‘released’ 5TGM1 cells from dormancy *in vivo*, resulting in increased tumour burden. Axl expression has also been shown to initiate, but not

maintain, prostate cancer cell dormancy[185]. One study suggested that a molecular switch between dominant Axl and Tyro3 expression regulates prostate cancer cell dormancy. When Axl is highly expressed, prostate cancer cells become dormant, but when Tyro3 is highly expressed, cells are reactivated[207]. Conversely, other studies have shown that knockdown or knockout of Axl decreases tumour burden *in vivo* in models of lung cancer[203] and breast cancer[187]. Although Mer expression in MM PCs promotes their proliferation[166, 188], recent studies attribute the tumourigenic effects of Mer expression in other cancers to immune suppression. These studies suggested a role for Mer in promoting an immune suppressive tumour microenvironment[187, 238], with some studies suggesting that Mer may regulate immune checkpoint signalling through the PD-1/PD-L1 axis[215, 251, 252]. A role for Tyro3 in myeloma has not been established, and due to negligible Tyro3 expression by MM PCs[166], the main focus of this study will be Axl and Mer. To further characterise their specific functions in myeloma, single TAM receptor expressing cell lines and a control TAM receptor null cell line were generated.

The 5TGM1/KaLwRij model of MM and *in vitro* assays were used to assess the function of Axl and Mer in myeloma pathogenesis. The GFP and firefly luciferase expressing-5TGM1 cell line, when intravenously inoculated into C57BL/KaLwRij mice, homes to the axial and appendicular skeleton and forms multiple tumours over the course of 4 weeks. Tumour burden can be monitored weekly by bioluminescence imaging and at the end point by enumeration of GFP+ cells in the bone marrow and assessment of 5TGM1-secreted serum paraprotein levels. As previous studies on Mer in myeloma were conducted using human myeloma cell lines[166], it was only possible to observe the effects of Mer on MM tumour burden in xenografts in immunodeficient mice. The advantage of the 5TGM1 cell line is that it can be inoculated into both the immune competent syngeneic KaLwRij mice as well as immune compromised NSG mice. Therefore, the generation of Mer positive and Mer negative 5TGM1 cell lines enabled, for the first time, the evaluation of the immune-mediated effects of Mer expression on tumour burden in myeloma. Previous studies[213] showed that Axl inhibition in the 5TGM1/KaLwRij model of MM, resulted in increased numbers of GFP+ 5TGM1 cells in the bone marrow at the experimental endpoint, and reduced numbers of dormant 5TGM1 cells. However, it should be noted that the Axl inhibitor would also target Axl expressed by cells in the

BM microenvironment, including macrophages[217] and osteoclasts[184]. Furthermore, the results observed in these studies[213], could be, in part, attributed to off target effects of the Axl inhibitor which could target multiple receptor tyrosine kinases including other TAM receptors[213]. Therefore, utilising a model of 5TGM1 Axl positive and Axl negative cell lines enabled us to identify whether Axl, expressed specifically by MM PCs, can initiate and maintain cellular dormancy *in vivo*.

In this chapter, the CRISPR-Cas9 system and retroviral mediated transduction were used to generate single TAM receptor expressing 5TGM1 murine myeloma cell lines. Parental 5TGM1 cells, which express both Axl and Tyro, were targeted with Axl and/or Tyro3 single guide RNAs (sgRNAs) to generate 5TGM1 Axl or Tyro3 clonal knockout cell lines and 5TGM1 TAM null cell lines. Sanger sequencing was used to identify homozygous or heterozygous putative frameshift mutations. Tyro3 protein expression and Axl cell surface expression in knockout cell lines were then assessed compared to the unaltered 5TGM1 cell line. Baseline proliferation and bioluminescence levels of 5TGM1 Tyro3 knockout, Axl knockout and TAM null cell lines compared to the unaltered 5TGM1 cell line were then examined. To provide a source of ligand for *in vitro* experiments, NIH3T3 cells expressing HA-tagged-Gas6 or Pros1 were generated. Proliferation of 5TGM1 Tyro3 knockout, Axl knockout and TAM null cell lines was assessed in response to ligand enriched NIH3T3 conditioned media. Multiple 5TGM1 Axl knockout, Tyro3 knockout and TAM null cell lines were then inoculated i.v. into the KaLwRij model of MM to determine whether independent clones with the same genetic knockout status produced a similar effect on MM disease development *in vivo*. Following this, a 5TGM1 Mer cell line and a 5TGM1 Axl cell line were generated by retroviral transduction of a candidate 5TGM1 TAM null cell line with Mer or Axl.

3.2 Results

3.2.1 Mer and Gas6 are expressed by MM patient PCs.

Previous studies showed that the MM PCs of the majority of myeloma patients express Mer and Gas6[166], whereas Axl is either not expressed, or expressed at low levels[213]. To confirm this in an independent analysis, TAM receptor and ligand expression in CD-138 selected BM PCs of newly diagnosed myeloma patients was

assessed in the publicly available CoMMpass RNA seq datasets (https://registry.opendata.aws/mmrf-commpass/). As shown in Figure 3.1, MM PCs from the majority of myeloma patients express Mer and Gas6, while only a subset of patients display Axl expression. Tyro3 and Pros1 showed little to no expression in MM PCs (Figure 3.1).

3.2.2 CRISPR-Cas9 mediated gene targeting and retroviral transduction were utilised to generate 5TGM1 single TAM receptor expressing cell lines.

The CRISPR-Cas9 system and retroviral transduction were utilised to generate 5TGM1 MM cell lines expressing a single TAM receptor. As the 5TGM1 cell line expresses both Axl and Tyro3, it was initially necessary to knock out Axl, Tyro3 or both receptors. The CRISPR Cas9 system functions by targeting the Cas9 nuclease to a specific genomic DNA locus using a single guide RNA (sgRNA), where Cas9 mediates a double stranded break (DSB) in the DNA helix[243]. DSBs are re-ligated through homology-directed repair (HDR) or non-homologous end joining (NHEJ), with the latter occurring at higher frequencies creating random insertion/deletion mutations (in/dels). Some in/dels result in frameshift mutations and the generation of premature termination codons (PTCs) in the targeted gene. The mRNA that encodes PTCs is commonly targeted for degradation via nonsense mediated decay (NMD)[253]. Therefore, PTCs generated through CRISPR-Cas9 gene targeting result in either NMD of mRNA and subsequently little to no full-length protein production, or the production of truncated and non-functional proteins. CRISPR-Cas9-mediated knockout of Axl and Tyro3 was performed by targeting 5TGM1 cells using either Axl or Tyro3 sgRNAs. 5TGM1 Tyro3 knockout cell lines were subsequently targeted with Axl sgRNA to generate 5TGM1 double knockout cell lines, or “TAM null” cell lines, that do not express any TAM receptors. 5TGM1 Mer cell lines were generated by retroviral transduction of 5TGM1 TAM null cell lines with pRufimCh2.Mer (Figure 3.2a). To target Tyro3 and Axl in 5TGM1 cells, Tyro3 and Axl sgRNAs were cloned into the px458.SFFV.cer2 CRISPR plasmid vector. This vector encodes the SpCas9 nuclease/cerulean reporter fusion protein, the SFFV murine haematopoietic promoter[254] from pLEGO vectors, and the U6 ubiquitous promoter for small RNA expression[255] (Figure 3.2b). After transfection with the Tyro3 or Axl sgRNA encoding px458.SFFV.cer2 CRISPR vector, 5TGM1 cells were sorted for cerulean expression

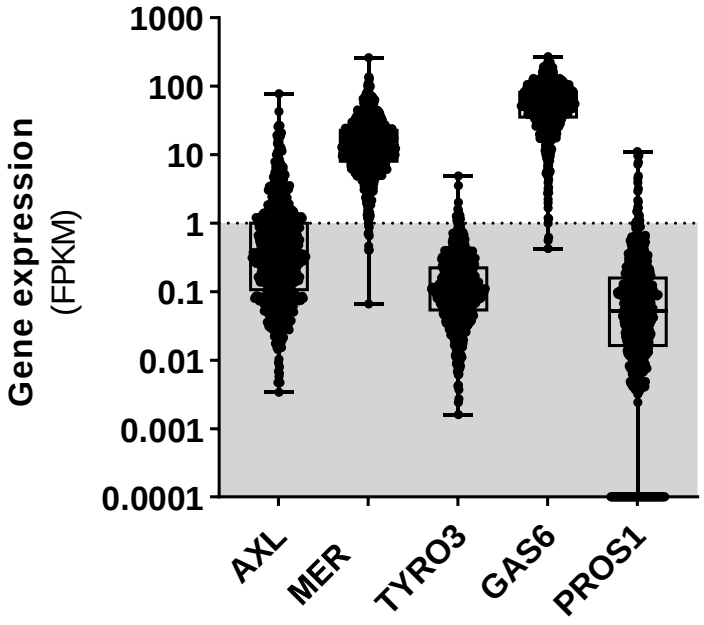

Figure 3.1. Mer and Gas6 are highly expressed by newly diagnosed MM patient PCs. *In silico* analysis of newly diagnosed MM patients from the CoMMPass dataset assessed TAM receptor and ligand RNA expression in CD-138 selected BM PCs of newly diagnosed myeloma patients (*n*=764). Gene expression data is presented as fragments per kilobase of exon per million mapped reads (FPKM), with a gene expression cut off of 1 FPKM.

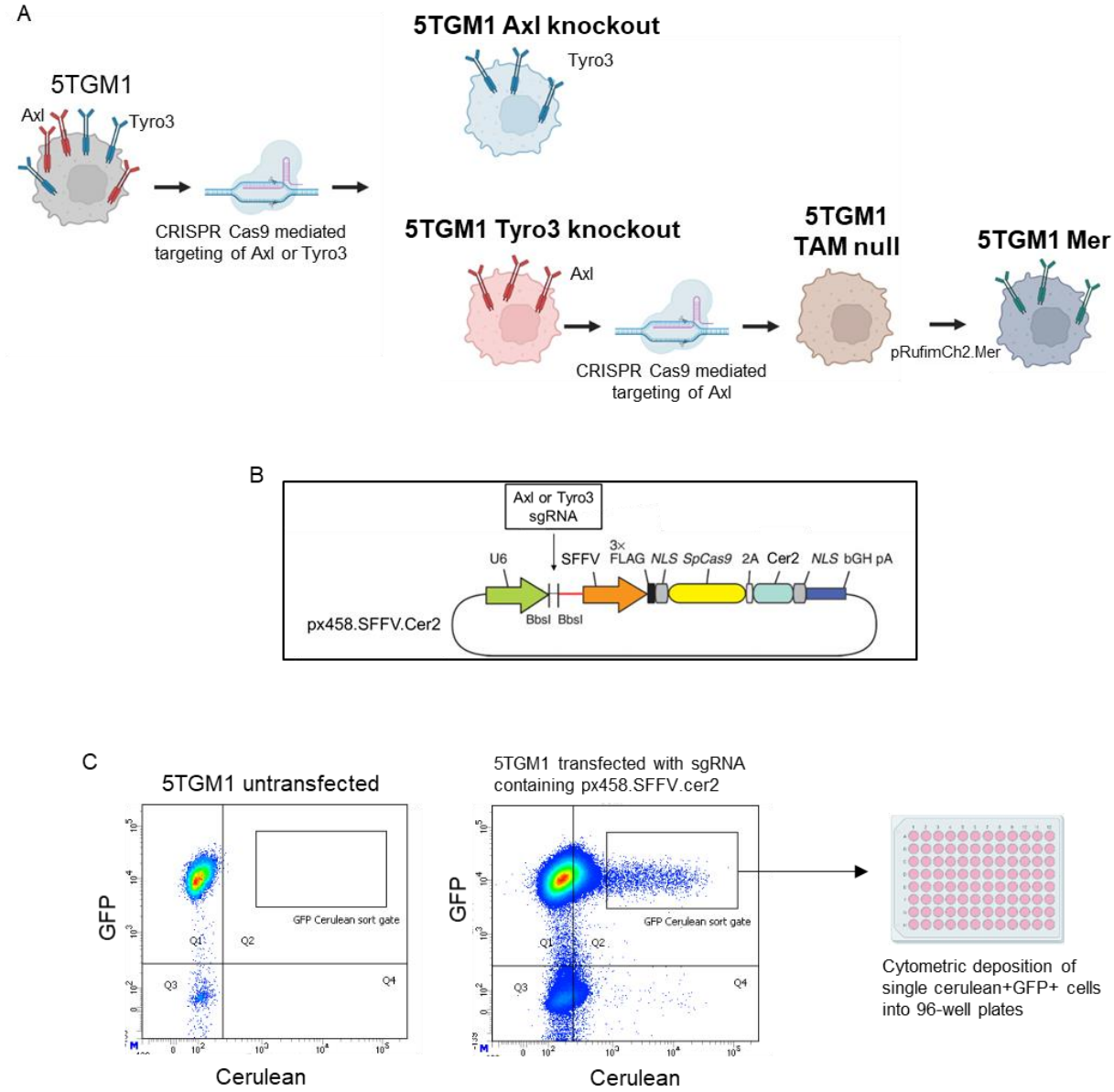
A
5TGM1
Axl
Tyro3
CRISPR Cas9 mediated targeting of Axl or Tyro3
5TGM1 Axl knockout
Tyro3
5TGM1 Tyro3 knockout
Axl
CRISPR Cas9 mediated targeting of Axl
5TGM1 TAM null
pRufimCh2.Mer
5TGM1 Mer
B
Axl or Tyro3 sgRNA
U6
SFFV
3x FLAG
NLS
SpCas9
2A
Cer2
NLS
bGH pA
BbsI
BbsI
px458.SFFV.Cer2
C
5TGM1 untransfected
5TGM1 transfected with sgRNA containing px458.SFFV.cer2
GFP
Cerulean
GFP Cerulean sort gate
Q1
Q2
Q3
Q4
Cytometric deposition of single cerulean+GFP+ cells into 96-well plates

Figure 3.2. CRISPR-Cas9 mediated gene targeting and retroviral transduction were utilised to generate 5TGM1 single TAM receptor expressing cell lines. (A) 5TGM1 cells initially expressing Axl and Tyro3 were targeted using either Axl or Tyro3 sgRNAs to generate 5TGM1 Axl knockout and 5TGM1 Tyro3 knockout clonal cell lines. 5TGM1 Tyro3 knockout cell lines were retargeted with Axl sgRNA to generate 5TGM1 double knockout cell lines that do not express any TAM receptors. 5TGM1 Mer cell lines were generated by retroviral transduction of 5TGM1 double knockout cell lines with pRufimCh2.Mer. **(B)** sgRNA guide sequences were cloned into an expression plasmid bearing a sgRNA scaffold backbone, Cas9, the U6 promoter, the SFFV promoter and the cerulean reporter (Cer2), figure adapted from Ran, *et al.,* 2013[242]. **(C)** 5TGM1 cells were transiently transfected with the px458.SFFV.cer2 vector encoding Axl or Tyro3 sgRNA (middle) compared to untransfected 5TGM1 cells (left) Single GFP+ cerulean+ cells were deposited into 96-well plates. 5TGM1 clonal knockout cell lines were then expanded from single cells.

and single cells were deposited into 96-well plates and clonal cell lines were expanded (Figure 3.2c).

3.2.3 Exon maps depicting sgRNA targeting of Axl and Tyro3.

Tyro3 and Axl sgRNAs were designed to target the portion of the Axl and Tyro3 genes encoding the signal peptide and/or Gas6 binding domain. Targeting these regions would ideally generate truncated and non-functional proteins that are missing essential domains. A sgRNA was designed to target the first wholly protein coding exon of Tyro3 (Ensembl.org Transcript ID: ENSMUST00000110783.8) exon 2 at nucleotides 498 to 517 of the cDNA sequence (Figure 3.3a). Due to targeting inefficiencies of Axl sgRNAs, two separate sgRNAs were designed to target the first exon of Axl (Ensembl.org Transcript ID: ENSMUST00000002677.11) at nucleotides 232 to 251, and nucleotides 251 to 270 of the cDNA sequence respectively. (Figure 3.3b). PCR primers to Tyro3 and Axl were designed to screen entire exons targeted by sgRNA, exon 2 of Tyro3 and exon 1 of Axl.

3.2.4 Confirmation of CRISPR-Cas9 mediated Tyro3 knockout in clonal 5TGM1 cell lines.

Clonal 5TGM1 cell lines were assessed for in/del mutations in Tyro3 induced by CRISPR-Cas9 targeting with a Tyro3 sgRNA. To identify potential in/dels surrounding the sgRNA binding site, PCR products amplifying Tyro3 exon 2 of genomic DNA from clonal 5TGM1 cell lines were subjected to Sanger sequencing. This revealed compound heterozygous frameshift in/del mutations in clones #1, #3 and #5 compared to the Tyro3 reference sequence (Figure 3.4a, Supplementary Figure 1). Larger, overtly homozygous deletions were detected in clones #2 and #4, with a 130bp deletion at the exon 2/intron 2 boundary identified in clone #2, and a 581bp deletion including complete deletion of the 184 bp exon 2 detected in clone #4. PCR products from candidate Tyro3 KO cell lines #1, #3 and #5 were also cloned into a plasmid vector. Individual cloned PCR products were sequenced to confirm the exact sequences of the two mutant alleles inferred from the original Sanger sequence chromatogram (Supplementary figure 2). RT-PCR analysis of the large deletions in 5TGM1 potential knockout clones #2 and #4 revealed alternative exon splicing events (Supplementary Figure 3). To predict the consequences of these

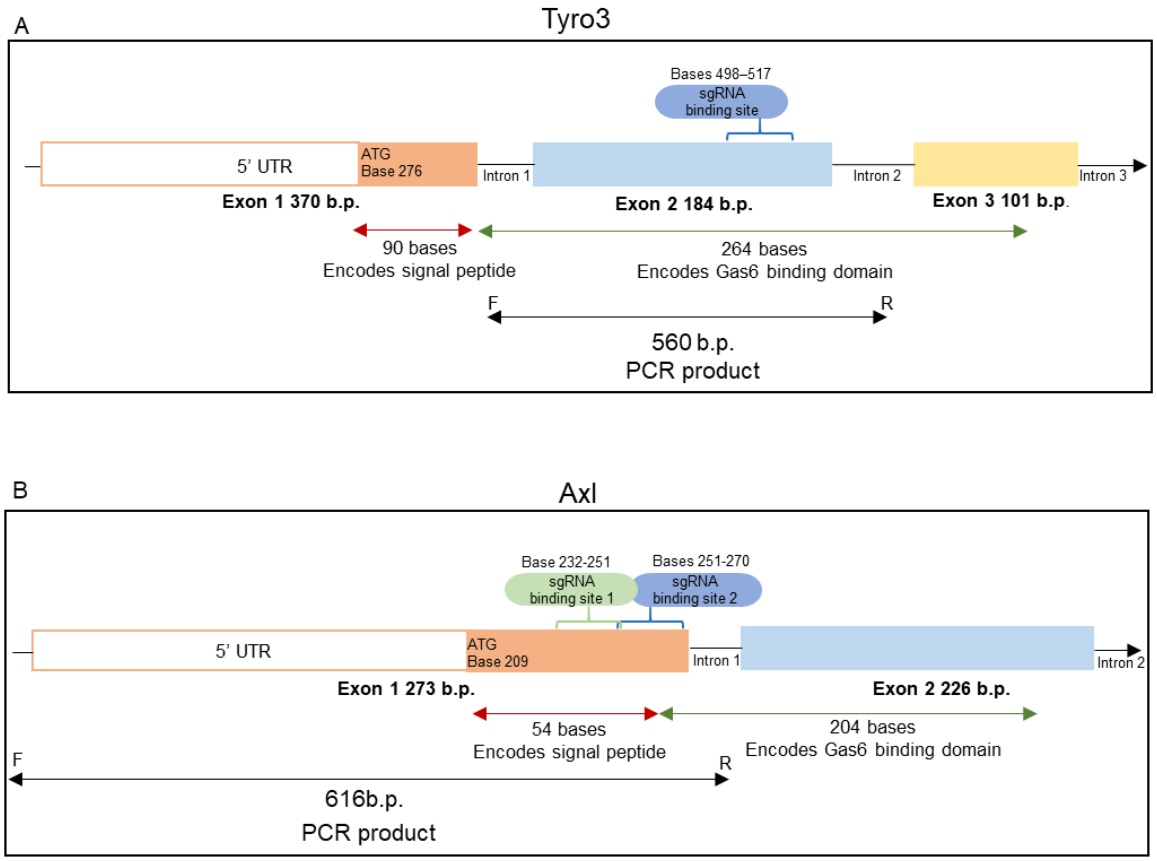

Figure 3.3. Exon maps depicting sgRNA targeting of Axl and Tyro3. Exon maps depicting nucleotide binding locations of **(A)** Tyro3 sgRNA and **(B)** Axl sgRNAs. Also shown are regions encoding the signal peptide and Gas6 binding domain, as well as PCR primers used to amplify regions of Axl and Tyro3 to be screened for mutations using Sanger sequencing. Lengths of exons, PCR products, are displayed in base pairs (b.p.) Gas6 binding domains and signal peptides and sgRNA binding sites are shown in bases/nucleotides. The nucleotide location of the initiating methionine (ATG) of Tyro3 and Axl are shown within exon 1.

in/dels on Tyro3 protein production compared to the unmutated Tyro3 gene, mutant allele DNA sequences were translated into amino acids using the ExPASy Translate tool (https://web.expasy.org/translate/). As a consequence of the frameshift mutations/exon deletions, it was anticipated that all of the Tyro3 mutant alleles would likely produce either severely truncated proteins ranging from 32aa to 98aa in length or be subject to NMD of Tyro3 mRNA (Figure 3.4b, Supplementary Figure 4). The predicted severely truncated Tyro3 receptor would lack virtually all functional domains and was predicted to be non-functional. There also remained a possibility that each mutant allele could potentially utilise an alternative downstream initiating methionine. Whilst there is no evidence that these alternative translational start sites are ever utilised, if the next downstream methionine codon was used as a translation start site, then N-terminal truncated proteins ranging from 518aa to 812aa in length would be generated. The Tyro3 proteins produced using these internal initiating methionines would have no, or incomplete, Gas6 binding domains as well as no signal peptide. Lack of a signal peptide would prevent trafficking to the plasma membrane[256], rendering Tyro3 non-functional.

Whole cell protein lysates from 5TGM1 clonal cell lines with frameshift mutations/exon deletions of Tyro3 were subjected to western blotting with an antibody to Tyro3. This revealed complete lack of detectable Tyro3 protein expression in clones #1, #3 and #5, highlighted in red boxes in Figure 3.4c, compared to wild type Tyro3 expression in the unaltered 5TGM1 cell line. Clone #2 produced a band at ~48kDa, and clone #4 produced a band at ~110-120kDA, which were not as predicted (Figure 3.3c). If clones #2 and #4 had produced the predicted 518aa truncated proteins, this would result in a ~58kDa band. As Sanger sequencing detected apparent homozygous deletions in clones #2 and #4, it was conceivable that the other allele of Tyro3 was refractory to the sequencing method utilised in this study. This could be due to in/dels of PCR primer binding sites of one allele of clone #2 and #4, preventing primer binding and sequencing. As clone #4 produces almost full length Tyro3 protein, potentially due to one allele of Tyro3 being largely intact, this clone was excluded from all future studies. Subsequent functional studies were restricted to clones #1, #3 and #5 for which both mutant alleles had been fully characterised at the genomic DNA level.

A

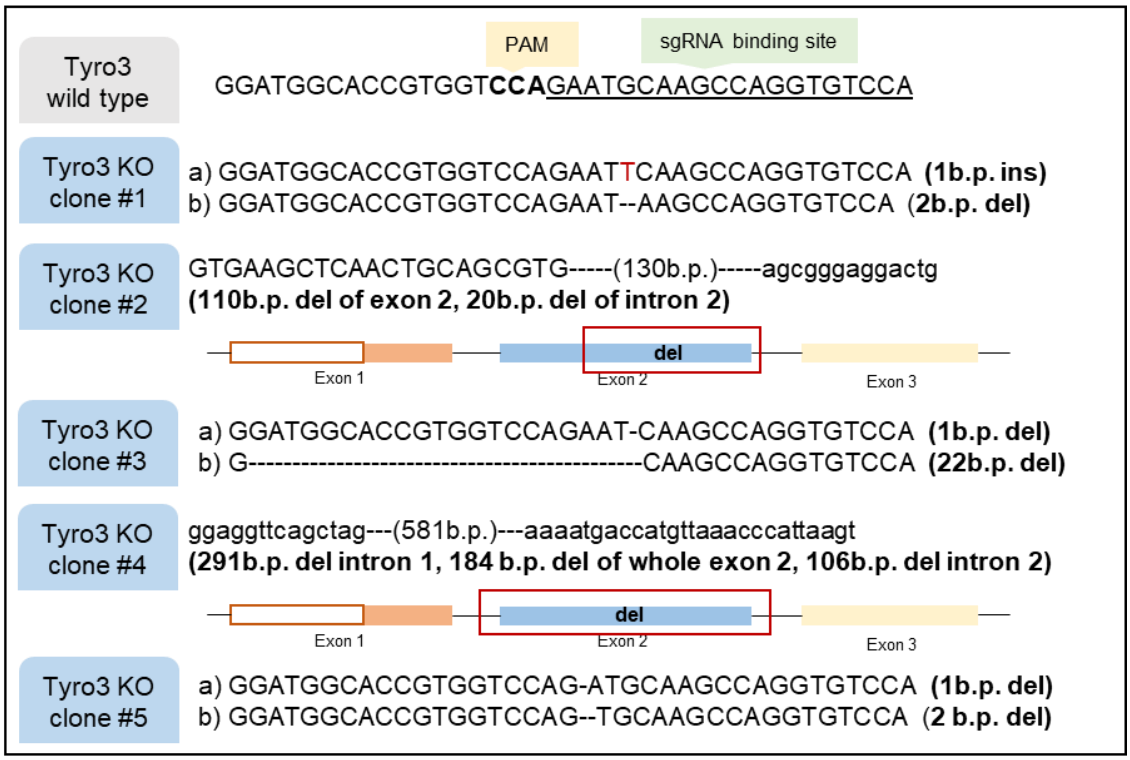
PAM
sgRNA binding site
Tyro3 wild type
GGATGGCACCGTGGTCCAGAATGCAAGCCAGGTGTCCA
Tyro3 KO clone #1
a) GGATGGCACCGTGGTCCAGAATTCAAGCCAGGTGTCCA (1b.p. ins)
b) GGATGGCACCGTGGTCCAGAAT--AAGCCAGGTGTCCA (2b.p. del)
Tyro3 KO clone #2
GTGAAGCTCAACTGCAGCGTG-----(130b.p.)-----agcgggaggactg
(110b.p. del of exon 2, 20b.p. del of intron 2)
del
Exon 1
Exon 2
Exon 3
Tyro3 KO clone #3
a) GGATGGCACCGTGGTCCAGAAT-CAAGCCAGGTGTCCA (1b.p. del)
b) G----------CAAGCCAGGTGTCCA (22b.p. del)
Tyro3 KO clone #4
ggaggttcagctag---(581b.p.)---aaaatgaccatgttaaacccattaagt
(291b.p. del intron 1, 184 b.p. del of whole exon 2, 106b.p. del intron 2)
del
Exon 1
Exon 2
Exon 3
Tyro3 KO clone #5
a) GGATGGCACCGTGGTCCAG-ATGCAAGCCAGGTGTCCA (1b.p. del)
b) GGATGGCACCGTGGTCCAG--TGCAAGCCAGGTGTCCA (2 b.p. del)

B

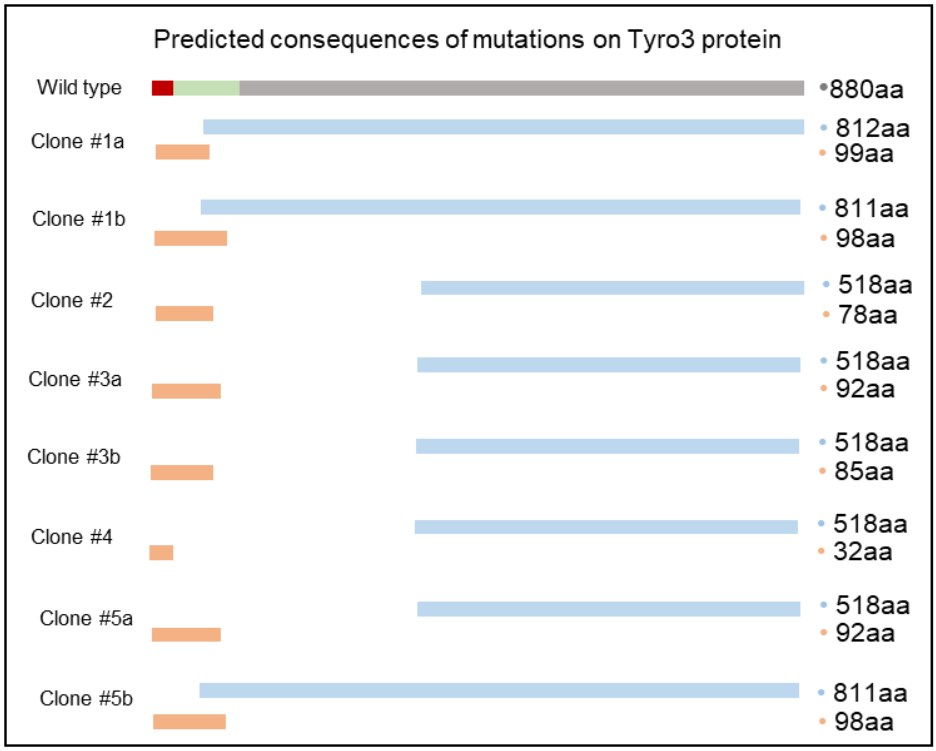
Predicted consequences of mutations on Tyro3 protein
Wild type
880aa
Clone #1a
812aa
99aa
Clone #1b
811aa
98aa
Clone #2
518aa
78aa
Clone #3a
518aa
92aa
Clone #3b
518aa
85aa
Clone #4
518aa
32aa
Clone #5a
518aa
92aa
Clone #5b
811aa
98aa

C

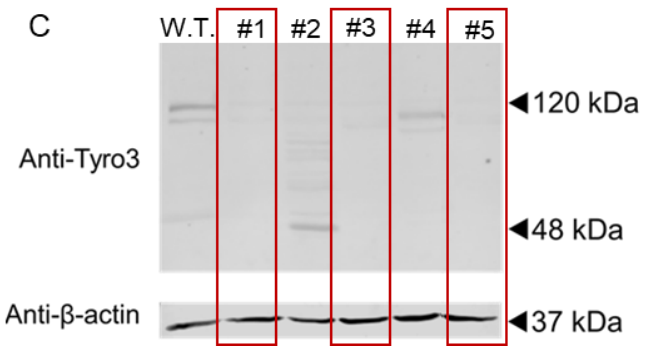
W.T.
#1
#2
#3
#4
#5
Anti-Tyro3
120 kDa
48 kDa
Anti-β-actin
37 kDa

Figure 3.4. Confirmation of CRISPR-Cas9 mediated Tyro3 knockout in clonal 5TGM1 cell lines. (A) Sanger sequencing results of PCR products amplifying Tyro3 exon 2 genomic DNA from clonal 5TGM1 cell lines targeted with Tyro3 sgRNA was compared to wild type Tyro3 sequence. The Tyro3 sgRNA binding site (underlined) and 5' PAM sequence (bold) are shown in the wild type Tyro3 sequence. Insertion (in) and deletion (del) mutations in individual clones are shown as red text (N) and dashes (-), respectively. Mutations were either heterozygous (clones 1, 3 and 5) or homozygous (clones 2 and 4). Larger deletions in clones #2 and #4 are depicted below sequences, with deletions shown by red boxes. **(B)** Predicted consequences of mutant Tyro3 alleles on encoded Tyro3 protein. Unmutated, wild type Tyro3 is indicated in grey at the top, with a green band overlain to indicate the Gas6 binding domain and red to indicate the signal peptide. Sizes of potential Tyro3 proteins that could be produced by mutant alleles are indicated. Orange bars start at the established initiating methionine, blue bars start at putative alternative downstream methionines. **(C)** Proteins from clonal Tyro3 knockout cell lines were subjected to western blotting using an anti-Tyro3 primary antibody. β-actin was used as a loading control. Red boxes identify 5TGM1 Tyro3 knockout clones that do not produce any detectable Tyro3 protein.

3.2.5 Confirmation of CRISPR-Cas9 mediated Axl knockout in clonal 5TGM1 cell lines.

Putative clonal 5TGM1 Axl knockout cell lines were assessed for in/del mutations induced by CRISPR-Cas9 mediated targeting with an Axl sgRNA. To identify in/dels surrounding the sgRNA binding site, PCR products amplifying genomic DNA from Axl exon 1 of putative 5TGM1 Axl knockout cell lines were subjected to Sanger sequencing. This revealed homozygous frameshift mutations in these Axl knockout clones targeted with sgRNA 1 (clones KO1#1 and KO1#2), or sgRNA 2 (clone KO2#3) compared to the Axl wild type reference sequence (Figure 3.5a, Supplementary Figure 5). Compound heterozygous frameshift deletion mutations were identified in clone KO2#4. PCR products from clone 2#4 were also cloned into a plasmid vector and sequencing performed on each of the two mutated alleles that were inferred from the original Sanger sequence trace (Supplementary Figure 6). To predict the consequences of these deletions on Axl protein production, DNA sequences were translated into amino acids using the ExPASy Translate tool (https://web.expasy.org/translate/). As a consequence of the frameshift mutations/exon deletions, it was predicted that all of the Axl mutant alleles would likely produce either severely truncated proteins ranging from 18aa to 68aa in length or be subject to NMD of Axl mRNA (Figure 3.5b, Supplementary Figure 7). Furthermore, the predicted amino acid lengths of these severely truncated Axl proteins only display partially conserved wild type amino acid sequences ranging from 8 to 18aa (Supplementary Figure 7), suggesting that the Gas6 binding domain would not be intact and would be unable to facilitate functional Gas6/Axl signalling. Furthermore, these truncated Axl proteins would be missing their tyrosine kinase domains. Like the predicted Tyro3 proteins described in section 3.2.3, there remains the potential that internal initiating methionines could be utilised to generate N-terminal truncated Axl proteins of 777aa in length. However, these proteins would be missing the signal peptide and entire Gas6 binding domain and would be non-functional. Axl cell surface expression in the putative 5TGM1 Axl knockout cell lines was assessed by flow cytometry compared to the unaltered 5TGM1 cell line. All 5TGM1 Axl knockout cell lines expressed no Axl on the cell surface compared to the unaltered 5TGM1 cell line (Figure 3.5c).

A

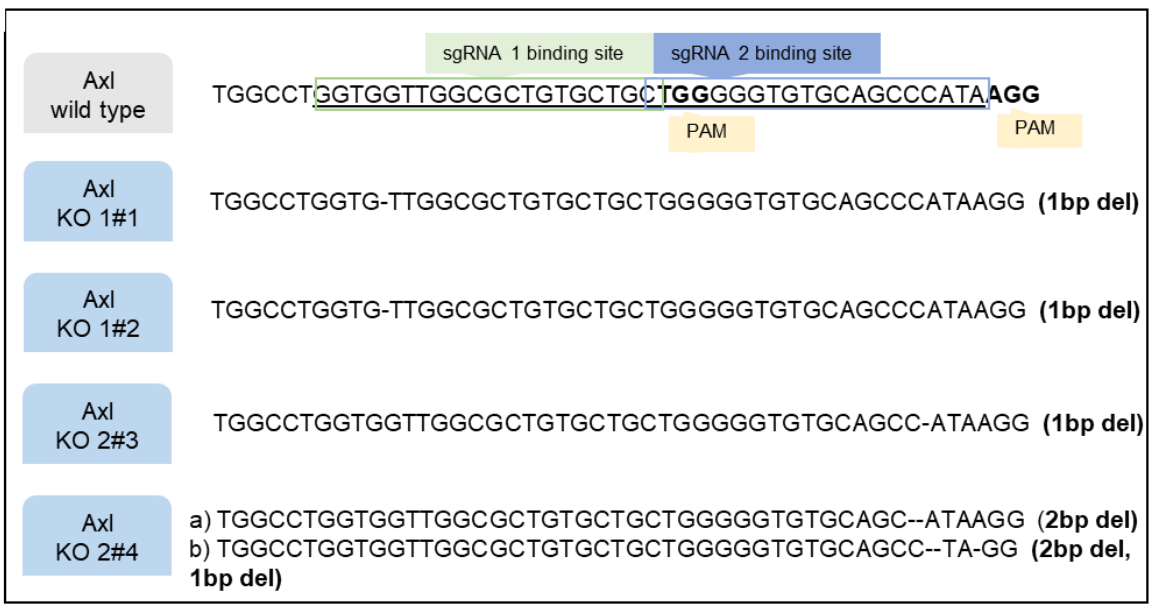
sgRNA 1 binding site
sgRNA 2 binding site
Axl wild type
TGGCCTGGTGGTTGGCGCTGTGCTGCTGGGGGTGTGCAGCCCATAAGG
PAM
PAM
Axl KO 1#1
TGGCCTGGTG-TTGGCGCTGTGCTGCTGGGGGTGTGCAGCCCATAAGG (1bp del)
Axl KO 1#2
TGGCCTGGTG-TTGGCGCTGTGCTGCTGGGGGTGTGCAGCCCATAAGG (1bp del)
Axl KO 2#3
TGGCCTGGTGGTTGGCGCTGTGCTGCTGGGGGTGTGCAGCC-ATAAGG (1bp del)
Axl KO 2#4
a) TGGCCTGGTGGTTGGCGCTGTGCTGCTGGGGGTGTGCAGC--ATAAGG (2bp del)
b) TGGCCTGGTGGTTGGCGCTGTGCTGCTGGGGGTGTGCAGCC--TA-GG (2bp del, 1bp del)

B

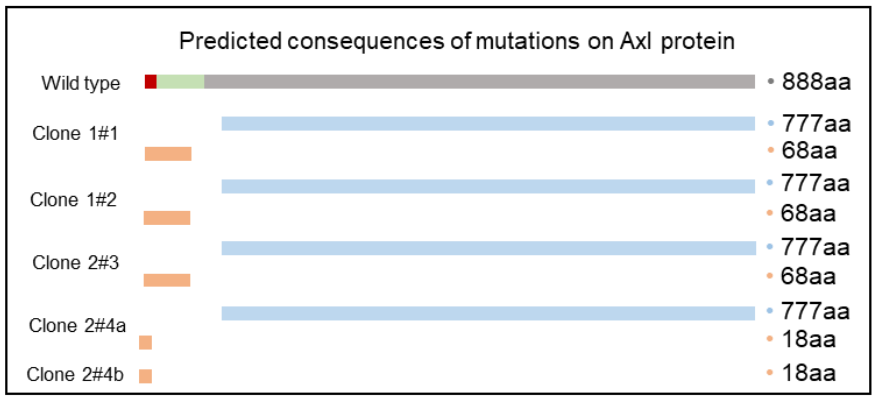
Predicted consequences of mutations on Axl protein
Wild type
888aa
Clone 1#1
777aa
68aa
Clone 1#2
777aa
68aa
Clone 2#3
777aa
68aa
Clone 2#4a
777aa
18aa
Clone 2#4b
18aa

C

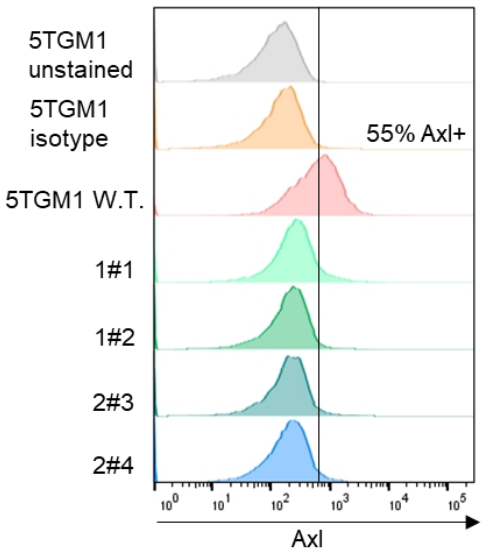
5TGM1 unstained
5TGM1 isotype
55% Axl+
5TGM1 W.T.
1#1
1#2
2#3
2#4
Axl

Figure 3.5. Confirmation of CRISPR-Cas9 mediated Axl knockout in clonal 5TGM1 cell lines. (A) Sanger sequencing results of PCR products amplifying Axl exon 1 genomic DNA from clonal 5TGM1 cell lines targeted with Axl sgRNA was compared to wild type Axl sequence. The Axl sgRNA 1 binding site (green box) and Axl sgRNA 2 binding site (blue box) and 5' PAM sequence (bold) are shown in the wild type Axl sequence. Deletion (del) mutations in individual clones are shown as dashes (-). Mutations were either homozygous (clones 1, 2 and 3) or heterozygous (clone 4). **(B)** Axl protein produced by wild type Axl gene is indicated in grey, with a green band overlayed to indicate the Gas6 binding domain and red to indicate the signal peptide. Sizes of potential Axl proteins that could be produced by mutant alleles are indicated. Orange bars start at the established initiating methionine, blue bars start at a putative alternative downstream methionine. **(C)** 5TGM1 Axl knockout cell lines were subjected to antibody staining for Axl expression and analysis by flow cytometry. Axl expression was compared to unaltered 5TGM1 cells and unstained and isotype controls.

3.2.6 Confirmation of CRISPR-Cas9 mediated Axl knockout in clonal 5TGM1 Tyro3 knockout cell lines.

To generate 5TGM1 double Tyro3 and Axl knockout cell lines, or 5TGM1 "TAM null" cell lines, 5TGM1 Tyro3 knockout clone #5 was retargeted with Axl sgRNA1. To identify in/dels surrounding the sgRNA binding site, PCR products amplifying genomic DNA from Axl exon 1 of putative 5TGM1 TAM null cell lines were subjected to Sanger sequencing. This identified heterozygous frameshift mutations of Axl in 5TGM1 potential TAM null cell lines #1, #2, #3, #4 and #5 compared to the Axl wild type reference sequence (Figure 3.6a, Supplementary Figure 8). For two of the putative TAM null clonal cell lines, #3 and #5, PCR products were cloned into a plasmid vector and both mutant alleles inferred from the original Sanger sequencing chromatogram were confirmed by the sequencing of multiple cloned PCR products (Supplementary Figure 9). To predict the consequences of these in/dels on Axl protein production compared to wild type Axl, DNA sequences were translated into amino acids using the ExPASy Translate tool (https://web.expasy.org/translate/). Because of the frameshift mutations/exon deletions, it was predicted that all of the Axl mutant alleles would likely produce either severely truncated proteins ranging from 18aa to 68aa in length or be subject to NMD of Axl mRNA (Figure 3.6b, Supplementary Figure 10). These truncated Axl proteins only display 7-10aa conserved from wild type Axl protein and would therefore lack any functional domains. There remains the potential that internal initiating methionines could be utilised to generate N-terminal truncated Axl proteins of 777aa in length. However, these proteins would be missing the signal peptide and entire Gas6 binding domain and would be non-functional. Axl cell surface expression in the potential 5TGM1 Axl knockout cell lines was assessed by flow cytometry compared to the unaltered 5TGM1 cell line. All 5TGM1 Axl knockout cell lines expressed no Axl on the cell surface compared to the unaltered 5TGM1 cell line (Figure 3.6d). The lack of detectable Tyro3 expression by Western blot was also confirmed in all 5 TAM null clonal cell lines (Figure 3.6c).

3.2.7 Screening of clonal 5TGM1 Axl knockout, Tyro3 knockout and TAM null cell lines for differences in baseline proliferation rates and bioluminescence.

To select at least two 5TGM1 Axl knockout, two 5TGM1 Tyro3 knockout and two 5TGM1 TAM null cell lines for *in vitro* and *in vivo* studies, baseline proliferation and

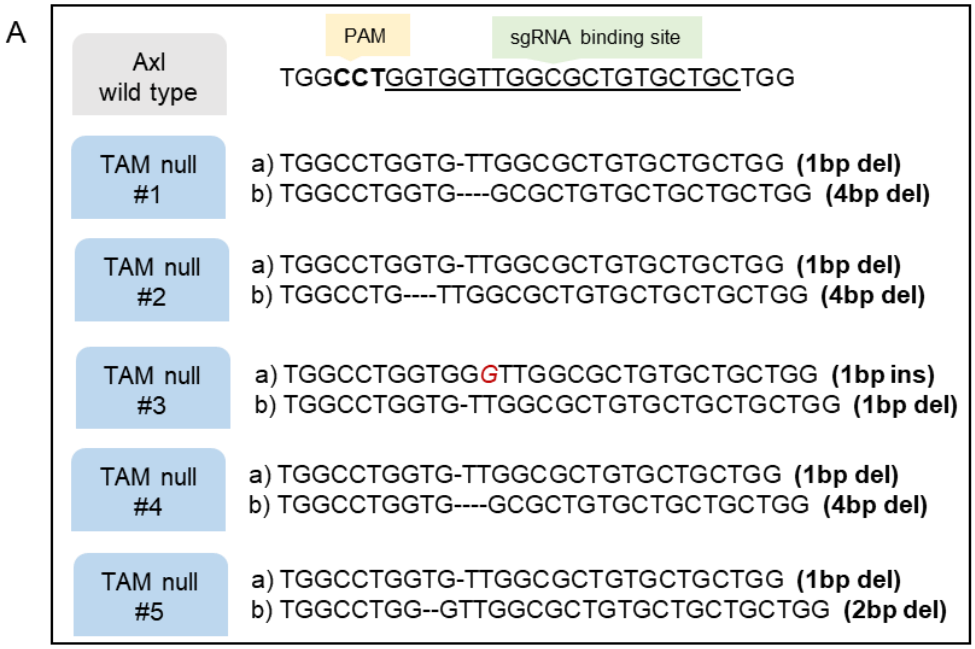
A
PAM
sgRNA binding site
Axl wild type
TGGCCTGGTGGTTGGCGCTGTGCTGCTGG
TAM null #1
a) TGGCCTGGTG-TTGGCGCTGTGCTGCTGG (1bp del)
b) TGGCCTGGTG----GCGCTGTGCTGCTGCTGG (4bp del)
TAM null #2
a) TGGCCTGGTG-TTGGCGCTGTGCTGCTGG (1bp del)
b) TGGCCTG----TTGGCGCTGTGCTGCTGCTGG (4bp del)
TAM null #3
a) TGGCCTGGTGGGTTGGCGCTGTGCTGCTGG (1bp ins)
b) TGGCCTGGTG-TTGGCGCTGTGCTGCTGCTGG (1bp del)
TAM null #4
a) TGGCCTGGTG-TTGGCGCTGTGCTGCTGG (1bp del)
b) TGGCCTGGTG----GCGCTGTGCTGCTGCTGG (4bp del)
TAM null #5
a) TGGCCTGGTG-TTGGCGCTGTGCTGCTGG (1bp del)
b) TGGCCTGG--GTTGGCGCTGTGCTGCTGCTGG (2bp del)

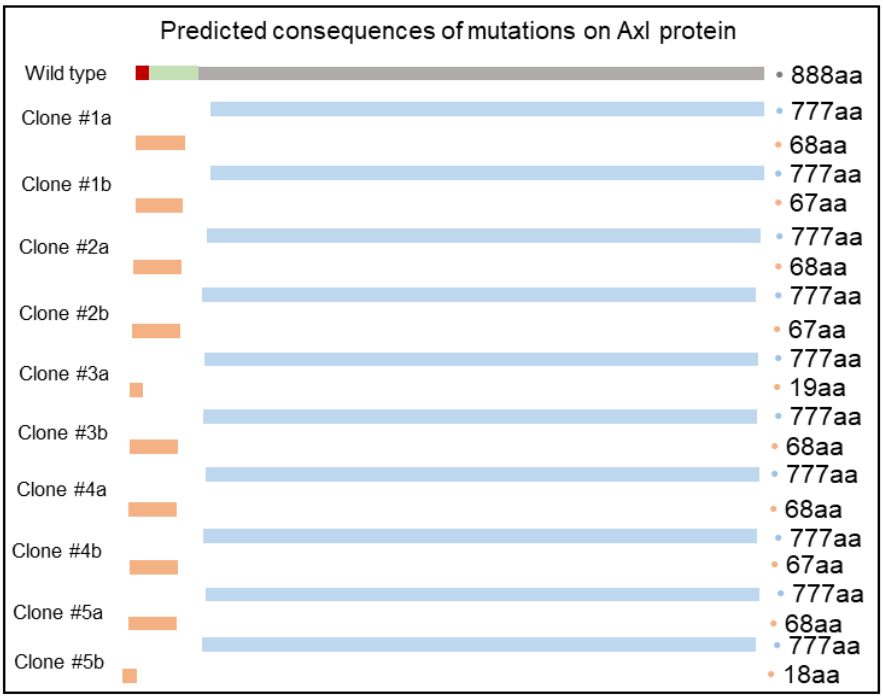
B
Predicted consequences of mutations on Axl protein
Wild type
888aa
Clone #1a
777aa
68aa
Clone #1b
777aa
67aa
Clone #2a
777aa
68aa
Clone #2b
777aa
67aa
Clone #3a
777aa
19aa
Clone #3b
777aa
68aa
Clone #4a
777aa
68aa
Clone #4b
777aa
67aa
Clone #5a
777aa
68aa
Clone #5b
777aa
18aa

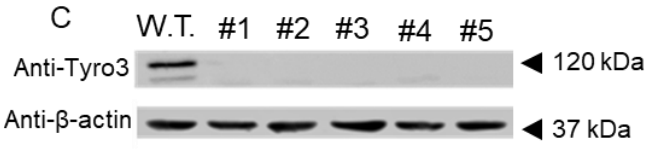
C
W.T. #1 #2 #3 #4 #5
Anti-Tyro3
120 kDa
Anti-β-actin
37 kDa

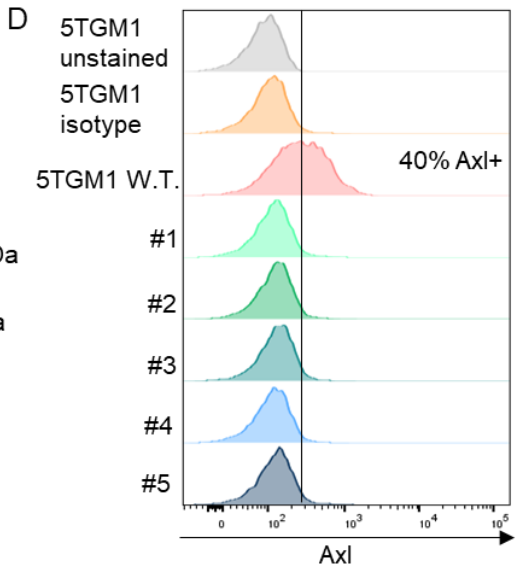
D
5TGM1 unstained
5TGM1 isotype
5TGM1 W.T.
40% Axl+
#1
#2
#3
#4
#5
Axl

Figure 3.6. Confirmation of CRISPR-Cas9 mediated Axl knockout in clonal 5TGM1 Tyro3 knockout cell lines. (A) Sanger sequencing results of PCR products amplifying Axl exon 1 genomic DNA from clonal 5TGM1 Tyro3 knockout cell lines targeted with Axl sgRNA1 was compared to wild type Axl sequence. The Axl sgRNA1 binding site (underlined) and 5' PAM sequence (bold) are shown in the wild type Axl sequence. Insertion (In) and deletion (del) mutations in individual mutant alleles are shown as red text (N) and dashes (-) respectively. Mutations were all heterozygous. **(B)** Axl protein produced by unmutated, wild type Axl gene is indicated in grey, with a green band overlayed to indicate the Gas6 binding domain and red to indicate the signal peptides. Sizes of potential Axl proteins that could be produced by mutant alleles are indicated. Orange bars start at the established initiating methionine, blue bars start at a putative alternative downstream methionine. **(C)** Proteins from 5TGM1 TAM null cell lines were subjected to western blotting using an anti-Tyro3 primary antibody. B-actin was used as a loading control. **(D)** 5TGM1 double knockout cell lines were subjected to antibody staining for cell surface Axl expression and analysis by flow cytometry. Axl expression was compared to unaltered 5TGM1 cells and unstained and istotype controls.

bioluminescence levels were assessed compared to the unaltered 5TGM1 cell line. Outlier clonal knockout cell lines that displayed significantly different proliferation rates or bioluminescence levels relative to each other and to the unaltered 5TGM1 cell line were then excluded from further studies. After 72 hours of culture in IMDM media, no significant differences in cell proliferation were observed between the unaltered 5TGM1 cell line and the 5TGM1 Axl knockout cell lines (Figure 3.7a), the 5TGM1 Tyro3 knockout cell lines (Figure 3.7b), or the 5TGM1 TAM null cell lines (Figure 3.7c). However, with the exception of clone #3 (Figure 3.7d), the 5TGM1 Tyro3 knockout cell lines (Figure 3.7e) and in all 5TGM1 TAM null cell lines (Figure 3.7f), significant decreases in bioluminescence levels compared to the unaltered 5TGM1 cell line were identified in all 5TGM1 Axl knockout cell lines (Figure 3.7d. Accordingly, the decreased bioluminescence levels in all clonal knockout cell lines needed to be considered when interpreting *in vivo* BLI results, particularly when tumour burden of clonal knockout cell lines was compared to that of the unaltered 5TGM1 cell line.

3.2.8 Retroviral mediated generation of NIH3T3 cells overexpressing Gas6 or Pros1.

To generate a source of TAM ligands for *in vitro* experiments, NIH3T3 murine fibroblasts overexpressing Gas6 or Pros1 were generated, as well as an empty vector control cell line. NIH3T3 cells express low levels of Gas6 and Pros1, making this cell line an ideal candidate for Gas6 and Pros1 overexpression. NIH3T3 cells were transduced with a pRufiG2.Gas6-HA, pRufiG2.Pros1-HA or an empty pRufiG2 vector. To select for transduced NIH3T3 cells, GFP+ cells were sorted by flow cytometry and expanded in culture (Figure 3.8a). Importantly, as described in previous studies[257, 258], the HA-tags located at the C-terminal should not interfere with ligand functionality. HA-tagged ligand expression was assessed by Western blot in NIH3T3 Gas6 (left) and NIH3T3 Pros1 (right) cell lines compared to NIH3T3 EV cells (Figure 3.8b). Increased ligand secretion into conditioned media (CM) was confirmed by immunoprecipitation of HA-tagged ligands and revealed the presence of HA-tagged ligand in NIH3T3 Gas6 CM and NIH3T3 Pros1 CM but not in NIH3T3 EV CM (Figure 3.8c). Gas6 expression in conditioned media of NIH3T3 Gas6 cells and NIH3T3 EV cell was also assessed by ELISA with an anti-Gas6 antibody, identifying a significant increase in Gas6 expression in the NIH3T3 Gas6

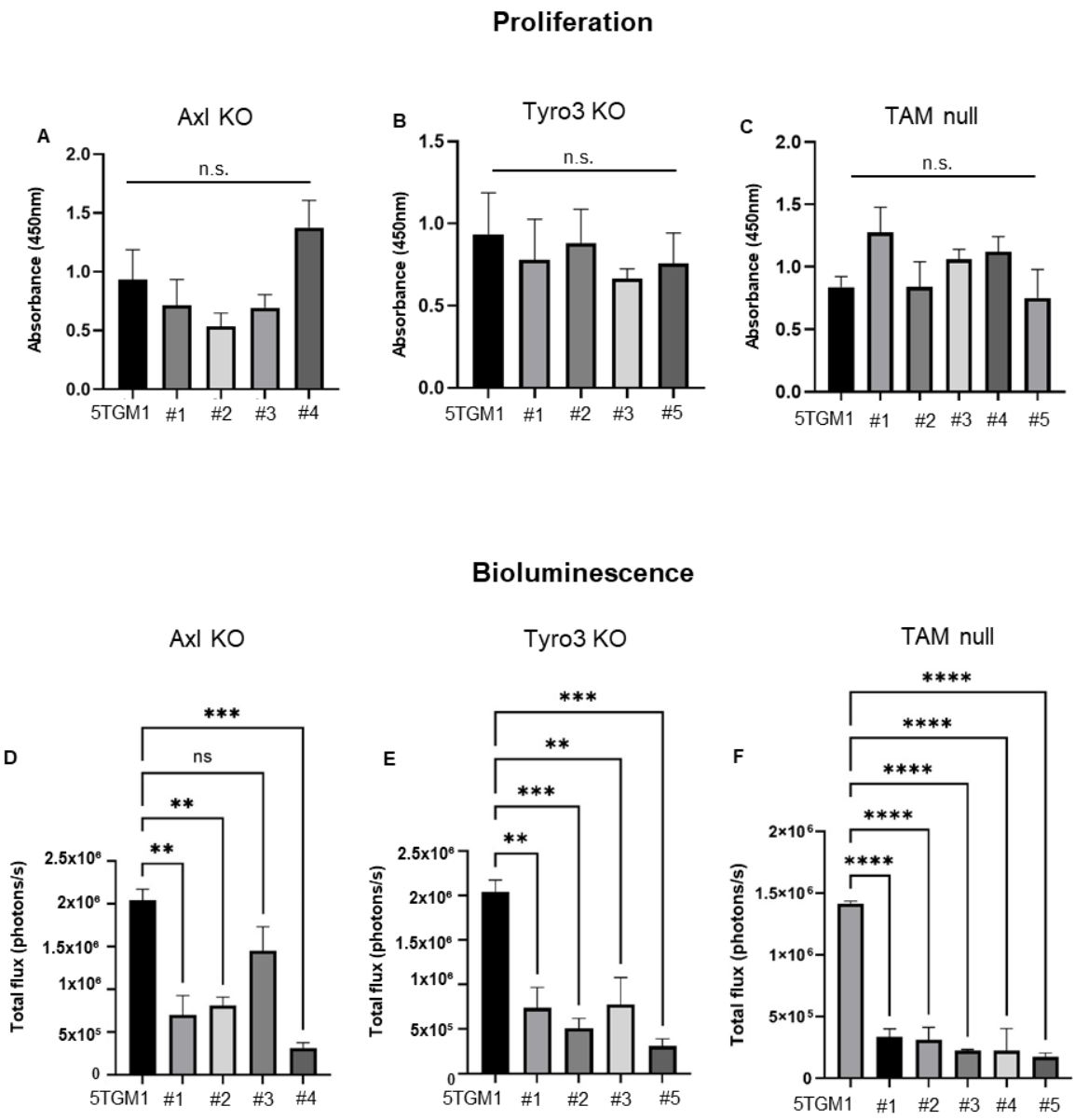

Figure 3.7. Screening of clonal 5TGM1 Axl knockout, Tyro3 knockout and TAM null cell lines for differences in baseline proliferation rates and bioluminescence. Clonal knockout cell lines were assessed for baseline proliferation and bioluminescence compared to the unaltered 5TGM1 cell line to identify any significant outliers. Proliferation of **(A)** 5TGM1 Axl knockout, **(B)** Tyro3 knockout and **(C)** TAM null cell lines were compared to the unaltered 5TGM1 cell line after 72 hours by a WST-1 assay. Results were displayed as absorbance (450nm) at 72 hours. Bioluminescence of **(D)** 5TGM1 Axl knockout, **(E)** Tyro3 knockout and **(F)** TAM null cell lines were compared to the unaltered 5TGM1 cell line using an *in vitro* luciferase assay. Graphs depict mean ± SEM, *n*=3, One-way ANOVA with Tukey's multiple comparisons, **p<0.01, ***p<0.001, ****p<0.0001.

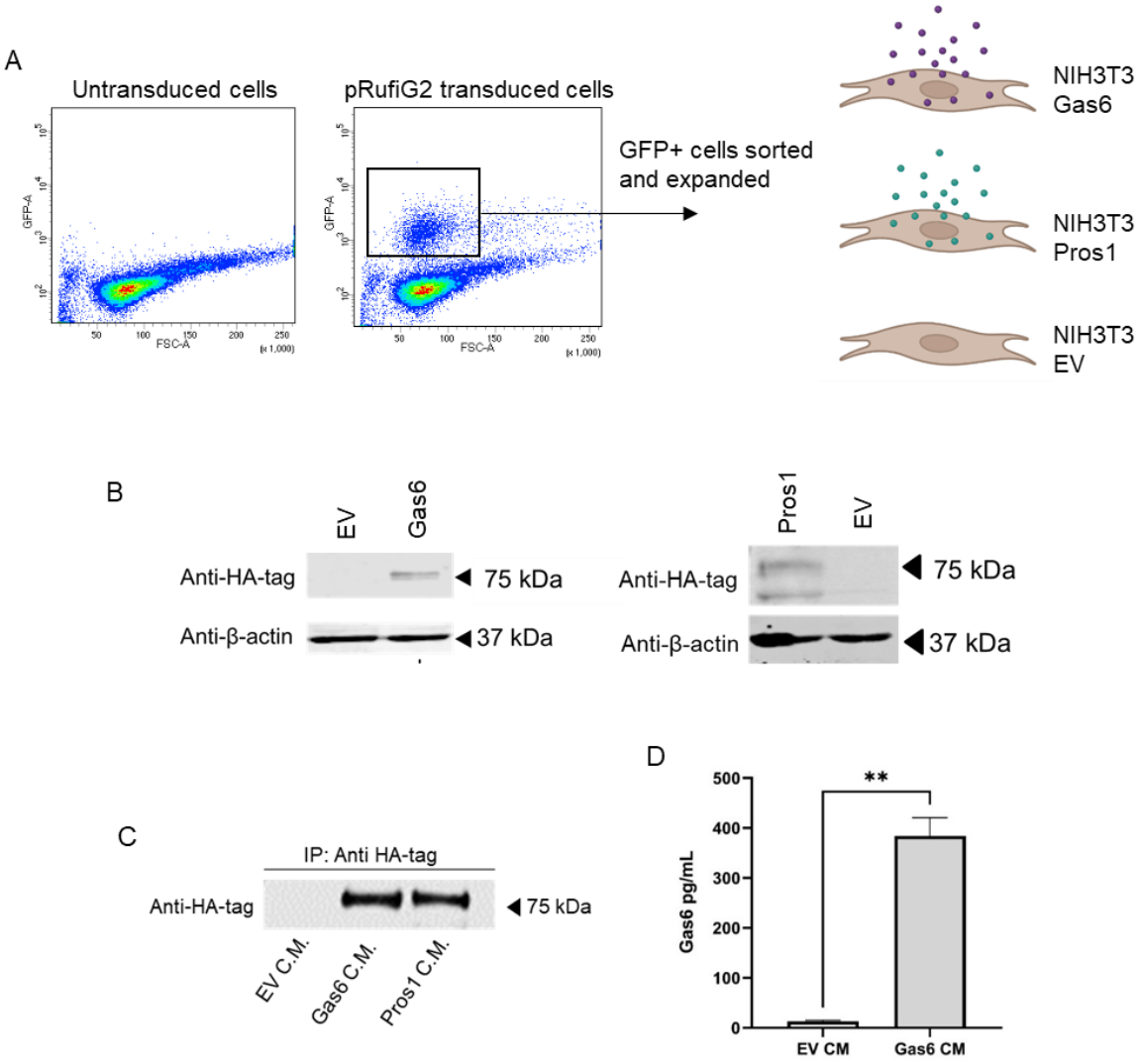

Figure 3.8. Retroviral mediated generation of NIH3T3 cells overexpressing Gas6 or Pros1 transgenes. (A) NIH3T3 cells were transduced with the pRufiG2.Gas6-HA, pRufiG2.Pros1-HA or empty vector retroviruses and GFP+ cells were sorted and expanded. Representative FAC plots with sort gate is shown. **(B)** Protein lysates from NIH3T3 EV compared to NIH3T3 Gas6 (left) and NIH3T3 Pros1 (right) cell lines were subjected to western blot using an anti-HA-tag primary antibody with β-actin used as a loading control. **(C)** Conditioned media was collected from the NIH3T3 cell lines and subjected to immunoprecipitation using an anti-HA-tag antibody. Purified proteins were then subjected to immunoblotting with anti-HA-tag antibody. **(D)** Conditioned media from the NIH3T3 EV and NIH3T3 Gas6 cell lines was used in an ELISA for Gas6, data presented as mean ± SEM, *n*=3, Student's t-test **p<0.01.

conditioned media (Figure 3.8d). A working ELISA kit for Pros1 was not available and accordingly, was not performed in this study.

3.2.9 There is no difference in the proliferation rates of 5TGM1 Axl knockout, Tyro3 knockout or TAM null cell lines compared to the unaltered 5TGM1 cell line.

The proliferation rates of 5TGM1 Axl knockout, 5TGM1 Tyro3 knockout and 5TGM1 TAM null cell lines, compared to the unaltered 5TGM1 cell line, was assessed by WST-1 assays. Given that Axl expression is associated with 5TGM1 cell dormancy[129, 213], and Tyro3 overexpression is associated with prostate cancer cells reactivation, it was hypothesised that 5TGM1 Axl knockout cells would display increased proliferation compared to the unaltered 5TGM1 cell line. Conversely, when Axl is the sole TAM receptor expressed, it was hypothesised that a dormant phenotype would be observed as evidenced by a decrease in cell proliferation. However no significant differences in proliferation between 5TGM1 Axl knockout cell lines (Figure 3.9a) or 5TGM1 Tyro3 knockout cell lines (Figure 3.9b) and the unaltered 5TGM1 cell line were identified when cells were cultured in NIH3T3 EV CM, NIH3T3 Gas6 CM or NIH3T3 Pros1 CM. Although 5TGM1 TAM null cell lines displayed slightly decreased cell proliferation compared to the unaltered 5TGM1 cell line in all three types of media, this did not reach statistical significance (Figure 3.9c).

3.2.10 Clonal 5TGM1 cell lines with the same Axl or Tyro3 knockout status display extreme heterogeneity in tumour burden in the KaLwRij model of MM.

To assess whether Axl and Tyro3 expression influences tumour burden *in vivo*, the unaltered 5TGM1 cell line, as well as 5TGM1 Axl knockout and 5TGM1 Tyro3 knockout cell lines, were i.v. inoculated into KaLwRij mice and tumour burden was monitored at weeks 2, 3 and 4 using BLI. Given that in a previous study[213], Axl inhibition using a small molecule inhibitor resulted in increased tumour burden *in vivo*, it was anticipated that 5TGM1 Axl knockout cells would produce increased tumour burden in comparison to the unaltered 5TGM1 cell line. However, the Axl knockout cell line #1 produced similar tumour burden in comparison to the unaltered 5TGM1 cell line, while Axl knockout cell line #4 produced no detectable tumour burden (Figure 3.10a-b). When Axl is the sole TAM receptor expressed in Tyro3

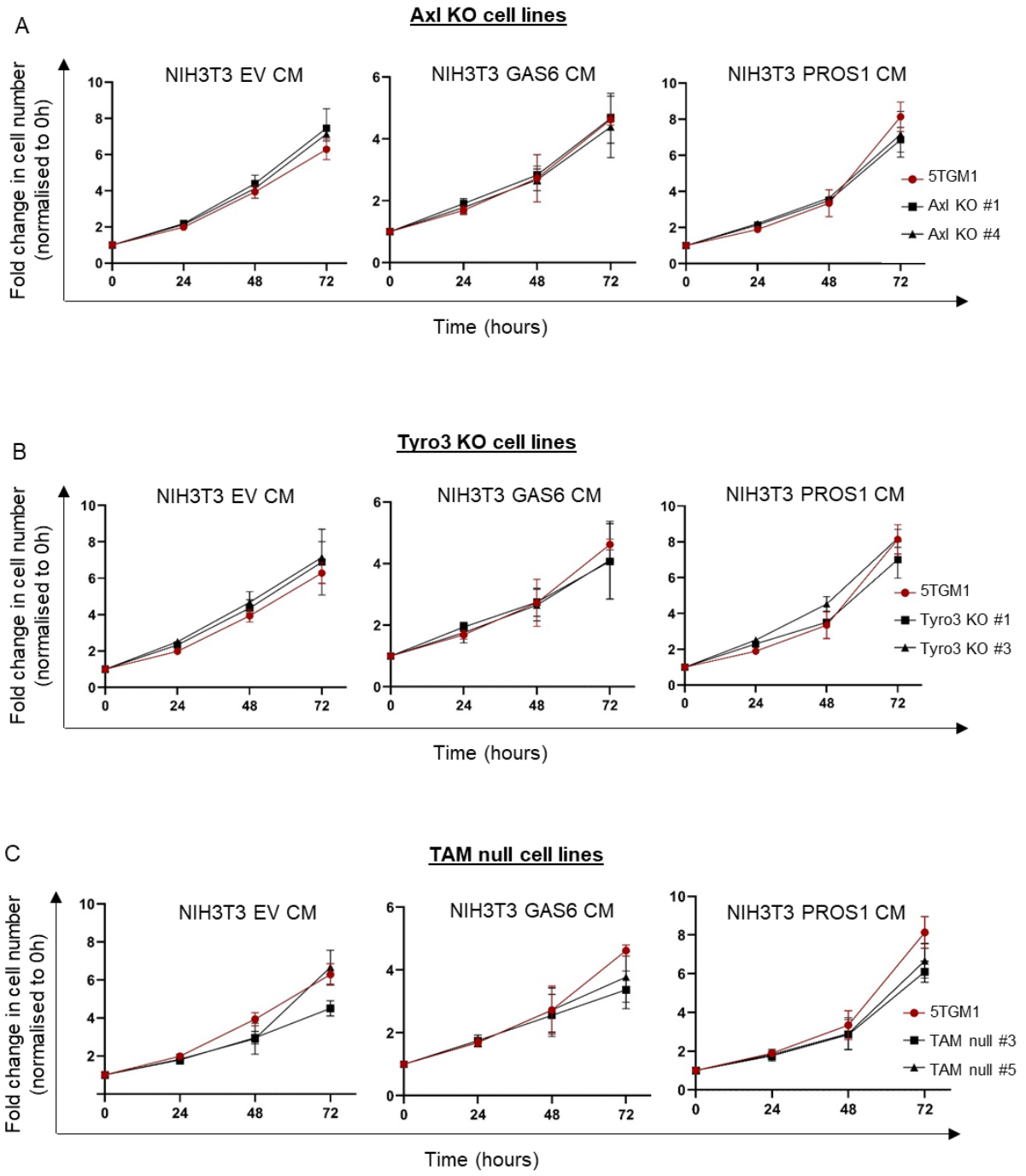

Figure 3.9. There is no difference in proliferation rates of 5TGM1 Axl knockout, Tyro3 knockout or TAM null cell lines compared to the unaltered 5TGM1 cell line. Proliferation of **(A)** 5TGM1 Axl knockout cell lines, **(B)** Tyro3 knockout cell lines and **(C)** TAM null cell lines were compared to unaltered 5TGM1 cells over 72 hours by a WST-1 assay. Cells were cultured in either NIH3T3 empty vector conditioned media (CM) (left), NIH3T3 Gas6 conditioned media (middle) or NIH3T3 Pros1 conditioned media (right). Results were displayed as fold change in absorbance (450nm) over 72 hours. Graphs depict mean ± SEM, *n*=3, two-way ANOVA with Tukey's multiple comparisons.

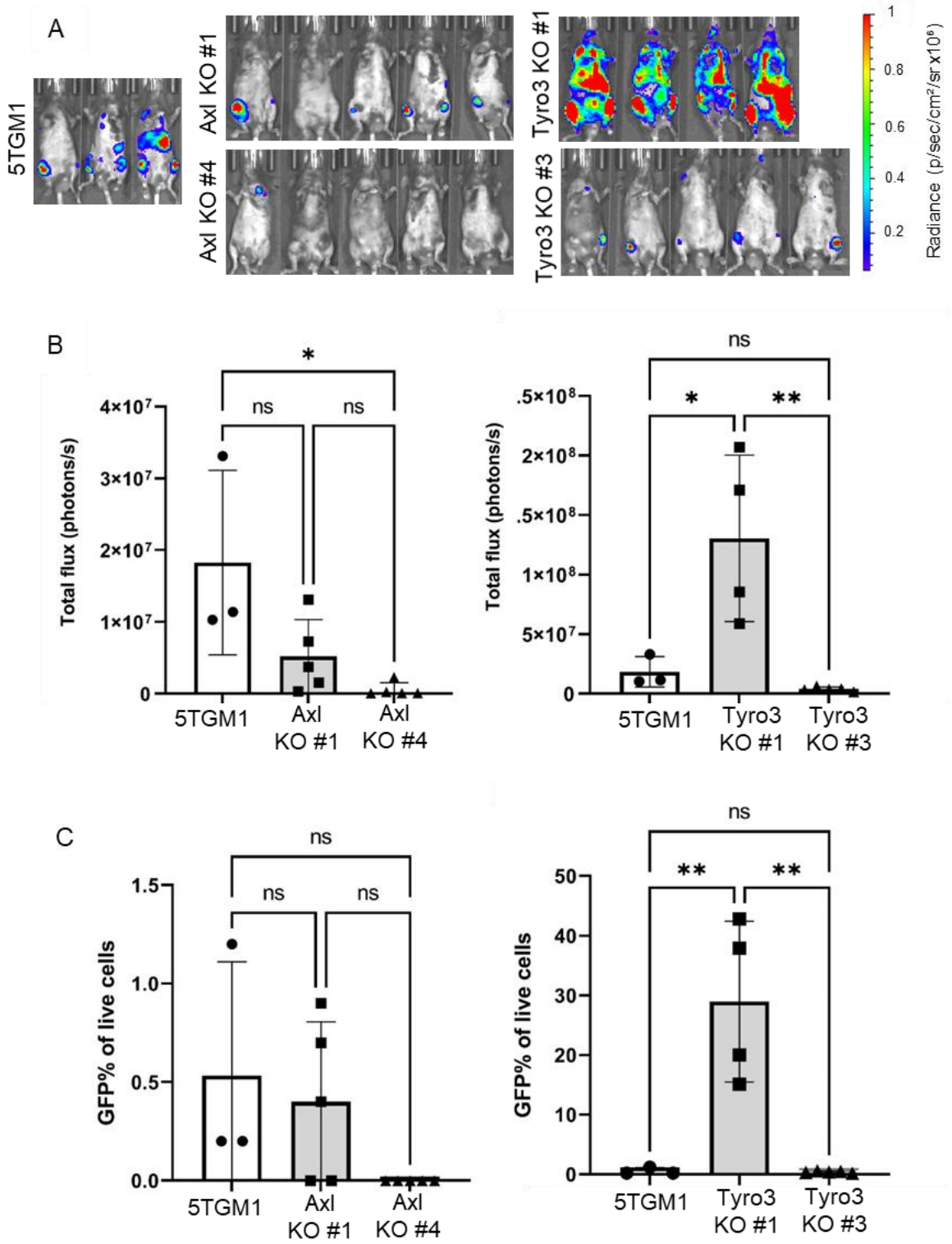
A
5TGM1
Axl KO #1
Axl KO #4
Tyro3 KO #1
Tyro3 KO #3
Radiance (p/sec/cm²/sr x10⁶)
B
Total flux (photons/s)
ns
*
**
5TGM1
Axl KO #1
Axl KO #4
Tyro3 KO #1
Tyro3 KO #3
C
GFP% of live cells

Figure 3.10. Clonal 5TGM1 cell lines with the same Axl or Tyro3 knockout status produce very different tumour burden after 4 weeks in the C57BL/KaLwRij model of MM. KaLwRij mice were inoculated with $5x10^5$ 5TGM1 Axl knockout clonal cell lines #1 and #4 or 5TGM1 Tyro3 clonal knockout cell lines #1 and #3 and disease burden was subsequently monitored by whole animal BLI and flow cytometry.**(A)** Ventral BLI scans depict tumour burden at week 4. **(B)** Graphs of the bioluminescence/total flux at week 4 from ventral scans are shown. **(C)** GFP+ % of live cells from the hind limbs of mice at week 4 is shown. Graphs depict the mean ± SD of *n*=3-5 mice per cell line. One-way ANOVA with Tukey's multiple comparisons.

knockout cell lines, it was anticipated that a dormancy phenotype may be initiated in 5TGM1 cells, resulting in decreased tumour burden. The Tyro3 knockout cell line #1 produced significantly increased tumour burden compared to the unaltered 5TGM1 cell line, whereas the Tyro3 knockout cell line #3 displayed similar levels of tumour burden to the unaltered 5TGM1 cell line (Figure 3.10a,b). This was supported by enumeration of GFP+ 5TGM1 cells in the BM of mice (Figure 3.10c-e). These data suggest significant heterogeneity in tumour burden between different clonal cell lines with the same Axl or Tyro3 knockout status. Therefore, the *in vivo* phenotypes identified using these cells lines may be artefacts of clonal expansion, rather than the biological product of specific receptor expression. In view of these results, it was decided that 5TGM1 single TAM receptor expressing cell lines should be generated from a candidate 5TGM1 TAM null cell line that would be retrovirally transduced with Axl or Mer transgenes.

3.2.11 Identification of a candidate 5TGM1 TAM null cell line to use as a basis for re-expressing the TAM receptors.

5TGM1 Axl or Tyro3 knockout clones, with the same genetic knockout status, produced heterogeneous disease burden *in vivo,* likely due to the effects of clonal expansion. To ensure that the functional studies were not influenced by the effects of clonal expansion, a candidate 5TGM1 TAM null cell line that produced good bilateral tumour burden *in vivo* was identified. This cell line would be used as a basis for generating single TAM receptor expressing 5TGM1 cell lines. 5TGM1 TAM null cell lines #3 and #5 were i.v. inoculated into KaLwRij mice and tumour burden was monitored at weeks 2, 3 and 4 using BLI. Analysis of whole-body ventral BLI scans revealed that 5TGM1 TAM null cell line #3 produced consistent bilateral tumour burden compared to 5TGM1 TAM null cell line #5 (Figure 3.11a-b). This was supported by enumeration of GFP+ cells in the bone marrow of mice (Figure 3.11c).

3.2.12 Generation of single TAM receptor expressing cell lines through retroviral transduction of 5TGM1 TAM null cell line #3 with Axl and Mer transgenes.

To generate a model of single TAM receptor expressing cell lines that was not affected by interclonal heterogeneity in relation to *in vivo* tumour burden, 5TGM1

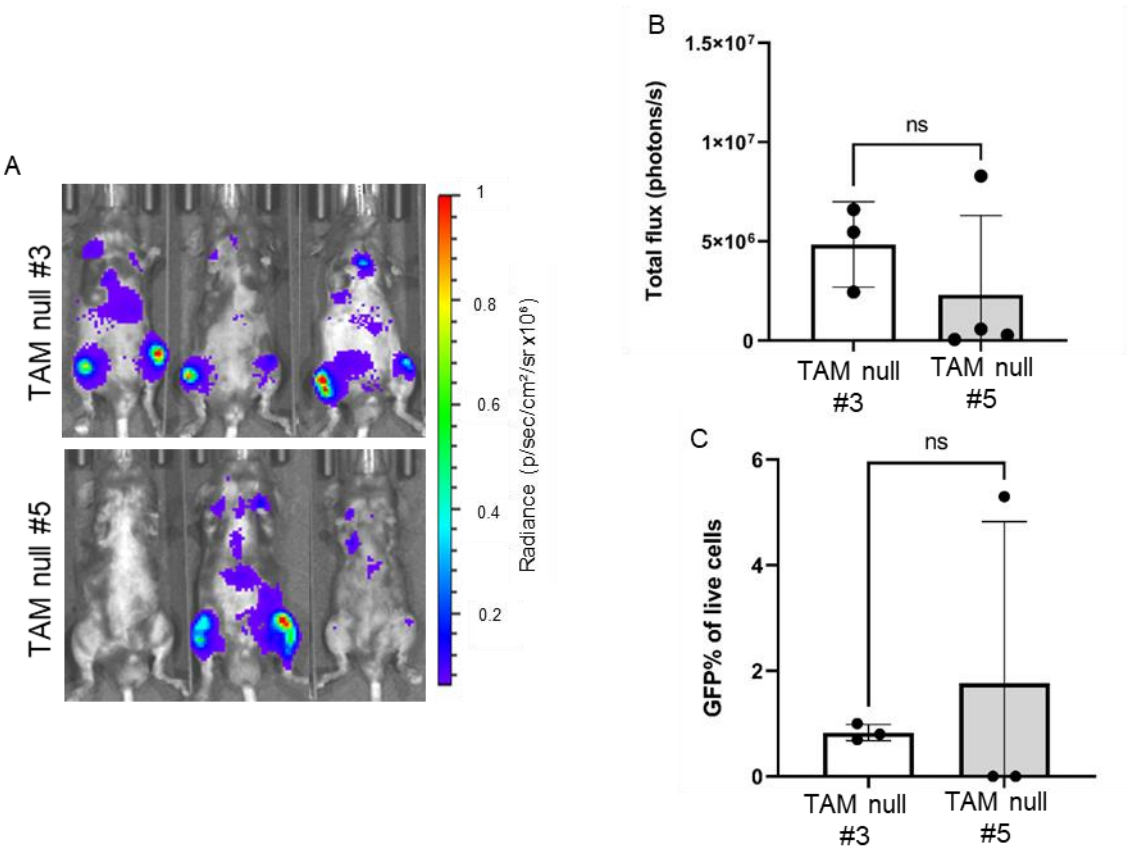

Figure 3.11. Identification of a candidate 5TGM1 TAM null cell line to use as a basis for re-expressing the TAM receptors. KaLwRij mice were inoculated with 5x10⁵ 5TGM1 TAM null clonal cell lines #3 and #5 and subsequent disease burden was monitored by whole animal BLI and flow cytometry. **(A)** Ventral BLI scans depict tumour burden at week 4. **(B)** A graph of the total flux at week 4 from ventral scans is shown. **(C)** GFP+ % of live cells from the hind limbs of mice at week 4 is shown. Graphs depict the mean ± SD of *n*=3 mice per cell line, Student's t-test.

TAM null cell line #3 was used as a target for retroviral mediated expression of either Axl or Mer. The 5TGM1 TAM null cell line was transduced with pRufimCh2 encoding Axl, Mer or the empty vector to generate the 5TGM1 Axl cell line, 5TGM1 Mer cell line and 5TGM1 EV cell line (Figure 3.12a). The 5TGM1 Axl, 5TGM1 Mer and 5TGM1 EV cell lines were sorted for mCherry expression, and double mCherry and GFP expression was confirmed compared to untransfected cells (Figure 3.12b). Flow cytometry was used to assess Axl and Mer expression on the cell surface of 5TGM1 Axl cells and 5TGM1 Mer cells, respectively. Results of staining with an Axl antibody showed that 5TGM1 Axl cells express Axl on the cell surface compared to the 5TGM1 EV cell line (Figure 3.12c). Results of staining with a Mer antibody show that 5TGM1 Mer cells express Mer on the cell surface compared to 5TGM1 EV cells, which display a small amount of background staining (Figure 3.12d).

3.3 Discussion

The TAM family of tyrosine kinase cell surface receptors have been studied in the context of numerous cancers and have been the subject of therapeutic targeting[213, 215]. To this end, a number of Axl, Mer and pan-TAM tyrosine kinase inhibitors and monoclonal antibodies are currently undergoing clinical trials[259]. However, the context-dependent functions of Axl and Mer in myeloma remain poorly understood. Myeloma patient PCs express Mer and Gas6, indicating that the Mer/Gas6 pathway may be important in MM pathogenesis. In contrast, MM patient-derived plasma cells express low or no Axl, Tyro3 and Pros1. This is consistent with Axl being expressed by only a subset of dormant myeloma cells[213] as a proportion of the bulk tumour. Analysis of patient samples using scRNA seq may be more useful to identify subsets of Axl-expressing myeloma cells at single cell resolution. To further understand the role of Axl and Mer expression by MM PCs in promoting myeloma disease progression, a model of single TAM receptor expressing 5TGM1 murine myeloma cell lines was generated.

Initially, CRISPR Cas9 was utilised to generate clonal 5TGM1 Axl and Tyro3 knockout cell lines. A 5TGM1 Tyro3 knockout cell line was then retargeted with an Axl sgRNA-directed CRISPR Cas9 nuclease to generate clonal 5TGM1 TAM null cell lines. Sanger sequencing of clonal cell lines identified insertion/deletion

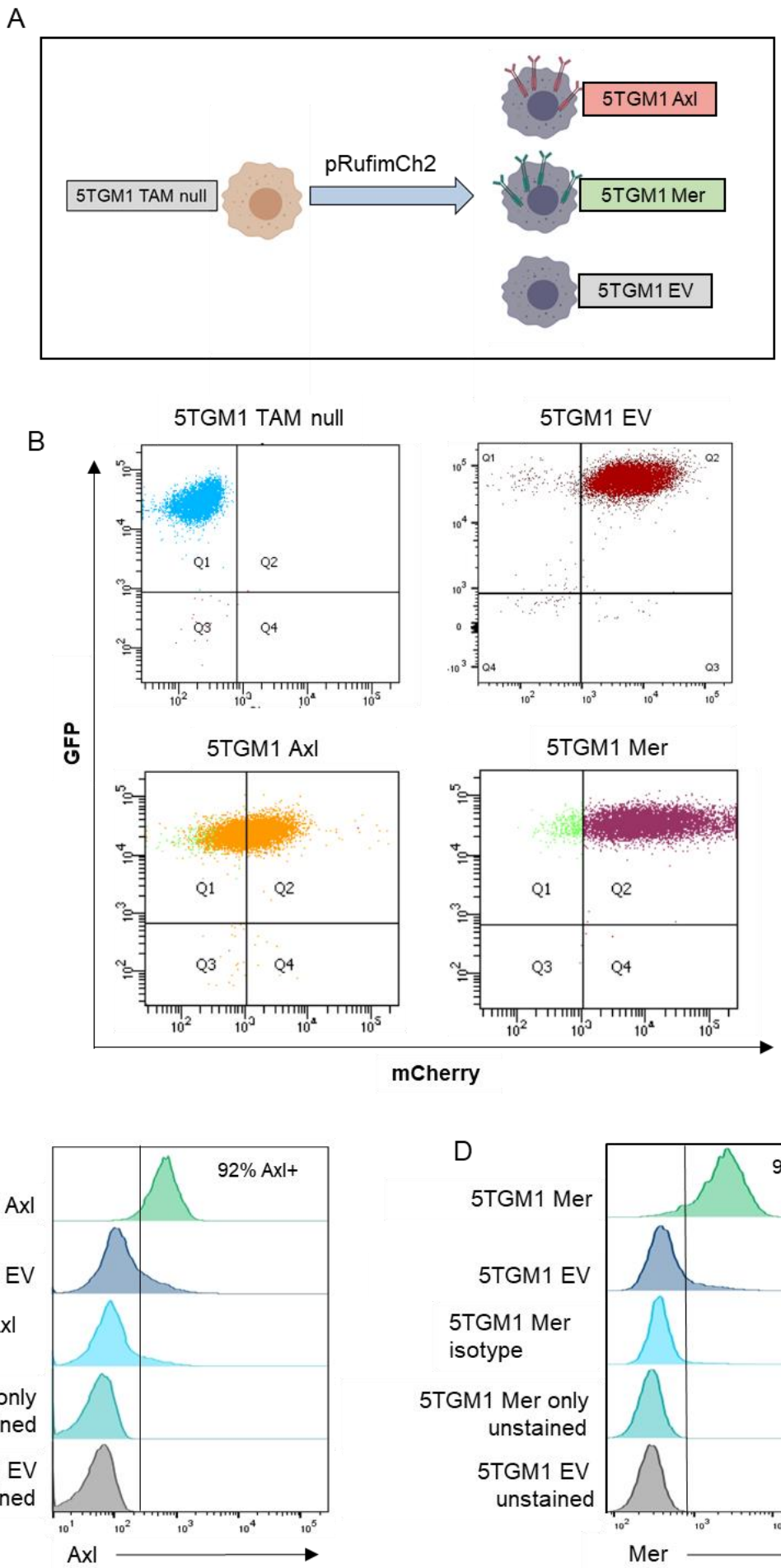
A
5TGM1 TAM null
pRufimCh2
5TGM1 Axl
5TGM1 Mer
5TGM1 EV
B
5TGM1 TAM null
5TGM1 EV
5TGM1 Axl
5TGM1 Mer
Q1
Q2
Q3
Q4
GFP
mCherry
C
92% Axl+
5TGM1 Axl
5TGM1 EV
5TGM1 Axl isotype
5TGM1 Axl only unstained
5TGM1 EV unstained
Axl
D
95% Mer+
5TGM1 Mer
5TGM1 EV
5TGM1 Mer isotype
5TGM1 Mer only unstained
5TGM1 EV unstained
Mer

Figure 3.12. Generation of single TAM receptor expressing cell lines through retroviral transduction of 5TGM1 TAM null cell line #3 with Axl and Mer transgenes. (A) Single Axl and Mer expressing cell lines were generated by retroviral transduction of a candidate 5TGM1 TAM null cell line with gene encoding pRufimCh2 vectors. **(B)** 5TGM1 TAM null cells were transduced with the pRufimCh2.Axl, pRufimCh2.Mer or the empty vector and cells were assessed for GFP and mCherry expression post-sort. **(C)** 5TGM1 Axl and 5TGM1 EV cells were stained with an anti-Axl antibody and analysed by flow cytometry compared to unstained and isotype controls. **(D)** 5TGM1 Mer and 5TGM1 EV cells were stained with an anti-Mer antibody and analysed by flow cytometry compared to unstained and isotype controls.

mutations of Axl or Tyro3 respectively. Many of the mutations produced frameshifts which were associated premature termination codons. Several clones harboured only alleles that would encode severely truncated proteins or mRNA species that may be subject to nonsense-mediated decay. Clonal cell lines expressing no Axl-encoding or Tyro3-encoding protein were identified using either flow cytometry or Western blotting. When 5TGM1 Axl knockout and 5TGM1 Tyro3 knockout cell lines were inoculated into the KaLwRij mouse model, significant heterogeneity in tumour burden was observed in clones with the same genetic Axl or Tyro3 knockout. It was decided that this model could not provide evidence of the true phenotype of TAM receptor knockout. Therefore, a candidate 5TGM1 TAM null cell line that provided consistent bilateral tumour burden *in vivo* was chosen as a basis for expressing Axl and Mer using retroviral transduction. This 5TGM1 TAM null cell line was transduced with Axl, Mer or an empty retroviral vector to generate single TAM receptor expressing cell lines, 5TGM1 Axl and 5TGM1 Mer, and a control cell line expressing no TAM receptors, 5TGM1 EV. NIH3T3 cell lines overexpressing TAM receptor ligands Gas6 and Pros1, and an EV cell line expressing low levels of Gas6 and Pros1 were also generated to provide a source of TAM ligand for *in vitro* experiments. The 5TGM1 Axl, 5TGM1 Mer and 5TGM1 EV cell lines, as well as the Gas6 and Pros1-overexpressing NIH3T3 cell lines, represent the tools that will be utilised throughout this study to explore the specific roles of Axl and Mer in myeloma.

Investigating the biological functions of Axl in cancer using CRISPR-Cas9 mediated Axl knockout cell lines has been performed in recent studies[185, 187]. CRISPR-Cas9 offers complete receptor knockout compared to targeting with shRNA or siRNA[243], and greater specificity in ablating genes of interest in MM PCs compared to the systemic use of an inhibitor. Therefore, in the current study it was decided to use the CRISPR Cas9 system to generate a model of single TAM receptor expressing 5TGM1 cell lines. However, significant interclonal heterogeneity in *in vivo* tumour burden between 5TGM1 Axl and Tyro3 knockout clones was identified. This result emphasises the potential variability that can arise from the process of clonal expansion of a cell line from a single progenitor cell. This process is subject to selection pressures that may produce undesired genetic and epigenetic alterations in the cell line, resulting in a biological phenotype independent of the gene of interest[260]. Future studies using single-cell clonal expansion of CRISPR-Cas9

knockout clones should derive multiple independent knockout clones to ensure that the result are not reflective of artefacts of clonal expansion. An alternative to the isolation of single cells to generate clones is the use of a pooled population of cells that have been successfully transfected with the CRISPR vector[243]. Provided that sgRNA targeting is efficient, gene expression can be significantly reduced in the pooled cell line. However, due to the inefficient targeting of the two Axl sgRNAs designed for this study, sgRNA targeting of Axl would need to be revised. Rescue experiments could have also been conducted in which Axl was re-expressed in a clonal Axl knockout cell line using retroviral transduction[261]. This should reverse the phenotype observed when Axl is knocked out, showing that the Axl knockout is the true cause of the phenotype, rather than an artefact of clonal expansion.

The 5TGM1 Axl, 5TGM1 Mer and 5TGM1 EV cell lines produced in this chapter are novel resources that will complement the findings of previous studies. Firstly, 5TGM1 cell lines can be inoculated into both the KaLwRij immune competent murine model of MM and the NSG immune compromised model. Therefore, the immune mediated effects of Mer expression on myeloma tumour burden can be investigated for the first time using 5TGM1 Mer and 5TGM1 EV cell lines. Secondly, the 5TGM1 Axl and the 5TGM1 EV cell line should enable the identification of whether high Axl expression alone is sufficient to initiate features of myeloma dormancy *in vitro* and *in vivo*. The studies in the following chapters will utilise 5TGM1 Mer, 5TGM1 Axl and 5TGM1 EV cell lines to understand the functions of Axl and Mer expression in myeloma. These studies will identify whether there may be therapeutic benefit in targeting Axl or Mer expressed by MM patient PCs.

4. Axl expression does not drive multiple myeloma cellular dormancy

4.1 Introduction

Multiple myeloma (MM) is a fatal haematological malignancy with a 5-year survival rate of 54.9%[6]. Despite the success of treatments such as proteasome inhibitors, immunomodulatory imide drugs (IMiDs), autologous stem cell transplant (ASCT), and monoclonal antibodies targeting SLAMF7 and CD38[53], almost all MM patients will inevitably relapse. Disease relapse is common in many cancers, notably breast and prostate cancer patients are known to experience relapse up to decades following removal of the primary tumour. This is indicative of cancer cells disseminating early in the disease course from the primary site to secondary sites, often within the bone marrow, where they reside long term in a 'dormant' state[262, 263]. MM relapse is also thought to arise from dormant subpopulations of MM PCs that evade targeting by the immune system and therapeutics, and persist long term in specialised BM niches as Minimal Residual Disease (MRD)[212, 264]. Dormant MM PCs can become reactivated, giving rise to clinical relapse[265] that can be driven the expansion of a single clonal initiating cell[266], or by the expansion of PCs at multiple skeletal sites. Dormant MM PCs are difficult to detect and target clinically, and the mechanisms of MM PC dormancy and reactivation remain poorly understood. Despite the advent of novel targeted therapies, frequent relapses in myeloma patients threaten the potential to achieve long term remission. Therefore, identifying the mechanisms of MM PC dormancy initiation and subsequent reactivation is essential to therapeutic targeting of dormant cells to prevent disease relapse.

Dormant cells are niche dependant, and in MM, and metastatic prostate cancer and breast cancer, cells disseminate to multiple sites throughout the skeleton, engage with specialised niches, and become dormant[129, 267, 268]. After arriving at the niche, dormant cancer cells are typically growth arrested in the G0 phase of the cell cycle, and enter a state of mitotic and metabolic quiescence and do not proliferate[212]. They are able to evade cytotoxic chemotherapy[129] as well as the host immune system[269], allowing them to persist long term in a dormant state. However, cellular dormancy is reversible, and cells can become reactivated, re-enter the cell cycle, and begin actively proliferating. Studying dormant myeloma cells and their interactions with the bone marrow microenvironment *in vivo* is technically challenging, however the 5TGM1/KaLwRij murine model of myeloma has proven to be an invaluable resource. To this end, Lawson, *et. al.,* labelled 5TGM1 mouse myeloma cells with a lipophilic membrane DiD label, identifying non-proliferative cells that retained the

DiD label as a DiD^{hi} dormant population[129]. DiD labelled 5TGM1 cells were i.v. inoculated into C57BL/KaLwRij mice and their colonisation of bone marrow niches was monitored using intravital two-photon microscopy. 5TGM1 cells colonised the endosteal niche, where they underwent growth arrest and retained the DiD label long term. Subsequent treatment of the mice with osteoclast activation factor sRANKL increased osteoclast activity and remodelling of the endosteal niche, displacing 5TGM1 DiD^{hi} cells from the niche. This process effectively released 5TGM1 cells from dormancy, resulting in increased bone marrow tumour burden and a reduced proportion of DiD^{hi} 5TGM1 cells as assessed by flow cytometry. Furthermore, 5TGM1 cells co-cultured with the MC3T3 pre-osteoblastic cell line retained the DiD label compared to 5TGM1 cells in monoculture. Taken together, these suggest that crosstalk between 5TGM1 cells and cells of the endosteal niche, such as osteoblasts, support tumour cell dormancy.

Using scRNAseq technologies to compare the transcriptome of dormant 5TGM1 DiD^{hi} cells and reactivated 5TGM1 DiD^{neg} cells revealed a specific dormancy transcriptome signature[213]. Genes highly expressed by dormant 5TGM1 cells harvested from the BM of mice included transcription factors *Irf7* and *Spic*, and adhesion molecules and receptors *Vcam1*, *Axl*, *Fcerg1*, *Mpeg1*, and *Sirpa*. 5TGM1 cell dormancy was induced *in vitro* by contact co-culture with MC3T3 cells, which also resulted in the induction of, and increased mRNA expression of these dormancy-associated genes. As *Axl* was one of the most highly upregulated genes expressed by dormant 5TGM1 cells, it was selected for targeting *in vivo* using a small molecule inhibitor, BMS-777607. Treatment with BMS-777607 in the KaLwRij/5TGM1 model of myeloma significantly reduced the proportion of 5TGM1 DiD^{hi} cells and increased tumour burden. Notably, BMS-777607 was initially marketed as a Met kinase inhibitor[214], and has recently shown efficacy in targeting other TAM receptors Tyro3 and Mer[215], and the receptor tyrosine kinase Ron[216]. Therefore, treatment with BMS-777607 *in vivo* has the ability to target Axl, Tyro3, Mer, Met and Ron on 5TGM1 cells, in addition to Axl expressed by macrophages[217], and Met expressed by osteoblasts[218], cells that form part of the myeloma supportive tumour microenvironment. Interestingly, high Axl expression in prostate cancer cell lines was sufficient to induce dormancy of disseminated prostate cancer cells in the bone marrow of mice[185, 206, 207], warranting the investigation of whether Axl

expressed by MM PCs promotes myeloma dormancy. Consequently, the aim of the studies detailed in this chapter was to determine whether high Axl expression in MM cancer cells is sufficient to drive MM cellular dormancy.

To investigate whether Axl expression alone, was sufficient to initiate MM dormancy, this study utilised 5TGM1 Axl positive (5TGM1 Axl) and 5TGM1 Axl negative (5TGM1 EV) cell lines. Notably, these cells were engineered to express no other TAM receptors. If Axl expression was able to induce MM PC dormancy, it would be anticipated that 5TGM1 Axl cells would exhibit the hallmarks of dormancy compared to 5TGM1 EV cells. It was hypothesised that 5TGM1 Axl cells would exhibit decreased cell proliferation, accumulation in the G0/G1 phases of the cell cycle, increased DiD dye retention and reduced tumour burden *in vivo* compared to the 5TGM1 EV cell line. In this chapter, 5TGM1 Axl and 5TGM1 EV cell lines were evaluated for their *in vitro* proliferation and cell cycle distribution in response to TAM-ligand enriched conditioned media. Additionally, 5TGM1 Axl and 5TGM1 EV cell lines were DiD labelled and dye retention was monitored when cells were cultured in MC3T3 conditioned media or in direct contact co-culture. The 5TGM1 Axl and 5TGM1 EV cell lines were inoculated both i.v. and i.t. into the KaLwRij model of MM, and the effects of Axl expression on tumour burden was assessed.

4.2 Results

4.2.1 Axl expression has no effect on 5TGM1 cell proliferation.

Given that reduced cell proliferation is a feature of cellular dormancy[270], it was hypothesised that Axl expression may confer a reduction in 5TGM1 cell proliferation in short term proliferation assays. As shown in Figure 4.1a, no difference in proliferation between 5TGM1 Axl and 5TGM1 EV cells was observed when cultured in serum-supplemented IMDM media. Similarly, 5TGM1 Axl and 5TGM1 EV cells also displayed no difference in proliferation when cultured in NIH3T3 EV control conditioned IMDM media (Figure 4.1b), which contains low levels of Gas6 and Pros1 (see Chapter 2, section 2.2.4.2 for NIH3T3 cell line construction). 5TGM1 Axl and 5TGM1 EV cells were then cultured in NIH3T3 Gas6 or NIH3T3 Pros1 conditioned IMDM media enriched for TAM-ligands Gas6 (Figure 4.1c) or Pros1 (Figure 4.1d), and no difference in cell proliferation was detected.

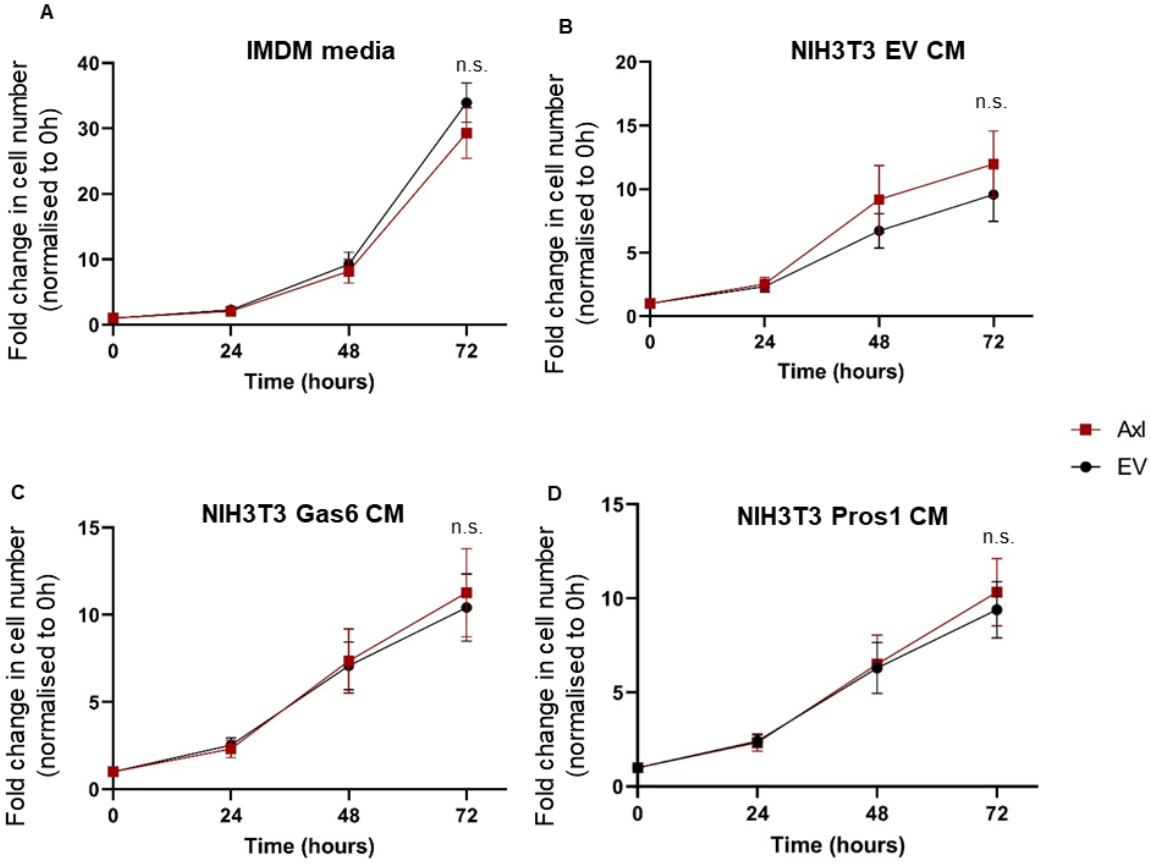

Figure 4.1. Axl expression has no effect on 5TGM1 cell proliferation. Proliferation of 5TGM1 Axl cells was compared to that of 5TGM1 EV cells over 72 hours by WST-1 assay. Cells were cultured in either **(A)** IMDM media, **(B)** NIH3T3 EV conditioned media (CM) or NIH3T3 CM enriched for TAM ligands **(C)** Gas6, or **(D)** Pros1. Results were displayed as fold change in absorbance (450nm) over 72 hours. Results are shown as the mean ± SEM of three independent experiments performed in triplicate, two-way ANOVA with Tukey's multiple comparisons.

4.2.2 Axl expression has no effect on 5TGM1 cell cycle distribution.

Cell cycle arrest in G0 is another hallmark feature of cancer cell dormancy[129, 271], in which cells exit the cell cycle and remain in a state of metabolic and mitotic quiescence. It was hypothesised that 5TGM1 Axl cells would have a significantly increased proportion of cells in phase G0 compared to 5TGM1 EV cells. Cells in G0 have low DNA and RNA content, which can be identified using double Hoechst and Pyronin Y staining (Figure 4.2a). Cell cycle analysis was performed in IMDM complete media (Figure 4.2b), or in response to NIH3T3 Gas6 (Figure 4.2c) or NIH3T3 Pros1 (Figure 4.2d) ligand enriched conditioned media. Under all media conditions no significant differences were seen in the proportions of cells in any of the phases of the cell cycle between 5TGM1 Axl and 5TGM1 EV cells.

4.2.3 Axl expression has no effect on 5TGM1 cell DiD dye retention.

Labelling cells using the heritable membrane dye DiD can be used as a method to identify dormant, non-proliferating cells, which retain the DiD label (DiD^{hi}), compared to actively proliferating cells, which undergo membrane dye dilution (DiD^{neg})[129]. 5TGM1 Axl and 5TGM1 EV cell lines were labelled with DiD, and it was hypothesised that there would be a significantly higher proportion of GFP+ DiD^{hi} 5TGM1 Axl cells compared to GFP+ DiD^{hi} 5TGM1 EV cells over time. However, when cells were cultured in IMDM media, there were no differences in DiD dye retention over 10 days (Figure 4.3a). To simulate 5TGM1 cell engagement with endosteal niche cells *in vivo* such as Gas6-expressing osteoblasts 5TGM1 Axl and 5TGM1 EV cells were DiD labelled and co-cultured with the pre-osteoblastic MC3T3 cell line, recapitulating experiments conducted by Lawson, *et al.,*[129] and Khoo, *et.al.,*[213]. It was hypothesised that Gas6 signalling through Axl under direct co-culture conditions would suppress the growth of 5TGM1 Axl cells, resulting in a significantly increased GFP+ DiD^{hi} population compared to 5TGM1 EV cells. However, under direct co-culture conditions, 5TGM1 cell growth was suppressed completely, regardless of Axl expression, and all cells retained the DiD dye over 7 days (Figure 4.3b). Therefore, it was not possible to compare DiD dye retention in 5TGM1 Axl cells and 5TGM1 EV cells in direct co-culture with MC3T3 cells. As an alternative to direct co-culture, the 5TGM1 cell lines were cultured in MC3T3 conditioned media. However, there were no differences in DiD dye retention

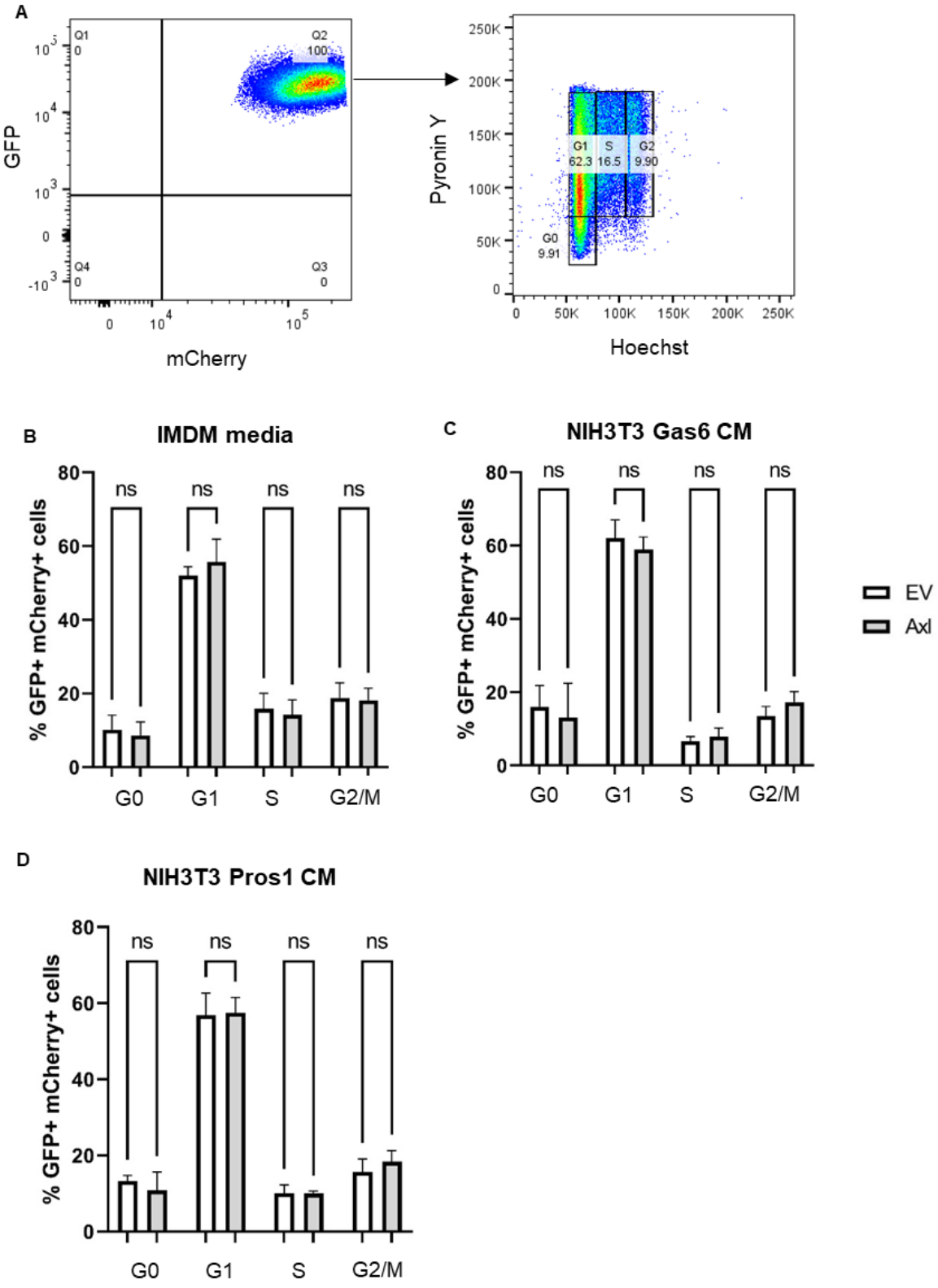
A
Q1
0
Q2
100
Q4
0
Q3
0
GFP
mCherry
Pyronin Y
Hoechst
G1
62.3
S
16.5
G2
9.90
G0
9.91
B
IMDM media
C
NIH3T3 Gas6 CM
D
NIH3T3 Pros1 CM
% GFP+ mCherry+ cells
ns
G0
G1
S
G2/M
EV
Axl

Figure 4.2. Axl expression has no effect on 5TGM1 cell cycle distribution. Cell cycle analysis was conducted using 5TGM1 Axl compared to 5TGM1 EV cells, including isolation of the G0 population**. (A)** A representative plot of GFP+ mCherry+ 5TGM1 EV cells (left), and the gating strategy for cell cycle analysis of the Hoechst and Pyronin Y stained GFP+ mCherry+ population (right). Cell cycle analysis was performed, comparing 5TGM1 Axl and 5TGM1 EV cells following overnight culture in **(B)** IMDM media, or NIH3T3 conditioned media (CM) enriched for TAM ligands **(C)** Gas6 and **(D)** Pros1. . Results are shown as the mean ± SEM of three independent experiments, Students t-test.

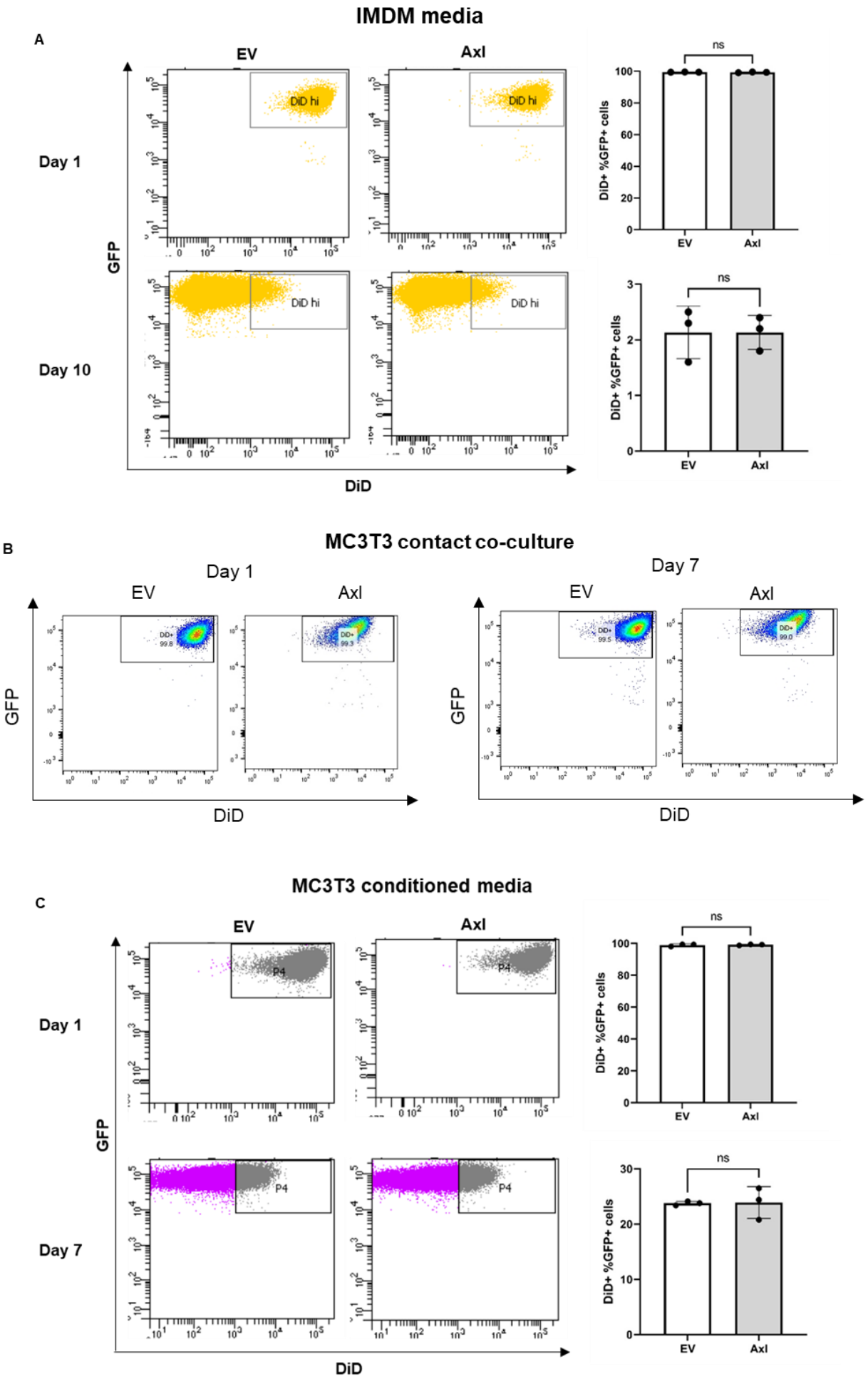
IMDM media
A
EV
Axl
Day 1
Day 10
GFP
DiD
DiD hi
ns
DiD+ %GFP+ cells
B
MC3T3 contact co-culture
Day 1
Day 7
C
MC3T3 conditioned media
P4

Figure 4.3. Axl expression has no effect on 5TGM1 cell DiD dye retention. 5TGM1 Axl cells and 5TGM1 EV cells were DiD labelled and DiD dye retention was monitored using flow cytometry. 5TGM1 cells were either maintained in monoculture, contact co-culture with MC3T3 pre-osteoblastic cells, or in MC3T3 conditioned media. **(A)** Representative flow cytometry plots of DiD retention in GFP+ 5TGM1 EV and 5TGM1 Axl cells on Day 1 and Day 10 when cultured in IMDM media are shown (left). Graphs depict the percentages of GFP+ DID+ cells (right), from three independent biological replicates. **(B)** Flow cytometry plots of DiD retention in GFP+ 5TGM1 EV and 5TGM1 Axl cells in contact co-culture with MC3T3 cells on Day 1 and Day 7 are shown, *n*=1. **(C)** Representative flow cytometry plots of DiD retention in GFP+ 5TGM1 Axl and 5TGM1 EV cells when cultured in MC3T3 conditioned media on Day 1 and Day 7 (left). Graphs depict the percentages of GFP+ DiD+ cells (right), from three independent biological replicates. All data was presented as mean ± SD, Student's t-test.

between 5TGM1 Axl and 5TGM1 EV cells cultured in MC3T3 conditioned media over 7 days (Figure 4.3c).

4.2.4 Axl expression has no effect on tumour burden in the KaLwRij model of MM.

To assess whether Axl expression induces a dormancy phenotype *in vivo*, 5TGM1 Axl and 5TGM1 EV cell lines were i.v. inoculated into KaLwRij mice and tumour burden was monitored at weeks 2, 3 and 4 using BLI. It was hypothesised that if high Axl expression could initiate features of cellular dormancy *in vivo,* such as cell cycle arrest and reduced cell proliferation, mice inoculated with 5TGM1 Axl cells would have reduced tumour burden compared to mice inoculated with 5TGM1 EV cells. Analysis of whole body ventral BLI scans from week 4 (Figure 4.4a-b), as well as hind limb only scans (Figure 4.4c) revealed that 5TGM1 Axl cells displayed a trend towards greater tumour burden *in vivo* compared to 5TGM1 EV cells, however this effect did not reach statistical significance (p=0.095, unpaired t-test). This was confirmed by flow cytometric analysis of GFP+ tumour cells as a percentage of total bone marrow cells (Figure 4.4d). SPEP results supported results from BLI scans and flow cytometric analysis of GFP (Figure 4.4e). These results indicate that Axl expression does not reduce *in vivo* tumour burden by promoting features of cellular dormancy.

4.2.5 Axl cell surface expression is maintained by the majority of GFP+ BM cells 4 weeks post i.v. inoculation with 5TGM1 Axl cells.

Axl cell surface expression, assessed by flow cytometry in the unaltered 5TGM1 cell line, was found to fluctuate at different cell culture densities (data not shown). Therefore, it was hypothesised that Axl cell surface expression may be lost after 4 weeks *in vivo*, preventing dormancy initiation. To investigate this, 5TGM1 Axl cells were analysed for Axl cell surface expression at the time of injection after being cultured *in vitro*, and after 4 weeks *in vivo*, with 5TGM1 EV cells used as a negative control (Figure 4.5a-c). Results indicated that Axl expression was significantly higher in 5TGM1 Axl cells cultured *in vitro* compared to 5TGM1 Axl cells harvested from mouse hind limbs after 4 weeks (****p<0.0001, One-way ANOVA with Tukey's multiple comparisons). However, Axl expression was maintained in the majority of

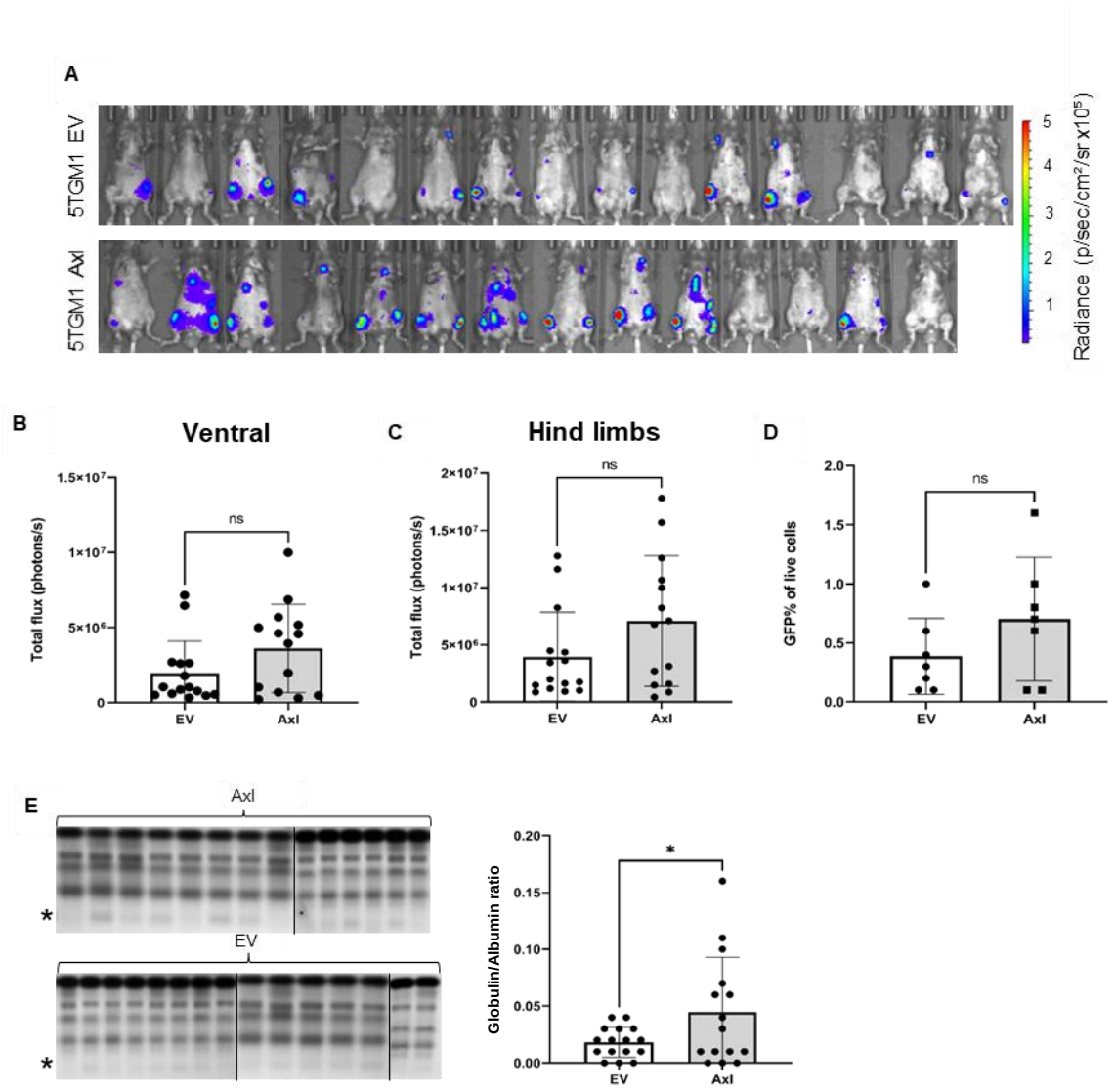

Figure 4.4. Axl expression has no effect on tumour burden in the KaLwRij model of MM. KaLwRij mice were inoculated with 5x10⁵ 5TGM1 EV cells or 5TGM1 Axl only cells and disease burden was monitored by whole animal BLI, serum paraprotein electrophoresis and flow cytometry. **(A)** Ventral BLI scans depict tumour burden at week 4. A graph of the total flux at week 4 from **(B)** ventral and **(C)** hind limb only scans are shown. **(D)** GFP+ % of live cells from the hind limbs of mice at week 4 is shown (*n*=7 mice/group) **(F)** Serum was collected from the mice after four weeks and the M-spikes were measured by SPEP. M-spikes (*) on the SPEP gel (left) and the quantitated Globulin/Albumin ratio (right) are shown. Black lines indicate separation between different gels. Graphs depict the mean ± SD of *n*=14-15 mice per cell line, Student's t-test.

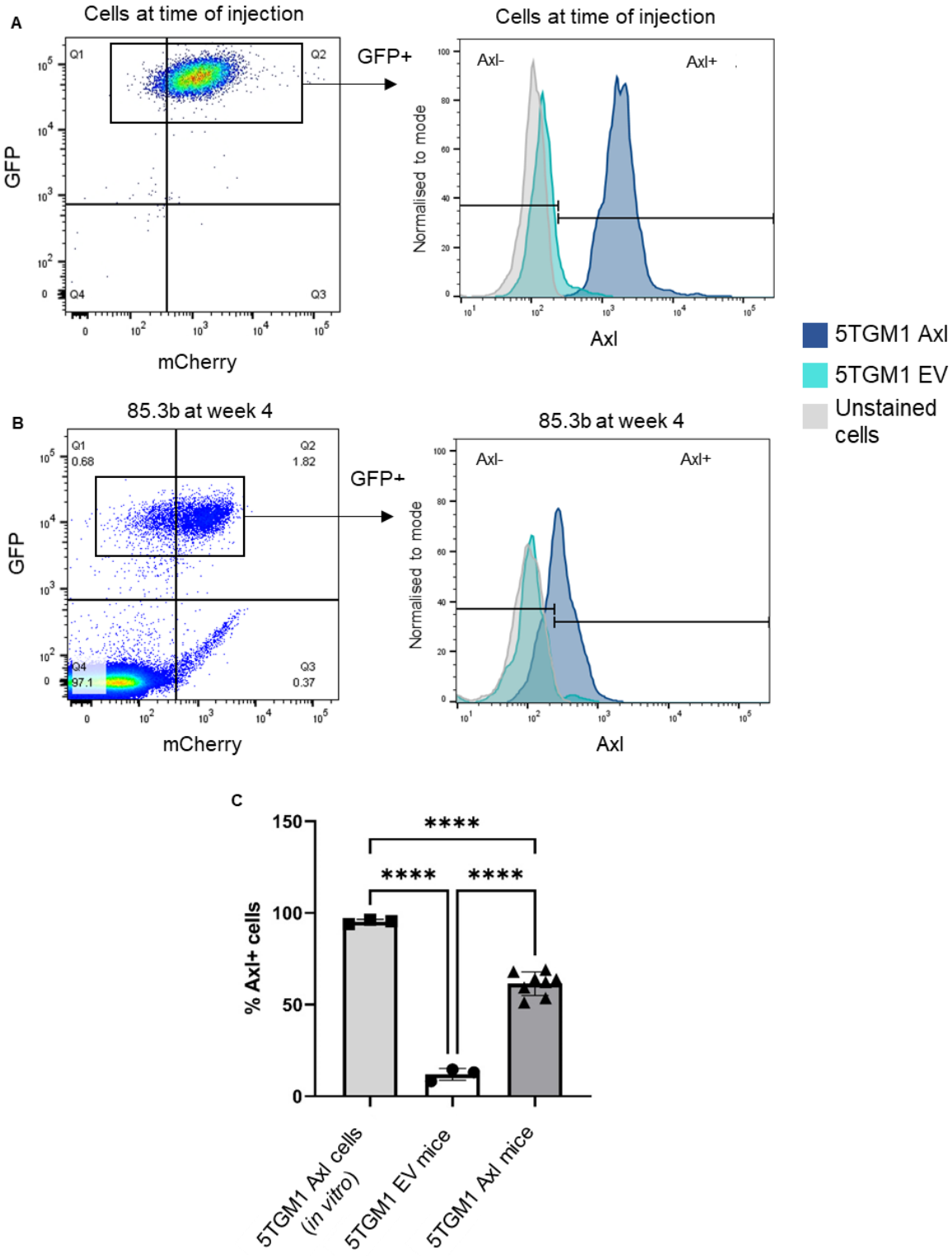
A
Cells at time of injection
Q1
Q2
Q4
Q3
GFP
mCherry
GFP+
Cells at time of injection
Axl-
Axl+
Normalised to mode
Axl
5TGM1 Axl
5TGM1 EV
Unstained cells
B
85.3b at week 4
Q1
0.68
Q2
1.82
Q4
97.1
Q3
0.37
GFP
mCherry
GFP+
85.3b at week 4
Axl-
Axl+
Normalised to mode
Axl
C
% Axl+ cells
150
100
50
0
****
****
****
5TGM1 Axl cells (in vitro)
5TGM1 EV mice
5TGM1 Axl mice

Figure 4.5. Axl cell surface expression is maintained by the majority of GFP+ BM cells 4 weeks post i.v. inoculation with 5TGM1 Axl cells. Cell surface expression of Axl was evaluated in 5TGM1 Axl cells cultured in IMDM media and in 5TGM1 Axl cells harvested from the hind limb BM of KaLwRij mice after 4 weeks of tumour growth. **(A)** A representative FACS plot depicts GFP+ 5TGM1 Axl cells cultured in IMDM media (left). A histogram depicts Axl expression in 5TGM1 Axl cells compared to 5TGM1 EV cells and unstained cells cultured in IMDM media (right). C57BL/KaLwRij mice were inoculated with $5x10^5$ 5TGM1 EV cells or 5TGM1 Axl only cells. Plots are representative of three independent biological replicates. **(B)** A representative FACS plot depicts GFP+ 5TGM1 Axl cells harvested from the BM of KaLwRij mice 4 weeks after injection (left). At the week 4 experimental endpoint Axl expression in GFP+ BM cells from a single mouse (ID 85.3b) was assessed compared to GFP+ cells from a 5TGM1 EV inoculated mouse and unstained controls. **(C)** Graph depicts the percentage of GFP+ cells that are Axl+, either directly from in vitro cultures (left), or harvested from the hind limbs of mice inoculated with 5TGM1 Axl cells (*n*=8) or 5TGM1 EV cells (*n*=3). Data was presented as mean ± SD, One-way ANOVA with Tukey's multiple comparisons, ****p<0.0001.

5TGM1 Axl cells harvested from mouse hind limbs after 4 weeks, with a mean percentage of Axl+ cells 61.41±6.37 (SD). Therefore, the loss of Axl expression did not account for the lack of dormancy induction in the i.v. KaLwRij model of MM.

4.2.6 Axl expression has no effect on BM homing of 5TGM1 cells *in vivo*.

It was hypothesised that the trend towards increased tumour burden when 5TGM1 Axl cells were inoculated into the KaLwRij model may be due to enhanced BM homing ability of 5TGM1 Axl cells compared to 5TGM1 EV cells. This enhanced ability to home to the bone marrow may increase rates of successful tumour engraftment and overall tumour burden. To determine whether the KalwRij tumour model results could be explained by a BM homing advantage in 5TGM1 Axl cells compared to 5TGM1 EV cells, a 24 hour BM homing assay was conducted. 5TGM1 Axl and 5TGM1 EV cells were i.v. inoculated into mice, and GFP+ cells from the hind limb BM were enumerated by flow cytometry compared to a GFP 'spiked' BM control (Figure 4.6a). Results indicated that there was no difference in the percentage of GFP+ cells detected in BM from mice inoculated with 5TGM1 Axl cells compared with BM from mice inoculated with 5TGM1 EV cells (Figure 4.6b).

4.2.7 Axl expression has no effect on the growth of primary or secondary tumours following i.t. injection of cells.

Rather than intravenously inoculating KaLwRij mice with 5TGM1 Axl and 5TGM1 EV cells, cells were injected directly into the tibiae of KaLwRij mice, bypassing the BM homing mechanism. Analysis of ventral BLI scans of the injected leg after 3 weeks revealed no difference in tumour burden between mice inoculated with 5TGM1 Axl cells and mice inoculated with 5TGM1 EV cells (Figure 4.7a-b). Moreover, there was no difference in metastatic tumour burden in the non-injected leg between mice inoculated with 5TGM1 Axl cells and mice inoculated with 5TGM1 EV cells (Figure 4.7a,c). These findings were confirmed by flow cytometric analysis of GFP+ tumour cells as a percentage of total bone marrow cells in the injected and non-injected legs (Figure 4.7d-e). SPEP results also supported results from BLI scans and flow cytometric analysis of GFP (Figure 4.7f).

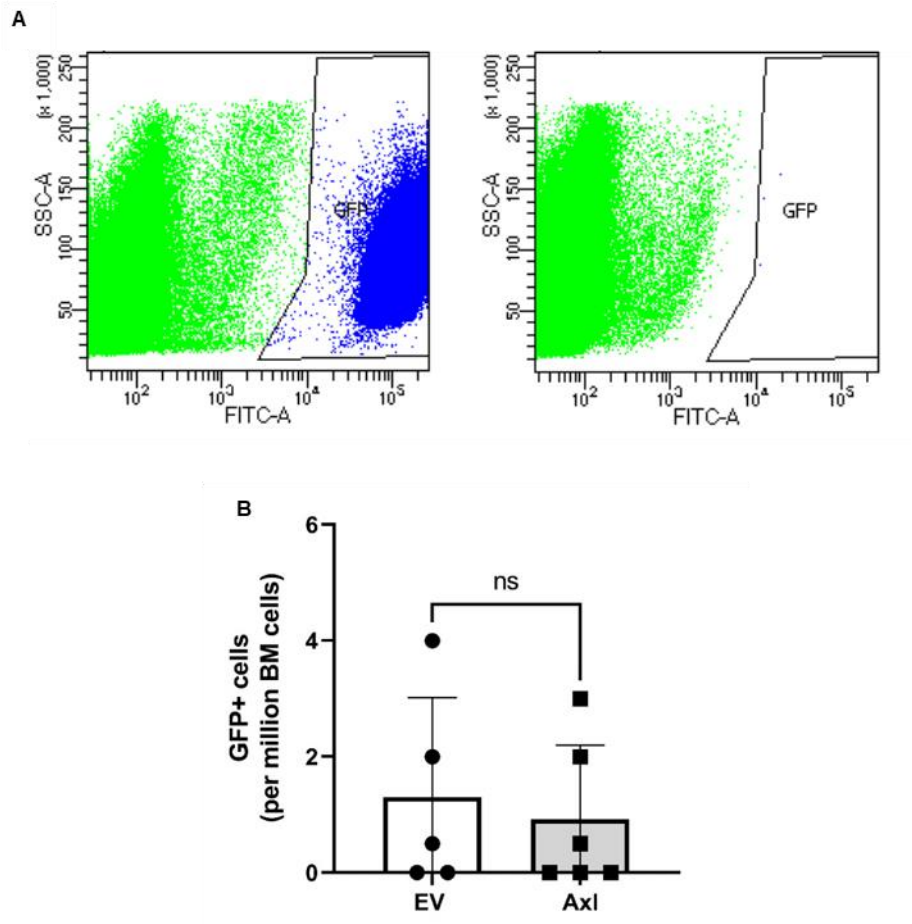

Figure 4.6. Axl expression has no effect on the BM homing of 5TGM1 cells *in vivo*. C57BL/KaLwRij mice were inoculated with 5x10⁶ 5TGM1 Axl or 5TGM1 EV cells, and 24 hours later were humanely culled, and GFP+ cells were assessed in hind limb BM. **(A)** Representative FACS plots showing GFP+ % of live cells from the hind limbs of a single mouse inoculated with 5TGM1 EV cells (right) compared to mouse BM 'spiked' with GFP+ cells (left). **(B)** The number of GFP+ cells was compared between mice inoculated with 5TGM1 Axl only and EV cells. Graphs depict the mean ± SEM of n=6 mice per cell line, Student's t-test.

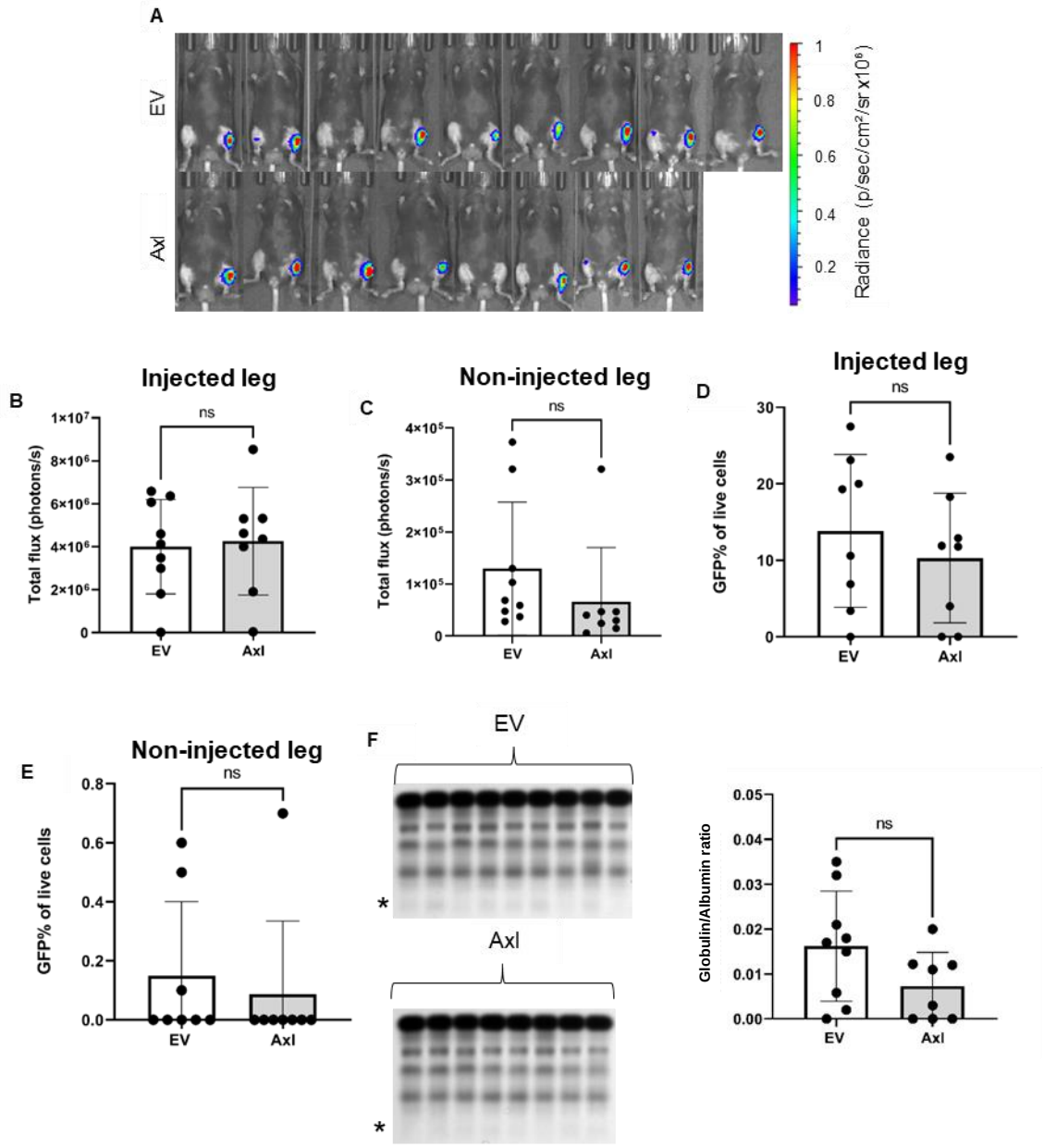
A
EV
Axl
1
0.8
0.6
0.4
0.2
Radiance (p/sec/cm²/sr x10⁶)
B
Injected leg
ns
Total flux (photons/s)
1×10⁷
8×10⁶
6×10⁶
4×10⁶
2×10⁶
0
EV
Axl
C
Non-injected leg
ns
Total flux (photons/s)
4×10⁵
3×10⁵
2×10⁵
1×10⁵
0
EV
Axl
D
Injected leg
ns
GFP% of live cells
30
20
10
0
EV
Axl
E
Non-injected leg
ns
GFP% of live cells
0.8
0.6
0.4
0.2
0.0
EV
Axl
F
EV
*
Axl
*
Globulin/Albumin ratio
ns
0.05
0.04
0.03
0.02
0.01
0.00
EV
Axl

Figure 4.7. Axl expression has no effect on the growth of primary or secondary tumours following i.t. injection of cells. C57BL/KaLwRij mice were inoculated intratibially with 1x10^5 5TGM1 EV cells or 5TGM1 Axl cells and disease burden was monitored by whole animal BLI, serum paraprotein electrophoresis and flow cytometry. **(A)** Ventral BLI scans depict tumour burden at 3 weeks. A graph of the total flux at 3 weeks from **(B)** the injected leg and **(C)** the non-injected leg are shown. GFP+ % of live cells from the **(D)** injected tibiae and **(E)** non-injected leg of mice after 3.5 weeks is shown. **(F)** Serum was collected from the mice after 3 weeks and the M-spikes were measured by SPEP. M-spikes (*) on the SPEP gel (left) and the quantitated Globulin/Albumin ratio (right), are shown. Graphs depict the mean ± SEM of n=8-9 mice per cell line from three independent experiments, Student's t-test.

4.3 Discussion

Dormant MM PCs are thought to stably reside long term within specialised bone marrow niches, evading conventional therapeutic targeting, whilst retaining the ability to become reactivated[129]. Reactivated MM PCs re-enter the cell cycle and begin proliferating, forming new tumours and giving rise to clinical relapse. Understanding the mechanisms of MM PC dormancy could lead to therapeutic targeting of dormant PCs to either maintain long term dormancy or enable reactivation prior to targeting by conventional therapy. *Axl* was previously identified as one of the genes most highly expressed by dormant 5TGM1 murine MM PCs[129, 213], and targeting Axl using the small molecule inhibitor BMS-777607 released 5TGM1 cells from dormancy[213]. However, as BMS-777607 also targets Met,[214] Tyro3, Mer[215], and Ron[216], the aim of this chapter was to use a model of Axl positive and Axl negative 5TGM1 cell lines to investigate whether high 5TGM1 Axl expression alone was sufficient to initiate MM dormancy.

Firstly, some of the hallmark features of cellular dormancy, reduced cell proliferation and cell cycle arrest were investigated in 5TGM1 Axl and 5TGM1 EV cell lines. Previous studies of Axl expressing- prostate cancer cell lines PC3 and DU145 showed that cell proliferation was reduced *in vitro* when cells were exposed to Gas6[164, 185]. Therefore it was hypothesised that 5TGM1 Axl cells may display reduced cell proliferation compared to 5TGM1 EV cells, particularly in response to ligand signalling. However no differences in cell proliferation were observed in short term proliferation assays. Interestingly, all the types of NIH3T3 conditioned IMDM media slowed the growth of both 5TGM1 Axl and 5TGM1 EV cells, but this effect does not appear to be due to Gas6 or Pros1 ligands. Cell cycle arrest in G0 has previously been detected in dormant 5TGM1 cells harvested from mouse BM[129], and in Axl expressing-PC3 prostate cancer cells *in vitro* after exposure to Gas6[164]. Therefore it was anticipated that 5TGM1 Axl cells would have a greater distribution of total cells in G0 compared to 5TGM1 EV cells, particularly in response to ligand signalling. However no differences in the distribution of cells in the G0 phase of the cell cycle were observed, nor any differences in any other cell cycle phases. Although proliferation assays and cell cycle analysis failed to identify any features of dormancy in 5TGM1 Axl expressing cells, these short term assays may lack the sensitivity to identify non-proliferative sub-populations of cells.

Labelling cells with heritable dyes is a reliable method for identifying long-term non-proliferating cells, which retain the label over time. To assess whether more 5TGM1 Axl cells retained the DiD label compared to 5TGM1 EV cells, these two cell lines were DiD labelled and cultured in IMDM media. No differences in the proportions of each cell line remaining DiD^{hi} were observed over 10 days. However, previous studies in both MM and prostate cancer found that DiD^{hi} cell populations were significantly increased when cells were in contact co-culture with pre-osteoblastic MC3T3 cells[129, 206]. Furthermore, 5TGM1 cells overexpress dormancy associated genes, including *Axl*, when in contact co-culture with MC3T3 cells[213]. 5TGM1 Axl cells and 5TGM1 EV cells were DiD labelled and placed in contact co-culture with MC3T3 cells, and after 7 days both 5TGM1 Axl cells and 5TGM1 EV cells completely retained the DiD label. Therefore contact with MC3T3 cells provided 5TGM1 cells with potent growth suppression signals, and this growth suppression was not dependent on Axl signalling. As a complement to direct co-culture with MC3T3 cells, 5TGM1 Axl cells and 5TGM1 EV cells were cultured in MC3T3 conditioned media, however no differences in DiD dye retention were observed. This is unsurprising, as it has previously been shown that increases in Axl expression and expression of other dormancy genes was only induced in 5TGM1 cells in direct co-culture with MC3T3 cells, not when they were cultured with MC3T3 conditioned media[213]. Future studies should include the assessment of dormancy signature genes in 5TGM1 Axl and 5TGM1 EV cell lines following co-culture with MC3T3 cells, to identify whether any of these genes are specifically co-expressed with Axl.

Engagement of 5TGM1 cells with endosteal niche cells is important for the initiation and maintenance of dormancy. *In vitro* studies lack the complexity of the BM microenvironment and 5TGM1 Axl cells may require contact with the endosteal niche *in vivo* to induce features of dormancy. Inhibition of Axl using BMS-777607 released 5TGM1 cells from dormancy and increased BM tumour burden[213]. It was hypothesised that 5TGM1 Axl cells would result in significantly reduced tumour burden in KaLwRij mice compared to 5TGM1 EV cells. However there was no statistically significant difference in tumour burden between mice inoculated with 5TGM1 Axl cells and mice inoculated with 5TGM1 EV cells. Although DiD labelling of 5TGM1 Axl and 5TGM1 EV cells was performed prior to i.v. inoculation into

KaLwRij mice in this study, no DiD+ cells were recovered from BM of mice after 28 days (data not shown). To identify differences in DiD^{hi} populations between 5TGM1 Axl and 5TGM1 EV inoculated mice, future studies should optimise *in vivo* DiD labelling at time points of 7, 14 and 21 days. As Axl cell surface expression assessed by flow cytometry in the unaltered 5TGM1 cell line has been shown to fluctuate at different cell culture densities, it was hypothesised that a loss of Axl expression over 4 weeks *in vivo* may be responsible for the lack of *in vivo* difference in tumour burden. However, *in vivo* Axl expression was maintained in the majority of 5TGM1 Axl cells, indicating that loss of Axl expression was not responsible for the lack of *in vivo* difference in tumour burden.

Knockdown of Axl in PC3 and DU145 prostate cancer cell lines significantly impaired their ability to migrate towards Gas6 *in vitro*[272]. Furthermore Axl knockdown reduced migration of triple negative breast cancer cells from the primary tumour to secondary sites in the lungs *in vivo*[273]. Given the results of the KaLwRij model in which cells are injected intravenously and must home to the bone marrow, it was hypothesised that 5TGM1 Axl cells had a migration or bone marrow homing advantage over 5TGM1 EV cells. Therefore, a 24 hour BM homing assay was conducted, revealing no differences in homing ability between 5TGM1 Axl and 5TGM1 EV cells. However it should be noted that this assay lacks sensitivity, with only small numbers of GFP+ cells being detected. The 5TGM1 Axl and 5TGM1 EV cell lines were then inoculated directly into the bone marrow microenvironment of KaLwRij mice via the tibia, bypassing the BM homing mechanism in the i.v. model. When cells were injected intratibially, there was a slight but not statistically significant decrease in tumour burden in the injected legs of mice inoculated with 5TGM1 Axl cells compared to 5TGM1 EV cells by GFP and SPEP. This was not supported by the whole body BLI data displaying no differences between groups, indicating that there is no reduction in tumour burden with Axl expression in either the KaLwRij i.v. or i.t. models. There were also no differences in metastasis to the non-injected leg in 5TGM1 Axl compared to 5TGM1 EV inoculated mice. Therefore, these data provide no evidence that Axl expression promotes 5TGM1 cell migration. The process of 5TGM1 cells forming tumours within the BM following i.v. injection into KaLwRij mice involves not only migration but also successful engraftment. It is possible that Axl promotes

engraftment and establishment of tumours in the BM, resulting in the modest increase in tumour burden in the i.v. KaLwRij model.

Axl expression has been associated with 5TGM1 cell dormancy in previous studies[129], and use of a small molecule inhibitor with targets including Axl released 5TGM1 cells from dormancy *in vivo*[213]. The studies in this chapter provide no evidence that high Axl expression in 5TGM1 cells promotes features of dormancy when compared to a control 5TGM1 cell line that does not express Axl. A recent study in prostate cancer found that Axl expression was not necessary for dormancy *in vivo* and without Axl expression prostate cancer cells were still able to disseminate to secondary sites, undergo a period of dormancy, become reactivated and form new tumours[185]. It is possible that Axl is a 'passenger' expressed highly by dormant cells, whereas one of the other genes identified by Khoo, *et.al.,*[213] *Irf7, Spic, Vcam1*, *Fcerg1*, *Mpeg1*, or *Sirpa* may be a 'driver' of dormancy induction and maintenance in myeloma. Furthermore, BMS-777607 also targets Met[214], Tyro3, Mer[215], and Ron[216], meaning that these targets either expressed by 5TGM1 cells or other cells within the BM microenvironment could be responsible for the 'release' of 5TGM1 cells from dormancy *in vivo* identified by Khoo, *et.al.,*[213] Therefore, previous studies have identified a total of 10 candidate genes other than Axl that can be investigated in further studies as potential drivers of dormancy in myeloma. In a recent study Irf7-expressing MR20 breast cancer cells were inoculated into mice and the resulting tumours were treated with chemotherapy, leading to long periods of dormancy[274]. Interestingly, shRNA-mediated knockdown of Irf7 abrogated dormancy, instead resulting in significantly increased tumour burden and metastatic disease following chemotherapy cessation. Given that the proteasome inhibitor bortezomib can be successfully utilised in the 5TGM1/KaLwRij model of MM[275], further studies should also incorporate bortezomib treatment of 5TGM1 tumours in KaLwRij mice and monitoring of subsequent relapse by BLI. Using a panel of 5TGM1 cell lines expressing individual candidate genes and a 5TGM1/KaLwRij model monitoring relapse post-bortezomib treatment, it may be possible to identify one of these genes as a novel drug target to limit MM relapse.

5. Mer expression promotes multiple myeloma disease progression

5.1 Introduction

Multiple myeloma is a haematological malignancy characterised by the unchecked clonal proliferation of malignant plasma cells in the bone marrow[2]. MM PCs, situated in specialised BM niches, establish paracrine interactions with stromal, immune and osteolineage cells that are mediated by cell surface receptor signalling[250]. Early in the disease course, MM PCs rely on interactions with BM microenvironment cells, via both direct cell-cell interactions, soluble factors and cytokines, which support clonal expansion[276]. As MM tumours develop, interactions between cell surface receptor signalling and stromal cell-derived ligands enables MM PCs to 'reprogram' the BM microenvironment to favour PC proliferation and immune evasion, leading to further disease progression[106, 277]. Disrupting cell surface receptor – ligand interactions through the use of novel targeted therapeutics, such as small molecule inhibitors, represents an opportunity to limit MM disease burden[278]. However, the roles of many cell surface receptors and ligands expressed by patient MM PCs in supporting tumour development remain ill-defined.

The TAM receptor, Mer, and its ligand, Gas6, have previously been proposed as important factors for MM PC growth and survival[166, 188]. Both Mer and Gas6 are expressed by MM patient-derived PCs, with Gas6 being expressed at higher levels in MM patient-derived PCs compared to healthy control PCs[166]. Our own RNAseq analysis has demonstrated that PCs express abundant Gas6 and Mer, but negligible Axl and Tyro3 (Chapter 3, Figure 3.1). shRNA mediated silencing of Mer (shMer) in the human myeloma cell lines, RPMI8226 and U266, reduced cell proliferation *in vitro*[166]. Inoculation of mice with the shMer U266 cells resulted in reduced myeloma burden and increased survival time compared to control shRNA-transduced cells. Furthermore, shRNA-mediated knockdown of Gas6 resulted in RPMI8226 and U266 cell death, whereas overexpression of Gas6 increased cell proliferation *in vitro.* Waizenegger *et al.,*[166] also showed that mice administered with Gas6 overexpressing U266 cells also had reduced survival times compared to mice administered control U266 cells. Treatment of mice, inoculated with U266 cells, with the Vitamin K antagonist Warfarin, which inhibits important post-translational modification of Gas6, reduced myeloma burden and increased survival time. These data suggest that Gas6 and Mer expression promotes MM cell proliferation and survival *in vitro* and blockade of either Gas6 or Mer reduces myeloma burden *in*

vivo. Given the expression of Gas6 and Mer by MM patient PCs, they may represent clinically relevant proteins, and therapeutic targeting of this receptor-ligand axis may limit disease burden.

Furukawa, *et al.,* showed that both autocrine and paracrine Gas6 signalling promoted human myeloma cell line survival and proliferation through activation of Mer *in vitro*[188]. The authors also showed that Gas6 is secreted not only by the RPMI8226 human myeloma cells but also from the HS-5 human BM stromal cells. Furthermore, Gas6 neutralising antibody treatments reduced RPMI8226 cell proliferation and increased apoptosis under standard cell culture conditions and when cells were cultured with HS-5 cell conditioned media. Findings from this study indicated that recombinant Gas6, or HS-5 conditioned media, resulted in the phosphorylation of Mer and downstream signalling pathway intermediates. Therefore, both autocrine and paracrine Gas6 signalling, mediates RPMI8226 cell proliferation and survival *in vitro,* likely through activation of Mer. Waizenegger, *et al.,* showed that Gas6 overexpressing U266 cells produce greater myeloma tumour burden *in vivo* compared to control cells, suggesting that autocrine Gas6 signalling also promotes the survival and proliferation of human MM PCs *in vivo*[166]. However, the effects of myeloma cell lines differentially expressing Mer and Gas6 has not been fully assessed *in vivo.* Therefore, it remains unknown whether there is an additive effect of both Mer and Gas6 expression in promoting MM tumour burden.

Although it is possible that Mer and Gas6 are simply pro-proliferative in MM PCs, the exact mechanism responsible for the increased myeloma burden, identified *in vivo* when Gas6 and Mer are both expressed[166], is yet to be established. In other cancers Mer and Gas6 have been shown to promote disease progression through increased cancer cell migration[279, 280], acquisition of drug resistance[281], and the promotion of an immune-suppressive tumour microenvironment [175, 186]. Interestingly, previous studies have shown that both Mer and Axl are able to regulate the expression of the immune checkpoint protein PD-L1 in breast cancer and cervical cancer cell lines *in vitro*[175, 232]. Expression of cell surface PD-L1 was upregulated when cells were stimulated with Gas6 and a source of phosphatidylserine to maximise Gas6 signalling. Furthermore, Mer inhibition in a murine model of acute lymphoblastic leukaemia (ALL) decreased PD-1 expression

on T cells and increased both CD4+ and CD8+ T cell activation[186]. The authors showed that Mer inhibition increased survival time and decreased leukaemia burden in immune compromised mice bearing Mer-positive human ALL xenografts, suggesting a direct effect of Mer expressed by leukaemia cells in promoting disease progression. Mer inhibition in immune competent C57BL/6 mice, inoculated with Mer-negative ALL cells, also significantly prolonged survival time, but had no effect in an immune compromised NSG model inoculated with the same Mer-negative cells. These findings suggest that Mer can also have indirect anti-cancer effects mediated through the adaptive immune system. PD-1/PD-L1 inhibitors have been successful used in a number of cancers, but clinical trials involving these inhibitors have been put on hold in MM due to high toxicities[231]. Therefore, studying the Mer/PD-L1 axis in MM may provide an alternative strategy for targeting both Mer and, indirectly, the PD-1/PD-L1 pathway. Additionally, there are other immune checkpoint pathways that may promote MM immune escape such as Galectin9/Tim3[282] and PVR/TIGIT[283]. To date, the effects of Mer expression on MM tumour burden *in vivo* have yet to be compared between immune competent and immune compromised murine models of MM.

To investigate the function of Mer in promoting myeloma disease progression, this study utilised 5TGM1 Mer positive (5TGM1 Mer) and 5TGM1 Mer negative (5TGM1 EV) cell lines. To generate these cell lines, CRISPR Cas9 mediated knockout of Tyro3 and Axl in 5TGM1 cells was performed, and these 5TGM1 TAM null cells were then retrovirally transduced to express Mer (Chapter 3, Figure 3.11). If Mer expression was able to promote MM PC proliferation, it was hypothesised that 5TGM1 Mer cells would display increased cell proliferation *in vitro*, display evidence of accumulation in the S phase of the cell cycle, and produce increased tumour burden *in vivo*, compared to 5TGM1 EV cells. If Mer expression promoted myeloma tumour burden through immune subversion, it was hypothesised that no differences in tumour burden would be observed between mice inoculated with 5TGM1 Mer or 5TGM1 EV cells in an immune compromised mouse model. Further to this, it was hypothesised that immune checkpoint protein expression, of PD-L1 or other immune checkpoint proteins, would be increased in 5TGM1 Mer cells compared to 5TGM1 EV cells. To identify whether Mer expression plays a role in MM PC migration, this study was designed to compare different modes of 5TGM1 cell delivery to mice. To investigate the relative effects of paracrine versus autocrine Gas6-Mer signalling, a

panel of four 5TGM1 cell lines were generated from the 5TGM1 Mer and 5TGM1 EV cell lines with differential Mer and Gas6 expression. It was hypothesised that if having both a source of paracrine and autocrine Gas6 signalling, like myeloma patient PCs, stimulated MM disease progression, 5TGM1 cells expressing both Mer and Gas6 would produce increased tumour burden *in vivo* in comparison to 5TGM1 cells expressing only Mer or Gas6 alone.

5.2 Results

5.2.1 Mer expression increases 5TGM1 cell proliferation when cells are cultured in IMDM media and NIH3T3 conditioned media.

Given that Mer knockdown in human myeloma cell lines RPMI-8226 and U266 was previously shown to reduce cell proliferation *in vitro*[166], it was hypothesised that 5TGM1 Mer cells would display increased cell proliferation compared to 5TGM1 empty vector (EV) cells. Proliferation assays performed in IMDM media showed that 5TGM1 Mer cells displayed increased proliferation at the 72 hour time point compared to 5TGM1 EV cells (Figure 5.1a). This effect was reproduced when cells were cultured in NIH3T3 empty vector (EV) control conditioned media, which contains low levels of Gas6 and Pros1 (Figure 5.1b). However, no differences in cell proliferation were detected when 5TGM1 Mer and 5TGM1 EV cells were culture in either NIH3T3 Gas6 (Figure 5.1c) or NIH3T3 Pros1 (Figure 5.1d) conditioned media enriched for TAM ligands through retroviral mediated transgene expression. In contrast to results obtained from proliferation assays, in which cells were cultured in IMDM media or NIH3T3 EV media, assays in which cells were cultured in ligand enriched conditioned media produced significant variability between replicates.

5.2.2 Mer expression has no effect on cell cycle distribution.

As 5TGM1 Mer cells displayed increased cell proliferation in IMDM media and NIH3T3 EV media compared to 5TGM1 EV cells, it was hypothesised that 5TGM1 Mer cells would have a significantly increased proportion of cells in the S phase of the cell cycle compared to 5TGM1 EV cells. Cells in G0, G1, S and G2/M phases of the cell cycle were identified by their differential DNA and RNA content using double Hoechst (RNA) and Pyronin Y (DNA) staining (Figure 5.2a). Cell cycle analysis was

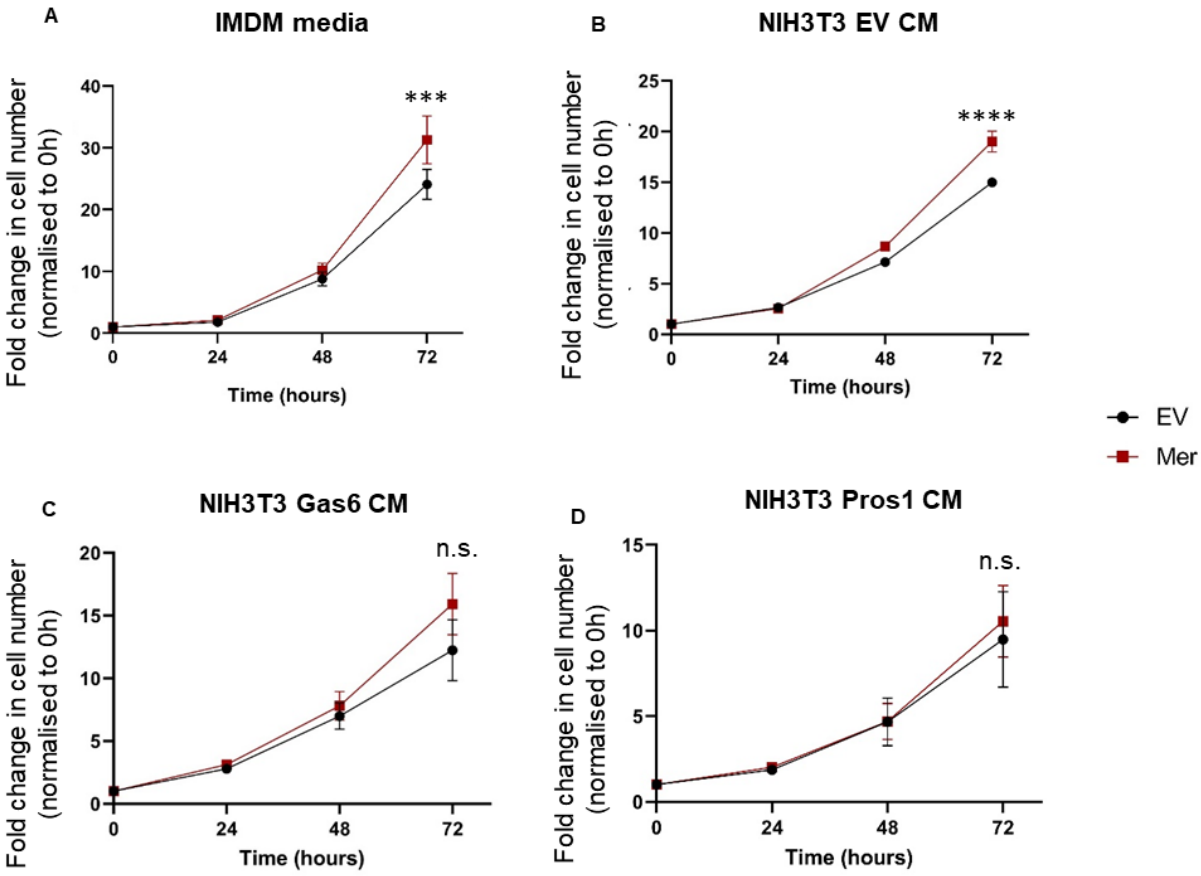

Figure 5.1. Mer expression increases 5TGM1 cell proliferation when cultured in IMDM media and NIH3T3 conditioned media. Proliferation of 5TGM1 Mer expressing cells was compared to that of 5TGM1 EV cells over 72 hours by a WST-1 assay. Cells were cultured in either **(A)** IMDM media, **(B)** NIH3T3 EV conditioned media, **(C)** NIH3T3 Gas6 CM or **(D)** NIH3T3 Pros1 CM. Results were displayed as fold change in absorbance (450nm) over 72 hours. Results are shown as the mean ± SEM of three independent experiments performed in triplicate, two-way ANOVA with Tukey's multiple comparisons, ****p<.0001, ***p<.0001, n.s. p> .05.

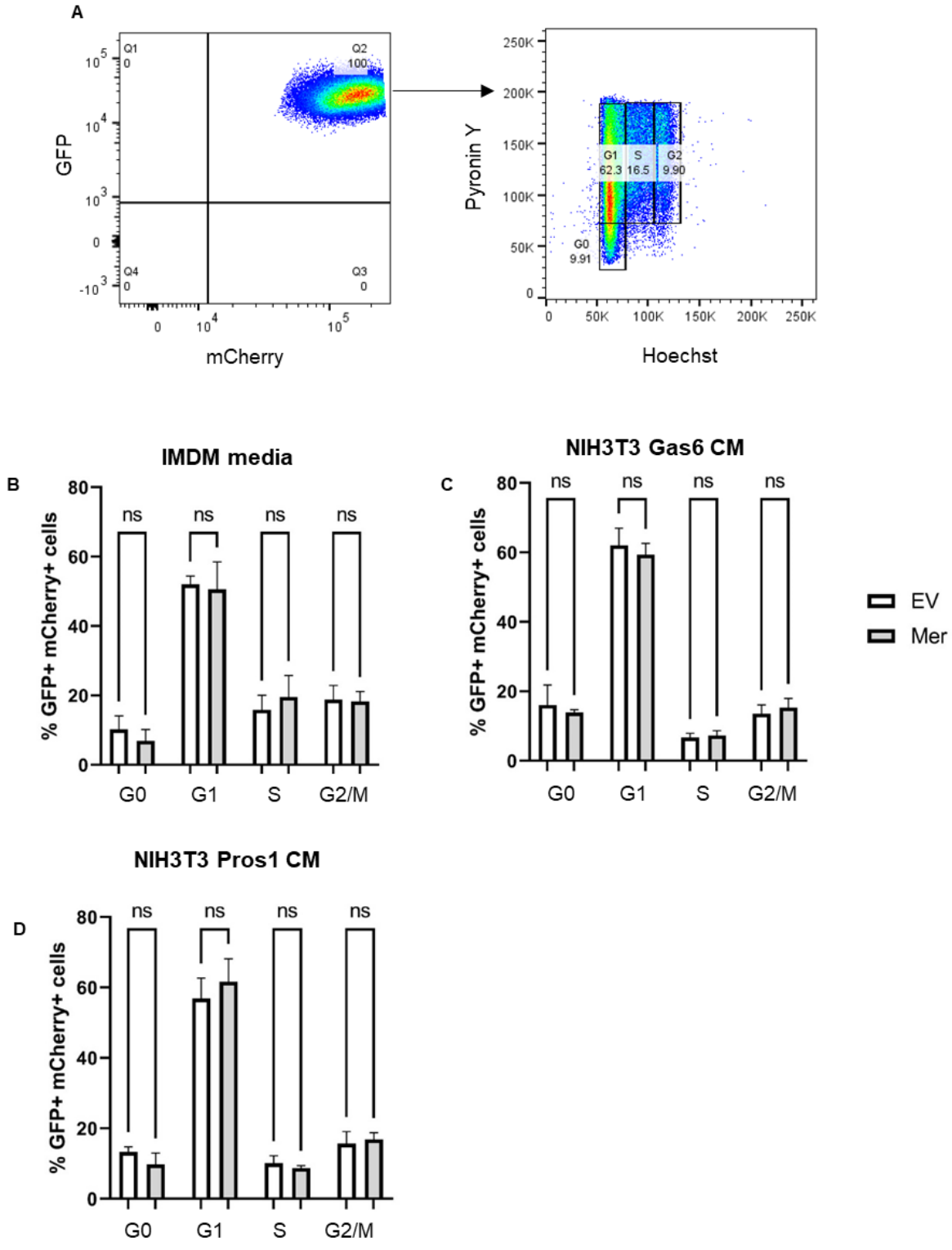
A
Q1
0
Q2
100
Q4
0
Q3
0
GFP
mCherry
Pyronin Y
Hoechst
G1
62.3
S
16.5
G2
9.90
G0
9.91
B
IMDM media
C
NIH3T3 Gas6 CM
D
NIH3T3 Pros1 CM
% GFP+ mCherry+ cells
ns
G0
G1
S
G2/M
EV
Mer

Figure 5.2. Mer expression has no effect on cell cycle distribution. Cell cycle analysis was conducted using 5TGM1 Mer compared to 5TGM1 EV cells, including isolation of the G0 population**. (A)** A representative plot of GFP+ mCherry+ 5TGM1 EV cells (left), and the gating strategy for cell cycle analysis of the Hoechst and Pyronin Y stained GFP+ mCherry+ population (right). Cell cycle analysis was performed, comparing 5TGM1 Mer and 5TGM1 EV cells following overnight culture in **(B)** IMDM media, **(C)** NIH3T3 Gas6 CM and **(D)** NIH3T3 Pros1 CM. Percentages of cells in each phase of the cell cycle are indicated. Results are shown as the mean ± SEM of three independent experiments, Students t-test, n.s. p>.05.

performed in IMDM media (Figure 5.2b), or in response to NIH3T3 Gas6 (Figure 5.2c) or NIH3T3 Pros1 (Figure 5.2d) ligand enriched conditioned media. Under all media conditions no significant differences were identified in the proportions of 5TGM1 Mer and 5TGM1 EV cells in any of the phases of the cell cycle. In both the 5TGM1 Mer and 5TGM1 EV cell lines, there was an increased proportion of cells in the S phase of the cell cycle when cultured in IMDM media (EV: mean 15.9% ± s.d. 4.16%, Mer: mean 19.53% ± s.d. 6.21%) compared to NIH3T3 Gas6 enriched media (EV: mean 6.69% ± s.d. 1.26%, Mer: mean 7.26% ± s.d.1.42%) or NIH3T3 Pros1 enriched media (EV: mean 10.11% ± s.d. 2.14%, Mer: mean 8.72% ± s.d. 0.71%). Therefore, when cells are cultured in IMDM media they proliferate at an increased rate compared to when they are cultured in NIH3T3 conditioned media, shown by both increased proportion of cells in S-phase and increased WST-1 absorbance (Figure 5.1).

5.2.3 Mer expression increases tumour burden in the KaLwRij model of MM.

To assess whether Mer expression promotes tumour burden *in vivo*, 5TGM1 Mer and 5TGM1 EV cell lines were i.v. inoculated into KaLwRij mice and tumour burden was monitored at week 4 using BLI. Previous studies showed that shRNA knockdown of Mer in U266 human myeloma cells inoculated into mice produced a significant reduction in myeloma burden[166]. Therefore, it was hypothesised that 5TGM1 Mer cells would produce significantly increased tumour burden in the KaLwRij model of MM compared to 5TGM1 EV cells. Analysis of whole-body ventral BLI scans from week 4 (Figure 5.3a-b), as well as hind limb only scans (Figure 5.3c), revealed that 5TGM1 Mer cells produce greater *in vivo* tumour burden (mean $5.68x10^6$ ± s.d. $4.31x10^6$ photons/s) compared to 5TGM1 EV cells (mean $2.44x10^6$ ± s.d. $2.56x10^6$ photons/s). GFP+ cells were enumerated from the hind limb bone marrow of tumour bearing mice, and showed a slight but not statistically significant increase in the percentage of GFP+ cells in 5TGM1 Mer inoculated mice compared to 5TGM1 EV inoculated mice (Figure 5.3d). There was also a small but statistically non-significant increase in M-spike intensity in the 5TGM1 Mer inoculated mice compared to 5TGM1 EV inoculated mice (Figure 5.3e). However, significantly increased numbers of mice inoculated with 5TGM1 Mer cells compared to 5TGM1 EV cells had detectable tumour burden by SPEP (Figure 5.3f). To assess whether, at the week 4 time point, 5TGM1 Mer cells were proliferating more rapidly in

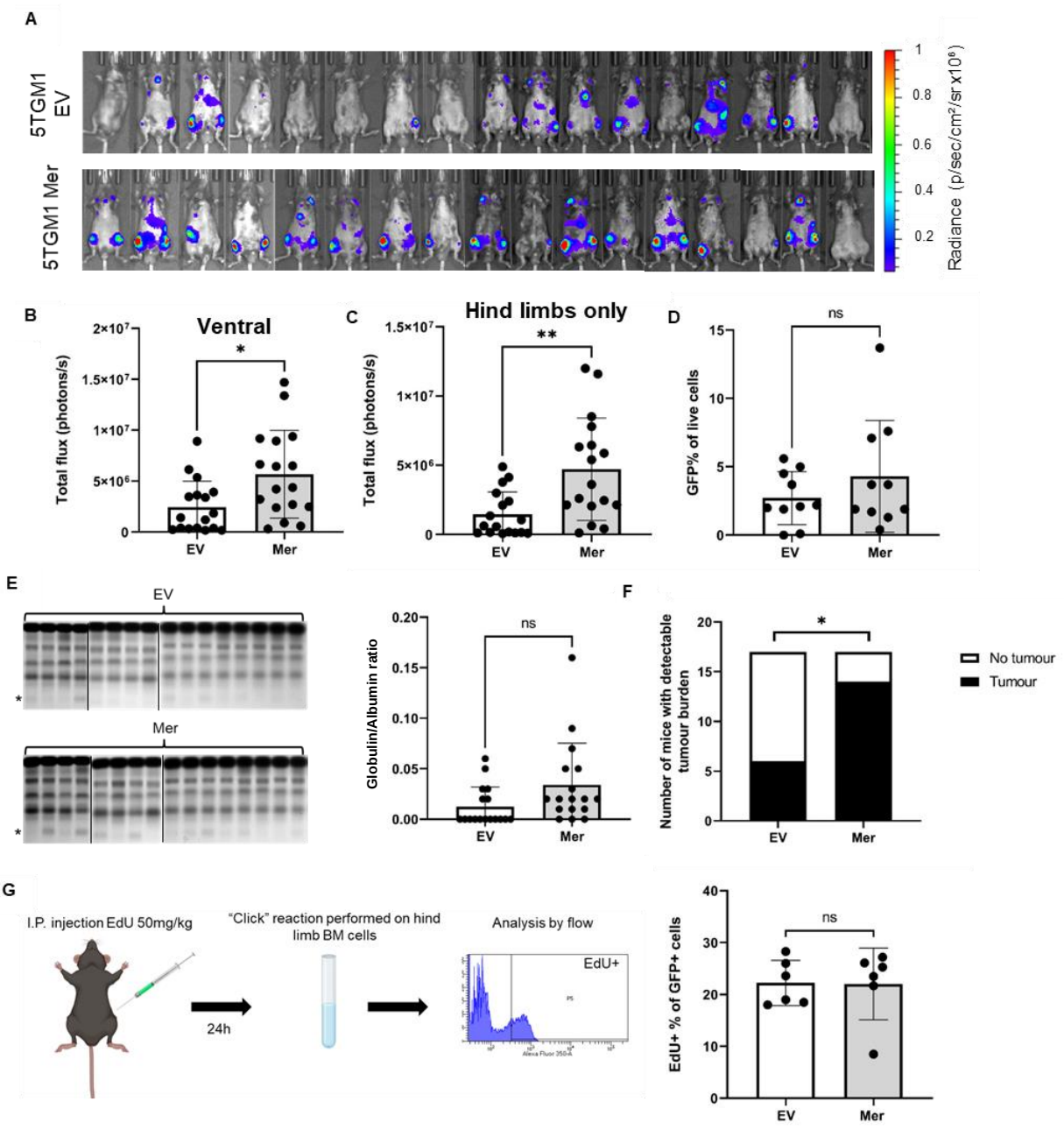
A
5TGM1 EV
5TGM1 Mer
Radiance (p/sec/cm²/sr x10⁶)
B
Ventral
Total flux (photons/s)
EV
Mer
C
Hind limbs only
D
GFP% of live cells
ns
E
EV
Mer
Globulin/Albumin ratio
F
Number of mice with detectable tumour burden
No tumour
Tumour
G
I.P. injection EdU 50mg/kg
24h
"Click" reaction performed on hind limb BM cells
Analysis by flow
EdU+
EdU+ % of GFP+ cells

Figure 5.3. Mer expression increases tumour burden in the KaLwRij model of MM. KaLwRij mice were inoculated with either 5x10^5 5TGM1 EV cells or 5TGM1 Mer cells via the tail vein, and subsequent disease burden was monitored by whole animal BLI, SPEP and flow cytometry. **(A)** Ventral BLI scans depicting tumour burden at week 4. A graph of the total flux at week 4 from **(B)** ventral and **(C)** hind limb only scans are shown. **(D)** GFP+ % of live cells from the hind limbs of *n*=10 mice/group at week 4 is shown. **(E)** Serum was collected from the mice after four weeks and the M-spikes were measured by SPEP. M-spikes (*) on the SPEP gel (left) and the quantitated Globulin/Albumin ratio (right), are shown. Black lines indicate separation between gels. **(F)**The number of mice with detectable tumour burden by SPEP were compared between groups, Fisher exact test. **(G)** *n*=6 mice/group were inoculated with 50mg/kg EdU 24 hours before the endpoint (left) to assess the proportion of 5TGM1 EV cells compared to 5TGM1 Mer cells that were actively dividing. EdU+% of GFP+ cells from the hind limbs of mice were compared between groups using flow cytometry (right). Graphs depict the mean ± SD of *n*=17 mice per cell line, Students t-test, unless otherwise indicated. *p<0.05, **p<0.01, n.s. p>.05.

comparison to 5TGM1 EV cells, *in vivo* measurement of the rates of DNA synthesis in tumour cells was performed. Mice were i.p. inoculated with the nucleotide analogue EdU 24 hours prior to being humanely euthanised. BM cells were harvested from mouse hind limbs and EdU incorporation into newly synthesised DNA was detected via conjugation to a fluorescent reporter. EdU+ GFP+ 5TGM1 cells were enumerated by flow cytometry, revealing no difference in the proportions of actively proliferating EdU+ cells between 5TGM1 Mer and 5TGM1 EV tumours (Figure 5.3g).

5.2.4 Mer expression has no effect on tumour burden in the immune compromised NSG model.

To assess whether Mer expression promotes tumour burden in an immune compromised mouse model, 5TGM1 Mer and 5TGM1 EV cell lines were i.v. inoculated into NSG mice and tumour burden was monitored at week 4 using BLI. NSG mice carry two mutations on the NOD/ShiLtJ genetic background: severe combined immune deficiency (scid) and a complete null allele of the IL2 receptor common gamma chain ($IL2rg^{null}$). These mutations render the mice B, T and NK cell deficient, with defective macrophages and dendritic cells. Previous studies have identified that Mer may play a role in tumour cell escape from immune surveillance through modulation of the PD-1/PD-L1 axis[175, 186, 215]. If the presence of an adaptive immune system was important for the increased myeloma burden identified in KaLwRij mice inoculated with 5TGM1 Mer cells compared to 5TGM1 EV cells, it was hypothesised that there would be no difference in tumour burden based on Mer expression in the NSG model. Analysis of whole-body ventral BLI scans from week 4 did indeed reveal no difference in tumour burden between mice inoculated with 5TGM1 Mer cells compared to 5TGM1 EV cells (Figure 5.4a-b). Enumeration of GFP+ 5TGM1 cells in the bone marrow of the hind legs by flow cytometry at week 4 showed no significant difference between mice inoculated with 5TGM1 Mer cells and mice inoculated with 5TGM1 EV cells (Figure 5.4c). However, this analysis was only performed in a subset of the total number of mice shown in BLI and SPEP data. In keeping with the results obtained by BLI, SPEP analysis revealed no difference in whole animal tumour burden between mice inoculated with 5TGM1 Mer compared to mice inoculated with 5TGM1 EV cells (Figure 5.4d).

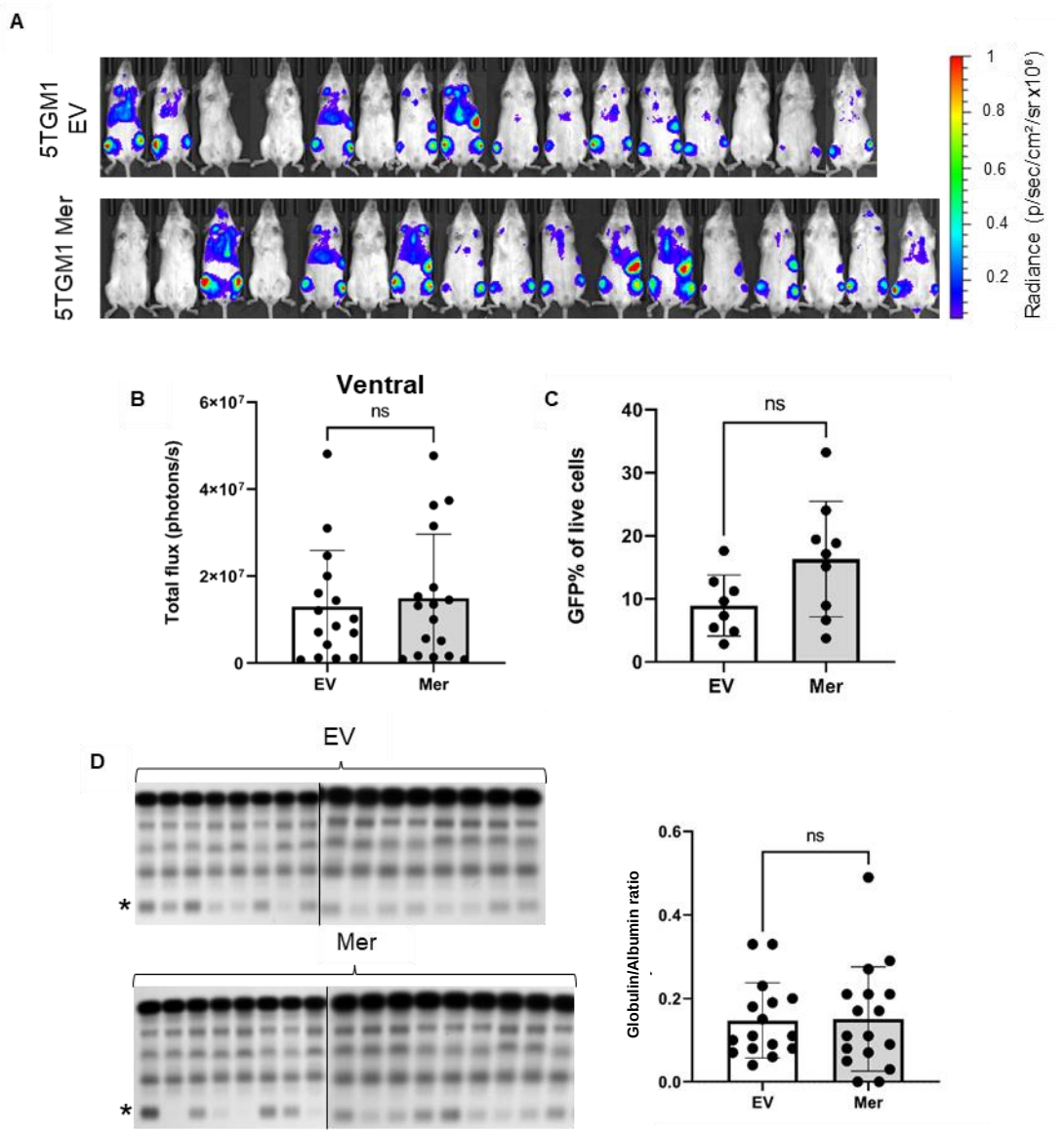

Figure 5.4. Mer expression has no effect on tumour burden in the immune compromised NSG model. NSG mice were inoculated with either 5x10⁵ 5TGM1 EV cells or 5TGM1 Mer cells via the tail vein and disease burden was subsequently monitored by whole animal BLI, SPEP and flow cytometry. **(A)** Ventral BLI scans depict tumour burden at week 4. **(B)** A graph of the total flux at week 4 from ventral scans are shown. **(C)** GFP+ % of live cells from the hind limbs of *n*=8-9 mice/group at week 4 is shown. **(D)** Serum was collected from the mice after 4 weeks and the M-spikes were measured by SPEP. M-spikes (*) on the SPEP gel (left) and the quantitated Globulin/Albumin ratio (right), are shown. Black lines indicate separation between gels. Graphs depict the mean ± SD of *n*=16-17 mice per cell line, Students t-test, n.s. p>.05.

5.2.5 NSG mice have increased mRNA expression of TAM ligands Pros1 and Galectin 3 in compact bone compared to KaLwRij mice.

To identify whether any differences in ligand expression in the bone marrow microenvironment may be responsible for the results observed in the KaLwRij model compared to the NSG model, mRNA expression of TAM ligands were compared between tumour naïve mice of the two strains. It was hypothesised that if there is increased ligand expression in the bone marrow or compact bone of KaLwRij mice compared to NSG mice, then increased ligand signalling through Mer could be responsible for the tumour-promoting effects of Mer seen only in KaLwRij mice. Relative mRNA expression levels of the TAM ligands Gas6, Pros1, and Galectin 3 were compared in compact bone and bone marrow extracted from KaLwRij and NSG mice. This showed no significant difference in Gas6 expression levels between compact bone of KaLwRij and NSG mice (Figure 5.5a). In contrast, we observed a significant increase in mRNA expression of Pros1 in NSG compact bone compared to KaLwRij compact bone (Figure 5.5b, NSG: mean 0.003 ± s.d. 0.0002, KaLwRij: mean 0.0002 ± s.d. 0.00004). There was also a significant increase in mRNA expression of Galectin 3 in NSG compact bone compared to KaLwRij compact bone (Figure 5.5c, NSG: mean 0.04 ± s.d. 0.008, KaLwRij: mean 0.021 ± s.d. 0.005). Notably, Gas6 and Pros1 expression were not detectable in bone marrow of either mouse strain (data not shown), and there was no significant difference in Galectin 3 mRNA expression between KaLwRij and NSG bone marrow samples (Figure 5.5d). Therefore, the KaLwRij-specific effects of Mer on 5TGM1 tumour growth are not due to increased expression levels of any of the TAM ligands in the bone microenvironment of this mouse strain.

5.2.6 Mer expression increases mRNA expression of immune checkpoint proteins Galectin 9, PD-L1 and PVR.

Previous studies identified that Mer expression could increase cancer cell expression of PD-L1[175, 232]. Therefore, it was hypothesised that if Mer plays an immune suppressive role in MM, expression of Mer may similarly produce an increase in mRNA expression of PD-L1. MM patient PCs are known to express ligands of other immune checkpoints[284], and therefore in this study mRNA expression of Galectin 9, PVR and TNFSF9 were also evaluated. Indeed, compared to 5TGM1 EV cells, 5TGM1 Mer cells cultured in IMDM media displayed a 2.6 fold

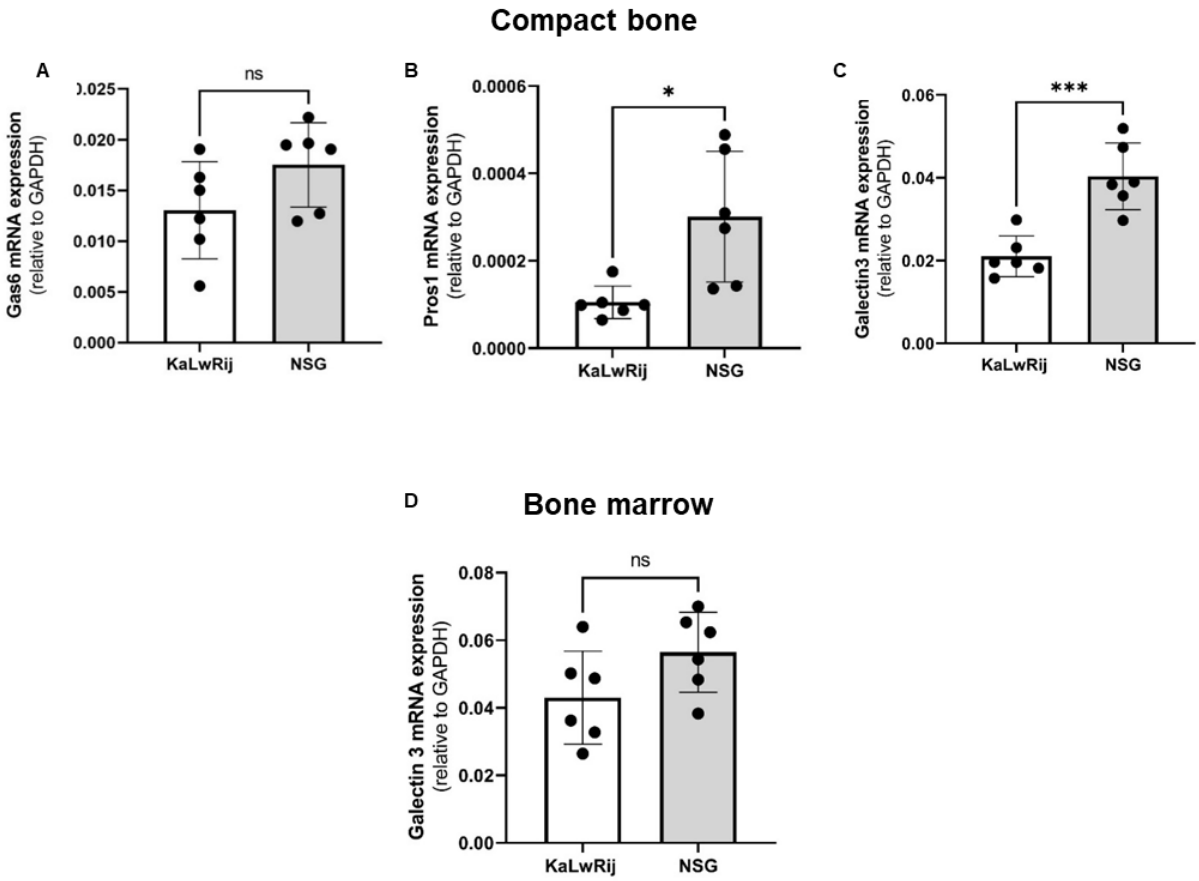

Figure 5.5. NSG mice have increased mRNA expression of TAM ligands Pros1 and Galectin 3 in compact bone compared to KaLwRij mice. RT-qPCR was performed on cDNA generated from compact bone and bone marrow of KaLwRij and NSG mice to compare ligand expression in the bone marrow microenvironment between mouse models. mRNA expression of **(A)** Gas6, **(B)** Pros1, **(C&D)** Galectin 3 were assessed. Gene expression levels are shown as relative to GAPDH. Graphs depict mean ± SD of *n*=6 mice/group, Student's t-test, *p<.05, ***p<.001, n.s. p>.05.

increase in Galectin 9 (Figure 5.6a), a 3.04 fold increase in PD-L1 (Figure 5.6b) and a 1.61 fold increase in PVR (Figure 5.6c). There was no significant difference in mRNA expression of TNFSF9 between the 5TGM1 Mer and 5TGM1 EV cell lines (Figure 5.6d). Of note, TNFSF9 differs from the other ligands investigated as it is a positive regulator of the immune system, expression of which, is commonly downregulated, allowing cancer cells to evade the immune system[285].

5.2.7 PD-L1 cell surface expression does not change in response to Mer expression or Gas6 stimulation.

As PD-L1 mRNA expression was upregulated in 5TGM1 Mer cells compared to 5TGM1 EV cells, it was hypothesised that PD-L1 expression at the cell surface would also be increased with Mer expression. Previous studies have shown increased cell surface PD-L1 expression when cancer cells were stimulated with Gas6 and a source of phosphatidylserine from apoptotic cells[175, 232]. To mimic these studies, 5TGM1 Mer cells and 5TGM1 EV cells were either cultured in IMDM media, NIH3T3 Gas6 conditioned media (CM), IMDM media with apoptotic cells or NIH3T3 Gas6 CM with apoptotic cells. Although PD-L1 expression was robust, no significant differences in cell surface expression were observed between the 5TGM1 Mer and 5TGM1 EV cell lines under any of the four media conditions (Figure 5.7a). Small differences in mean fluorescence intensity (MFI) of PD-L1 antibody staining were identified between 5TGM1 Mer (mean 4464 ± s.d. 226.1) and 5TGM1 EV (mean 3765 ± s.d. 642.7) cells cultured in IMDM media alone (“untreated”, Figure 5.7a), however this failed to reach statistical significance (Figure 5.7b).

5.2.8 Mer expression has no effect on the growth of primary or secondary tumours following i.t. injection.

Another possible explanation for the significantly increased tumour burden in KaLwRij mice intravenously inoculated with 5TGM1 Mer cells compared to 5TGM1 EV cells is that Mer expression confers a KaLwRij strain-specific advantage in 5TGM1 cell BM homing and establishment. To investigate this, the 5TGM1 Mer and 5TGM1 EV cell lines were inoculated intratibially into KaLwRij mice and tumour burden was monitored at week 3 using BLI. When 5TGM1 Mer and 5TGM1 EV cells are inoculated i.t. into KaLwRij mice, any differences in the abilities of these two cell

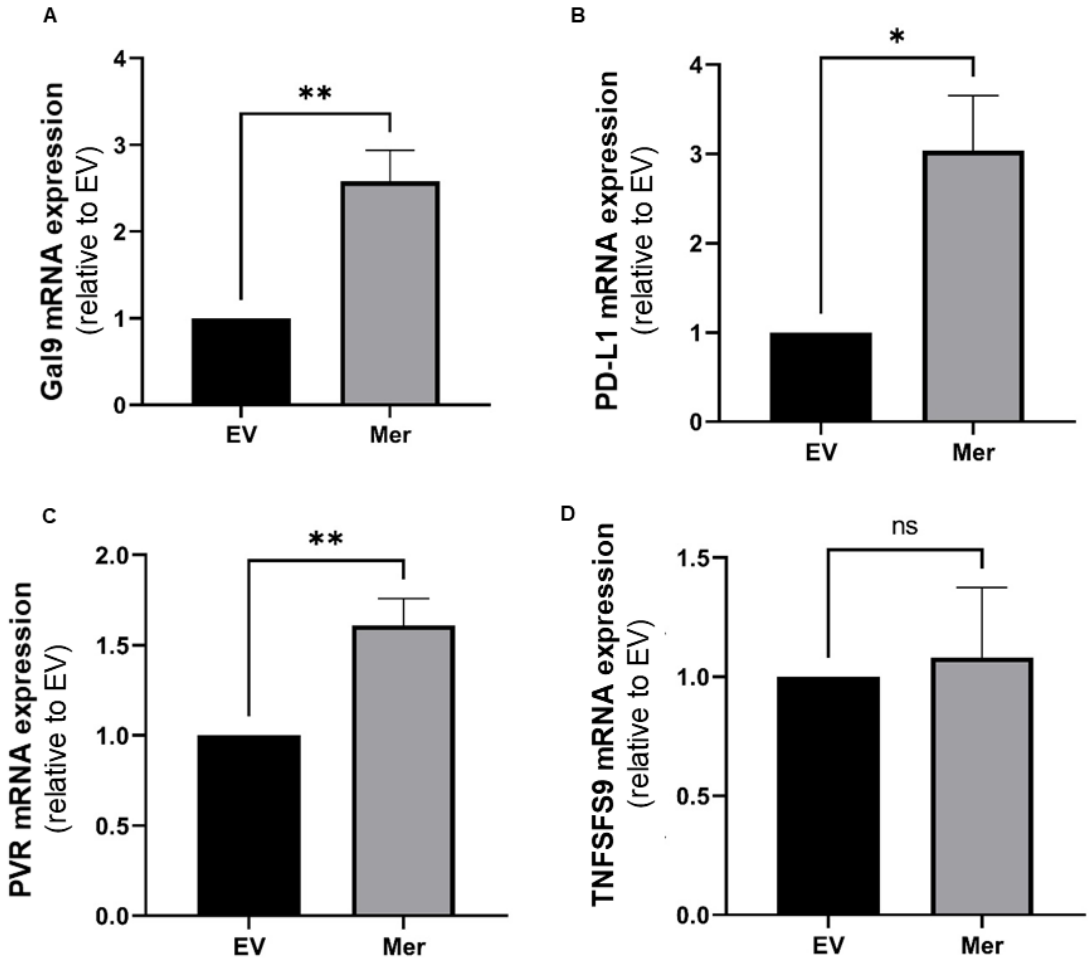

Figure 5.6. Mer expression increases mRNA expression levels of immune checkpoint proteins Galectin 9, PD-L1 and PVR. To identify changes in immune checkpoint mRNA expression with Mer expression**,** RT-qPCR was performed on cDNA generated from 5TGM1 Mer and 5TGM1 EV cells cultured in IMDM media. mRNA expression levels of **(A)** Galectin 9, **(B)** PD-L1, **(C)** PVR and **(D)** TNFSF9 were assessed in both 5TGM1 EV cells and 5TGM1 Mer cells. Gene expression levels are shown as normalised to *Hprt* and relative to 5TGM1 EV. Graphs depict mean ± SEM of four independent biological replicates performed in triplicate, Student's t-test. **p*<0.05, ***p*<0.01, n.s. p>.05.

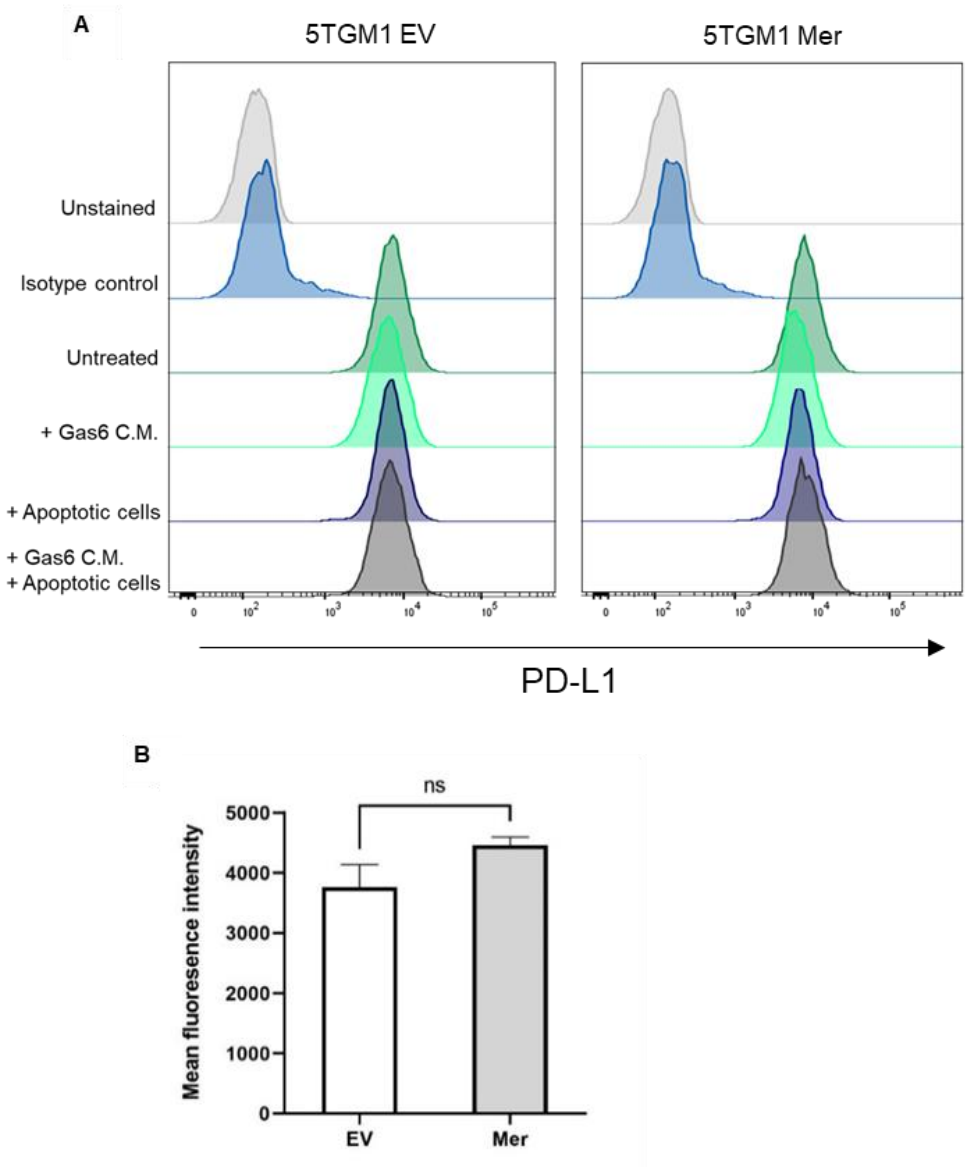

Figure 5.7. PD-L1 expression does not change in response to Mer expression or Gas6 stimulation. Cell surface PD-L1 expression was compared between GFP+ 5TGM1 EV cells and 5TGM1 Mer cells in response to a source of Gas6 and a source of phosphatidylserine using flow cytometry and an anti-PD-L1 antibody. **(A)** Representative histograms of PD-L1 cell surface expression of PD-L1 assessed when cells were cultured in IMDM media, 50% NIH3T3 Gas6 conditioned media, IMDM media with apoptotic cells, or both NIH3T3 Gas6 CM and apoptotic cells. Histograms are representative of three independent biological replicates. **(B)** Mean fluorescence intensity of PD-L1 was compared between GFP+ 5TGM1 Mer and 5TGM1 EV cells cultured in IMDM media. Graph depicts mean ± SD of three independent biological replicates, Student's t-test, n.s. p>.05.

lines to migrate to and become established in the BM will be bypassed. Intratibial injection also provides a means of directly determining whether Mer expression confers a cellular growth advantage when inoculated directly into the bone marrow microenvironment. Analysis of whole-body ventral BLI scans from week 3 revealed no significant differences in tumour burden in the injected leg between mice inoculated with 5TGM1 Mer cells and mice inoculated with 5TGM1 EV cells (Figure 5.8a-b). Additionally, a modest increase in the number of mice with substantial metastasis to the non-injected leg was identified in mice inoculated with 5TGM1 Mer cells (*n*=5 >250,000 photons/s) compared to mice inoculated with 5TGM1 EV cells (*n* = 3 >250,000 photons/s), however, a statistically significant difference in mean BLI signal between the two groups of mice was not observed (Figure 5.8c). Flow cytometric enumeration of the numbers of GFP+ tumour cells in the bone marrow showed similar results, with no difference in tumour burden between 5TGM1 Mer and 5TGM1 EV inoculated mice in the injected tibiae (Figure 5.8d), and a modest but not statistically significant increase in metastasis to the non-injected leg in mice inoculated with 5TGM1 Mer cells compared to 5TGM1 EV cells (Figure 5.8e). SPEP analysis also revealed no difference in whole animal tumour burden between mice inoculated with 5TGM1 Mer cells and 5TGM1 EV cells (Figure 5.8f). Although, it should be noted that the intensity of the paraprotein band is typically weak in such a localised tumour growth model and SPEP analysis may lack sensitivity in this instance. A previous study found that soluble recombinant Axl ectodomains could act as a Gas6 “sponge” and block Mer activation on breast cancer cell lines[219]. It was hypothesised that 5TGM1 Mer tumours may produce sMer, which would also have the potential to act as a Gas6 “sponge” and reduce systemic Gas6. Therefore, serum Gas6 levels were assessed by ELISA. These investigations revealed no difference in serum Gas6 levels between mice inoculated with 5TGM1 EV cells and mice inoculated with 5TGM1 Mer cells (Figure 5.8g).

5.2.9 Mer expression has no effect on the migration of 5TGM1 cells towards media or recombinant TAM ligands.

A modest but not statistically significant increase in metastasis to the non-injected legs of KaLwRij mice inoculated with 5TGM1 Mer compared to 5TGM1 EV cells was identified. To further investigate a potential pro-migratory phenotype conferred by Mer expression *in vitro* transwell migration assays were conducted. In a previous

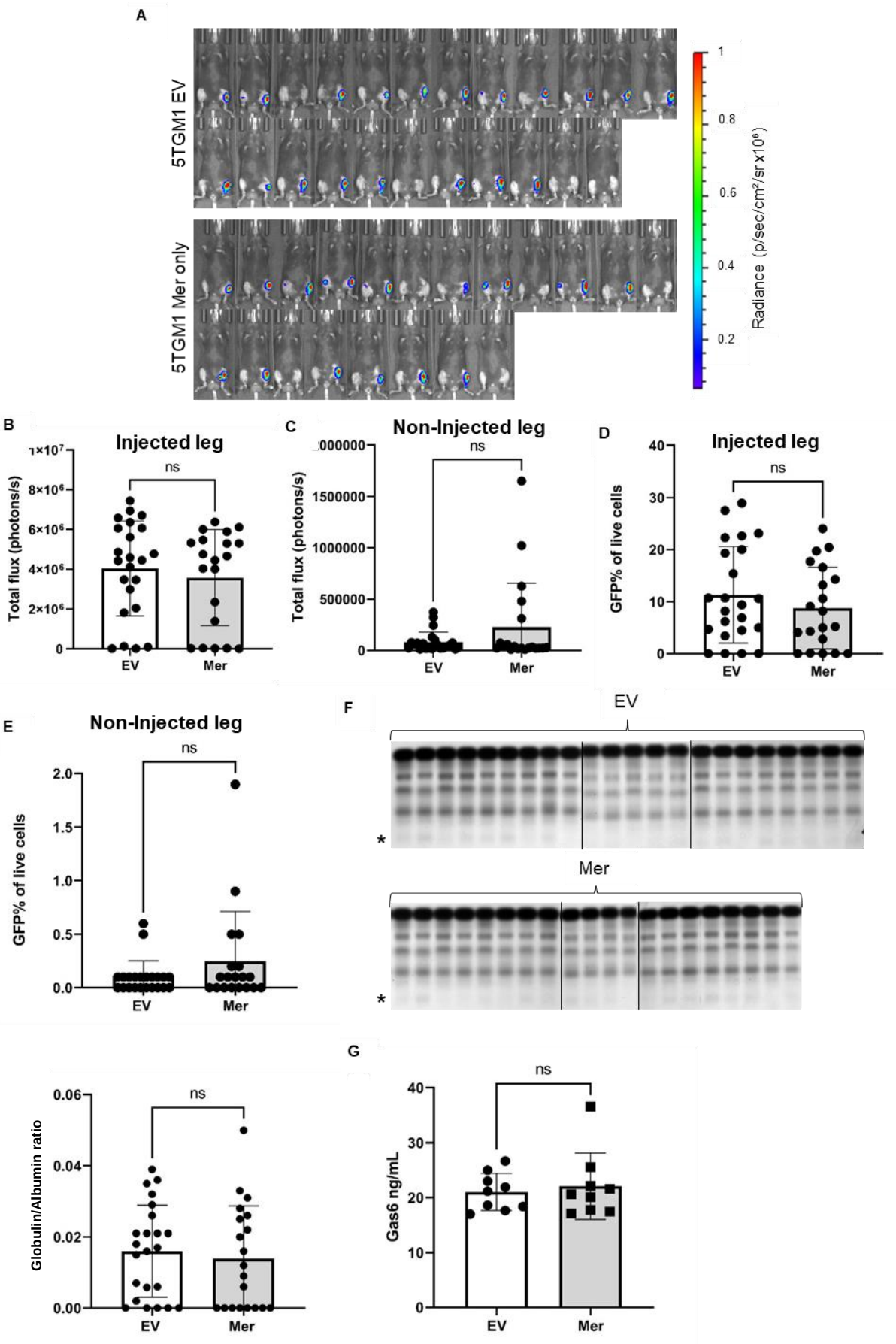
A
5TGM1 EV
5TGM1 Mer only
Radiance (p/sec/cm²/sr x10⁶)
1
0.8
0.6
0.4
0.2
B
Injected leg
Total flux (photons/s)
ns
EV
Mer
C
Non-Injected leg
Total flux (photons/s)
ns
EV
Mer
D
Injected leg
GFP% of live cells
ns
EV
Mer
E
Non-Injected leg
GFP% of live cells
ns
EV
Mer
F
EV
Mer
G
Globulin/Albumin ratio
ns
EV
Mer
Gas6 ng/mL
ns
EV
Mer

Figure 5.8. Mer expression has no effect on the growth of primary or secondary tumours following i.t. injection. C57BL/KaLwRij mice were i.t. inoculated with $1x10^5$ 5TGM1 EV cells or 5TGM1 Mer cells and disease burden was subsequently monitored by whole animal BLI, SPEP and flow cytometry. **(A)** Ventral BLI scans depict tumour burden at 3 weeks. A graph of the total flux after 3 weeks from **(B)** the injected leg and **(C)** the non-injected leg are shown. GFP+ % of live cells from the **(D)** injected tibiae and **(E)** non-injected leg of mice at 3.5 weeks is shown. **(F)** Serum was collected from the mice after 3 weeks and the M-spikes were measured by SPEP. M-spikes (*) on the SPEP gel and the quantitated Globulin/Albumin ratio are shown. Black lines indicate separation between gels. **(G)** Gas6 ng/mL in mouse serum from mice inoculated with 5TGM1 EV cells was compared to 5TGM1 Mer cells, *n*=9 mice/group. Graphs depict the mean ± SD of *n*=20-23 mice per cell line unless otherwise stated, Student's t-test, n.s. p>.05.

study, Mer expressing-B cell precursor ALL cell line RCH-ACV displayed increased migration in a transwell migration assay towards a source of Gas6 compared to media alone[279]. Therefore, it was hypothesised that 5TGM1 Mer cells may display an enhanced ability to migrate towards a source of ligand. 5TGM1 EV and 5TGM1 Mer cells were seeded into the top well of a transwell plate and allowed to migrate to the bottom well containing IMDM media or IMDM media containing a source of recombinant Gas6 or Pros1 over 24 hours. GFP+ cells were then enumerated by flow cytometry and absolute cells/well were calculated using counting beads (Figure 5.9a). Modest, but not statistically significant increases in migration of 5TGM1 Mer cells, compared to 5TGM1 EV cells, were observed in IMDM media alone (Figure 5.9b), IMDM media with the addition of recombinant Gas6 (Figure 5.9c), and IMDM media with the addition of recombinant Pros1 (Figure 5.9d).

5.2.10 Retroviral mediated generation of a panel of 5TGM1 Mer and Gas6 differentially expressing cells.

Previous studies showed that myeloma patient-derived MM PCs express Mer and Gas6 at the mRNA level.[166] To investigate the effects of paracrine versus autocrine Gas6 signalling, a panel of 5TGM1 cells, differentially expressing Mer and Gas6 were generated. 5TGM1 Mer and 5TGM1 EV cells were transduced with a novel pRufimPlum retroviral vector encoding Gas6, or the empty vector, to generate four cell lines expressing different combinations of Mer and Gas6 (Supplementary Figure 11, Figure 5.10a). Expression of the mPlum reporter was confirmed using flow cytometry in all four cell lines (Figure 5.10b). Expression of HA-tagged Gas6 was assessed by western blot, showing HA-tagged transgene expression in 5TGM1 Mer Gas6 cells and 5TGM1 EV Gas6 cells compared to 5TGM1 Mer EV cells and 5TGM1 EV EV cells (Figure 5.10c).

5.2.11 Differential Mer and Gas6 expression have no effect on cell proliferation *in vitro* or tumour burden *in vivo*.

It was anticipated that 5TGM1 Mer Gas6 cells would display increased *in vitro* proliferation compared to 5TGM1 Mer EV, 5TGM1 EV Gas6 and 5TGM1 EV EV cell lines. Proliferation assays performed in IMDM media showed no differences in rates of proliferation between any of the four cell lines at the 72-hour time point (Figure

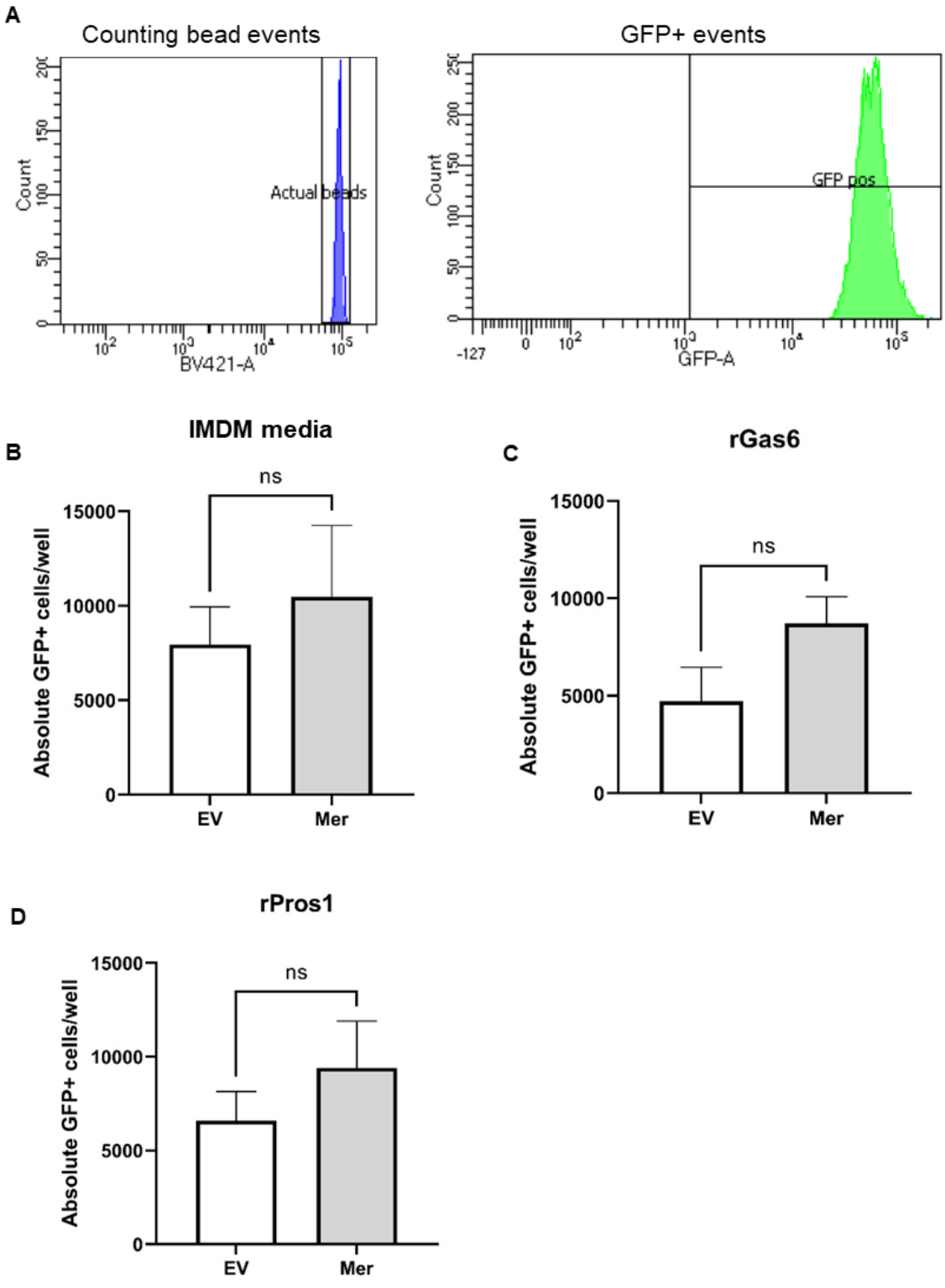
A
Counting bead events
Count
Actual beads
BV421-A
GFP+ events
Count
GFP pos
GFP-A
B
IMDM media
ns
Absolute GFP+ cells/well
15000
10000
5000
0
EV
Mer
C
rGas6
ns
Absolute GFP+ cells/well
15000
10000
5000
0
EV
Mer
D
rPros1
ns
Absolute GFP+ cells/well
15000
10000
5000
0
EV
Mer

Figure 5.9. Mer expression has no effect on the migration of 5TGM1 cells towards media or recombinant TAM ligands. 5x10^5 5TGM1 Mer or 5TGM1 EV cells were seeded into the upper chamber of transwell plates and allowed to migrate to the bottom chamber over 24 hours. **(A)** Representative plots showing counting bead events (left) used to calculate the absolute number of GFP+ cells/well, and GFP+ events from the bottom chamber of transwells (right). 5TGM1 EV and 5TGM1 Mer cell migration towards **(B)** IMDM media, **(C)** IMDM media with rGas6 and **(D)** IMDM media with rPros1 was compared. Graphs are presented as mean ± SEM of 5 independent biological replicates, performed in triplicate, Students t-test, n.s. p>.05.

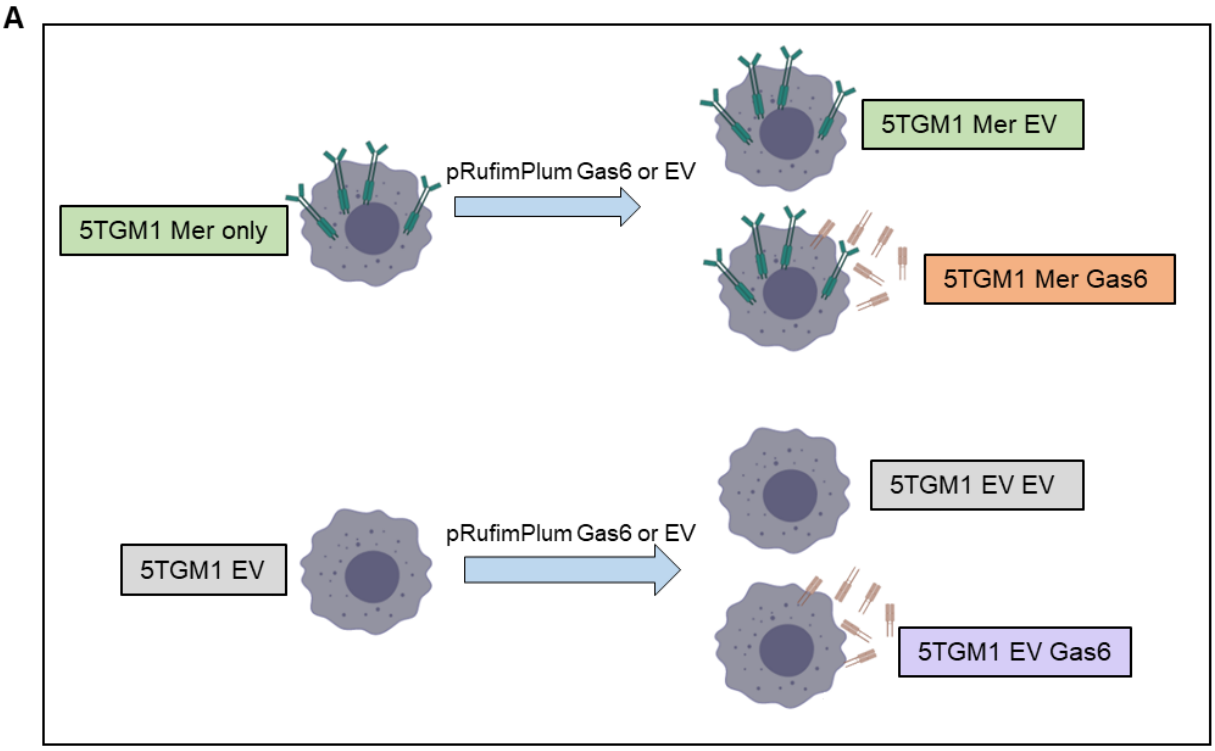
A
5TGM1 Mer only
pRufimPlum Gas6 or EV
5TGM1 Mer EV
5TGM1 Mer Gas6
5TGM1 EV
pRufimPlum Gas6 or EV
5TGM1 EV EV
5TGM1 EV Gas6

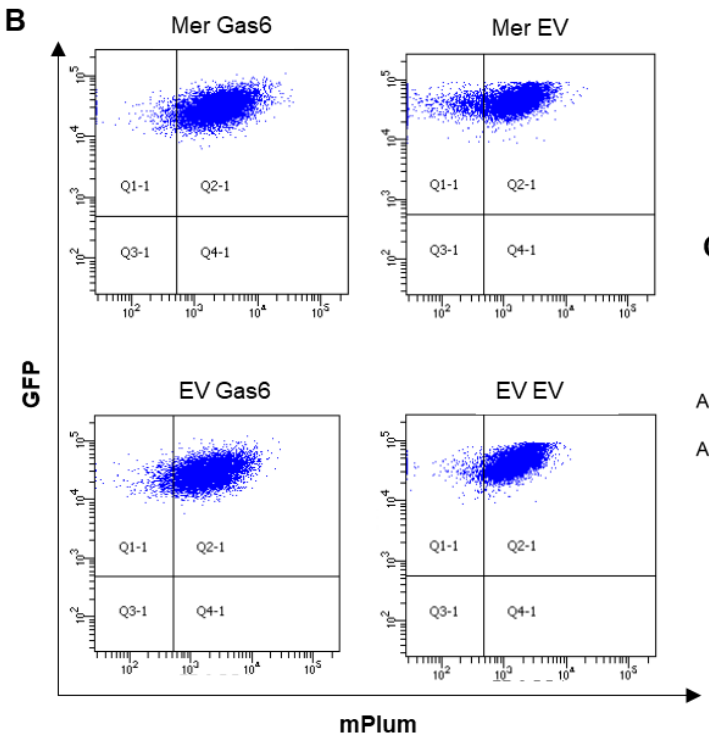
B
Mer Gas6
Mer EV
EV Gas6
EV EV
Q1-1
Q2-1
Q3-1
Q4-1
GFP
mPlum

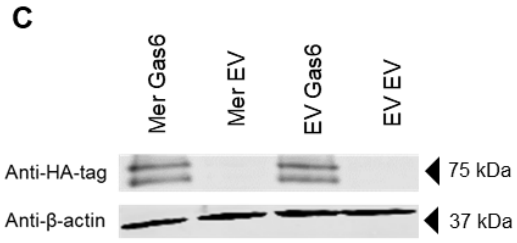
C
Mer Gas6
Mer EV
EV Gas6
EV EV
Anti-HA-tag
75 kDa
Anti-β-actin
37 kDa

Figure 5.10. Retroviral mediated generation of a panel of 5TGM1 Mer and Gas6 differentially expressing cells. To further elucidate the importance of autocrine vs. paracrine Gas6 signalling in MM pathogenesis, a panel of 5TGM1 Mer and Gas6 differentially expressing cell lines were generated. **(A)** 5TGM1 Mer and 5TGM1 EV cells were retrovirally transduced with pRufimPlum EV or pRufimPlum encoding HA-tagged Gas6 to generate four cell lines expressing different combinations of Mer and Gas6. **(B)** Double GFP and mPlum reporter expression is shown in successfully transfected 5TGM1 Mer Gas6 cells, 5TGM1 Mer EV cells, 5TGM1 EV Gas6 cells and 5TGM1 EV EV cells. **(C)** The panel of 5TGM1 cell lines differentially expressing Mer and Gas6 was subjected to western blotting using an anti-HA-tag antibody. β-actin was used as a loading control.

5.11a). To assess whether concomitant expression of both Mer and Gas6 promoted tumour burden *in vivo*, 5TGM1 Mer Gas6, 5TGM1 Mer EV, 5TGM1 EV Gas6 and 5TGM1 EV EV cell lines were i.v. inoculated into KaLwRij mice and tumour burden was subsequently monitored at week 5 using BLI. It was hypothesised that a source of autocrine Gas6 *in vivo,* when KaLwRij mice are inoculated with 5TGM1 Mer Gas6 cells, would promote an increase in MM tumour burden compared to other combinations of Mer and Gas6 expression. Analysis of whole-body ventral BLI scans from week 5 revealed no differences in tumour burden between groups of mice inoculated with the four different cell lines (Figure 5.11b-c). Although it did not reach statistical significance, there was an increase in mean BLI signal in mice injected with 5TGM1 Mer EV cells (mean $1.28x10^7$ ± s.d. $3.67x10^6$ photons/s) compared to that detected in mice injected with 5TGM1 EV cells (mean $3.1x10^6$ ± s.d. $1.11x10^6$ photons/s). Therefore, this does not contradict previous results indicating that 5TGM1 Mer cells produce greater *in vivo* tumour burden compared to 5TGM1 EV cells (Figure 5.3). The GFP+ tumour cell percentage of total BM cells was assessed in mice that had detectable tumour burden by BLI, which provided similar results to BLI (Figure 5.11d). SPEP analysis from all mice again showed no differences in myeloma burden between any of the groups of mice inoculated with any of the four 5TGM1 cell lines differentially expressing Mer and Gas6 (5.11e).

5.3 Discussion

MM PC growth and disease progression is supported by the communication between the PCs and the BM microenvironment facilitated by cell surface receptor-ligand signalling. The tyrosine kinase receptor Mer, and its ligand Gas6, have previously been shown to promote MM PC survival and proliferation *in vitro* and *in vivo*[6, 7]. Due to the widespread expression of Mer and Gas6 by MM patient PCs[6], this receptor-ligand axis represents a clinically targetable pathway. In other cancers, Mer and Gas6 signalling have also been implicated in cancer cell escape from immune surveillance[11, 12, 15] and increased cancer cell migration to distal sites[8]. Therefore, in addition to providing MM PCs with a proliferative or survival advantage, Mer receptor expression may also promote MM disease progression through these other mechanisms. In this chapter, a model of Mer positive and Mer negative 5TGM1 murine myeloma cell lines was utilised to further investigate the function of the Mer/Gas6 signalling pathway in MM.

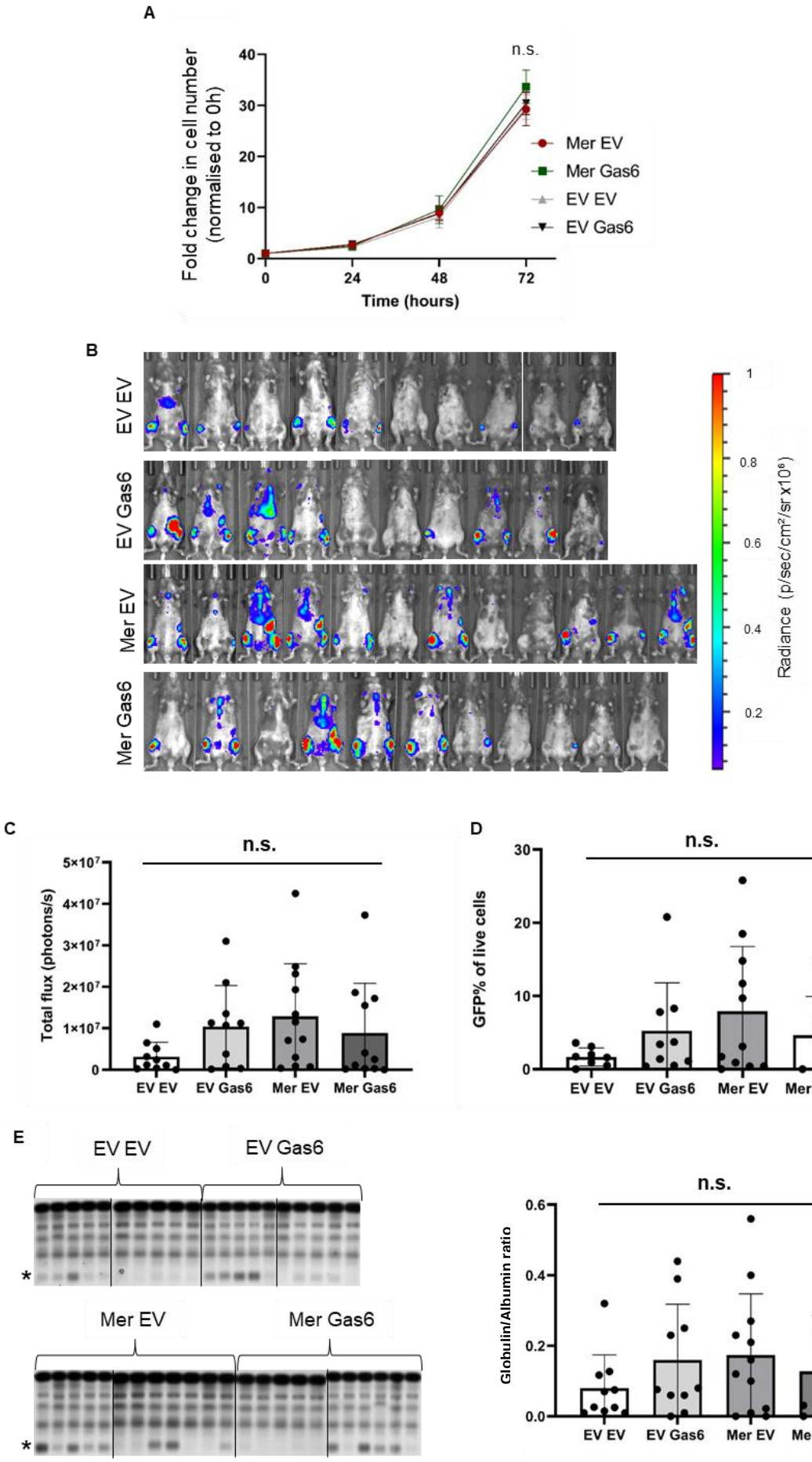
A
n.s.
Fold change in cell number (normalised to 0h)
Time (hours)
Mer EV
Mer Gas6
EV EV
EV Gas6
B
EV EV
EV Gas6
Mer EV
Mer Gas6
Radiance (p/sec/cm²/sr x10⁶)
C
n.s.
Total flux (photons/s)
D
n.s.
GFP% of live cells
E
EV EV
EV Gas6
Mer EV
Mer Gas6
n.s.
Globulin/Albumin ratio

Figure 5.11. Differential Mer and Gas6 expression have no effect on cell proliferation *in vitro* or tumour burden *in vivo*. (A) Proliferation of a panel of differential Mer and Gas6 expressing cell lines was monitored over 72 hours by a WST-1 assay in IMDM media. Results were displayed as fold change in absorbance (450nm) over 72 hours. Graphs depict mean ± SEM of three independent biological replicates performed in triplicate, Two-way ANOVA with Tukey's multiple comparisons. **(B-E)** KaLwRij mice were inoculated with $5x10^5$ 5TGM1 EV EV, 5TGM1 EV Gas6, 5TGM1 Mer EV or 5TGM1 Mer Gas6 cells and disease burden was subsequently monitored by whole animal BLI, SPEP and flow cytometry. **(B)** Ventral BLI scans depict tumour burden at week 5. **(C)** A graph of the total flux at week 5 from ventral scans is shown. **(D)** GFP+ tumour cell % of live cells from the bone marrow of the hind limbs of tumour bearing mice was assessed. Serum was collected from the mice after 5 weeks and the M-spikes were measured by SPEP. **(E)** M-spikes (*) on the SPEP gel (left) and the quantitated Globulin/Albumin ratio (right), are shown. Black lines indicate separation between different gels. Graphs depict the mean ± SD of *n*=10-12 mice per cell line, One way ANOVA with Tukey's multiple comparisons, n.s. p>.05.

Previous studies identified that Mer and Gas6 expression provides MM PCs with a proliferative advantage[166, 188], and Mer has been shown to promote the proliferation of lung cancer and leukaemia cell lines[252, 286]. Therefore, it was anticipated that Mer-expressing 5TGM1 cells would provide a proliferative advantage *in vitro* and *in vivo* compared to control 5TGM1 cells. Mer expression did, in fact, increase proliferation of 5TGM1 cells cultured in IMDM media and NIH3T3 EV media, the latter containing low levels of the Mer ligands Gas6 and Pros1. Although statistically significant, the fold changes in proliferation rates were modest. At the 72-hour time point, 5TGM1 Mer cells displayed a 1.3-fold increase in mean cell number compared to 5TGM1 EV cells when cultured in IMDM media, and a 1.27-fold increase when cultured in NIH3T3 EV media. Previous studies identified a greater magnitude of change in proliferation rates due to Mer expression in human myeloma cell lines[166, 188]. Given that the human myeloma cell lines utilised in these other studies express Gas6, whereas 5TGM1 cells do not, this suggests that autocrine Mer/Gas6 signalling may support MM PC proliferation. The results of cell cycle analysis performed in the present study, showed a slight increase in proportions of 5TGM1 Mer cells in S phase compared to 5TGM1 EV cells when cultured in IMDM media, although this did not reach statistical significance. These data suggest that Mer expression promotes a modest increase in 5TGM1 cell proliferation *in vitro*, although this was not observed when cells were cultured in NIH3T3 conditioned media enriched for Mer ligands. The 5TGM1 Mer and 5TGM1 EV cell lines were inoculated intravenously into KaLwRij mice, and consistent with results from a previous study[6], Mer expression did confer greater *in vivo* myeloma burden. Assessment of cell proliferation at the experimental endpoint using the nucleotide analogue EdU revealed no differences in tumour cell proliferation in mice inoculated with 5TGM1 Mer cells compared to mice inoculated with 5TGM1 EV cells. Therefore, the increased proliferation rates of 5TGM1 Mer compared to 5TGM1 EV cells observed *in vitro* were not evident in the complex cellular milieu of the BM microenvironment *in vivo*. Future studies should conduct the *in vivo* EdU assay at earlier time points such as 7, 14 and 21 days, as it is possible that differences in cell proliferation may occur at an earlier stage in tumour establishment. To further investigate the mechanism by which Mer promotes MM tumour burden, 5TGM1 Mer and 5TGM1 EV cells were evaluated in alternative *in vivo* models. When cells were injected intratibially into the KaLwRij BM microenvironment, bypassing the BM homing mechanism, no differences in tumour burden due to Mer expression were identified.

5TGM1 Mer and 5TGM1 EV cells were also inoculated intravenously into the immune compromised NSG mouse model, again resulting in no differences in tumour burden with Mer expression. Therefore, Mer expression does not confer a proliferation advantage to MM PCs *in vivo*. These data suggest that enhanced BM homing and the presence of an adaptive immune system are important for the role of Mer in promoting MM tumour burden in these model systems.

Previous studies suggested that Mer promotes cancer cell evasion of immune surveillance through modulation of the PD-1/PD-L1 axis[11, 12]. In the current study, using the immune competent KaLwRij mouse model, we found that Mer expression promoted 5TGM1 tumour burden when cells were administered intravenously but not when administered intratibially. Results from a previous study indicate that when 5TGM1 cells are intratibially inoculated directly into the BM of KaLwRij mice, a state of immune tolerance can occur as the large number of tumour cells overwhelm the immune system[287]. This did not occur in micro metastases, where only small numbers of cells colonise the BM. Therefore, when 5TGM1 Mer and 5TGM1 EV cells are inoculated intratibially into KaLwRij mice it is possible that immune tolerance occurs regardless of Mer expression. Like previous studies, immune checkpoint pathways that function by signalling through T-cell receptors, such as PD-L1/PD-1, may be modulated by 5TGM1 Mer expression in KaLwRij mice, resulting in immune suppression and increased tumour burden[175, 186]. However, future studies should include a broader analysis of immune cell subsets in KaLwRij mice bearing 5TGM1 Mer tumours compared to 5TGM1 EV tumours using mass cytometry or scRNA seq analysis. Mass cytometry enables single cell analysis of immune cell subsets including T-cells, B-cells and NK cells[288], and has been used successfully in previous studies to identify changes in T-cell populations in acute myeloid leukaemia[289]. A recent study was performed in which scRNA seq on MM patient samples was used to investigate the transcriptome profile of PCs and their immune microenvironment throughout MM disease development[290]. In this study, the authors found that the composition of the immune microenvironment was dynamic across disease stages and across patients. Therefore, mass cytometry or scRNA seq could be used to identify whether Mer expression in MM PCs can alter immune cell subsets in the BM microenvironment of KaLwRij mice, providing a

greater understanding of the mechanism by which Mer potentially promotes immune suppression.

In a previous study, immune checkpoint profiling performed on BM PCs from MM patients and healthy controls identified 10 immune checkpoint pairs that have dysregulated expression in MM[284]. The immune checkpoint axes identified in this study included PD-L1/PD-1, Galectin9/Tim3, PVR/TIGIT and TNFSF9/TNFRSF9. In the present study, significantly increased mRNA expression of PD-L1, Galectin 9 and PVR in 5TGM1 Mer compared to 5TGM1 EV cells was observed. However, this was not associated with an increase in cell surface expression of PD-L1. Cell surface expression of Galectin 9 and PVR was not investigated in this study due to time constraints. This result contrasts the results from a previous study, which showed increased cell surface expression of PD-L1 in TAM receptor expressing-breast and cervical cancer cell lines following exposure to Gas6 and phosphatidylserine[175]. These data indicate that the proposed immune suppression facilitated by Mer expression in the 5TGM1/KaLwRij model of MM is occurring via mechanisms outside of these three T-cell immune checkpoint axes. Future studies should assess the potential co-expression of Mer, PD-L1 and other immune checkpoint proteins in MM patient PCs using the freely available COMMpass dataset (https://portal.gdc.cancer.gov/projects/MMRF-COMMPASS). Cell surface expression of PD-L1 and other immune checkpoint proteins should also be assessed by flow cytometry in human myeloma cell lines with differential Mer expression levels. In addition to changes in T-cell function, NK cell function is commonly supressed in late stage MM, contributing to MM PC immune escape[236]. The NK cell stimulatory receptor NGKD2 is activated by binding of its ligand MICA, which is expressed by human MM cells. A recent study found that Gas6/Mer signalling can downregulate MICA expression in human MM cell lines SKO-007(J3), U266 and ARP1, identifying a potential mechanism of NK cell suppression by MM PCs[237]. MICA expression was not assessed in the current study as expression of its ligand, NKG2DL, is not conserved in mice and thus is not a potential mechanism of immune evasion in murine cancer models[291]. However, numerous potential mechanisms of immune evasion have recently been identified at the gene-expression level in MM patient PCs[292]. MM PCs expressed classic and non-classic MHC class I molecules, and genes such as LILRB1 and LILRB4, which may deliver

inhibitory signals to NK cells, as well as TNFSF10, which can trigger aberrant T-cell activation. Therefore, RNA seq should be performed on 5TGM1 Mer tumours compared to 5TGM1 EV tumours from KaLwRij mice to assess broader differences in genes that may be associated with immune suppression in this model. Investigating whether Mer expressed by MM PCs can promote an immune suppressive tumour microenvironment may identify Mer as a potential therapeutic target to limit immune suppression in MM.

In the current study, 5TGM1 Mer cells produced greater tumour burden compared to 5TGM1 EV cells when inoculated intravenously into the KaLwRij model. In contrast, no difference in tumour burden was detected in primary tumours when cells were inoculated intratibially. However, in the latter experiments, a slightly increased incidence of tumours in the non-injected leg was detected in 5TGM1 Mer inoculated mice compared with 5TGM1 EV inoculated mice. Given that the BM homing mechanism is bypassed in the intratibial model, it was hypothesised that it is by this mechanism that Mer promotes MM tumour burden when cells are delivered intravenously. A previous study showed that Mer expressing-B cell precursor ALL cell line RCH-ACV displayed increased migration towards a source of Gas6 *in vitro* compared to media alone[8]. Therefore *in vitro* migration assays were performed, revealing that 5TGM1 Mer cells display a modest, but not statistically significant increase in migration compared to 5TGM1 EV cells regardless of the presence of ligand. This was consistent with the small increase in the incidence of metastasis of 5TGM1 Mer cells compared to 5TGM1 EV cells to the non-injected leg in the i.t. KaLwRij model. As cells within the KaLwRij BM microenvironment express Gas6, it was hypothesised that Gas6 may act as a chemokine in the KaLwRij model, promoting the BM homing of Mer expressing cells. However, results of a 24-hour BM homing assay showed no difference in the number of GFP+ cells detected in the BM of mice inoculated with 5TGM1 Mer cells compared with 5TGM1 EV cells (data not shown). Notably, this assay lacks sensitivity, with only 0.5-1 GFP+ cells detected per million BM cells. The 24-hour time point utilised in this assay also does not directly compare to the metastases that are established over 2-3 weeks in the i.t. model.

The dissemination of myeloma cells is a multi-step process that is subject to

selection pressures within the BM microenvironment[293]. DNA barcoding studies have tracked the fates of MM PC clones *in vivo*, revealing that primary tumours result from the clonal expansion of only a small number of individual clonal cells[248, 294]. Shen, *et. al.,*[248] found that both circulating cells and sites of secondary tumours displayed even less clonal diversity, suggesting multiple bottlenecks exist in the migration, bone marrow establishment, and growth of MM PCs. Due to these *in vivo* selection pressures, the i.v. injection of 5TGM1 cells into KaLwRij mice is highly inefficient, with less than 0.01% of injected cells contributing to the final tumour burden[129, 293, 294]. In the present study, the combined immunosuppressive and migration advantages conferred by Mer expression could enable 5TGM1 cells to overcome selection pressures, disseminate and establish within the BM of KaLwRij mice more readily. Further studies are warranted to identify whether targeting Mer in MM PCs prior to the progression to metastatic disease may have therapeutic efficacy in limiting the selective outgrowth of Mer-expressing PC clones.

Myeloma patient PCs express both Mer and Gas6, and a previous study identified that autocrine Gas6 signalling supported MM PC growth *in vitro* and *in vivo*[166]. To identify which combination of Mer and Gas6 expression supports MM pathogenesis in the 5TGM1/KaLwRij model, four 5TGM1 cell lines differentially expressing Mer and Gas6 were generated. It was anticipated that the 5TGM1 Mer Gas6 cell line would produce the greatest tumour burden *in vivo* as there would be the potential for both autocrine and paracrine Gas6 signalling to support MM disease progression. However results showed no statistically significant differences in tumour burden based on Mer and Gas6 expression, which contradicts the results of a previous study[166]. The numbers of mice inoculated with each cell line in this experiment were significantly lower (Figure 5.11, *n*=10-12 mice/group) compared to the i.v. KaLwRij model using 5TGM1 Mer cells and 5TGM1 EV cells (Figure 5.3, *n*=17 mice/group). Thus, there may be insufficient power to detect differences in tumour burden between 5TGM1 cell lines differentially expressing Mer and Gas6. Due to consecutive rounds of genetic manipulation of these cell lines, their ability to engraft within the bone marrow may be impaired in comparison to 5TGM1 Mer and 5TGM1 EV cell lines. Therefore, future studies utilising these cell lines should consider an additional passage through the bone marrow of KaLwRij mice prior to their use. Results from this chapter suggest that in the KaLwRij model, cells in the

BM microenvironment, such as osteoblasts, produce sufficient Gas6 to support 5TGM1 Mer EV cell growth and disease progression, and an additional source of autocrine Gas6 in 5TGM1 Mer Gas6 cells is not required for optimal tumour growth. Interestingly, mice inoculated with 5TGM1 EV Gas6 cells displayed similar levels of tumour burden compared with mice inoculated with 5TGM1 Mer EV or 5TGM1 Mer Gas6 cell lines. Gas6 expressed and secreted by 5TGM1 cells could signal through TAM receptors expressed by other BM microenvironment cells, such as tumour associated macrophages, which may support MM PC growth and tumour development. A previous study, examining oral squamous carcinoma, provides evidence of this, with results suggesting that Gas6-expressing cancer cells polarised tumour-associated macrophages towards a pro-tumoural M2 phenotype through Gas6/Axl signalling, thus supporting cancer cell growth[295]. Further to this, macrophage depletion, via clodronate liposome pre-treatment, abrogated 5TGM1 tumour development in the KaLwRij model of MM, indicating that in this model macrophages support disease progression[296]. However, further studies are required to understand the role of Gas6 paracrine signalling between MM PCs and BM microenvironment cells.

In this study, Mer expression in the murine 5TGM1 cell line was found to increase 5TGM1 tumour burden in the KaLwRij model of myeloma. Our findings indicate that the mechanism of action of Mer in potentiating MM tumour burden may be through increased 5TGM1 BM homing and promotion of an immune suppressive tumour microenvironment. It is possible that Mer expression may promote engraftment of 5TGM1 cells and tumour establishment in specialised BM niches, rather than promoting migration per se, leading to increased tumour burden. This could be due to factors such as engagement with Gas6-expressing BM cells, such as osteoblasts, and immune suppression through immune checkpoint inhibition, however, further investigation is warranted to fully elucidate these mechanisms. Further studies to explore the possible role of Mer in promoting immune suppression in human MM are also needed. Mer inhibitors and Pan-TAM tyrosine kinase inhibitors have been used with success to limit *in vivo* tumour burden in pre-clinical models[186, 222, 232, 297]. Therefore, understanding the specific roles of the Mer/Gas6 axis in MM will identify whether using these Mer small molecule inhibitors will have therapeutic efficacy in MM patients.

6. Final Discussion

MM is a haematological malignancy characterised by the uncontrolled clonal expansion of MM PCs within the bone marrow[1]. The current 5-year survival rate from date of MM diagnosis is 54.9% in Australia, which remains lower than other common cancers such as colorectal, breast and prostate cancers[6]. Myeloma is a genetic disease in which each patient displays a unique combination of primary and secondary genetic events that contribute to disease initiation and progression[70]. Despite constant improvements in treatment options for MM patients, which include autologous stem cell transplants, immunomodulatory imide drugs, proteasome inhibitors and biological agents, almost all patients will inevitably relapse[45]. MM PCs manipulate the bone marrow microenvironment to support their proliferation and tumour formation, immune evasion, and eventual disease relapse[108]. MM relapse is thought to arise from dormant subpopulations of MM PCs that evade the immune system and therapeutic targeting and persist long term in the bone marrow until they are reactivated to form new tumours [212, 264]. The molecular mechanisms that govern dormant cell reactivation and MM disease progression is the subject of intense investigation. Interactions between MM PCs and other cells that comprise the bone marrow microenvironment are facilitated by adhesion molecules, cytokine signalling and cell surface receptor and ligand signalling[109]. Therefore, cell surface receptors and ligands expressed by MM PCs represent potential therapeutic targets to limit MM disease progression.

MM PC dormancy occurs when cells enter a state of growth arrest, which is thought to be maintained by contact with osteoblasts at the endosteal bone surface[129]. Dormant MM PCs reside long term within the endosteal niche, evading targeting by conventional therapies, which target rapidly dividing cells[211]. Dormant MM PCs can become reactivated when favourable conditions arise and can re-enter the cell cycle, begin proliferating, and contribute to disease relapse[212]. However, the mechanisms controlling MM PC dormancy and reactivation remain poorly understood. Previous studies using the 5TGM1/ KaLwRij murine model of MM showed that expression of the TAM tyrosine kinase cell surface receptor Axl was associated with 5TGM1 MM cell dormancy[129, 213]. Initial studies indicated that osteoclast-mediated bone turnover ‘released’ 5TGM1 cells from dormancy *in vivo* by ceasing their contact with osteoblasts[131]. Therapeutic blockade of Axl by Khoo, *et al.*,[213] *in vivo* in tumour-bearing mice also ‘released’ 5TGM1 cells from dormancy

and resulted in increased tumour burden compared to untreated mice. These studies suggest that cell-cell interactions between osteoblasts and MM PCs such as the Gas6/Axl axis may be important for MM PC dormancy. The role of Axl in initiating and maintaining MM PC dormancy was further investigated in the current study using genetically modified Axl-positive (5TGM1 Axl) and Axl-negative (5TGM1 EV) 5TGM1 cell lines. It was hypothesised that inoculation of KaLwRij mice with 5TGM1 Axl cells would result in significantly reduced tumour burden compared to mice inoculated with 5TGM1 EV cells. However, no statistically significant differences in tumour burden were observed between mice bearing Axl-positive compared to Axl-negative tumours. Moreover, the 5TGM1 Axl cells did not display evidence of an Axl-specific dormancy phenotype in either *in vitro* DiD-labelling assays or cell cycle analysis compared to 5TGM1 EV cells. Therefore, the results of the present study do not provide evidence that high Axl expression by 5TGM1 cells alone is sufficient to initiate myeloma dormancy.

Khoo, *et al.*,[213] identified genes other than Axl that were highly expressed by dormant 5TGM1 cells harvested from the BM of mice. These genes included *Irf7*, *Spic*, *Vcam1*, *Fcerg1*, *Mpeg1*, and *Sirpa,* and should be investigated for their capacity to induce dormancy in future studies. Notably, when Khoo, *et al*., treated mice with the Axl, Met kinase[214],Tyro3 Mer[215], and Ron[216] inhibitor BMS-777607, mice displayed increased tumour burden and a reduction in dormant MM PC numbers. These studies may suggest that Axl, or one of the other targets of BMS-777607, may be involved in MM PC dormancy maintenance even if they do not play a role in dormancy initiation. Dormant MM PCs which are not susceptible to conventional therapies targeting actively cycling cells may provide a reservoir of malignant PC clones for future disease relapse. Reactivating dormant cells prior to therapy could reduce this reservoir of cells, preventing or delaying MM relapse. In the context of acute myeloid leukemia (AML), *in vivo* treatment of human AML tumour bearing-mice with granulocyte colony-stimulating factor (GCSF), a stimulator of myeloid cell differentiation, maturation and proliferation, reactivated dormant AML cells at the endosteal niche[298]. Notably, in these studies, Saito, *et al.,*[298] transplanted GCSF treated or untreated bone marrow from AML tumour bearing mice into recipient mice, which were treated with the chemotherapeutic agent cytarabine. GCSF treatment prior to cytarabine increased survival time

compared to cytarabine treatment alone, indicating therapeutic efficacy of dormant AML cell reactivation prior to chemotherapy. A recent meta-analysis of leukemia studies showed that GCSF treatment in leukemia patients increases overall survival and decreases chance of relapse[299]. An alternate strategy to prevent relapse in MM would be to maintain long term cancer cell dormancy by preventing their reactivation. A previous study by Lawson, *et al*.[129] showed that osteoclast remodelling of the endosteal niche released 5TGM1 cells from dormancy by limiting contact with osteoblasts. Therefore, it is necessary for future studies to identify specific mechanisms of MM PC reactivation, which could form the basis of novel treatment strategies to maintain long term MM PC dormancy and prevent relapse.

Previous studies identified that the Gas6/Mer axis promotes the proliferation of human MM PCs[166, 188]. Malignant PCs from the majority of MM patients express both Gas6 and Mer at the mRNA level, with Gas6 expression increased compared to that seen in healthy control PCs [166, 188]. Given that Gas6 and Mer are expressed by the majority of patient MM PCs[166], the Gas6/Mer axis is an attractive therapeutic target to limit MM disease progression. The role of Mer in promoting MM PC proliferation was further investigated in this study using genetically modified Mer-positive (5TGM1 Mer) and Mer-negative (5TGM1 Mer) 5TGM1 cell lines. Studies in this thesis revealed that 5TGM1 Mer cells produce significantly greater myeloma tumour burden *in vivo* in comparison to 5TGM1 EV cells following intravenous inoculation into the C57BL/KaLwRij mouse model. Previous studies suggested that Mer promotes cancer cell evasion of immune surveillance through modulation of the PD-1/PD-L1 axis[186, 215]. Therefore, it was hypothesised that the ability of Mer in promoting tumour burden in the KaLwRij model of MM may, in part, depend on the presence of an adaptive immune system. In fact, when 5TGM1 Mer cells and 5TGM1 EV cells were inoculated intravenously into immune compromised NSG mice, no difference in tumour burden with Mer expression was identified after 4 weeks. Furthermore, significantly increased mRNA expression of immune checkpoint proteins PD-L1, Galectin 9 and PVR in 5TGM1 Mer compared to 5TGM1 EV cells was observed. However, this was not associated with an increase in cell surface expression of PD-L1. Future studies should more broadly examine the role of Mer in mediating MM immune suppression through RNA seq analysis performed on 5TGM1 Mer tumours compared to 5TGM1 EV tumours from KaLwRij mice to

assess differences in immune suppression related genes. Therapeutic strategies that combine immunotherapies with distinct mechanisms of action such as IMiDs, monoclonal antibodies SLAMF7 and CD38, and other novel agents are becoming attractive strategies for heavily pre-treated patients and those with immunotherapeutic resistance [300]. Further characterisation of the role of Mer in MM could provide a novel immunotherapeutic target that contributes to future MM immunotherapy regimens.

Several Mer inhibitors are currently in development and have shown anti-cancer activity in pre-clinical models. Results of a recent study using a selective Mer small molecule inhibitor, R992, showed that treating NSG mice inoculated with human MM cell lines reduced MM tumour burden and increased bone-forming osteoblast activity, thereby reducing MM disease-induced osteolysis[301]. Due to similarities in the molecular structure of the TAM receptors, many inhibitors target multiple TAM receptors as well as other receptor tyrosine kinases[302]. Previous preclinical studies have shown that Mer inhibitors can have both a direct effect on reducing tumour burden *in vivo* as well as an immune mediated effect[186, 215]. To this end, the Axl/Mer inhibitor INCB081776 reduced tumour burden when used as a monotherapy in murine breast and bladder cancer models, and further enhanced when used in combination with PD-L1 blockade[303]. In the same study, using a model of murine colon adenocarcinoma, the combination of INCB081776 with anti-PD-1 treatment significantly increased CD4+ and CD8+ T cell proliferation. The Mer inhibitor MRX-2843, was recently shown to reduce peripheral blood leukemic burden *in vivo* in murine models of T-cell acute lymphoblastic leukemia (T-ALL)[304]. Additionally, MRX-2843 in combination with the BCL-2 inhibitor venetoclax increased T-ALL cell apoptosis *in vitro*. The Axl/Mer inhibitor ONO-7475 was found to induce apoptosis in venetoclax-resistant acute myeloid leukemia (AML) cell lines *in vitro* as a monotherapy as well as decrease leukemic burden and increase survival time in models of AML *in vivo*[305]. ONO-7475 was also found to synergise with venetoclax, with the combination therapy showing increased potency against AML cell lines and PDX *in vivo*. Numerous small molecule inhibitors including INCB081776, MRX-2843 and ONO-7475 targeting Mer and other receptor tyrosine kinases including Axl are currently in Phase I clinical trials for advanced or metastatic solid tumours[302] and leukemia[304, 306] (Table 6.1). It is possible that these compounds could be repurposed

for the future treatment of myeloma. Future studies should evaluate the efficacy of Mer inhibition in immune competent mouse models of MM and should consider the potential synergy of Mer inhibitors with IMiDs to support anti-MM immune activation.

Compound	Known Targets	Phase	Clinical trial ID
MRX-2843	MERTK, FLT3	I/Ib	NCT03510104 NCT04762199
S49076	AXL, MET, EGFR, ISRC, FGFR1/2/3	I/II	ISRCTN00759419
ASLAN002 (BMS-777607)	AXL, MERTK, and MET	I/II	NCT01721148 NCT00605618
INCB081776	AXL, MERTK	I	NCT03522142
RXDX106	AXL, MERTK, TYRO3, MET	I	NCT03454243
Bosutinib (SKI-606/PF-5208763)	AXL, Src, Abl, TGFB, BMP	I/II	NCT00195260 NCT00319254
Amuvatinib (MP470)	AXL, c-KIT, PDGFR, FLT3, RAD51, RET	I/Ib/II	NCT00894894 NCT00881166 NCT01357395
Gilteritinib (ASP2215)	AXL, FLT3	I/II/III	NCT02014558 NCT02421939 NCT02752035 NCT02927262 NCT02997202 NCT03182244 NCT02561455 NCT02456883
Glesatinib (MGCD265)	AXL, MET, VEGFR	I/II	NCT00697632 NCT00975767
Ningetinib	VEGFR2, MET, AXL, MERTK, FLT3, RON	I/II	NCT03758287 NCT04577703
Merestinib (LY2801653)	MET, RON, FLT3, AXL	I/II	NCT01285037 NCT03027284 NCT02711553
Crizotinib (PF-02341066)	ALK, MET, ROS1, AXL	Ib/II	NCT02034981 NCT02511184
ONO-7475	AXL, MERTK	I/II	NCT03176277 NCT03730337
Sunitinib (SU11248)	KIT, FLT3, PDGFR, VEGFR2, AXL	II	NCT01499121 NCT01034878 NCT00864721
Cabozantinib (XL184)	AXL, MET, VEGFR2, RET, Kit, Flt-1/3/4, Tie2	II/III	NCT01639508 NCT01708954 NCT01866410

Table 6.1. Small molecule Mer/Axl inhibitors in clinical trials. A summary of Axl and/or Mer inhibitors that are currently in Phase I, II or III clinical trials. The table shows each compound name, known targets, clinical trial phase and clinical trial identification number. Table modified from Yan, *et. al*. (2021).[306]

As TAM receptors are responsible for many normal biological functions, primarily in the phagocytosis of dead cells by immune cells such as macrophages, potential systemic toxicities may arise from therapeutic TAM receptor inhibition[158]. Previous studies of TAM triple knockout mice have noted the acquisition of autoimmune conditions, and in Mer knockout mice, progressive blindness due to gradual photoreceptor death[176, 307]. Therefore, it is possible that a 'therapeutic window' may exist, in which anti-TAM receptor therapeutics can be safely used prior to the acquisition of debilitating side effects[308]. A further consideration should be the potential off target effects of TAM receptor targeting on other TAM receptor expressing cells within the tumour immune microenvironment. Inhibition of Mer in an *in vivo* model of acute myeloid leukaemia led to macrophage M1 repolarisation and inhibited macrophage mediated immunosuppression[309]. As Mer has recently been identified as a T-cell co-stimulatory molecule[310], inhibiting Mer in the tumour microenvironment may reduce the anti-tumour effects of T-cells. The adverse effects of TAM receptor targeting, particularly in combination with conventional chemotherapies used for the treatment of MM must be assessed in future immunocompetent preclinical studies. Novel drug delivery strategies, currently in development, are focussed on mitigating some of the potential adverse effects of systemic TAM receptor inhibition. To this end, targeting TAM receptor inhibition to bone using bone targeting moieties such as bisphosphonates may reduce systemic side effects[311]. The use of nanoparticle drug delivery systems with bone-targeting or MM PC-targeting moieties may be instrumental in future anti-TAM receptor MM treatments that avoid toxicities whilst maximising anti-tumour effects[312, 313].

The studies in this thesis have provided further evidence that Mer expression promotes MM tumour burden *in vivo*. Furthermore, this study has demonstrated, for the first time, that the presence of an adaptive immune system may be necessary for the *in vivo* tumourigenic activity of Mer in MM. Future studies are necessary to determine the molecular mechanisms by which Mer mediates increased MM tumour burden. In the present study it was hypothesised that Mer may modulate T-cell immune checkpoint axes such as PD-L1/PD-1. Future studies should consider a broader characterisation of the composition of the immune microenvironment in mice bearing Mer-positive vs. Mer-negative tumours. Targeting Mer in myeloma could provide a novel precision therapy that stimulates an anti-MM immune

response, reduces MM-induced osteolysis and limits MM tumour burden. Novel precision therapeutics such as Mer small molecule inhibitors in combination with existing anti-myeloma agents may present an opportunity to provide patients with increased options for therapy and improved outcomes.

7. References

1. Kumar SK, Rajkumar V, Kyle RA, van Duin M, Sonneveld P, Mateos MV, Gay F & Anderson KC (2017). Multiple myeloma. *Nat Rev Dis Primers* **3**, 17046.
2. Rajkumar SV (2022). Multiple myeloma: 2022 update on diagnosis, risk stratification, and management. *American Journal of Hematology* **97**, 1086-1107.
3. Davies FE, Pawlyn C, Usmani SZ, San-Miguel JF, Einsele H, Boyle EM, Corre J, Auclair D, Cho HJ, Lonial S, Sonneveld P, Stewart AK, Bergsagel PL, Kaiser MF, Weisel K, Keats JJ, Mikhael JR, Morgan KE, Ghobrial IM, Orlowski RZ, Landgren CO, Gay F, Caers J, Chng WJ, Chari A, Walker BA, Kumar SK, Costa LJ, Anderson KC & Morgan GJ (2022). Perspectives on the Risk-Stratified Treatment of Multiple Myeloma. *Blood Cancer Discov* **3**, 273-284.
4. Bazarbachi AH, Al Hamed R, Malard F, Harousseau JL & Mohty M (2019). Relapsed refractory multiple myeloma: a comprehensive overview. *Leukemia* **33**, 2343-2357.
5. Rajkumar SV, Dimopoulos MA, Palumbo A, Blade J, Merlini G, Mateos MV, Kumar S, Hillengass J, Kastritis E, Richardson P, Landgren O, Paiva B, Dispenzieri A, Weiss B, LeLeu X, Zweegman S, Lonial S, Rosinol L, Zamagni E, Jagannath S, Sezer O, Kristinsson SY, Caers J, Usmani SZ, Lahuerta JJ, Johnsen HE, Beksac M, Cavo M, Goldschmidt H, Terpos E, Kyle RA, Anderson KC, Durie BG & Miguel JF (2014). International Myeloma Working Group updated criteria for the diagnosis of multiple myeloma. *Lancet Oncol* **15**, e538-48.
6. Health AIo & Welfare, *Cancer data in Australia*. 2022, AIHW: Canberra.
7. Ludwig H, Novis Durie S, Meckl A, Hinke A & Durie B (2020). Multiple Myeloma Incidence and Mortality Around the Globe; Interrelations Between Health Access and Quality, Economic Resources, and Patient Empowerment. *Oncologist* **25**, e1406-e1413.
8. Gebregziabher M, Bernstein L, Wang Y & Cozen W (2006). Risk patterns of multiple myeloma in Los Angeles County, 1972-1999 (United States). *Cancer Causes Control* **17**, 931-8.
9. Kaur G, Mejia Saldarriaga M, Shah N, Catamero DD, Yue L, Ashai N, Goradia N, Heisler J, Xiao Z, Ghalib N, Aaron T, Cole D, Foreman R, Mantzaris I, Derman O, Bachier L, Sica RA, Kornblum N, Braunschweig I, Shastri A, Goel S, Verma A & Janakiram M (2021). Multiple Myeloma in Hispanics: Incidence, Characteristics, Survival, Results of Discovery, and Validation Using Real-World and Connect MM Registry Data. *Clinical Lymphoma, Myeloma and Leukemia* **21**, e384-e397.
10. Sneyd MJ, Cox B & Morison IM (2019). Trends in myeloma incidence, mortality and survival in New Zealand (1985-2016). *Cancer Epidemiol* **60**, 55-59.
11. Cowan AJ, Allen C, Barac A, Basaleem H, Bensenor I, Curado MP, Foreman K, Gupta R, Harvey J, Hosgood HD, Jakovljevic M, Khader Y, Linn S, Lad D, Mantovani L, Nong VM, Mokdad A, Naghavi M, Postma M, Roshandel G, Shackelford K, Sisay M, Nguyen CT, Tran TT, Xuan BT, Ukwaja KN, Vollset SE, Weiderpass E, Libby EN & Fitzmaurice C (2018). Global Burden of Multiple Myeloma: A Systematic Analysis for the Global Burden of Disease Study 2016. *JAMA Oncology* **4**, 1221-1227.
12. Swann R, McPhail S, Witt J, Shand B, Abel GA, Hiom S, Rashbass J, Lyratzopoulos G & Rubin G (2018). Diagnosing cancer in primary care: results from the National Cancer Diagnosis Audit. *Br J Gen Pract* **68**, e63-e72.
13. Georg WH, Ralph W, Lukas K, Hagen S, Evangelos T & Monika E (2020). Prevention of bone disease and early detection of impending fractures in multiple myeloma patients can reduce morbidity and mortality: the necessity of interdisciplinary state-of-the-art treatment. *Haematologica* **105**, 859-861.
14. Terpos E, Christoulas D & Gavriatopoulou M (2018). Biology and treatment of myeloma related bone disease. *Metabolism* **80**, 80-90.
15. Kyriakou C, Molloy S, Vrionis F, Alberico R, Bastian L, Zonder JA, Giralt S, Raje N, Kyle RA & Roodman DG (2019). The role of cement augmentation with percutaneous vertebroplasty and balloon kyphoplasty for the treatment of vertebral compression fractures in multiple myeloma: a consensus statement from the International Myeloma Working Group (IMWG). *Blood cancer journal* **9**, 1-10.

16. Goldner W (2016). Cancer-Related Hypercalcemia. *J Oncol Pract* **12**, 426-32.
17. Farrugia AN, Atkins GJ, To LB, Pan B, Horvath N, Kostakis P, Findlay DM, Bardy P & Zannettino AC (2003). Receptor activator of nuclear factor-kappaB ligand expression by human myeloma cells mediates osteoclast formation in vitro and correlates with bone destruction in vivo. *Cancer Res* **63**, 5438-45.
18. Bernstein ZS, Kim EB & Raje N (2022). Bone Disease in Multiple Myeloma: Biologic and Clinical Implications. *Cells* **11**,
19. Nierste BA, Glackin CA & Kirshner J (2014). Dkk-1 and IL-7 in plasma of patients with multiple myeloma prevent differentiation of mesenchymal stem cells into osteoblasts. *Am J Blood Res* **4**, 73-85.
20. Zagouri F, Kastritis E, Zomas A, Terpos E, Katodritou E, Symeonidis A, Delimpasi S, Pouli A, Vassilakopoulos TP, Michalis E, Giannouli S, Kartasis Z, Christoforidou A, Kokoviadou K, Hatzimichael E, Gika D, Megalakaki C, Papaioannou M, Kyrtsonis M-C, Konstantopoulos K, Dimopoulos MA & Group tGMS (2017). Hypercalcemia remains an adverse prognostic factor for newly diagnosed multiple myeloma patients in the era of novel antimyeloma therapies. *European Journal of Haematology* **99**, 409-414.
21. Kundu S, Jha SB, Rivera AP, Flores Monar GV, Islam H, Puttagunta SM, Islam R & Sange I (2022). Multiple Myeloma and Renal Failure: Mechanisms, Diagnosis, and Management. *Cureus* **14**, e22585.
22. Liu L, Yu Z, Cheng H, Mao X, Sui W, Deng S, Wei X, Lv J, Du C, Xu J, Huang W, Xia S, An G, Zhou W, Ma X, Cheng T, Qiu L & Hao M (2020). Multiple myeloma hinders erythropoiesis and causes anaemia owing to high levels of CCL3 in the bone marrow microenvironment. *Sci Rep* **10**, 20508.
23. Raje NS, Anaissie E, Kumar SK, Lonial S, Martin T, Gertz MA, Krishnan A, Hari P, Ludwig H, O'Donnell E, Yee A, Kaufman JL, Cohen AD, Garderet L, Wechalekar AF, Terpos E, Khatry N, Niesvizky R, Yi Q, Joshua DE, Saikia T, Leung N, Engelhardt M, Mothy M, Branagan A, Chari A, Reiman AJ, Lipe B, Richter J, Rajkumar SV, Miguel JS, Anderson KC, Stadtmauer EA, Prabhala RH, McCarthy PL & Munshi NC (2022). Consensus guidelines and recommendations for infection prevention in multiple myeloma: a report from the International Myeloma Working Group. *Lancet Haematol* **9**, e143-e161.
24. Kyle RA, Therneau TM, Rajkumar SV, Larson DR, Plevak MF, Offord JR, Dispenzieri A, Katzmann JA & Melton LJ, 3rd (2006). Prevalence of monoclonal gammopathy of undetermined significance. *N Engl J Med* **354**, 1362-9.
25. Kyle RA, Therneau TM, Rajkumar SV, Offord JR, Larson DR, Plevak MF & Melton LJ, 3rd (2002). A long-term study of prognosis in monoclonal gammopathy of undetermined significance. *N Engl J Med* **346**, 564-9.
26. Rajkumar SV, Kyle RA, Therneau TM, Melton LJ, 3rd, Bradwell AR, Clark RJ, Larson DR, Plevak MF, Dispenzieri A & Katzmann JA (2005). Serum free light chain ratio is an independent risk factor for progression in monoclonal gammopathy of undetermined significance. *Blood* **106**, 812-7.
27. Kyle RA, Durie BG, Rajkumar SV, Landgren O, Blade J, Merlini G, Kröger N, Einsele H, Vesole DH, Dimopoulos M, San Miguel J, Avet-Loiseau H, Hajek R, Chen WM, Anderson KC, Ludwig H, Sonneveld P, Pavlovsky S, Palumbo A, Richardson PG, Barlogie B, Greipp P, Vescio R, Turesson I, Westin J & Boccadoro M (2010). Monoclonal gammopathy of undetermined significance (MGUS) and smoldering (asymptomatic) multiple myeloma: IMWG consensus perspectives risk factors for progression and guidelines for monitoring and management. *Leukemia* **24**, 1121-7.
28. Rajkumar SV, Kyle RA & Buadi FK (2010). Advances in the diagnosis, classification, risk stratification, and management of monoclonal gammopathy of undetermined significance: implications for recategorizing disease entities in the presence of evolving scientific evidence. *Mayo Clin Proc* **85**, 945-8.
29. Rajkumar SV, Gupta V, Fonseca R, Dispenzieri A, Gonsalves WI, Larson D, Ketterling RP, Lust JA, Kyle RA & Kumar SK (2013). Impact of primary molecular

cytogenetic abnormalities and risk of progression in smoldering multiple myeloma. *Leukemia* **27**, 1738-44.
30. Brighton TA, Khot A, Harrison SJ, Ghez D, Weiss BM, Kirsch A, Magen H, Gironella M, Oriol A, Streetly M, Kranenburg B, Qin X, Bandekar R, Hu P, Guilfoyle M, Qi M, Nemat S & Goldschmidt H (2019). Randomized, Double-Blind, Placebo-Controlled, Multicenter Study of Siltuximab in High-Risk Smoldering Multiple Myeloma. *Clin Cancer Res* **25**, 3772-3775.
31. Lonial S, Jacobus S, Fonseca R, Weiss M, Kumar S, Orlowski RZ, Kaufman JL, Yacoub AM, Buadi FK, O'Brien T, Matous JV, Anderson DM, Emmons RV, Mahindra A, Wagner LI, Dhodapkar MV & Rajkumar SV (2020). Randomized Trial of Lenalidomide Versus Observation in Smoldering Multiple Myeloma. *J Clin Oncol* **38**, 1126-1137.
32. Mateos MV, Hernández MT, Salvador C, Rubia J, de Arriba F, López-Corral L, Rosiñol L, Paiva B, Palomera L, Bargay J, Oriol A, Prosper F, López J, Arguiñano JM, Bladé J, Lahuerta JJ & San-Miguel J (2022). Lenalidomide-dexamethasone versus observation in high-risk smoldering myeloma after 12 years of median follow-up time: A randomized, open-label study. *Eur J Cancer* **174**, 243-250.
33. Musto P, Engelhardt M, Caers J, Bolli N, Kaiser M, van de Donk N, Terpos E, Broijl A, de Larrea CF, Gay F, Goldschmidt H, Hajek R, Vangsted AJ, Zamagni E, Zweegman S, Cavo M, Dimopoulos M, Einsele H, Ludwig H, Barosi G, Boccadoro M, Mateos M-V, Sonneveld P & Miguel JS (2021). 2021 European Myeloma Network review and consensus statement on smoldering multiple myeloma: how to distinguish (and manage) Dr. Jekyll and Mr. Hyde. *Haematologica* **106**, 2799-2812.
34. Lonial S, Dhodapkar MV & Rajkumar SV (2020). Smoldering Myeloma and the Art of War. *J Clin Oncol* **38**, 2363-2365.
35. Dimopoulos MA, Moreau P, Terpos E, Mateos MV, Zweegman S, Cook G, Delforge M, Hájek R, Schjesvold F, Cavo M, Goldschmidt H, Facon T, Einsele H, Boccadoro M, San-Miguel J, Sonneveld P & Mey U (2021). Multiple myeloma: EHA-ESMO Clinical Practice Guidelines for diagnosis, treatment and follow-up(†). *Ann Oncol* **32**, 309-322.
36. Palumbo A, Avet-Loiseau H, Oliva S, Lokhorst HM, Goldschmidt H, Rosinol L, Richardson P, Caltagirone S, Lahuerta JJ, Facon T, Bringhen S, Gay F, Attal M, Passera R, Spencer A, Offidani M, Kumar S, Musto P, Lonial S, Petrucci MT, Orlowski RZ, Zamagni E, Morgan G, Dimopoulos MA, Durie BG, Anderson KC, Sonneveld P, San Miguel J, Cavo M, Rajkumar SV & Moreau P (2015). Revised International Staging System for Multiple Myeloma: A Report From International Myeloma Working Group. *J Clin Oncol* **33**, 2863-9.
37. Mikhael JR, Dingli D, Roy V, Reeder CB, Buadi FK, Hayman SR, Dispenzieri A, Fonseca R, Sher T, Kyle RA, Lin Y, Russell SJ, Kumar S, Bergsagel PL, Zeldenrust SR, Leung N, Drake MT, Kapoor P, Ansell SM, Witzig TE, Lust JA, Dalton RJ, Gertz MA, Stewart AK, Rajkumar SV, Chanan-Khan A & Lacy MQ (2013). Management of newly diagnosed symptomatic multiple myeloma: updated Mayo Stratification of Myeloma and Risk-Adapted Therapy (mSMART) consensus guidelines 2013. *Mayo Clin Proc* **88**, 360-76.
38. van de Donk NWCJ, Lokhorst HM, Anderson KC & Richardson PG (2012). How I treat plasma cell leukemia. *Blood* **120**, 2376-2389.
39. Fernández de Larrea C, Kyle RA, Durie BGM, Ludwig H, Usmani S, Vesole DH, Hajek R, San Miguel JF, Sezer O, Sonneveld P, Kumar SK, Mahindra A, Comenzo R, Palumbo A, Mazumber A, Anderson KC, Richardson PG, Badros AZ, Caers J, Cavo M, LeLeu X, Dimopoulos MA, Chim CS, Schots R, Noeul A, Fantl D, Mellqvist UH, Landgren O, Chanan-Khan A, Moreau P, Fonseca R, Merlini G, Lahuerta JJ, Bladé J, Orlowski RZ, Shah JJ & on behalf of the International Myeloma Working G (2013). Plasma cell leukemia: consensus statement on diagnostic requirements, response criteria and treatment recommendations by the International Myeloma Working Group. *Leukemia* **27**, 780-791.

40. Ravi P, Kumar SK, Roeker L, Gonsalves W, Buadi F, Lacy MQ, Go RS, Dispenzieri A, Kapoor P, Lust JA, Dingli D, Lin Y, Russell SJ, Leung N, Gertz MA, Kyle RA, Bergsagel PL & Rajkumar SV (2018). Revised diagnostic criteria for plasma cell leukemia: results of a Mayo Clinic study with comparison of outcomes to multiple myeloma. *Blood Cancer J* **8**, 116.
41. Fernández de Larrea C, Kyle R, Rosiñol L, Paiva B, Engelhardt M, Usmani S, Caers J, Gonsalves W, Schjesvold F, Merlini G, Lentzch S, Ocio E, Garderet L, Moreau P, Sonneveld P, Badros A, Gahrton G, Goldschmidt H, Tuchman S, Einsele H, Durie B, Wirk B, Musto P, Hayden P, Kaiser M, Miguel JS, Bladé J, Rajkumar SV & Mateos MV (2021). Primary plasma cell leukemia: consensus definition by the International Myeloma Working Group according to peripheral blood plasma cell percentage. *Blood Cancer J* **11**, 192.
42. Cavo M, Terpos E, Nanni C, Moreau P, Lentzsch S, Zweegman S, Hillengass J, Engelhardt M, Usmani SZ, Vesole DH, San-Miguel J, Kumar SK, Richardson PG, Mikhael JR, da Costa FL, Dimopoulos MA, Zingaretti C, Abildgaard N, Goldschmidt H, Orlowski RZ, Chng WJ, Einsele H, Lonial S, Barlogie B, Anderson KC, Rajkumar SV, Durie BGM & Zamagni E (2017). Role of (18)F-FDG PET/CT in the diagnosis and management of multiple myeloma and other plasma cell disorders: a consensus statement by the International Myeloma Working Group. *Lancet Oncol* **18**, e206-e217.
43. Gagelmann N, Eikema DJ, Koster L, Caillot D, Pioltelli P, Lleonart JB, Reményi P, Blaise D, Schaap N, Trneny M, Passweg J, Porras RP, Cahn JY, Musso M, Poiré X, Fenk R, Itälä-Remes M, Pavone V, Fouillard L, Maertens J, Bron D, Pouli A, Schroyens W, Schönland S, Garderet L, Yakoub-Agha I & Kröger N (2019). Tandem Autologous Stem Cell Transplantation Improves Outcomes in Newly Diagnosed Multiple Myeloma with Extramedullary Disease and High-Risk Cytogenetics: A Study from the Chronic Malignancies Working Party of the European Society for Blood and Marrow Transplantation. *Biol Blood Marrow Transplant* **25**, 2134-2142.
44. Kristinsson SY, Anderson WF & Landgren O (2014). Improved long-term survival in multiple myeloma up to the age of 80 years. *Leukemia* **28**, 1346-8.
45. Rajkumar SV & Kumar S (2020). Multiple myeloma current treatment algorithms. *Blood Cancer J* **10**, 94.
46. Ito T & Handa H (2020). Molecular mechanisms of thalidomide and its derivatives. *Proc Jpn Acad Ser B Phys Biol Sci* **96**, 189-203.
47. Krönke J, Udeshi ND, Narla A, Grauman P, Hurst SN, McConkey M, Svinkina T, Heckl D, Comer E, Li X, Ciarlo C, Hartman E, Munshi N, Schenone M, Schreiber SL, Carr SA & Ebert BL (2014). Lenalidomide Causes Selective Degradation of IKZF1 and IKZF3 in Multiple Myeloma Cells. *Science* **343**, 301-305.
48. Gandhi AK, Kang J, Havens CG, Conklin T, Ning Y, Wu L, Ito T, Ando H, Waldman MF, Thakurta A, Klippel A, Handa H, Daniel TO, Schafer PH & Chopra R (2014). Immunomodulatory agents lenalidomide and pomalidomide co-stimulate T cells by inducing degradation of T cell repressors Ikaros and Aiolos via modulation of the E3 ubiquitin ligase complex CRL4CRBN. *British Journal of Haematology* **164**, 811-821.
49. Gandolfi S, Laubach JP, Hideshima T, Chauhan D, Anderson KC & Richardson PG (2017). The proteasome and proteasome inhibitors in multiple myeloma. *Cancer and Metastasis Reviews* **36**, 561-584.
50. Ntanasis-Stathopoulos I, Gavriatopoulou M, Kastritis E, Terpos E & Dimopoulos MA (2020). Multiple myeloma: Role of autologous transplantation. *Cancer Treatment Reviews* **82**, 101929.
51. Durie BGM, Hoering A, Abidi MH, Rajkumar SV, Epstein J, Kahanic SP, Thakuri M, Reu F, Reynolds CM, Sexton R, Orlowski RZ, Barlogie B & Dispenzieri A (2017). Bortezomib with lenalidomide and dexamethasone versus lenalidomide and dexamethasone alone in patients with newly diagnosed myeloma without intent for immediate autologous stem-cell transplant (SWOG S0777): a randomised, open-label, phase 3 trial. *The Lancet* **389**, 519-527.

52. Palumbo A, Rajkumar SV, Miguel JFS, Larocca A, Niesvizky R, Morgan G, Landgren O, Hajek R, Einsele H, Anderson KC, Dimopoulos MA, Richardson PG, Cavo M, Spencer A, Stewart AK, Shimizu K, Lonial S, Sonneveld P, Durie BGM, Moreau P & Orlowski RZ (2014). International Myeloma Working Group Consensus Statement for the Management, Treatment, and Supportive Care of Patients With Myeloma Not Eligible for Standard Autologous Stem-Cell Transplantation. *Journal of Clinical Oncology* **32**, 587-600.
53. Rajkumar SV (2019). Multiple myeloma: Every year a new standard? *Hematological Oncology* **37**, 62-65.
54. Palumbo A, Cavallo F, Gay F, Di Raimondo F, Ben Yehuda D, Petrucci MT, Pezzatti S, Caravita T, Cerrato C, Ribakovsky E, Genuardi M, Cafro A, Marcatti M, Catalano L, Offidani M, Carella AM, Zamagni E, Patriarca F, Musto P, Evangelista A, Ciccone G, Omedé P, Crippa C, Corradini P, Nagler A, Boccadoro M & Cavo M (2014). Autologous transplantation and maintenance therapy in multiple myeloma. *N Engl J Med* **371**, 895-905.
55. Lonial S & Anderson KC (2014). Association of response endpoints with survival outcomes in multiple myeloma. *Leukemia* **28**, 258-68.
56. Flores-Montero J, Sanoja-Flores L, Paiva B, Puig N, García-Sánchez O, Böttcher S, van der Velden VHJ, Pérez-Morán JJ, Vidriales MB, García-Sanz R, Jimenez C, González M, Martínez-López J, Corral-Mateos A, Grigore GE, Fluxá R, Pontes R, Caetano J, Sedek L, Del Cañizo MC, Bladé J, Lahuerta JJ, Aguilar C, Bárez A, García-Mateo A, Labrador J, Leoz P, Aguilera-Sanz C, San-Miguel J, Mateos MV, Durie B, van Dongen JJM & Orfao A (2017). Next Generation Flow for highly sensitive and standardized detection of minimal residual disease in multiple myeloma. *Leukemia* **31**, 2094-2103.
57. Offidani M, Boccadoro M, Di Raimondo F, Petrucci MT, Tosi P & Cavo M (2019). Expert Panel Consensus Statement for Proper Evaluation of First Relapse in Multiple Myeloma. *Curr Hematol Malig Rep* **14**, 187-196.
58. Moreau P (2017). How I treat myeloma with new agents. *Blood* **130**, 1507-1513.
59. Moreau P, Kumar SK, San Miguel J, Davies F, Zamagni E, Bahlis N, Ludwig H, Mikhael J, Terpos E, Schjesvold F, Martin T, Yong K, Durie BGM, Facon T, Jurczyszyn A, Sidana S, Raje N, van de Donk N, Lonial S, Cavo M, Kristinsson SY, Lentzsch S, Hajek R, Anderson KC, João C, Einsele H, Sonneveld P, Engelhardt M, Fonseca R, Vangsted A, Weisel K, Baz R, Hungria V, Berdeja JG, Leal da Costa F, Maiolino A, Waage A, Vesole DH, Ocio EM, Quach H, Driessen C, Bladé J, Leleu X, Riva E, Bergsagel PL, Hou J, Chng WJ, Mellqvist U-H, Dytfeld D, Harousseau J-L, Goldschmidt H, Laubach J, Munshi NC, Gay F, Beksac M, Costa LJ, Kaiser M, Hari P, Boccadoro M, Usmani SZ, Zweegman S, Holstein S, Sezer O, Harrison S, Nahi H, Cook G, Mateos M-V, Rajkumar SV, Dimopoulos MA & Richardson PG (2021). Treatment of relapsed and refractory multiple myeloma: recommendations from the International Myeloma Working Group. *The Lancet Oncology* **22**, e105-e118.
60. Dimopoulos MA, Leleu X, Palumbo A, Moreau P, Delforge M, Cavo M, Ludwig H, Morgan GJ, Davies FE, Sonneveld P, Schey SA, Zweegman S, Hansson M, Weisel K, Mateos MV, Facon T & Miguel JF (2014). Expert panel consensus statement on the optimal use of pomalidomide in relapsed and refractory multiple myeloma. *Leukemia* **28**, 1573-85.
61. Dimopoulos MA, Dytfeld D, Grosicki S, Moreau P, Takezako N, Hori M, Leleu X, LeBlanc R, Suzuki K, Raab MS, Richardson PG, Popa McKiver M, Jou YM, Shelat SG, Robbins M, Rafferty B & San-Miguel J (2018). Elotuzumab plus Pomalidomide and Dexamethasone for Multiple Myeloma. *N Engl J Med* **379**, 1811-1822.
62. Dimopoulos M, Quach H, Mateos MV, Landgren O, Leleu X, Siegel D, Weisel K, Yang H, Klippel Z, Zahlten-Kumeli A & Usmani SZ (2020). Carfilzomib, dexamethasone, and daratumumab versus carfilzomib and dexamethasone for patients with relapsed or refractory multiple myeloma (CANDOR): results from a randomised, multicentre, open-label, phase 3 study. *Lancet* **396**, 186-197.

63. Baertsch MA, Fougereau M, Hielscher T, Sauer S, Breitkreutz I, Jordan K, Müller-Tidow C, Goldschmidt H, Raab MS, Hillengass J & Giesen N (2021). Carfilzomib, Lenalidomide, and Dexamethasone Followed by Salvage Autologous Stem Cell Transplant with or without Maintenance for Relapsed or Refractory Multiple Myeloma. *Cancers (Basel)* **13**,
64. Gandhi UH, Cornell RF, Lakshman A, Gahvari ZJ, McGehee E, Jagosky MH, Gupta R, Varnado W, Fiala MA, Chhabra S, Malek E, Mansour J, Paul B, Barnstead A, Kodali S, Neppalli A, Liedtke M, Narayana S, Godby KN, Kang Y, Kansagra A, Umyarova E, Scott EC, Hari P, Vij R, Usmani SZ, Callander NS, Kumar SK & Costa LJ (2019). Outcomes of patients with multiple myeloma refractory to CD38-targeted monoclonal antibody therapy. *Leukemia* **33**, 2266-2275.
65. Mhaskar R, Kumar A, Miladinovic B & Djulbegovic B (2017). Bisphosphonates in multiple myeloma: an updated network meta-analysis. *Cochrane Database Syst Rev* **12**, Cd003188.
66. Guzdar A & Costello C (2020). Supportive Care in Multiple Myeloma. *Current Hematologic Malignancy Reports* **15**, 56-61.
67. Manohar S, Nasr SH & Leung N (2018). Light Chain Cast Nephropathy: Practical Considerations in the Management of Myeloma Kidney—What We Know and What the Future May Hold. *Current Hematologic Malignancy Reports* **13**, 220-226.
68. Bohlius J, Bohlke K, Castelli R, Djulbegovic B, Lustberg MB, Martino M, Mountzios G, Peswani N, Porter L, Tanaka TN, Trifirò G, Yang H & Lazo-Langner A (2019). Management of cancer-associated anemia with erythropoiesis-stimulating agents: ASCO/ASH clinical practice guideline update. *Blood Advances* **3**, 1197-1210.
69. Blimark C, Holmberg E, Mellqvist UH, Landgren O, Björkholm M, Hultcrantz M, Kjellander C, Turesson I & Kristinsson SY (2015). Multiple myeloma and infections: a population-based study on 9253 multiple myeloma patients. *Haematologica* **100**, 107-13.
70. Morgan GJ, Walker BA & Davies FE (2012). The genetic architecture of multiple myeloma. *Nature Reviews Cancer* **12**, 335-348.
71. Xu Z, Zan H, Pone EJ, Mai T & Casali P (2012). Immunoglobulin class-switch DNA recombination: induction, targeting and beyond. *Nature Reviews Immunology* **12**, 517-531.
72. Stavnezer J, Guikema JE & Schrader CE (2008). Mechanism and regulation of class switch recombination. *Annu Rev Immunol* **26**, 261-92.
73. González D, van der Burg M, García-Sanz R, Fenton JA, Langerak AW, González M, van Dongen JJM, San Miguel JF & Morgan GJ (2007). Immunoglobulin gene rearrangements and the pathogenesis of multiple myeloma. *Blood* **110**, 3112-3121.
74. Bergsagel PL, Chesi M, Nardini E, Brents LA, Kirby SL & Kuehl WM (1996). Promiscuous translocations into immunoglobulin heavy chain switch regions in multiple myeloma. *Proceedings of the National Academy of Sciences* **93**, 13931-13936.
75. Bal S, Kumar SK, Fonseca R, Gay F, Hungria VT, Dogan A & Costa LJ (2022). Multiple myeloma with t(11;14): unique biology and evolving landscape. *Am J Cancer Res* **12**, 2950-2965.
76. Fonseca R, Blood EA, Oken MM, Kyle RA, Dewald GW, Bailey RJ, Van Wier SA, Henderson KJ, Hoyer JD, Harrington D, Kay NE, Van Ness B & Greipp PR (2002). Myeloma and the t(11;14)(q13;q32); evidence for a biologically defined unique subset of patients. *Blood* **99**, 3735-3741.
77. Fu M, Wang C, Li Z, Sakamaki T & Pestell RG (2004). Minireview: Cyclin D1: Normal and Abnormal Functions. *Endocrinology* **145**, 5439-5447.
78. Kumar S, Kaufman JL, Gasparetto C, Mikhael J, Vij R, Pegourie B, Benboubker L, Facon T, Amiot M, Moreau P, Punnoose EA, Alzate S, Dunbar M, Xu T, Agarwal SK, Enschede SH, Leverson JD, Ross JA, Maciag PC, Verdugo M & Touzeau C (2017). Efficacy of venetoclax as targeted therapy for relapsed/refractory t(11;14) multiple myeloma. *Blood* **130**, 2401-2409.

79. Wang J, Zhu X, Dang L, Jiang H, Xie Y, Li X, Guo J, Wang Y, Peng Z, Wang M, Wang J, Wang S, Li Q, Wang Y, Wang Q, Ye L, Zhang L & Liu Z (2022). Epigenomic reprogramming via HRP2-MINA dictates response to proteasome inhibitors in multiple myeloma with t(4;14) translocation. *J Clin Invest* **132**,
80. Martinez-Garcia E, Popovic R, Min DJ, Sweet SM, Thomas PM, Zamdborg L, Heffner A, Will C, Lamy L, Staudt LM, Levens DL, Kelleher NL & Licht JD (2011). The MMSET histone methyl transferase switches global histone methylation and alters gene expression in t(4;14) multiple myeloma cells. *Blood* **117**, 211-20.
81. Manier S, Salem KZ, Park J, Landau DA, Getz G & Ghobrial IM (2017). Genomic complexity of multiple myeloma and its clinical implications. *Nature Reviews Clinical Oncology* **14**, 100-113.
82. Walker BA, Wardell CP, Murison A, Boyle EM, Begum DB, Dahir NM, Proszek PZ, Melchor L, Pawlyn C, Kaiser MF, Johnson DC, Qiang Y-W, Jones JR, Cairns DA, Gregory WM, Owen RG, Cook G, Drayson MT, Jackson GH, Davies FE & Morgan GJ (2015). APOBEC family mutational signatures are associated with poor prognosis translocations in multiple myeloma. *Nature Communications* **6**, 6997.
83. Chng WJ, Santana-Dávila R, Van Wier SA, Ahmann GJ, Jalal SM, Bergsagel PL, Chesi M, Trendle MC, Jacobus S, Blood E, Oken MM, Henderson K, Kyle RA, Gertz MA, Lacy MQ, Dispenzieri A, Greipp PR & Fonseca R (2006). Prognostic factors for hyperdiploid-myeloma: effects of chromosome 13 deletions and IgH translocations. *Leukemia* **20**, 807-813.
84. Smadja NVr, Bastard C, Brigaudeau C, Leroux D, Fruchart C & Hématologique obotGFadCnt (2001). Hypodiploidy is a major prognostic factor in multiple myeloma. *Blood* **98**, 2229-2238.
85. Kumar S, Fonseca R, Ketterling RP, Dispenzieri A, Lacy MQ, Gertz MA, Hayman SR, Buadi FK, Dingli D, Knudson RA, Greenberg A, Russell SJ, Zeldenrust SR, Lust JA, Kyle RA, Bergsagel L & Rajkumar SV (2012). Trisomies in multiple myeloma: impact on survival in patients with high-risk cytogenetics. *Blood* **119**, 2100-2105.
86. Pawlyn C, Melchor L, Murison A, Wardell CP, Brioli A, Boyle EM, Kaiser MF, Walker BA, Begum DB, Dahir NB, Proszek P, Gregory WM, Drayson MT, Jackson GH, Ross FM, Davies FE & Morgan GJ (2015). Coexistent hyperdiploidy does not abrogate poor prognosis in myeloma with adverse cytogenetics and may precede IGH translocations. *Blood* **125**, 831-840.
87. Kaufmann H, Ackermann J, Baldia C, Nösslinger T, Wieser R, Seidl S, Sagaster V, Gisslinger H, Jäger U, Pfeilstöcker M, Zielinski C & Drach J (2004). Both IGH translocations and chromosome 13q deletions are early events in monoclonal gammopathy of undetermined significance and do not evolve during transition to multiple myeloma. *Leukemia* **18**, 1879-82.
88. Avet-Loiseau H, Gerson F, Magrangeas F, Minvielle Sp, Harousseau J-L, Bataille Rg & Myélome ftIFd (2001). Rearrangements of the c-myc oncogene are present in 15% of primary human multiple myeloma tumors. *Blood* **98**, 3082-3086.
89. Walker BA, Leone PE, Chiecchio L, Dickens NJ, Jenner MW, Boyd KD, Johnson DC, Gonzalez D, Dagrada GP, Protheroe RKM, Konn ZJ, Stockley DM, Gregory WM, Davies FE, Ross FM & Morgan GJ (2010). A compendium of myeloma-associated chromosomal copy number abnormalities and their prognostic value. *Blood* **116**, e56-e65.
90. Fonseca R, Bergsagel PL, Drach J, Shaughnessy J, Gutierrez N, Stewart AK, Morgan G, Van Ness B, Chesi M, Minvielle S, Neri A, Barlogie B, Kuehl WM, Liebisch P, Davies F, Chen-Kiang S, Durie BG, Carrasco R, Sezer O, Reiman T, Pilarski L & Avet-Loiseau H (2009). International Myeloma Working Group molecular classification of multiple myeloma: spotlight review. *Leukemia* **23**, 2210-21.
91. Fonseca R, Blood E, Rue M, Harrington D, Oken MM, Kyle RA, Dewald GW, Van Ness B, Van Wier SA, Henderson KJ, Bailey RJ & Greipp PR (2003). Clinical and biologic implications of recurrent genomic aberrations in myeloma. *Blood* **101**, 4569-75.

92. Lodé L, Eveillard M, Trichet V, Soussi T, Wuillème S, Richebourg S, Magrangeas F, Ifrah N, Campion L, Traullé C, Guilhot F, Caillot D, Marit G, Mathiot C, Facon T, Attal M, Harousseau JL, Moreau P, Minvielle S & Avet-Loiseau H (2010). Mutations in TP53 are exclusively associated with del(17p) in multiple myeloma. *Haematologica* **95**, 1973-6.
93. Schmidt TM, Fonseca R & Usmani SZ (2021). Chromosome 1q21 abnormalities in multiple myeloma. *Blood Cancer J* **11**, 83.
94. Kastritis E, Migkou M, Dalampira D, Gavriatopoulou M, Fotiou D, Roussou M, Kanellias N, Ntanasis-Stathopoulos I, Malandrakis P, Theodorakakou F, Sevastoudi A, Eleutherakis-Papaiakovou E, Triantafyllou T, Terpos E, Katodritou E & Dimopoulos MA (2022). Chromosome 1q21 aberrations identify ultra high-risk myeloma with prognostic and clinical implications. *American Journal of Hematology* **97**, 1142-1149.
95. Miller A, Asmann Y, Cattaneo L, Braggio E, Keats J, Auclair D, Lonial S, Russell SJ & Stewart AK (2017). High somatic mutation and neoantigen burden are correlated with decreased progression-free survival in multiple myeloma. *Blood Cancer J* **7**, e612.
96. Chapman MA, Lawrence MS, Keats JJ, Cibulskis K, Sougnez C, Schinzel AC, Harview CL, Brunet JP, Ahmann GJ, Adli M, Anderson KC, Ardlie KG, Auclair D, Baker A, Bergsagel PL, Bernstein BE, Drier Y, Fonseca R, Gabriel SB, Hofmeister CC, Jagannath S, Jakubowiak AJ, Krishnan A, Levy J, Liefeld T, Lonial S, Mahan S, Mfuko B, Monti S, Perkins LM, Onofrio R, Pugh TJ, Rajkumar SV, Ramos AH, Siegel DS, Sivachenko A, Stewart AK, Trudel S, Vij R, Voet D, Winckler W, Zimmerman T, Carpten J, Trent J, Hahn WC, Garraway LA, Meyerson M, Lander ES, Getz G & Golub TR (2011). Initial genome sequencing and analysis of multiple myeloma. *Nature* **471**, 467-72.
97. Walker BA, Boyle EM, Wardell CP, Murison A, Begum DB, Dahir NM, Proszek PZ, Johnson DC, Kaiser MF, Melchor L, Aronson LI, Scales M, Pawlyn C, Mirabella F, Jones JR, Brioli A, Mikulasova A, Cairns DA, Gregory WM, Quartilho A, Drayson MT, Russell N, Cook G, Jackson GH, Leleu X, Davies FE & Morgan GJ (2015). Mutational Spectrum, Copy Number Changes, and Outcome: Results of a Sequencing Study of Patients With Newly Diagnosed Myeloma. *J Clin Oncol* **33**, 3911-20.
98. Salomon-Perzyński A, Jamroziak K & Głodkowska-Mrówka E (2021). Clonal Evolution of Multiple Myeloma-Clinical and Diagnostic Implications. *Diagnostics (Basel)* **11**,
99. Bolli N, Avet-Loiseau H, Wedge DC, Van Loo P, Alexandrov LB, Martincorena I, Dawson KJ, Iorio F, Nik-Zainal S, Bignell GR, Hinton JW, Li Y, Tubio JM, McLaren S, S OM, Butler AP, Teague JW, Mudie L, Anderson E, Rashid N, Tai YT, Shammas MA, Sperling AS, Fulciniti M, Richardson PG, Parmigiani G, Magrangeas F, Minvielle S, Moreau P, Attal M, Facon T, Futreal PA, Anderson KC, Campbell PJ & Munshi NC (2014). Heterogeneity of genomic evolution and mutational profiles in multiple myeloma. *Nat Commun* **5**, 2997.
100. Dutta AK, Fink JL, Grady JP, Morgan GJ, Mullighan CG, To LB, Hewett DR & Zannettino ACW (2019). Subclonal evolution in disease progression from MGUS/SMM to multiple myeloma is characterised by clonal stability. *Leukemia* **33**, 457-468.
101. Dutta AK, Alberge J-B, Sklavenitis-Pistofidis R, Lightbody ED, Getz G & Ghobrial IM (2022). Single-cell profiling of tumour evolution in multiple myeloma — opportunities for precision medicine. *Nature Reviews Clinical Oncology* **19**, 223-236.
102. Morgan GJ, Walker BA & Davies FE (2012). The genetic architecture of multiple myeloma. *Nat Rev Cancer* **12**, 335-348.
103. Abe M (2011). Targeting the interplay between myeloma cells and the bone marrow microenvironment in myeloma. *International Journal of Hematology* **94**, 334-343.

104. Iannozzi NT, Marchica V, Toscani D, Burroughs Garcìa J, Giuliani N & Storti P (2022). Molecular Features of the Mesenchymal and Osteoblastic Cells in Multiple Myeloma. *Int J Mol Sci* **23**,
105. Chauhan D, Uchiyama H, Akbarali Y, Urashima M, Yamamoto K-I, Libermann TA & Anderson KC (1996). Multiple Myeloma Cell Adhesion-Induced Interleukin-6 Expression in Bone Marrow Stromal Cells Involves Activation of NF-κB. *Blood* **87**, 1104-1112.
106. Liang Y, He H, Wang W, Wang H, Mo S, Fu R, Liu X, Song Q, Xia Z & Wang L (2022). Malignant clonal evolution drives multiple myeloma cellular ecological diversity and microenvironment reprogramming. *Molecular Cancer* **21**, 182.
107. Yaccoby S, Wezeman MJ, Henderson A, Cottler-Fox M, Yi Q, Barlogie B & Epstein J (2004). Cancer and the Microenvironment: Myeloma-Osteoclast Interactions as a Model. *Cancer Research* **64**, 2016-2023.
108. Lomas OC, Tahri S & Ghobrial IM (2020). The microenvironment in myeloma. *Current Opinion in Oncology* **32**, 170-175.
109. Li L & Xie T (2005). Stem cell niche: structure and function. *Annual review of cell and developmental biology* **21**, 605-631.
110. Noll JE, Williams SA, Purton LE & Zannettino AC (2012). Tug of war in the haematopoietic stem cell niche: do myeloma plasma cells compete for the HSC niche? *Blood Cancer J* **2**, e91.
111. Kopp H-G, Avecilla ST, Hooper AT & Rafii S (2005). The Bone Marrow Vascular Niche: Home of HSC Differentiation and Mobilization. *Physiology* **20**, 349-356.
112. Abkowitz JL, Robinson AE, Kale S, Long MW & Chen J (2003). Mobilization of hematopoietic stem cells during homeostasis and after cytokine exposure. *Blood* **102**, 1249-1253.
113. Bowers M, Zhang B, Ho Y, Agarwal P, Chen C-C & Bhatia R (2015). Osteoblast ablation reduces normal long-term hematopoietic stem cell self-renewal but accelerates leukemia development. *Blood* **125**, 2678-2688.
114. Iriuchishima H, Takubo K, Miyakawa Y, Nakamura-Ishizu A, Miyauchi Y, Fujita N, Miyamoto K, Miyamoto T, Ikeda E, Kizaki M, Nojima Y & Suda T (2012). Neovascular niche for human myeloma cells in immunodeficient mouse bone. *PLoS One* **7**, e30557.
115. Ribatti D, Nico B & Vacca A (2006). Importance of the bone marrow microenvironment in inducing the angiogenic response in multiple myeloma. *Oncogene* **25**, 4257-4266.
116. Bianco P, Riminucci M, Gronthos S & Robey PG (2001). Bone Marrow Stromal Stem Cells: Nature, Biology, and Potential Applications. *STEM CELLS* **19**, 180-192.
117. Dar A, Kollet O & Lapidot T (2006). Mutual, reciprocal SDF-1/CXCR4 interactions between hematopoietic and bone marrow stromal cells regulate human stem cell migration and development in NOD/SCID chimeric mice. *Experimental Hematology* **34**, 967-975.
118. Peled A, Klein S, Beider K, Burger JA & Abraham M (2018). Role of CXCL12 and CXCR4 in the pathogenesis of hematological malignancies. *Cytokine* **109**, 11-16.
119. Pellegrino A, Ria R, Pietro GD, Cirulli T, Surico G, Pennisi A, Morabito F, Ribatti D & Vacca A (2005). Bone marrow endothelial cells in multiple myeloma secrete CXC-chemokines that mediate interactions with plasma cells. *British Journal of Haematology* **129**, 248-256.
120. Waldschmidt JM, Simon A, Wider D, Müller SJ, Follo M, Ihorst G, Decker S, Lorenz J, Chatterjee M, Azab AK, Duyster J, Wäsch R & Engelhardt M (2017). CXCL12 and CXCR7 are relevant targets to reverse cell adhesion-mediated drug resistance in multiple myeloma. *British Journal of Haematology* **179**, 36-49.
121. Roccaro AM, Sacco A, Purschke WG, Moschetta M, Buchner K, Maasch C, Zboralski D, Zöllner S, Vonhoff S, Mishima Y, Maiso P, Reagan MR, Lonardi S, Ungari M, Facchetti F, Eulberg D, Kruschinski A, Vater A, Rossi G, Klussmann S & Ghobrial IM (2014). SDF-1 inhibition targets the bone marrow niche for cancer therapy. *Cell Rep* **9**, 118-128.

122. Azab AK, Runnels JM, Pitsillides C, Moreau AS, Azab F, Leleu X, Jia X, Wright R, Ospina B, Carlson AL, Alt C, Burwick N, Roccaro AM, Ngo HT, Farag M, Melhem MR, Sacco A, Munshi NC, Hideshima T, Rollins BJ, Anderson KC, Kung AL, Lin CP & Ghobrial IM (2009). CXCR4 inhibitor AMD3100 disrupts the interaction of multiple myeloma cells with the bone marrow microenvironment and enhances their sensitivity to therapy. *Blood* **113**, 4341-51.
123. Suzuki R, Ogiya D, Ogawa Y, Kawada H & Ando K (2022). Targeting CAM-DR and Mitochondrial Transfer for the Treatment of Multiple Myeloma. *Curr Oncol* **29**, 8529-8539.
124. Liu Y, Liang HM, Lv YQ, Tang SM & Cheng P (2019). Blockade of SDF-1/CXCR4 reduces adhesion-mediated chemoresistance of multiple myeloma cells via interacting with interleukin-6. *J Cell Physiol* **234**, 19702-19714.
125. Vacca A, Di Loreto M, Ribatti D, Di Stefano R, Gadaleta-Caldarola G, Iodice G, Caloro D & Dammacco F (1995). Bone marrow of patients with active multiple myeloma: angiogenesis and plasma cell adhesion molecules LFA-1, VLA-4, LAM-1, and CD44. *Am J Hematol* **50**, 9-14.
126. Sherbenou DW, Su Y, Behrens CR, Aftab BT, Perez de Acha O, Murnane M, Bearrows SC, Hann BC, Wolf JL, Martin TG & Liu B (2020). Potent Activity of an Anti-ICAM1 Antibody-Drug Conjugate against Multiple Myeloma. *Clin Cancer Res* **26**, 6028-6038.
127. Matsumoto T & Abe M (2011). TGF-β-related mechanisms of bone destruction in multiple myeloma. *Bone* **48**, 129-34.
128. Takeuchi K, Abe M, Hiasa M, Oda A, Amou H, Kido S, Harada T, Tanaka O, Miki H, Nakamura S, Nakano A, Kagawa K, Yata K, Ozaki S & Matsumoto T (2010). Tgf-Beta inhibition restores terminal osteoblast differentiation to suppress myeloma growth. *PLoS One* **5**, e9870.
129. Lawson MA, McDonald MM, Kovacic N, Khoo WH, Terry RL, Down J, Kaplan W, Paton-Hough J, Fellows C, Pettitt JA, Dear TN, Van Valckenborgh E, Baldock PA, Rogers MJ, Eaton CL, Vanderkerken K, Pettit AR, Quinn JMW, Zannettino ACW, Phan TG & Croucher PI (2015). Osteoclasts control reactivation of dormant myeloma cells by remodelling the endosteal niche. *Nat Commun*
130. Abe M, Hiura K, Wilde J, Moriyama K, Hashimoto T, Ozaki S, Wakatsuki S, Kosaka M, Kido S, Inoue D & Matsumoto T (2002). Role for macrophage inflammatory protein (MIP)-1α and MIP-1β in the development of osteolytic lesions in multiple myeloma. *Blood* **100**, 2195-2202.
131. Han J-H, Choi SJ, Kurihara N, Koide M, Oba Y & Roodman GD (2001). Macrophage inflammatory protein-1α is an osteoclastogenic factor in myeloma that is independent of receptor activator of nuclear factor κB ligand. *Blood* **97**, 3349-3353.
132. Parrondo RD & Sher T (2019). Prevention Of Skeletal Related Events In Multiple Myeloma: Focus On The RANK-L Pathway In The Treatment Of Multiple Myeloma. *Onco Targets Ther* **12**, 8467-8478.
133. Abe M, Hiura K, Wilde J, Shioyasono A, Moriyama K, Hashimoto T, Kido S, Oshima T, Shibata H, Ozaki S, Inoue D & Matsumoto T (2004). Osteoclasts enhance myeloma cell growth and survival via cell-cell contact: a vicious cycle between bone destruction and myeloma expansion. *Blood* **104**, 2484-2491.
134. Moreaux J, Hose D, Kassambara A, Reme T, Moine P, Requirand G, Goldschmidt H & Klein B (2011). Osteoclast-gene expression profiling reveals osteoclast-derived CCR2 chemokines promoting myeloma cell migration. *Blood* **117**, 1280-1290.
135. Schinke C, Poos AM, Bauer M, John L, Johnson S, Deshpande S, Carrillo L, Alapat D, Rasche L, Thanendrarajan S, Zangari M, Al Hadidi S, van Rhee F, Davies F, Raab MS, Morgan G & Weinhold N (2022). Characterizing the role of the immune microenvironment in multiple myeloma progression at a single-cell level. *Blood Adv* **6**, 5873-5883.
136. Nakamura K, Smyth MJ & Martinet L (2020). Cancer immunoediting and immune dysregulation in multiple myeloma. *Blood* **136**, 2731-2740.

137. Desantis V, Savino FD, Scaringella A, Potenza MA, Nacci C, Frassanito MA, Vacca A & Montagnani M (2022). The Leading Role of the Immune Microenvironment in Multiple Myeloma: A New Target with a Great Prognostic and Clinical Value. *J Clin Med* **11**,
138. Suen H, Brown R, Yang S, Weatherburn C, Ho PJ, Woodland N, Nassif N, Barbaro P, Bryant C, Hart D, Gibson J & Joshua D (2016). Multiple myeloma causes clonal T-cell immunosenescence: identification of potential novel targets for promoting tumour immunity and implications for checkpoint blockade. *Leukemia* **30**, 1716-24.
139. Benson DM, Jr., Bakan CE, Mishra A, Hofmeister CC, Efebera Y, Becknell B, Baiocchi RA, Zhang J, Yu J, Smith MK, Greenfield CN, Porcu P, Devine SM, Rotem-Yehudar R, Lozanski G, Byrd JC & Caligiuri MA (2010). The PD-1/PD-L1 axis modulates the natural killer cell versus multiple myeloma effect: a therapeutic target for CT-011, a novel monoclonal anti-PD-1 antibody. *Blood* **116**, 2286-94.
140. Prabhala RH, Pelluru D, Fulciniti M, Prabhala HK, Nanjappa P, Song W, Pai C, Amin S, Tai YT, Richardson PG, Ghobrial IM, Treon SP, Daley JF, Anderson KC, Kutok JL & Munshi NC (2010). Elevated IL-17 produced by TH17 cells promotes myeloma cell growth and inhibits immune function in multiple myeloma. *Blood* **115**, 5385-92.
141. Noonan K, Marchionni L, Anderson J, Pardoll D, Roodman GD & Borrello I (2010). A novel role of IL-17-producing lymphocytes in mediating lytic bone disease in multiple myeloma. *Blood* **116**, 3554-63.
142. Scavelli C, Nico B, Cirulli T, Ria R, Di Pietro G, Mangieri D, Bacigalupo A, Mangialardi G, Coluccia AM, Caravita T, Molica S, Ribatti D, Dammacco F & Vacca A (2008). Vasculogenic mimicry by bone marrow macrophages in patients with multiple myeloma. *Oncogene* **27**, 663-74.
143. Sun J, Park C, Guenthner N, Gurley S, Zhang L, Lubben B, Adebayo O, Bash H, Chen Y, Maksimos M, Muz B & Azab AK (2022). Tumor-associated macrophages in multiple myeloma: advances in biology and therapy. *J Immunother Cancer* **10**,
144. Brown R, Suen H, Favaloro J, Yang S, Ho PJ, Gibson J & Joshua D (2012). Trogocytosis generates acquired regulatory T cells adding further complexity to the dysfunctional immune response in multiple myeloma. *Oncoimmunology* **1**, 1658-1660.
145. Alrasheed N, Lee L, Ghorani E, Henry JY, Conde L, Chin M, Galas-Filipowicz D, Furness AJS, Chavda SJ, Richards H, De-Silva D, Cohen OC, Patel D, Brooks A, Rodriguez-Justo M, Pule M, Herrero J, Quezada SA & Yong KL (2020). Marrow-Infiltrating Regulatory T Cells Correlate with the Presence of Dysfunctional CD4+PD-1+ Cells and Inferior Survival in Patients with Newly Diagnosed Multiple Myeloma. *Clinical Cancer Research* **26**, 3443-3454.
146. Bryant C, Suen H, Brown R, Yang S, Favaloro J, Aklilu E, Gibson J, Ho PJ, Iland H, Fromm P, Woodland N, Nassif N, Hart D & Joshua DE (2013). Long-term survival in multiple myeloma is associated with a distinct immunological profile, which includes proliferative cytotoxic T-cell clones and a favourable Treg/Th17 balance. *Blood Cancer J* **3**, e148.
147. Favaloro J, Brown R, Aklilu E, Yang S, Suen H, Hart D, Fromm P, Gibson J, Khoo L, Ho PJ & Joshua D (2014). Myeloma skews regulatory T and pro-inflammatory T helper 17 cell balance in favor of a suppressive state. *Leuk Lymphoma* **55**, 1090-8.
148. Dahlhoff J, Manz H, Steinfatt T, Delgado-Tascon J, Seebacher E, Schneider T, Wilnit A, Mokhtari Z, Tabares P, Böckle D, Rasche L, Martin Kortüm K, Lutz MB, Einsele H, Brandl A & Beilhack A (2022). Transient regulatory T-cell targeting triggers immune control of multiple myeloma and prevents disease progression. *Leukemia* **36**, 790-800.
149. Dyck L & Mills KHG (2017). Immune checkpoints and their inhibition in cancer and infectious diseases. *European Journal of Immunology* **47**, 765-779.
150. Dong H, Strome SE, Salomao DR, Tamura H, Hirano F, Flies DB, Roche PC, Lu J, Zhu G, Tamada K, Lennon VA, Celis E & Chen L (2002). Tumor-associated B7-H1

promotes T-cell apoptosis: A potential mechanism of immune evasion. *Nature Medicine* **8**, 793-800.
151. Rodig N, Ryan T, Allen JA, Pang H, Grabie N, Chernova T, Greenfield EA, Liang SC, Sharpe AH, Lichtman AH & Freeman GJ (2003). Endothelial expression of PD-L1 and PD-L2 down-regulates CD8+ T cell activation and cytolysis. *European Journal of Immunology* **33**, 3117-3126.
152. Kulikowska de Nałęcz A, Ciszak L, Usnarska-Zubkiewicz L, Frydecka I, Pawlak E, Szmyrka M & Kosmaczewska A (2021). Deregulated Expression of Immune Checkpoints on Circulating CD4 T Cells May Complicate Clinical Outcome and Response to Treatment with Checkpoint Inhibitors in Multiple Myeloma Patients. *Int J Mol Sci* **22**,
153. Salik B, Smyth MJ & Nakamura K (2020). Targeting immune checkpoints in hematological malignancies. *J Hematol Oncol* **13**, 111.
154. Endo H & Inoue M (2019). Dormancy in cancer. *Cancer Sci* **110**, 474-480.
155. Kostopoulos IV, Ntanasis-Stathopoulos I, Gavriatopoulou M, Tsitsilonis OE & Terpos E (2020). Minimal Residual Disease in Multiple Myeloma: Current Landscape and Future Applications With Immunotherapeutic Approaches. *Front Oncol* **10**, 860.
156. Dadzie TG & Green AC (2022). The role of the bone microenvironment in regulating myeloma residual disease and treatment. *Front Oncol* **12**, 999939.
157. Lai C & Lemke G (1991). An extended family of protein-tyrosine kinase genes differentially expressed in the vertebrate nervous system. *Neuron* **6**, 691-704.
158. Lemke G (2013). Biology of the TAM receptors. *Cold Spring Harbor Perspectives in Biology* **5**, 1-12.
159. Heiring C, Dahlbäck B & Muller YA (2004). Ligand Recognition and Homophilic Interactions in Tyro3: STRUCTURAL INSIGHTS INTO THE Axl/Tyro3 RECEPTOR TYROSINE KINASE FAMILY *. *Journal of Biological Chemistry* **279**, 6952-6958.
160. Sasaki T, Knyazev PG, Clout NJ, Cheburkin Y, Göhring W, Ullrich A, Timpl R & Hohenester E (2006). Structural basis for Gas6-Axl signalling. *Embo j* **25**, 80-7.
161. Caberoy NB, Zhou Y & Li W (2010). Tubby and tubby-like protein 1 are new MerTK ligands for phagocytosis. **29**, 3898-3910.
162. Caberoy NB, Alvarado G, Bigcas J-L & Li W (2012). Galectin-3 is a new MerTK-specific eat-me signal. *Journal of Cellular Physiology* **227**, 401-407.
163. Maillard C, Berruyer M, Serre CM, Dechavanne M & Delmas PD (1992). Protein-s, a vitamin k-dependent protein, is a bone matrix component synthesized and secreted by osteoblasts. *Endocrinology* **130**, 1599-1604.
164. Shiozawa Y, Pedersen EA, Patel LR, Ziegler AM, Havens AM, Jung Y, Wang J, Zalucha S, Loberg RD, Pienta KJ & Taichman RS (2010). GAS6/AXL axis regulates prostate cancer invasion, proliferation, and survival in the bone marrow niche. *Neoplasia* **12**, 116-127.
165. Ubil E, Caskey L, Holtzhausen A, Hunter D, Story C & Earp HS (2018). Tumor-secreted Pros1 inhibits macrophage M1 polarization to reduce antitumor immune response. *Journal of Clinical Investigation* **128**, 2356-2369.
166. Waizenegger JS, Ben-Batalla I, Weinhold N, Meissner T, Wroblewski M, Janning M, Riecken K, Binder M, Atanackovic D, Taipaleenmaeki H, Schewe D, Sawall S, Gensch V, Cubas-Cordova M, Seckinger A, Fiedler W, Hesse E, Kröger N, Fehse B, Hose D, Klein B, Raab MS, Pantel K, Bokemeyer C & Loges S (2015). Role of Growth arrest-specific gene 6-Mer axis in multiple myeloma. *Leukemia* **29**, 696-704.
167. Al Kafri N & Hafizi S (2019). Tumour-Secreted Protein S (ProS1) Activates a Tyro3-Erk Signalling Axis and Protects Cancer Cells from Apoptosis. *Cancers (Basel)* **11**,
168. Fang S, Luo Y, Zhang Y, Wang H, Liu Q, Li X & Yu T (2021). NTNG1 Modulates Cisplatin Resistance in Epithelial Ovarian Cancer Cells via the GAS6/AXL/Akt Pathway. *Front Cell Dev Biol* **9**, 652325.
169. Lemke G (2017). Phosphatidylserine Is the Signal for TAM Receptors and Their Ligands. *Trends in Biochemical Sciences* **42**, 738-748.

170. Vuckovic S, Vandyke K, Rickards DA, McCauley Winter P, Brown SHJ, Mitchell TW, Liu J, Lu J, Askenase PW, Yuriev E, Capuano B, Ramsland PA, Hill GR, Zannettino ACW & Hutchinson AT (2017). The cationic small molecule GW4869 is cytotoxic to high phosphatidylserine-expressing myeloma cells. *British Journal of Haematology* **177**, 423-440.
171. Sharma B & Kanwar SS (2018). Phosphatidylserine: A cancer cell targeting biomarker. *Semin Cancer Biol* **52**, 17-25.
172. Goruppi S, Ruaro E, Varnum B & Schneider C (1997). Requirement of phosphatidylinositol 3-kinase-dependent pathway and Src for Gas6-Axl mitogenic and survival activities in NIH 3T3 fibroblasts. *Molecular and Cellular Biology* **17**, 4442-4453.
173. Georgescu MM, Kirsch KH, Shishido T, Zong C & Hanafusa H (1999). Biological effects of c-Mer receptor tyrosine kinase in hematopoietic cells depend on the Grb2 binding site in the receptor and activation of NF-kappaB. *Mol Cell Biol* **19**, 1171-81.
174. Weinger JG, Gohari P, Yan Y, Backer JM, Varnum B & Shafit-Zagardo B (2008). In brain, Axl recruits Grb2 and the p85 regulatory subunit of PI3 kinase; in vitro mutagenesis defines the requisite binding sites for downstream Akt activation. *Journal of Neurochemistry* **106**, 134-146.
175. Kasikara C, Kumar S, Kimani S, Tsou W-I, Geng K, Davra V, Sriram G, Devoe C, Nguyen K-QN, Antes A, Krantz A, Rymarczyk G, Wilczynski A, Empig C, Freimark B, Gray M, Schlunegger K, Hutchins J, Kotenko SV & Birge RB (2017). Phosphatidylserine Sensing by TAM Receptors Regulates AKT-Dependent Chemoresistance and PD-L1 Expression. *Molecular Cancer Research* **15**, 753-764.
176. Lemke G & Burstyn-Cohen T (2010). TAM receptors and the clearance of apoptotic cells. *Ann N Y Acad Sci* **1209**, 23-9.
177. Linger RMA, Keating AK, Earp HS & Graham DK (2008). TAM Receptor Tyrosine Kinases: Biologic Functions, Signaling, and Potential Therapeutic Targeting in Human Cancer. In, edn, ed. 35-83. Elsevier.
178. Wanke F, Gutbier S, Rümmelin A, Steinberg M, Hughes LD, Koenen M, Komuczki J, Regan-Komito D, Wagage S, Hesselmann J, Thoma R, Brugger D, Christopeit T, Wang H, Point F, Hallet R, Ghosh S, Rothlin CV, Patsch C & Geering B (2021). Ligand-dependent kinase activity of MERTK drives efferocytosis in human iPSC-derived macrophages. *Cell Death Dis* **12**, 538.
179. Jiménez-García L, Mayer C, Burrola PG, Huang Y, Shokhirev MN & Lemke G (2022). The TAM receptor tyrosine kinases Axl and Mer drive the maintenance of highly phagocytic macrophages. *Front Immunol* **13**, 960401.
180. Lu Q, Gore M, Zhang Q, Camenisch T, Boast S, Casagranda F, Lai C, Skinner MK, Klein R, Matsushima GK, Earp HS, Goff SP & Lemke G (1999). Tyro-3 family receptors are essential regulators of mammalian spermatogenesis. *Nature* **398**, 723-8.
181. Duncan JL, LaVail MM, Yasumura D, Matthes MT, Yang H, Trautmann N, Chappelow AV, Feng W, Earp HS, Matsushima GK & Vollrath D (2003). An RCS-like retinal dystrophy phenotype in mer knockout mice. *Invest Ophthalmol Vis Sci* **44**, 826-38.
182. Al-Zaeed N, Budai Z, Szondy Z & Sarang Z (2021). TAM kinase signaling is indispensable for proper skeletal muscle regeneration in mice. *Cell Death & Disease* **12**, 611.
183. Lemke G & Rothlin CV (2008). Immunobiology of the TAM receptors. *Nat Rev Immunol* **8**, 327-336.
184. Tanaka M, Dykes SS & Siemann DW (2021). Inhibition of the Axl pathway impairs breast and prostate cancer metastasis to the bones and bone remodeling. *Clin Exp Metastasis* **38**, 321-335.
185. Axelrod HD, Valkenburg KC, Amend SR, Hicks JL, Parsana P, Torga G, DeMarzo AM & Pienta KJ (2019). AXL Is a Putative Tumor Suppressor and Dormancy Regulator in Prostate Cancer. *Molecular Cancer Research* **17**, 356-369.

186. Lee-Sherick AB, Jacobsen KM, Henry CJ, Huey MG, Parker RE, Page LS, Hill AA, Wang X, Frye SV, Earp HS, Jordan CT, Deryckere D & Graham DK (2018). MERTK inhibition alters the PD-1 axis and promotes anti-leukemia immunity. *JCI Insight* **3**,
187. Davra V, Kumar S, Geng K, Calianese D, Mehta D, Gadiyar V, Kasikara C, Lahey KC, Chang YJ, Wichroski M, Gao C, De Lorenzo MS, Kotenko SV, Bergsbaken T, Mishra PK, Gause WC, Quigley M, Spires TE & Birge RB (2021). Axl and Mertk Receptors Cooperate to Promote Breast Cancer Progression by Combined Oncogenic Signaling and Evasion of Host Antitumor Immunity. *Cancer Res* **81**, 698-712.
188. Furukawa M, Ohkawara H, Ogawa K, Ikeda K, Ueda K, Shichishima-Nakamura A, Ito E, Imai JI, Yanagisawa Y, Honma R, Watanabe S, Waguri S, Ikezoe T & Takeishi Y (2017). Autocrine and paracrine interactions between multiple myeloma cells and bone marrow stromal cells by growth arrest-specific gene 6 cross-talk with interleukin-6. *Journal of Biological Chemistry* **292**, 4280-4292.
189. Lee E, Decker AM, Cackowski FC, Kana LA, Yumoto K, Jung Y, Wang J, Buttitta L, Morgan TM & Taichman RS (2016). Growth Arrest-Specific 6 (GAS6) Promotes Prostate Cancer Survival by G1Arrest/S Phase Delay and Inhibition of Apoptosis During Chemotherapy in Bone Marrow. **117**, 2815-2824.
190. Ben-Batalla I, Schultze A, Wroblewski M, Erdmann R, Heuser M, Waizenegger JS, Riecken K, Binder M, Schewe D, Sawall S, Witzke V, Cubas-Cordova M, Janning M, Wellbrock J, Fehse B, Hagel C, Krauter J, Ganser A, Lorens JB, Fiedler W, Carmeliet P, Pantel K, Bokemeyer C & Loges S (2013). Axl, a prognostic and therapeutic target in acute myeloid leukemia mediates paracrine crosstalk of leukemia cells with bone marrow stroma. *Blood* **122**, 2443-2452.
191. Whitman SP, Kohlschmidt J, Maharry K, Volinia S, Mrózek K, Nicolet D, Schwind S, Becker H, Metzeler KH, Mendler JH, Eisfeld AK, Carroll AJ, Powell BL, Carter TH, Baer MR, Kolitz JE, Park IK, Stone RM, Caligiuri MA, Marcucci G & Bloomfield CD (2014). GAS6 expression identifies high-risk adult AML patients: potential implications for therapy. *Leukemia* **28**, 1252-1258.
192. Wei M, Wang Y, Liu Y, Li D & He X (2022). AXL, along with PROS1, is overexpressed in papillary thyroid carcinoma and regulates its biological behaviour. *World J Surg Oncol* **20**, 334.
193. Suleiman L, Muataz Y, Négrier C & Boukerche H (2021). Protein S-mediated signal transduction pathway regulates lung cancer cell proliferation, migration and angiogenesis. *Hematology/Oncology and Stem Cell Therapy*
194. Khamko R, Wasenang W, Daduang J, Settasatian C & Limpaiboon T (2022). Combined OPCML and AXL Expression as a Prognostic Marker and OPCML Enhances AXL Inhibitor in Cholangiocarcinoma. *In Vivo* **36**, 1168-1177.
195. Busch CJ, Hagel C, Becker B, Oetting A, Möckelmann N, Droste C, Möller-Koop C, Witt M, Blaurock M, Loges S, Rothkamm K, Betz C, Münscher A, Clauditz TS & Rieckmann T (2022). Tissue Microarray Analyses Suggest Axl as a Predictive Biomarker in HPV-Negative Head and Neck Cancer. *Cancers (Basel)* **14**,
196. Paccez JD, Vasques GJ, Correa RG, Vasconcellos JF, Duncan K, Gu X, Bhasin M, Libermann TA & Zerbini LF (2013). The receptor tyrosine kinase Axl is an essential regulator of prostate cancer proliferation and tumor growth and represents a new therapeutic target. *Oncogene* **32**, 689-698.
197. Nam RK, Benatar T, Wallis CJD, Kobylecky E, Amemiya Y, Sherman C & Seth A (2019). MicroRNA-139 is a predictor of prostate cancer recurrence and inhibits growth and migration of prostate cancer cells through cell cycle arrest and targeting IGF1R and AXL. *The Prostate* **79**, 1435-1451.
198. Park J-S, Lee C, Kim H-K, Kim D, Son JB, Ko E, Cho J-H, Kim N-D, Nan H-Y, Kim C-Y, Yoon S, Lee S-H & Choi HG (2016). Suppression of the metastatic spread of breast cancer by DN10764 (AZD7762)-mediated inhibition of AXL signaling. *Oncotarget* **7**,
199. Leconet W, Chentouf M, Du Manoir S, Chevalier C, Sirvent A, Aït-Arsa I, Busson M, Jarlier M, Radosevic-Robin N, Theillet C, Chalbos D, Pasquet J-M, Pèlegrin A,

Larbouret C & Robert B (2017). Therapeutic Activity of Anti-AXL Antibody against Triple-Negative Breast Cancer Patient-Derived Xenografts and Metastasis. *Clinical Cancer Research* **23**, 2806-2816.
200. Chang H, An R, Li X, Lang X, Feng J & Lv M (2021). Anti-Axl monoclonal antibodies attenuate the migration of MDA-MB-231 breast cancer cells. *Oncol Lett* **22**, 749.
201. Duan Y, Luo L, Qiao C, Li X, Wang J, Liu H, Zhou T, Shen B, Lv M & Feng J (2019). A novel human anti-AXL monoclonal antibody attenuates tumour cell migration. *Scandinavian Journal of Immunology* **90**, e12777.
202. Lewis Q, Penelope DO & Ingunn H (2015). Bone Metastasis: Molecular Mechanisms Implicated in Tumour Cell Dormancy in Breast and Prostate Cancer. *Current Cancer Drug Targets* **15**, 469-480.
203. Taniguchi H, Yamada T, Wang R, Tanimura K, Adachi Y, Nishiyama A, Tanimoto A, Takeuchi S, Araujo LH, Boroni M, Yoshimura A, Shiotsu S, Matsumoto I, Watanabe S, Kikuchi T, Miura S, Tanaka H, Kitazaki T, Yamaguchi H, Mukae H, Uchino J, Uehara H, Takayama K & Yano S (2019). AXL confers intrinsic resistance to osimertinib and advances the emergence of tolerant cells. *Nat Commun* **10**, 259.
204. Brown NE, Jones A, Hunt BG & Waltz SE (2022). Prostate tumor RON receptor signaling mediates macrophage recruitment to drive androgen deprivation therapy resistance through Gas6-mediated Axl and RON signaling. *The Prostate* **82**, 1422-1437.
205. Dumas P-Y, Villacreces A, Guitart AV, El-habhab A, Massara L, Mansier O, Bidet A, Martineau D, Fernandez S, Leguay T, Pigneux A, Vigon I, Pasquet J-M & Desplat V (2021). Dual Inhibition of FLT3 and AXL by Gilteritinib Overcomes Hematopoietic Niche-Driven Resistance Mechanisms in FLT3-ITD Acute Myeloid Leukemia. *Clinical Cancer Research* **27**, 6012-6025.
206. Yumoto K, Eber MR, Wang J, Cackowski FC, Decker AM, Lee E, Nobre AR, Aguirre-Ghiso JA, Jung Y & Taichman RS (2016). Axl is required for TGF-β2-induced dormancy of prostate cancer cells in the bone marrow. *Scientific Reports*
207. Taichman RS, Patel LR, Bedenis R, Wang J, Weidner S, Schumann T, Yumoto K, Berry JE, Shiozawa Y & Pienta KJ (2013). GAS6 Receptor Status Is Associated with Dormancy and Bone Metastatic Tumor Formation. *PLoS ONE*
208. Zhang KS, Pelleg T, Campbell S, Rubio C, Loschner AL & Ie S (2021). Pulmonary metastatic melanoma: current state of diagnostic imaging and treatments. *Melanoma Manag* **8**, Mmt58.
209. Fane ME, Chhabra Y, Alicea GM, Maranto DA, Douglass SM, Webster MR, Rebecca VW, Marino GE, Almeida F, Ecker BL, Zabransky DJ, Hüser L, Beer T, Tang H-Y, Kossenkov A, Herlyn M, Speicher DW, Xu W, Xu X, Jaffee EM, Aguirre-Ghiso JA & Weeraratna AT (2022). Stromal changes in the aged lung induce an emergence from melanoma dormancy. *Nature* **606**, 396-405.
210. Mohty M, Avet-Loiseau H & Harousseau J-L (2021). Requirements for operational cure in multiple myeloma. *Blood, The Journal of the American Society of Hematology* **138**, 1406-1411.
211. Innao V, Allegra A, Russo S, Gerace D, Vaddinelli D, Alonci A, Allegra AG & Musolino C (2017). Standardisation of minimal residual disease in multiple myeloma. *Eur J Cancer Care*
212. Aguirre-Ghiso JA (2007). Models, mechanisms and clinical evidence for cancer dormancy. *Nat Rev Cancer* **7**, 834-46.
213. Khoo WH, Ledergor G, Weiner A, Roden DL, Terry RL, McDonald MM, Chai RC, De Veirman K, Owen KL, Opperman KS, Vandyke K, Clark JR, Seckinger A, Kovacic N, Nguyen A, Mohanty ST, Pettitt JA, Xiao Y, Corr AP, Seeliger C, Novotny M, Lasken RS, Nguyen TV, Oyajobi BO, Aftab D, Swarbrick A, Parker B, Hewett DR, Hose D, Vanderkerken K, Zannettino ACW, Amit I, Phan TG & Croucher PI (2019). A niche-dependent myeloid transcriptome signature defines dormant myeloma cells. *Blood* **134**, 30-43.

214. Schroeder GM, An Y, Cai Z-W, Chen X-T, Clark C, Cornelius LAM, Dai J, Gullo-Brown J, Gupta A, Henley B, Hunt JT, Jeyaseelan R, Kamath A, Kim K, Lippy J, Lombardo LJ, Manne V, Oppenheimer S, Sack JS, Schmidt RJ, Shen G, Stefanski K, Tokarski JS, Trainor GL, Wautlet BS, Wei D, Williams DK, Zhang Y, Zhang Y, Fargnoli J & Borzilleri RM (2009). Discovery of N-(4-(2-Amino-3-chloropyridin-4-yloxy)-3-fluorophenyl)-4-ethoxy-1-(4-fluorophenyl)-2-oxo-1,2-dihydropyridine-3-carboxamide (BMS-777607), a Selective and Orally Efficacious Inhibitor of the Met Kinase Superfamily. *Journal of Medicinal Chemistry* **52**, 1251-1254.
215. Kasikara C, Davra V, Calianese D, Geng K, Spires TE, Quigley M, Wichroski M, Sriram G, Suarez-Lopez L, Yaffe MB, Kotenko SV, De Lorenzo MS & Birge RB (2019). Pan-TAM Tyrosine Kinase Inhibitor BMS-777607 Enhances Anti-PD-1 mAb Efficacy in a Murine Model of Triple-Negative Breast Cancer. *Cancer Res* **79**, 2669-2683.
216. Zeng JY, Sharma S, Zhou YQ, Yao HP, Hu X, Zhang R & Wang MH (2014). Synergistic activities of MET/RON inhibitor BMS-777607 and mTOR inhibitor AZD8055 to polyploid cells derived from pancreatic cancer and cancer stem cells. *Mol Cancer Ther* **13**, 37-48.
217. Tirado-Gonzalez I, Descot A, Soetopo D, Nevmerzhitskaya A, Schäffer A, Kur IM, Czlonka E, Wachtel C, Tsoukala I, Müller L, Schäfer AL, Weitmann M, Dinse P, Alberto E, Buck MC, Landry JJ, Baying B, Slotta-Huspenina J, Roesler J, Harter PN, Kubasch AS, Meinel J, Elwakeel E, Strack E, Quang CT, Abdel-Wahab O, Schmitz M, Weigert A, Schmid T, Platzbecker U, Benes V, Ghysdael J, Bonig H, Götze KS, Rothlin CV, Ghosh S & Medyouf H (2021). AXL Inhibition in Macrophages Stimulates Host-versus-Leukemia Immunity and Eradicates Naïve and Treatment-Resistant Leukemia. *Cancer Discov* **11**, 2924-2943.
218. Lee C, Whang YM, Campbell P, Mulcrone PL, Elefteriou F, Cho SW & Park SI (2018). Dual targeting c-met and VEGFR2 in osteoblasts suppresses growth and osteolysis of prostate cancer bone metastasis. *Cancer Letters* **414**, 205-213.
219. Nguyen KQ, Tsou WI, Calarese DA, Kimani SG, Singh S, Hsieh S, Liu Y, Lu B, Wu Y, Garforth SJ, Almo SC, Kotenko SV & Birge RB (2014). Overexpression of MERTK receptor tyrosine kinase in epithelial cancer cells drives efferocytosis in a gain-of-function capacity. *J Biol Chem* **289**, 25737-49.
220. Liu Y, Lan L, Li Y, Lu J, He L, Deng Y, Fei M, Lu JW, Shangguan F, Lu JP, Wang J, Wu L, Huang K & Lu B (2022). N-glycosylation stabilizes MerTK and promotes hepatocellular carcinoma tumor growth. *Redox Biol* **54**, 102366.
221. Shi C, Li X, Wang X, Ding N, Ping L, Shi Y, Mi L, Lai Y, Song Y & Zhu J (2018). The proto-oncogene Mer tyrosine kinase is a novel therapeutic target in mantle cell lymphoma. *J Hematol Oncol* **11**, 43.
222. DeRyckere D, Lee-Sherick AB, Huey MG, Hill AA, Tyner JW, Jacobsen KM, Page LS, Kirkpatrick GG, Eryildiz F, Montgomery SA, Zhang W, Wang X, Frye SV, Earp HS & Graham DK (2017). UNC2025, a MERTK Small-Molecule Inhibitor, Is Therapeutically Effective Alone and in Combination with Methotrexate in Leukemia Models. *Clin Cancer Res* **23**, 1481-1492.
223. Linger RM, Cohen RA, Cummings CT, Sather S, Migdall-Wilson J, Middleton DH, Lu X, Barón AE, Franklin WA, Merrick DT, Jedlicka P, DeRyckere D, Heasley LE & Graham DK (2013). Mer or Axl receptor tyrosine kinase inhibition promotes apoptosis, blocks growth and enhances chemosensitivity of human non-small cell lung cancer. *Oncogene* **32**, 3420-31.
224. Pilli VS, Datta A, Dorsey A, Liu B & Majumder R (2020). Modulation of protein S and growth arrest specific 6 protein signaling inhibits pancreatic cancer cell survival and proliferation. *Oncol Rep* **44**, 1322-1332.
225. Pardoll DM (2012). The blockade of immune checkpoints in cancer immunotherapy. *Nature Reviews Cancer* **12**, 252-264.
226. Bardhan K, Anagnostou T & Boussiotis VA (2016). The PD1:PD-L1/2 Pathway from Discovery to Clinical Implementation. **7**,
227. Tanaka T, Kutomi G, Kajiwara T, Kukita K, Kochin V, Kanaseki T, Tsukahara T, Hirohashi Y, Torigoe T, Okamoto Y, Hirata K, Sato N & Tamura Y (2017). Cancer-

associated oxidoreductase ERO1-α promotes immune escape through up-regulation of PD-L1 in human breast cancer. *Oncotarget* **8**,
228. Yoyen-Ermis D, Tunali G, Tavukcuoglu E, Horzum U, Ozkazanc D, Sutlu T, Buyukasik Y & Esendagli G (2019). Myeloid maturation potentiates STAT3-mediated atypical IFN-γ signaling and upregulation of PD-1 ligands in AML and MDS. *Scientific Reports* **9**,
229. Rosenblatt J, Glotzbecker B, Mills H, Vasir B, Tzachanis D, Levine JD, Joyce RM, Wellenstein K, Keefe W, Schickler M, Rotem-Yehudar R, Kufe D & Avigan D (2011). PD-1 Blockade by CT-011, Anti-PD-1 Antibody, Enhances Ex Vivo T-cell Responses to Autologous Dendritic Cell/Myeloma Fusion Vaccine. *Journal of Immunotherapy* **34**, 409-418.
230. Hallett WHD, Jing W, Drobyski WR & Johnson BD (2011). Immunosuppressive Effects of Multiple Myeloma Are Overcome by PD-L1 Blockade. *Biology of Blood and Marrow Transplantation* **17**, 1133-1145.
231. Tremblay-Lemay R, Rastgoo N & Chang H (2018). Modulating PD-L1 expression in multiple myeloma: an alternative strategy to target the PD-1/PD-L1 pathway. *Journal of Hematology & Oncology* **11**,
232. Kasikara C, Davra V, Calianese D, Geng K, Spires TE, Quigley M, Wichroski M, Sriram G, Suarez-Lopez L, Yaffe MB, Kotenko SV, De Lorenzo MS & Birge RB (2019). Pan-TAM Tyrosine Kinase Inhibitor BMS-777607 Enhances Anti–PD-1 mAb Efficacy in a Murine Model of Triple-Negative Breast Cancer. *Cancer Research* **79**, 2669.
233. Caetano MS, Younes AI, Barsoumian HB, Quigley M, Menon H, Gao C, Spires T, Reilly TP, Cadena AP, Cushman TR, Schoenhals JE, Li A, Nguyen QN, Cortez MA & Welsh JW (2019). Triple Therapy with MerTK and PD1 Inhibition Plus Radiotherapy Promotes Abscopal Antitumor Immune Responses. *Clin Cancer Res* **25**, 7576-7584.
234. Jung S-H, Park S-S, Lim J-Y, Sohn SY, Kim NY, Kim D, Lee SH, Chung Y-J & Min C-K (2022). Single-cell analysis of multiple myelomas refines the molecular features of bortezomib treatment responsiveness. *Experimental & Molecular Medicine*
235. Zhang Z, Wang W, Ma D, Xiong J, Kuang X, Zhang S, Fang Q & Wang J (2020). Heme oxygenase-1 inhibition mediates Gas6 to enhance bortezomib-sensitivity in multiple myeloma via ERK/STAT3 axis. *Aging (Albany NY)* **12**, 6611-6629.
236. Fionda C, Stabile H, Molfetta R, Soriani A, Bernardini G, Zingoni A, Gismondi A, Paolini R, Cippitelli M & Santoni A (2018). Translating the anti-myeloma activity of Natural Killer cells into clinical application. *Cancer Treatment Reviews* **70**, 255-264.
237. Kosta A, Mekhloufi A, Lucantonio L, Zingoni A, Soriani A, Cippitelli M, Gismondi A, Fazio F, Petrucci MT, Santoni A, Stabile H & Fionda C (2022). GAS6/TAM signaling pathway controls MICA expression in multiple myeloma cells. *Front Immunol* **13**, 942640.
238. Tormoen GW, Blair TC, Bambina S, Kramer G, Baird J, Rahmani R, Holland JM, McCarty OJT, Baine MJ, Verma V, Nabavizadeh N, Gough MJ & Crittenden M (2020). Targeting MerTK Enhances Adaptive Immune Responses After Radiation Therapy. *Int J Radiat Oncol Biol Phys* **108**, 93-103.
239. Jung Y, Decker AM, Wang J, Lee E, Kana LA, Yumoto K, Cackowski FC, Rhee J, Carmeliet P, Buttitta L, Morgan TM & Taichman RS (2016). Endogenous GAS6 and Mer receptor signaling regulate prostate cancer stem cells in bone marrow. *Oncotarget* **7**, 25698-25711.
240. Linger RMA, Lee-Sherick AB, DeRyckere D, Cohen RA, Jacobsen KM, McGranahan A, Brandão LN, Winges A, Sawczyn KK, Liang X, Keating AK, Tan AC, Earp HS & Graham DK (2013). Mer receptor tyrosine kinase is a therapeutic target in pre–B-cell acute lymphoblastic leukemia. *Blood* **122**, 1599-1609.
241. Livak KJ & Schmittgen TD (2001). Analysis of relative gene expression data using real-time quantitative PCR and the 2(-Delta Delta C(T)) Method. *Methods* **25**, 402-8.

242. Hanahan D (1983). Studies on transformation of Escherichia coli with plasmids. *J Mol Biol* **166**, 557-80.
243. Ran FA, Hsu PD, Wright J, Agarwala V, Scott DA & Zhang F (2013). Genome engineering using the CRISPR-Cas9 system. *Nature Protocols* **8**, 2281-2308.
244. Noll JE, Hewett DR, Williams SA, Vandyke K, Kok C, To LB & Zannettino ACW (2014). SAMSN1 Is a Tumor Suppressor Gene in Multiple Myeloma. *Neoplasia* **16**, 572-585.
245. Diamond P, Labrinidis A, Martin SK, Farrugia AN, Gronthos S, To LB, Fujii N, O'Loughlin PD, Evdokiou A & Zannettino AC (2009). Targeted disruption of the CXCL12/CXCR4 axis inhibits osteolysis in a murine model of myeloma-associated bone loss. *J Bone Miner Res* **24**, 1150-61.
246. Hanawa H, Kelly PF, Nathwani AC, Persons DA, Vandergriff JA, Hargrove P, Vanin EF & Nienhuis AW (2002). Comparison of various envelope proteins for their ability to pseudotype lentiviral vectors and transduce primitive hematopoietic cells from human blood. *Mol Ther* **5**, 242-51.
247. Eddaoudi A, Canning SL & Kato I (2018). Flow Cytometric Detection of G0 in Live Cells by Hoechst 33342 and Pyronin Y Staining. *Methods Mol Biol* **1686**, 49-57.
248. Shen YJ, Mishima Y, Shi J, Sklavenitis-Pistofidis R, Redd RA, Moschetta M, Manier S, Roccaro AM, Sacco A, Tai YT, Mercier F, Kawano Y, Su NK, Berrios B, Doench JG, Root DE, Michor F, Scadden DT & Ghobrial IM (2021). Progression signature underlies clonal evolution and dissemination of multiple myeloma. *Blood* **137**, 2360-2372.
249. Krejcik J, Barnkob MB, Nyvold CG, Larsen TS, Barington T & Abildgaard N (2021). Harnessing the Immune System to Fight Multiple Myeloma. *Cancers (Basel)* **13**,
250. Méndez-Ferrer S, Bonnet D, Steensma DP, Hasserjian RP, Ghobrial IM, Gribben JG, Andreeff M & Krause DS (2020). Bone marrow niches in haematological malignancies. *Nature Reviews Cancer* **20**, 285-298.
251. Lee-Sherick AB, Eisenman KM, Sather S, McGranahan A, Armistead PM, McGary CS, Hunsucker SA, Schlegel J, Martinson H, Cannon C, Keating AK, Earp HS, Liang X, Deryckere D & Graham DK (2013). Aberrant Mer receptor tyrosine kinase expression contributes to leukemogenesis in acute myeloid leukemia. *Oncogene* **32**, 5359-5368.
252. Du W, Zhu J, Zeng Y, Liu T, Zhang Y, Cai T, Fu Y, Zhang W, Zhang R, Liu Z & Huang JA (2021). KPNB1-mediated nuclear translocation of PD-L1 promotes non-small cell lung cancer cell proliferation via the Gas6/MerTK signaling pathway. *Cell Death Differ* **28**, 1284-1300.
253. Shi M, Zhang H, Wang L, Zhu C, Sheng K, Du Y, Wang K, Dias A, Chen S, Whitman M, Wang E, Reed R & Cheng H (2015). Premature termination codons are recognized in the nucleus in a reading-frame-dependent manner. *Cell Discovery* **1**, 15001.
254. Winiarska M, Nowis D, Firczuk M, Zagozdzon A, Gabrysiak M, Sadowski R, Barankiewicz J, Dwojak M & Golab J (2017). Selection of an optimal promoter for gene transfer in normal B cells. *Mol Med Rep* **16**, 3041-3048.
255. Lambeth LS, Moore RJ, Muralitharan M, Dalrymple BP, McWilliam S & Doran TJ (2005). Characterisation and application of a bovine U6 promoter for expression of short hairpin RNAs. *BMC Biotechnol* **5**, 13.
256. Huang Y, Wilkinson GF & Willars GB (2010). Role of the signal peptide in the synthesis and processing of the glucagon-like peptide-1 receptor. *Br J Pharmacol* **159**, 237-51.
257. Zhao X, Li G & Liang S (2013). Several Affinity Tags Commonly Used in Chromatographic Purification. *Journal of Analytical Methods in Chemistry* **2013**, 581093.
258. McCloskey P, Fridell YW, Attar E, Villa J, Jin Y, Varnum B & Liu ET (1997). GAS6 mediates adhesion of cells expressing the receptor tyrosine kinase Axl. *J Biol Chem* **272**, 23285-91.

259. Sang YB, Kim J-H, Kim C-G, Hong MH, Kim HR, Cho BC & Lim SM (2022). The Development of AXL Inhibitors in Lung Cancer: Recent Progress and Challenges. *Frontiers in Oncology* **12**,
260. Giuliano CJ, Lin A, Girish V & Sheltzer JM (2019). Generating Single Cell-Derived Knockout Clones in Mammalian Cells with CRISPR/Cas9. *Curr Protoc Mol Biol* **128**, e100.
261. Jin J, Xu Y, Huo L, Ma L, Scott AW, Pizzi MP, Li Y, Wang Y, Yao X, Song S & Ajani JA (2020). An improved strategy for CRISPR/Cas9 gene knockout and subsequent wildtype and mutant gene rescue. *PLOS ONE* **15**, e0228910.
262. Ramamoorthi G, Kodumudi K, Gallen C, Zachariah NN, Basu A, Albert G, Beyer A, Snyder C, Wiener D, Costa RLB & Czerniecki BJ (2022). Disseminated cancer cells in breast cancer: Mechanism of dissemination and dormancy and emerging insights on therapeutic opportunities. *Semin Cancer Biol* **78**, 78-89.
263. Singh DK, Patel VG, Oh WK & Aguirre-Ghiso JA (2021). Prostate Cancer Dormancy and Reactivation in Bone Marrow. *J Clin Med* **10**,
264. Kumar S, Paiva B, Anderson KC, Durie B, Landgren O, Moreau P, Munshi N, Lonial S, Bladé J, Mateos MV, Dimopoulos M, Kastritis E, Boccadoro M, Orlowski R, Goldschmidt H, Spencer A, Hou J, Chng WJ, Usmani SZ, Zamagni E, Shimizu K, Jagannath S, Johnsen HE, Terpos E, Reiman A, Kyle RA, Sonneveld P, Richardson PG, McCarthy P, Ludwig H, Chen W, Cavo M, Harousseau JL, Lentzsch S, Hillengass J, Palumbo A, Orfao A, Rajkumar SV, Miguel JS & Avet-Loiseau H (2016). International Myeloma Working Group consensus criteria for response and minimal residual disease assessment in multiple myeloma. *Lancet Oncol* **17**, e328-e346.
265. Phan TG & Croucher PI (2020). The dormant cancer cell life cycle. *Nature Reviews Cancer* **20**, 398-411.
266. Rasche L, Schinke C, Maura F, Bauer MA, Ashby C, Deshpande S, Poos AM, Zangari M, Thanendrarajan S, Davies FE, Walker BA, Barlogie B, Landgren O, Morgan GJ, van Rhee F & Weinhold N (2022). The spatio-temporal evolution of multiple myeloma from baseline to relapse-refractory states. *Nat Commun* **13**, 4517.
267. Shiozawa Y, Berry JE, Eber MR, Jung Y, Yumoto K, Cackowski FC, Yoon HJ, Parsana P, Mehra R, Wang J, McGee S, Lee E, Nagrath S, Pienta KJ & Taichman RS (2016). The marrow niche controls the cancer stem cell phenotype of disseminated prostate cancer. *Oncotarget* **7**, 41217-41232.
268. Sandiford OA, Donnelly RJ, El-Far MH, Burgmeyer LM, Sinha G, Pamarthi SH, Sherman LS, Ferrer AI, DeVore DE, Patel SA, Naaldijk Y, Alonso S, Barak P, Bryan M, Ponzio NM, Narayanan R, Etchegaray JP, Kumar R & Rameshwar P (2021). Mesenchymal Stem Cell-Secreted Extracellular Vesicles Instruct Stepwise Dedifferentiation of Breast Cancer Cells into Dormancy at the Bone Marrow Perivascular Region. *Cancer Res* **81**, 1567-1582.
269. Wong NKY, Dong X, Lin YY, Xue H, Wu R, Lin D, Collins C & Wang Y (2022). Framework of Intrinsic Immune Landscape of Dormant Prostate Cancer. *Cells* **11**,
270. Ju S, Wang F, Wang Y & Ju S (2020). CSN8 is a key regulator in hypoxia-induced epithelial–mesenchymal transition and dormancy of colorectal cancer cells. *Molecular Cancer* **19**, 168.
271. Phan TG & Croucher PI (2020). The dormant cancer cell life cycle. *Nat Rev Cancer* **20**, 398-411.
272. Mishra A, Wang J, Shiozawa Y, McGee S, Kim J, Jung Y, Joseph J, Berry JE, Havens A, Pienta KJ & Taichman RS (2012). Hypoxia stabilizes GAS6/Axl signaling in metastatic prostate cancer. *Molecular Cancer Research* **10**, 703-712.
273. Li Y, Ye X, Tan C, Hongo JA, Zha J, Liu J, Kallop D, Ludlam MJ & Pei L (2009). Axl as a potential therapeutic target in cancer: role of Axl in tumor growth, metastasis and angiogenesis. *Oncogene* **28**, 3442-55.
274. Lan Q, Peyvandi S, Duffey N, Huang YT, Barras D, Held W, Richard F, Delorenzi M, Sotiriou C, Desmedt C, Lorusso G & Rüegg C (2019). Type I interferon/IRF7

axis instigates chemotherapy-induced immunological dormancy in breast cancer. *Oncogene* **38**, 2814-2829.
275. Mrozik KM, Cheong CM, Hewett DR, Noll JE, Opperman KS, Adwal A, Russell DL, Blaschuk OW, Vandyke K & Zannettino ACW (2020). LCRF-0006, a small molecule mimetic of the N-cadherin antagonist peptide ADH-1, synergistically increases multiple myeloma response to bortezomib. *FASEB Bioadv* **2**, 339-353.
276. García-Ortiz A, Rodríguez-García Y, Encinas J, Maroto-Martín E, Castellano E, Teixidó J & Martínez-López J (2021). The Role of Tumor Microenvironment in Multiple Myeloma Development and Progression. *Cancers* **13**, 217.
277. Colombo M, Mirandola L, Platonova N, Apicella L, Basile A, Figueroa AJ, Cobos E, Chiriva-Internati M & Chiaramonte R (2013). Notch-directed microenvironment reprogramming in myeloma: a single path to multiple outcomes. *Leukemia* **27**, 1009-18.
278. Lind J, Czernilofsky F, Vallet S & Podar K (2019). Emerging protein kinase inhibitors for the treatment of multiple myeloma. *Expert Opin Emerg Drugs* **24**, 133-152.
279. Shiozawa Y, Pedersen EA & Taichman RS (2010). GAS6/Mer axis regulates the homing and survival of the E2A/PBX1-positive B-cell precursor acute lymphoblastic leukemia in the bone marrow niche. *Exp Hematol* **38**, 132-40.
280. Ohta S, Tago K, Kuchimaru T, Funakoshi-Tago M, Horie H, Aoki-Ohmura C, Matsugi J & Yanagisawa K (2022). The role of MerTK in promoting cell migration is enhanced by the oncogenic Ras/IL-33 signaling axis. *Febs j* **289**, 1950-1967.
281. Yan D, Huelse JM, Kireev D, Tan Z, Chen L, Goyal S, Wang X, Frye SV, Behera M, Schneider F, Ramalingam SS, Owonikoko T, Earp HS, DeRyckere D & Graham DK (2022). MERTK activation drives osimertinib resistance in EGFR-mutant non-small cell lung cancer. *J Clin Invest* **132**,
282. Lee BH, Park Y, Kim JH, Kang KW, Lee SJ, Kim SJ & Kim BS (2021). Prognostic Value of Galectin-9 Relates to Programmed Death-Ligand 1 in Patients With Multiple Myeloma. *Front Oncol* **11**, 669817.
283. Lozano E, Mena MP, Díaz T, Martin-Antonio B, León S, Rodríguez-Lobato LG, Oliver-Caldés A, Cibeira MT, Bladé J, Prat A, Rosiñol L & Fernández de Larrea C (2020). Nectin-2 Expression on Malignant Plasma Cells Is Associated with Better Response to TIGIT Blockade in Multiple Myeloma. *Clin Cancer Res* **26**, 4688-4698.
284. Wang J, Zheng Y, Tu C, Zhang H, Vanderkerken K, Menu E & Liu J (2020). Identification of the immune checkpoint signature of multiple myeloma using mass cytometry-based single-cell analysis. *Clin Transl Immunology* **9**, e01132.
285. Pennycuick A, Teixeira VH, AbdulJabbar K, Raza SEA, Lund T, Akarca AU, Rosenthal R, Kalinke L, Chandrasekharan DP, Pipinikas CP, Lee-Six H, Hynds RE, Gowers KHC, Henry JY, Millar FR, Hagos YB, Denais C, Falzon M, Moore DA, Antoniou S, Durrenberger PF, Furness AJ, Carroll B, Marceaux C, Asselin-Labat ML, Larson W, Betts C, Coussens LM, Thakrar RM, George J, Swanton C, Thirlwell C, Campbell PJ, Marafioti T, Yuan Y, Quezada SA, McGranahan N & Janes SM (2020). Immune Surveillance in Clinical Regression of Preinvasive Squamous Cell Lung Cancer. *Cancer Discov* **10**, 1489-1499.
286. KODA Y, ITOH M & TOHDA S (2018). Effects of MERTK Inhibitors UNC569 and UNC1062 on the Growth of Acute Myeloid Leukaemia Cells. *Anticancer Research* **38**, 199-204.
287. Friend NL, Hewett DR, Panagopoulos V, Noll JE, Vandyke K, Mrozik KM, Fitter S & Zannettino ACW (2020). Characterization of the role of Samsn1 loss in multiple myeloma development. *FASEB Bioadv* **2**, 554-572.
288. Stern L, McGuire H, Avdic S, Rizzetto S, Fazekas de St Groth B, Luciani F, Slobedman B & Blyth E (2018). Mass Cytometry for the Assessment of Immune Reconstitution After Hematopoietic Stem Cell Transplantation. *Front Immunol* **9**, 1672.
289. Herbrich S, Baran N, Cai T, Weng C, Aitken MJL, Post SM, Henderson J, Shi C, Richard-Carpentier G, Sauvageau G, Baggerly K, Al-Atrash G, Davis RE, Daver N,

Zha D & Konopleva M (2021). Overexpression of CD200 is a Stem Cell-Specific Mechanism of Immune Evasion in AML. *J Immunother Cancer* **9**,
290. Liu R, Gao Q, Foltz SM, Fowles JS, Yao L, Wang JT, Cao S, Sun H, Wendl MC, Sethuraman S, Weerasinghe A, Rettig MP, Storrs EP, Yoon CJ, Wyczalkowski MA, McMichael JF, Kohnen DR, King J, Goldsmith SR, O'Neal J, Fulton RS, Fronick CC, Ley TJ, Jayasinghe RG, Fiala MA, Oh ST, DiPersio JF, Vij R & Ding L (2021). Co-evolution of tumor and immune cells during progression of multiple myeloma. *Nature Communications* **12**, 2559.
291. Kim Y, Born C, Bléry M & Steinle A (2020). MICAgen Mice Recapitulate the Highly Restricted but Activation-Inducible Expression of the Paradigmatic Human NKG2D Ligand MICA. *Front Immunol* **11**, 960.
292. Ryu D, Kim SJ, Hong Y, Jo A, Kim N, Kim H-J, Lee H-O, Kim K & Park W-Y (2020). Alterations in the Transcriptional Programs of Myeloma Cells and the Microenvironment during Extramedullary Progression Affect Proliferation and Immune Evasion. *Clinical Cancer Research* **26**, 935-944.
293. Vandyke K (2021). Seed and soil revisited in multiple myeloma. *Blood* **137**, 2282-2283.
294. Hewett DR, Vandyke K, Lawrence DM, Friend N, Noll JE, Geoghegan JM, Croucher PI & Zannettino ACW (2017). DNA Barcoding Reveals Habitual Clonal Dominance of Myeloma Plasma Cells in the Bone Marrow Microenvironment. *Neoplasia* **19**, 972-981.
295. Chiu KC, Lee CH, Liu SY, Chou YT, Huang RY, Huang SM & Shieh YS (2015). Polarization of tumor-associated macrophages and Gas6/Axl signaling in oral squamous cell carcinoma. *Oral Oncol* **51**, 683-9.
296. Opperman KS, Vandyke K, Clark KC, Coulter EA, Hewett DR, Mrozik KM, Schwarz N, Evdokiou A, Croucher PI, Psaltis PJ, Noll JE & Zannettino AC (2019). Clodronate-Liposome Mediated Macrophage Depletion Abrogates Multiple Myeloma Tumor Establishment In Vivo. *Neoplasia* **21**, 777-787.
297. Sinik L, Minson KA, Tentler JJ, Carrico J, Bagby SM, Robinson WA, Kami R, Burstyn-Cohen T, Eckhardt SG, Wang X, Frye SV, Earp HS, DeRyckere D & Graham DK (2019). Inhibition of MERTK Promotes Suppression of Tumor Growth in BRAF Mutant and BRAF Wild-Type Melanoma. *Mol Cancer Ther* **18**, 278-288.
298. Saito Y, Uchida N, Tanaka S, Suzuki N, Tomizawa-Murasawa M, Sone A, Najima Y, Takagi S, Aoki Y, Wake A, Taniguchi S, Shultz LD & Ishikawa F (2010). Induction of cell cycle entry eliminates human leukemia stem cells in a mouse model of AML. *Nat Biotechnol* **28**, 275-80.
299. Feng X, Lan H, Ruan Y & Li C (2018). Impact on acute myeloid leukemia relapse in granulocyte colony-stimulating factor application: a meta-analysis. *Hematology* **23**, 581-589.
300. Cho SF, Xing L, Anderson KC & Tai YT (2021). Promising Antigens for the New Frontier of Targeted Immunotherapy in Multiple Myeloma. *Cancers (Basel)* **13**,
301. Engelmann J, Zarrer J, Gensch V, Riecken K, Berenbrok N, Luu TV, Beitzen-Heineke A, Vargas-Delgado ME, Pantel K, Bokemeyer C, Bhamidipati S, Darwish IS, Masuda E, Burstyn-Cohen T, Alberto EJ, Ghosh S, Rothlin C, Hesse E, Taipaleenmäki H, Ben-Batalla I & Loges S (2022). Regulation of bone homeostasis by MERTK and TYRO3. *Nat Commun* **13**, 7689.
302. Myers KV, Amend SR & Pienta KJ (2019). Targeting Tyro3, Axl and MerTK (TAM receptors): implications for macrophages in the tumor microenvironment. *Mol Cancer* **18**, 94.
303. Rios-Doria J, Favata M, Lasky K, Feldman P, Lo Y, Yang G, Stevens C, Wen X, Sehra S, Katiyar K, Liu K, Wynn R, Harris JJ, Ye M, Spitz S, Wang X, He C, Li YL, Yao W, Covington M, Scherle P & Koblish H (2020). A Potent and Selective Dual Inhibitor of AXL and MERTK Possesses Both Immunomodulatory and Tumor-Targeted Activity. *Front Oncol* **10**, 598477.
304. Summers RJ, Jain J, Vasileiadi E, Smith B, Chimenti ML, Yeung TY, Kelvin J, Wang X, Frye SV, Earp HS, Tyner JW, Dreaden EC, DeRyckere D & Graham DK

(2022). Therapeutic Targeting of MERTK and BCL-2 in T-Cell and Early T-Precursor Acute Lymphoblastic Leukemia. *Cancers (Basel)* **14**,
305. Post SM, Ma H, Malaney P, Zhang X, Aitken MJL, Mak PY, Ruvolo VR, Yasuhiro T, Kozaki R, Chan LE, Ostermann LB, Konopleva M, Carter BZ, DiNardo C, Andreeff MD, Khoury JD & Ruvolo PP (2022). AXL/MERTK inhibitor ONO-7475 potently synergizes with venetoclax and overcomes venetoclax resistance to kill FLT3-ITD acute myeloid leukemia. *Haematologica* **107**, 1311-1322.
306. Yan D, Earp HS, DeRyckere D & Graham DK (2021). Targeting MERTK and AXL in EGFR Mutant Non-Small Cell Lung Cancer. *Cancers (Basel)* **13**,
307. Lu Q & Lemke G (2001). Homeostatic regulation of the immune system by receptor tyrosine kinases of the Tyro 3 family. *Science* **293**, 306-311.
308. Linger RM, Keating AK, Earp HS & Graham DK (2008). TAM receptor tyrosine kinases: biologic functions, signaling, and potential therapeutic targeting in human cancer. *Adv Cancer Res* **100**, 35-83.
309. Cruz Cruz J, Allison KC, Page LS, Jenkins AJ, Wang X, Earp HS, Frye SV, Graham DK, Verneris MR & Lee-Sherick AB (2023). Inhibiting efferocytosis reverses macrophage-mediated immunosuppression in the leukemia microenvironment. *Front Immunol* **14**, 1146721.
310. Peeters MJW, Dulkeviciute D, Draghi A, Ritter C, Rahbech A, Skadborg SK, Seremet T, Carnaz Simões AM, Martinenaite E, Halldórsdóttir HR, Andersen MH, Olofsson GH, Svane IM, Rasmussen LJ, Met Ö, Becker JC, Donia M, Desler C & thor Straten P (2019). MERTK Acts as a Costimulatory Receptor on Human CD8+ T Cells. *Cancer Immunology Research* **7**, 1472-1484.
311. Stapleton M, Sawamoto K, Alméciga-Díaz CJ, Mackenzie WG, Mason RW, Orii T & Tomatsu S (2017). Development of Bone Targeting Drugs. *Int J Mol Sci* **18**,
312. Wang H, Liu H, Sun C, Liu C, Jiang T, Yin Y, Xu A, Pang Z, Zhang B & Hu Y (2021). Nanoparticles Dual Targeting Both Myeloma Cells and Cancer-Associated Fibroblasts Simultaneously to Improve Multiple Myeloma Treatment. *Pharmaceutics* **13**,
313. Lin CW, Lee CY, Lin SY, Kang L, Fu YC, Chen CH & Wang CK (2022). Bone-Targeting Nanoparticles of a Dendritic (Aspartic acid)(3)-Functionalized PEG-PLGA Biopolymer Encapsulating Simvastatin for the Treatment of Osteoporosis in Rat Models. *Int J Mol Sci* **23**,

Supplementary Figures

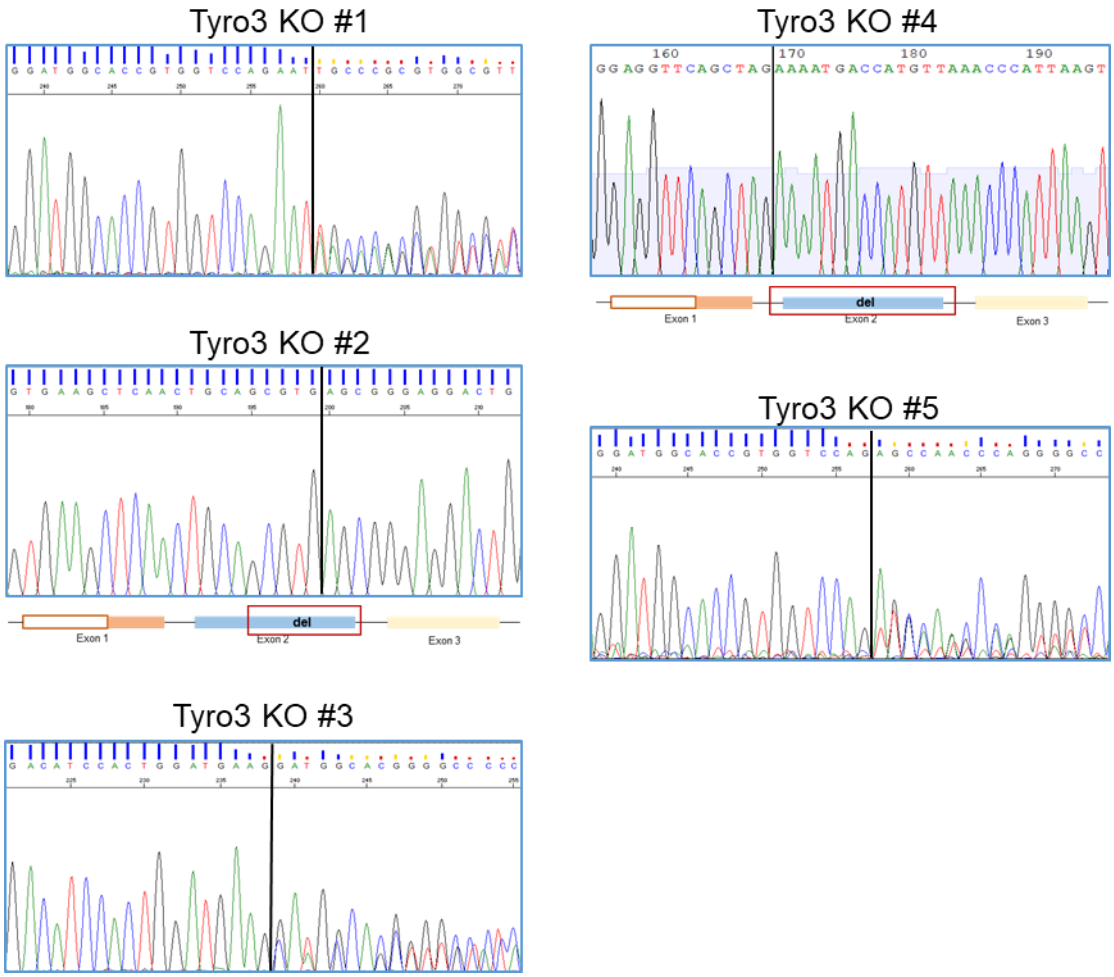

Supplementary Figure 1. Sequencing chromatograms of genomic DNA from 5TGM1 potential Tyro3 knockout cell lines. PCR products amplified from genomic DNA of 5TGM1 potential Tyro3 knockout clones were sequenced. Sequence chromatograms show location of insertion/deletion mutations. Larger deletions of exon 2 in clones #2 and #4 are depicted beneath chromatograms.

Tyro3 mutant allele cloning and sequencing summaries (cloned into pGEMTeasy)

Thesis Clone Tyro3KO#1

GC deletion – 7 clones; T insertion – 3 clones

GGATGAAGGATGGCACCGTGGTCCAGAAT**AAGCCAGGTGTCCATCTCCATCAGCGAGCACA

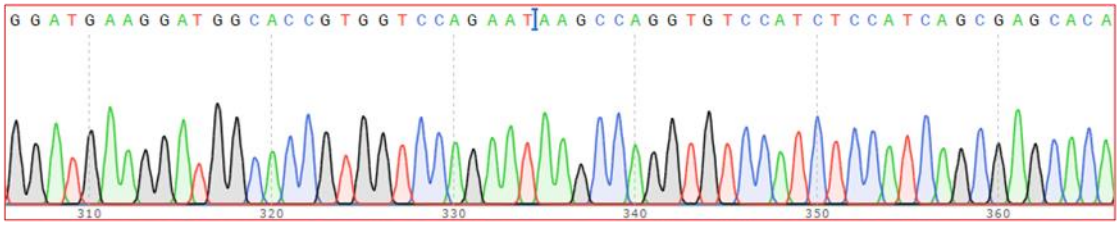

GGATGAAGGATGGCACCGTGGTCCAGAATTGCAAGCCAGGTGTCCATCTCCATCAGCGAGCACA

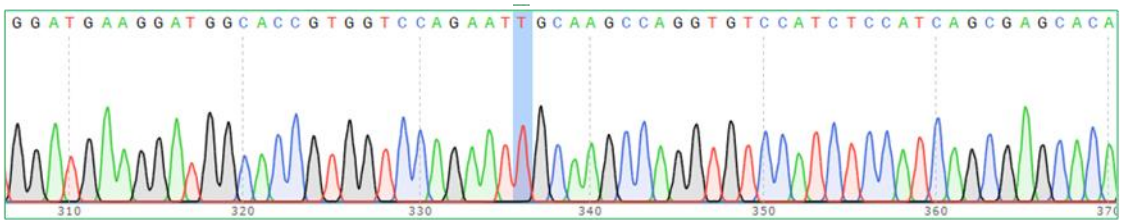

Thesis Clone Tyro3KO#3

22bp deletion – 7 clones; G deletion – 2 clones;

GGATGAAG**********CAAGCCAGGTGTCCATCTCCATCAGCGAGCACA

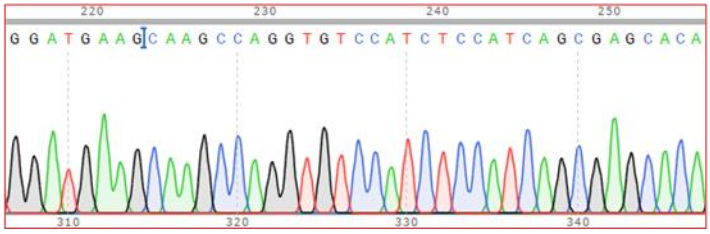

GGATGAAGGATGGCACCGTGGTCCAGAAT*CAAGCCAGGTGTCCATCTCCATCAGCGAGCACA

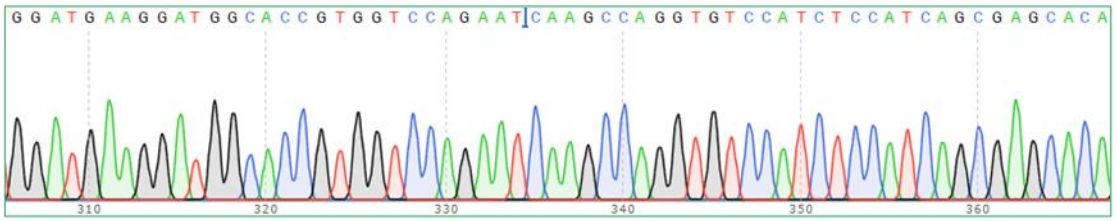

Thesis Clone Tyro3KO#5

AA deletion – 9 clones; A deletion – 4 clones

GGATGAAGGATGGCACCGTGGTCCAG**TGCAAGCCAGGTGTCCATCTCCATCAGCGAGCACA

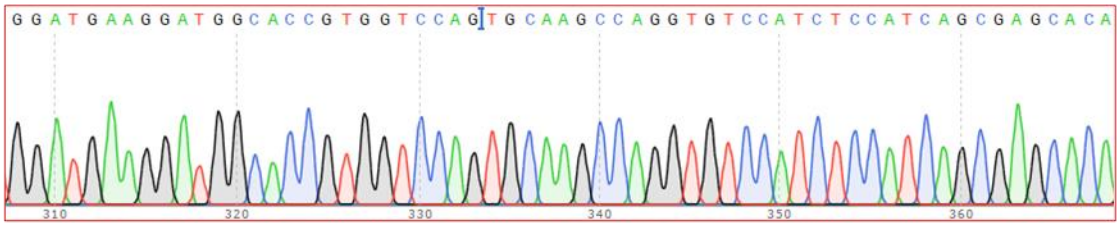

GGATGAAGGATGGCACCGTGGTCCAGA*TGCAAGCCAGGTGTCCATCTCCATCAGCGAGCACA

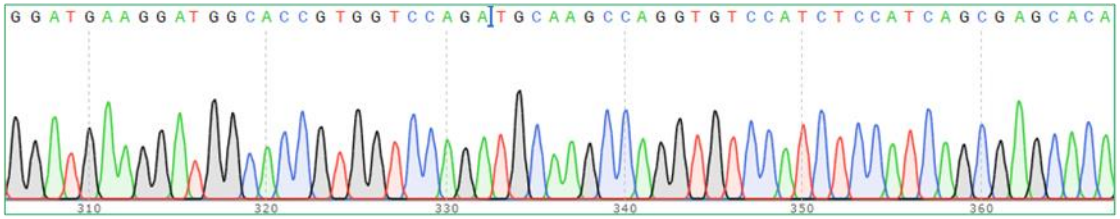

Supplementary Figure 2. Sequencing chromatograms of genomic DNA from 5TGM1 potential Tyro3 knockout cell lines #1, #3 and #5 cloned into a plasmid vector. PCR products amplified from genomic DNA of 5TGM1 potential Tyro3 knockout clones were cloned into a plasmid vector. Sequences were obtained from the two mutant alleles inferred from the original Sanger sequences traces. Sequence chromatograms show location of insertion/deletion mutations.

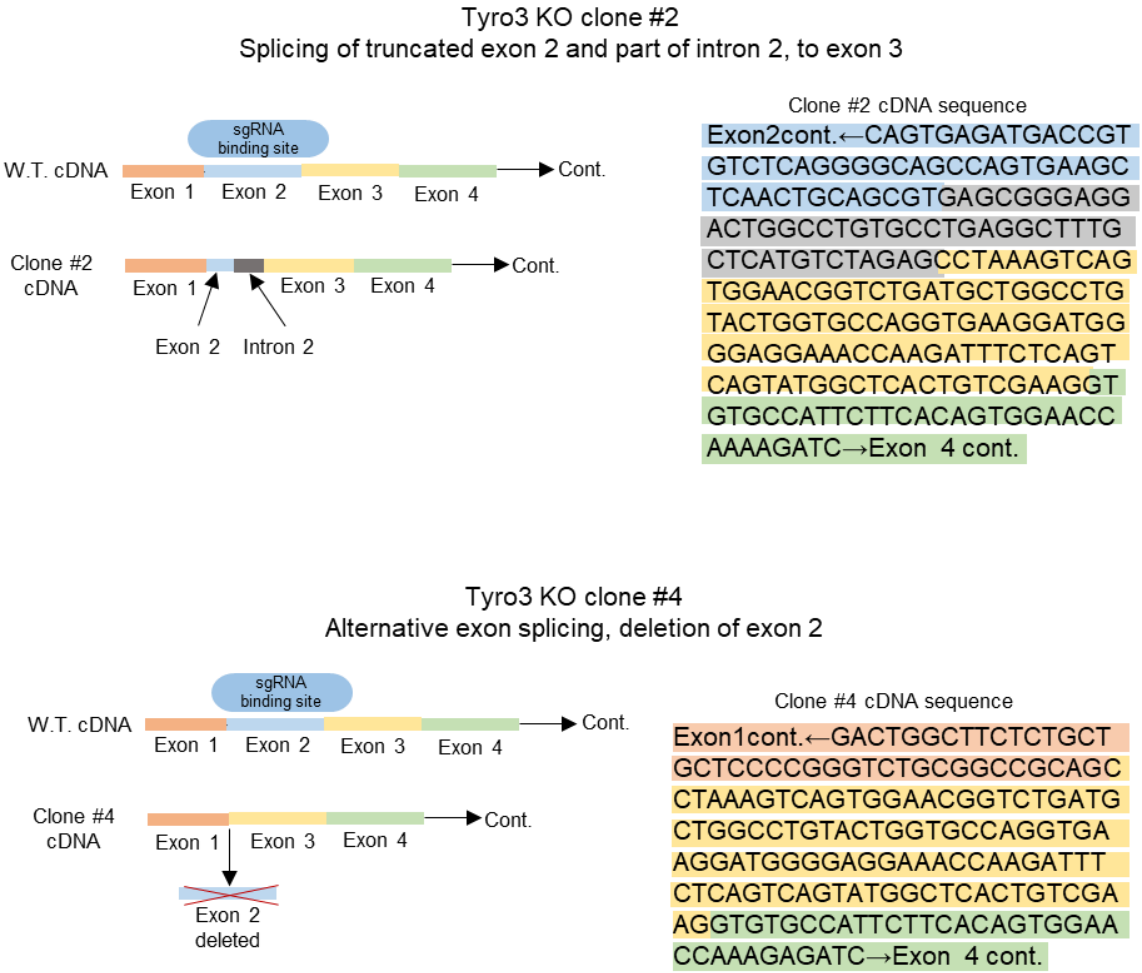

Supplementary Figure 3. 5TGM1 potential Tyro3 knockout clones #2 and #4 display alternative exon splicing. RT-PCR product sequencing of Tyro3 knockout clone #2 reveals partial deletion of exon 2, read through into part of intron 2, before splicing of a cryptic splice donor site to exon 3. RT-PCR products sequencing from Tyro3 knockout clone #4 reveals alternative exon splicing of exon 1 to exon 3 and complete deletion of exon 2. Figures depicting alternative splicing of Tyro3 potential knockout clones is shown compared to wild type Tyro3 (left) and corresponding cDNA sequences are shown (right).

Wild type Tyro3
880aa

MALRRSMGWPGLRPLLLAGLASLLLPGSAAAGLKLMGAPVKMTVSQGQPVKLNCSVEGMEDPDIHWMKDGTVV
QNASQVSISISEHSWIGLLSLKSVERSDAGLYWCQVKDGEETKISQSVWLTVEGVPFFTVEPKDLAVPPNAPF
QLSCEAVGPPEPVTIYWWRGLTKVGGPAPSPSVLNVTGVTQRTEFSCEARNIKGLATSRPAIVRLQAPPAAPF
NTTVTTISSYNASVAWVPGADGLALLHSCTVQVAHAPGEWEALAVVVPVPPFTCLLRNLAPATNYSLRVRCAN
ALGPSPYGDWVPFQTKGLAPARAPQNFHAIRTDSGLILEWEEVIPEDPGEGPLGPYKLSWVQENGTQDELMVE
GTRANLTDWDPQKDLILRVCASNAIGDGPWSQPLVVSSHDHAGRQGPPHSRTSWVPVVLGVLTALITAAALAL
ILLRKRRKETRFGQAFDSVMARGEPAVHFRAARSFNRERPERIEATLDSLGISDELKEKLEDVLIPEQQFTLG
RMLGKGEFGSVREAQLKQEDGSFVKVAVKMLKADIIASSDIEEFLREAACMKEFDHPHVAKLVGVSLRSRAKG
RLPIPMVILPFMKHGDLHAFLLASRIGENPFNLPLQTLVRFMVDIACGMEYLSSRNFIHRDLAARNCMLAEDM
TVCVADFGLSRKIYSGDYYRQGCASKLPVKWLALESLADNLYTVHSDVWAFGVTMWEIMTRGQTPYAGIENAE
IYNYLIGGNRLKQPPECMEEVYDLMYQCWSADPKQRPSFTCLRMELENILGHLSVLSTSQDPLYINIERAEQP
TESGSPEVHCGERSSSEAGDGSGVGAVGGIPSDSRYIFSPGGLSESPGQLEQQPESPLNENQRLLLLQQGLLP
HSSC-

Tyro3 KO #1a
Prediction 1: 812aa

MAPWSRIASQVSISISEHSWIGLLSLKSVERSDAGLYWCQVKDGEETKISQSVWLTVEGVPFFTVEPKDLAVP
PNAPFQLSCEAVGPPEPVTIYWWRGLTKVGGPAPSPSVLNVTGVTQRTEFSCEARNIKGLATSRPAIVRLQAP
PAAPFNTTVTTISSYNASVAWVPGADGLALLHSCTVQVAHAPGEWEALAVVVPVPPFTCLLRNLAPATNYSLR
VRCANALGPSPYGDWVPFQTKGLAPARAPQNFHAIRTDSGLILEWEEVIPEDPGEGPLGPYKLSWVQENGTQD
ELMVEGTRANLTDWDPQKDLILRVCASNAIGDGPWSQPLVVSSHDHAGRQGPPHSRTSWVPVVLGVLTALITA
AALALILLRKRRKETRFGQAFDSVMARGEPAVHFRAARSFNRERPERIEATLDSLGISDELKEKLEDVLIPEQ
QFTLGRMLGKGEFGSVREAQLKQEDGSFVKVAVKMLKADIIASSDIEEFLREAACMKEFDHPHVAKLVGVSLR
SRAKGRLPIPMVILPFMKHGDLHAFLLASRIGENPFNLPLQTLVRFMVDIACGMEYLSSRNFIHRDLAARNCM
LAEDMTVCVADFGLSRKIYSGDYYRQGCASKLPVKWLALESLADNLYTVHSDVWAFGVTMWEIMTRGQTPYAG
IENAEIYNYLIGGNRLKQPPECMEEVYDLMYQCWSADPKQRPSFTCLRMELENILGHLSVLSTSQDPLYINIE
RAEQPTESGSPEVHCGERSSSEAGDGSGVGAVGGIPSDSRYIFSPGGLSESPGQLEQQPESPLNENQRLLLLQ
QGLLPHSSC-

Tyro3 KO #1a Prediction 2: 99aa

MALRRSMGWPGLRPLLLAGLASLLLPGSAAAGLKLMGAPVKMTVSQGQPVKLNCSVEGMEDPDIHWMKDGTVV
QNCKPGVHLHQRAQLDWLTQPKVSGTV-

Tyro3 KO #1b
Prediction 1: 811aa

MAPWSRISQVSISISEHSWIGLLSLKSVERSDAGLYWCQVKDGEETKISQSVWLTVEGVPFFTVEPKDLAVPP
NAPFQLSCEAVGPPEPVTIYWWRGLTKVGGPAPSPSVLNVTGVTQRTEFSCEARNIKGLATSRPAIVRLQAPP
AAPFNTTVTTISSYNASVAWVPGADGLALLHSCTVQVAHAPGEWEALAVVVPVPPFTCLLRNLAPATNYSLRV
RCANALGPSPYGDWVPFQTKGLAPARAPQNFHAIRTDSGLILEWEEVIPEDPGEGPLGPYKLSWVQENGTQDE
LMVEGTRANLTDWDPQKDLILRVCASNAIGDGPWSQPLVVSSHDHAGRQGPPHSRTSWVPVVLGVLTALITAA
ALALILLRKRRKETRFGQAFDSVMARGEPAVHFRAARSFNRERPERIEATLDSLGISDELKEKLEDVLIPEQQ
FTLGRMLGKGEFGSVREAQLKQEDGSFVKVAVKMLKADIIASSDIEEFLREAACMKEFDHPHVAKLVGVSLRS
RAKGRLPIPMVILPFMKHGDLHAFLLASRIGENPFNLPLQTLVRFMVDIACGMEYLSSRNFIHRDLAARNCML
AEDMTVCVADFGLSRKIYSGDYYRQGCASKLPVKWLALESLADNLYTVHSDVWAFGVTMWEIMTRGQTPYAGI
ENAEIYNYLIGGNRLKQPPECMEEVYDLMYQCWSADPKQRPSFTCLRMELENILGHLSVLSTSQDPLYINIER
AEQPTESGSPEVHCGERSSSEAGDGSGVGAVGGIPSDSRYIFSPGGLSESPGQLEQQPESPLNENQRLLLLQQ
GLLPHSSC-

Tyro3 KO #1b, 5b
Prediction 2: 98aa

MALRRSMGWPGLRPLLLAGLASLLLPGSAAAGLKLMGAPVKMTVSQGQPVKLNCSVEGMEDPDIHWMKDGTVV
QNKPGVHLHQRAQLDWLTQPKVSGTV-

Tyro3 KO #2, 3a, 3b, 4, 5a
Prediction 1: 518aa

MVEGTRANLTDWDPQKDLILRVCASNAIGDGPWSQPLVVSSHDHAGRQGPPHSRTSWVPVVLGVLTALITAAA
LALILLRKRRKETRFGQAFDSVMARGEPAVHFRAARSFNRERPERIEATLDSLGISDELKEKLEDVLIPEQQF
TLGRMLGKGEFGSVREAQLKQEDGSFVKVAVKMLKADIIASSDIEEFLREAACMKEFDHPHVAKLVGVSLRSR
AKGRLPIPMVILPFMKHGDLHAFLLASRIGENPFNLPLQTLVRFMVDIACGMEYLSSRNFIHRDLAARNCMLA
EDMTVCVADFGLSRKIYSGDYYRQGCASKLPVKWLALESLADNLYTVHSDVWAFGVTMWEIMTRGQTPYAGIE
NAEIYNYLIGGNRLKQPPECMEEVYDLMYQCWSADPKQRPSFTCLRMELENILGHLSVLSTSQDPLYINIERA
EQPTESGSPEVHCGERSSSEAGDGSGVGAVGGIPSDSRYIFSPGGLSESPGQLEQQPESPLNENQRLLLLQQG
LLPHSSC-

Tyro3 #2
Prediction 2: 78aa

MALRRSMGWPGLRPLLLAGLASLLLPGSAAAGLKLMGAPVKMTVSQGQPVKLNCSVSGRTGLCLRLCSCLEPKVSGTV

Tyro3 KO #3a, 5a
Prediction 2: 92aa

MALRRSMGWPGLRPLLLAGLASLLLPGSAAAGLKLMGAPVKMTVSQGQPVKLNCSVEGMEDPDIHWMKDGTVV
QNQARCPSPSASTAGLAYSA-

Tyro3 KO #3b
Prediction 2: 85aa

MALRRSMGWPGLRPLLLAGLASLLLPGSAAAGLKLMGAPVKMTVSQGQPVKLNCSVEGMEDPDIHWMKQARCP
SPSASTAGLAYSA-

Tyro3 KO #4
Prediction 2: 32aa

MALRRSMGWPGLRPLLLAGLASLLLPGSAAAA-

Tyro3 KO #5b
Prediction 1: 811aa

MAPWSSASQVSISISEHSWIGLLSLKSVERSDAGLYWCQVKDGEETKISQSVWLTVEGVPFFTVEPKDLAVPPN
APFQLSCEAVGPPEPVTIYWWRGLTKVGGPAPSPSVLNVTGVTQRTEFSCEARNIKGLATSRPAIVRLQAPPAA
PFNTTVTTISSYNASVAWVPGADGLALLHSCTVQVAHAPGEWEALAVVVPVPPFTCLLRNLAPATNYSLRVRCA
NALGPSPYGDWVPFQTKGLAPARAPQNFHAIRTDSGLILEWEEVIPEDPGEGPLGPYKLSWVQENGTQDELMVE
GTRANLTDWDPQKDLILRVCASNAIGDGPWSQPLVVSSHDHAGRQGPPHSRTSWVPVVLGVLTALITAAALALI
LLRKRRKETRFGQAFDSVMARGEPAVHFRAARSFNRERPERIEATLDSLGISDELKEKLEDVLIPEQQFTLGRM
LGKGEFGSVREAQLKQEDGSFVKVAVKMLKADIIASSDIEEFLREAACMKEFDHPHVAKLVGVSLRSRAKGRLP
IPMVILPFMKHGDLHAFLLASRIGENPFNLPLQTLVRFMVDIACGMEYLSSRNFIHRDLAARNCMLAEDMTVCV
ADFGLSRKIYSGDYYRQGCASKLPVKWLALESLADNLYTVHSDVWAFGVTMWEIMTRGQTPYAGIENAEIYNYL
IGGNRLKQPPECMEEVYDLMYQCWSADPKQRPSFTCLRMELENILGHLSVLSTSQDPLYINIERAEQPTESGSP
EVHCGERSSSEAGDGSGVGAVGGIPSDSRYIFSPGGLSESPGQLEQQPESPLNENQRLLLLQQGLLPHSSC-

Supplementary Figure 4. Predicted consequences of Tyro3 mutations at the protein level in 5TGM1 potential Tyro3 knockout cell lines. Sequences of 5TGM1 potential Tyro3 knockout clonal cell line mutant alleles were translated into amino acids using Expasy Translate. Amino acid sequences were compared to wild type Tyro3, and open reading frames that code for sections of Tyro3 are shown. For each mutation between 1-2 predictions of total amino acid (aa) length are shown. Grey highlighted sections denote wild type Tyro3 protein sequence.

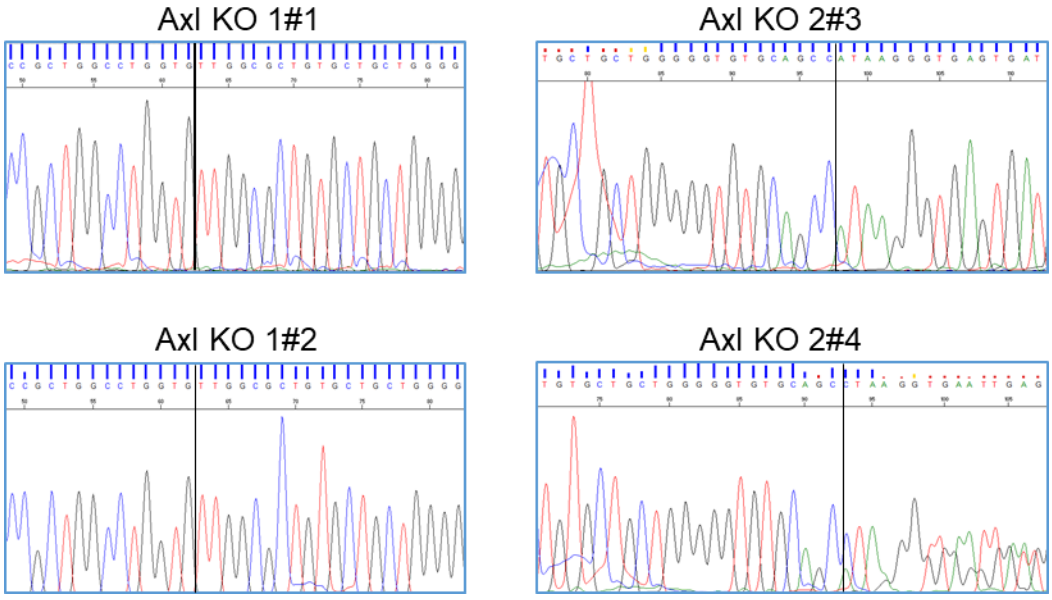

Supplementary Figure 5. Sequencing chromatograms of genomic DNA from 5TGM1 potential Axl knockout cell lines. PCR products amplified from genomic DNA of 5TGM1 potential Axl knockout clones were sequenced. Sequence chromatograms show location of insertion/deletion mutations.

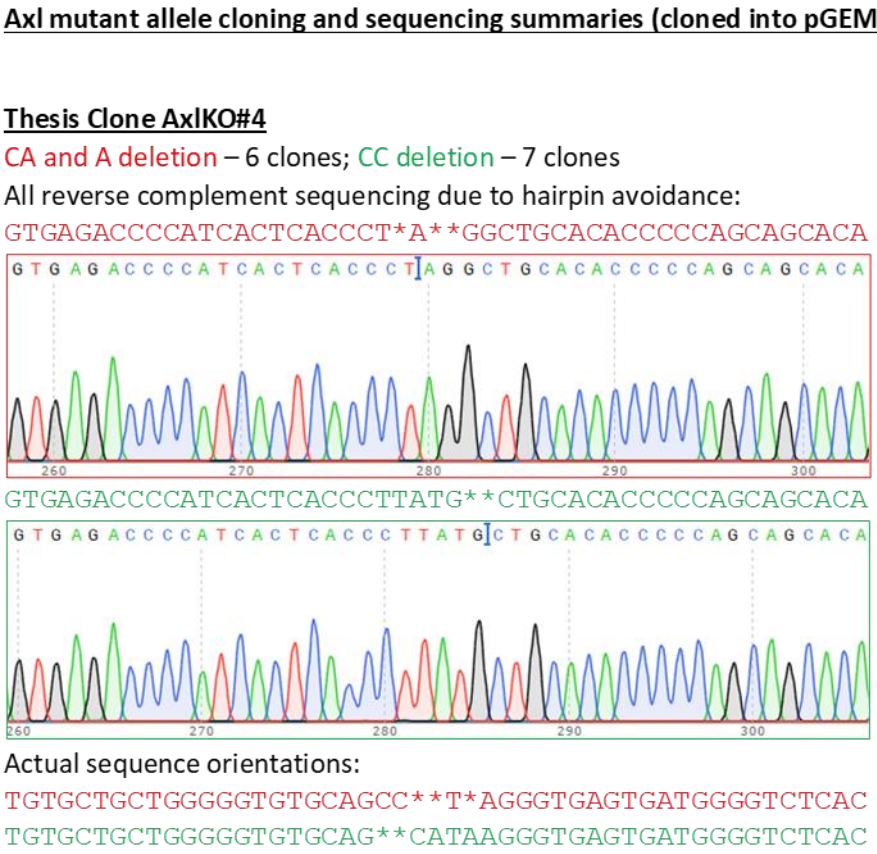

Supplementary Figure 6. Sequencing chromatograms of genomic DNA from 5TGM1 potential Axl knockout cell lines 2#4 cloned into a plasmid vector. PCR products amplified from genomic DNA of 5TGM1 potential Axl knockout clone 2#4 were cloned into a plasmid vector. Sequences were obtained from the two mutant alleles inferred from the original Sanger sequences trace. Sequence chromatograms show location of insertion/deletion mutations.

Wild type Axl
888aa

MGRVPLAWWLALCCWGCAAHKDTQTEAGSPFVGNPGNITGARGLTGTLRCELQVQGEPPEVVWLRDGQILELADNTQ
TQVPLGEDWQDEWKVVSQLRISALQLSDAGEYQCMVHLEGRTFVSQPGFVGLEGLPYFLEEPEDKAVPANTPFNLSC
QAQGPPEPVTLLWLQDAVPLAPVTGHSSQHSLQTPGLNKTSSFSCEAHNAKGVTTSRTATITVLPQRPHHLHVVSRQ
PTELEVAWTPGLSGIYPLTHCNLQAVLSDDGVGIWLGKSDPPEDPLTLQVSVPPHQLRLEKLLPHTPYHIRISCSSS
QGPSPWTHWLPVETTEGVPLGPPENVSAMRNGSQVLVRWQEPRVPLQGTLLGYRLAYRGQDTPEVLMDIGLTREVTL
ELRGDRPVANLTVSVTAYTSAGDGPWSLPVPLEPWRPGQGQPLHHLVSEPPPRAFSWPWWYVLLGALVAAACVLILA
LFLVHRRKKETRYGEVFEPTVERGELVVRYRVRKSYSRRTTEATLNSLGISEELKEKLRDVMVDRHKVALGKTLGEG
EFGAVMEGQLNQDDSILKVAVKTMKIAICTRSELEDFLSEAVCMKEFDHPNVMRLIGVCFQGSDREGFPEPVVILPF
MKHGDLHSFLLYSRLGDQPVFLPTQMLVKFMADIASGMEYLSTKRFIHRDLAARNCMLNENMSVCVADFGLSKKIYN
GDYYRQGRIAKMPVKWIAIESLADRVYTSKSDVWSFGVTMWEIATRGQTPYPGVENSEIYDYLRQGNRLKQPVDCLD
GLYALMSRCWELNPRDRPSFAELREDLENTLKALPPAQEPDEILYVNMDEGGSHLEPRGAAGGADPPTQPDPKDSCS
CLTAADVHSAGRYVLCPSTAPGPTLSADRGCPAPPGQEDGA-

Axl KO clones 1#1, 1#2, 2#3 and 2#4a
Prediction 1: 777aa

MVHLEGRTFVSQPGFVGLEGLPYFLEEPEDKAVPANTPFNLSCQAQGPPEPVTLLWLQDAVPLAPVTGHSSQHSLQT
PGLNKTSSFSCEAHNAKGVTTSRTATITVLPQRPHHLHVVSRQPTELEVAWTPGLSGIYPLTHCNLQAVLSDDGVGI
WLGKSDPPEDPLTLQVSVPPHQLRLEKLLPHTPYHIRISCSSSQGPSPWTHWLPVETTEGVPLGPPENVSAMRNGSQ
VLVRWQEPRVPLQGTLLGYRLAYRGQDTPEVLMDIGLTREVTLELRGDRPVANLTVSVTAYTSAGDGPWSLPVPLEP
WRPGQGQPLHHLVSEPPPRAFSWPWWYVLLGALVAAACVLILALFLVHRRKKETRYGEVFEPTVERGELVVRYRVRK
SYSRRTTEATLNSLGISEELKEKLRDVMVDRHKVALGKTLGEGEFGAVMEGQLNQDDSILKVAVKTMKIAICTRSEL
EDFLSEAVCMKEFDHPNVMRLIGVCFQGSDREGFPEPVVILPFMKHGDLHSFLLYSRLGDQPVFLPTQMLVKFMADI
ASGMEYLSTKRFIHRDLAARNCMLNENMSVCVADFGLSKKIYNGDYYRQGRIAKMPVKWIAIESLADRVYTSKSDVW
SFGVTMWEIATRGQTPYPGVENSEIYDYLRQGNRLKQPVDCLDGLYALMSRCWELNPRDRPSFAELREDLENTLKAL
PPAQEPDEILYVNMDEGGSHLEPRGAAGGADPPTQPDPKDSCSCLTAADVHSAGRYVLCPSTAPGPTLSADRGCPAP
PGQEDGA

Axl KO clone 2#4a 2#4b
Prediction 1: 18aa

MGRVPLAWWLALCCWGCAA

Axl KO clone 2#3
Prediction 2: 68aa

MGRVPLAWWLALCCWGCAAIRTHRPRLAARLWGTQGISQVPEDSRGHFGVSSRFRGNPLRWCGFEMDRS

Axl KO clone 1#1 and 1#2
Prediction 2: 68aa

MGRVPLAWCWRCAAGGVQPIRTHRPRLAARLWGTQGISQVPEDSRGHFGVSSRFRGNPLRWCGFEMDRS

Supplementary Figure 7. Predicted consequences of Axl mutations at the protein level in 5TGM1 potential Axl knockout cell lines. Sequences of 5TGM1 potential Axl knockout clonal cell line mutant alleles were translated into amino acids using Expasy Translate. Amino acid sequences were compared to wild type Axl, and open reading frames that code for sections of Axl are shown. For each mutation between 1-2 predictions of total amino acid (aa) length are shown. Grey highlighted sections denote wild type Axl protein sequence.

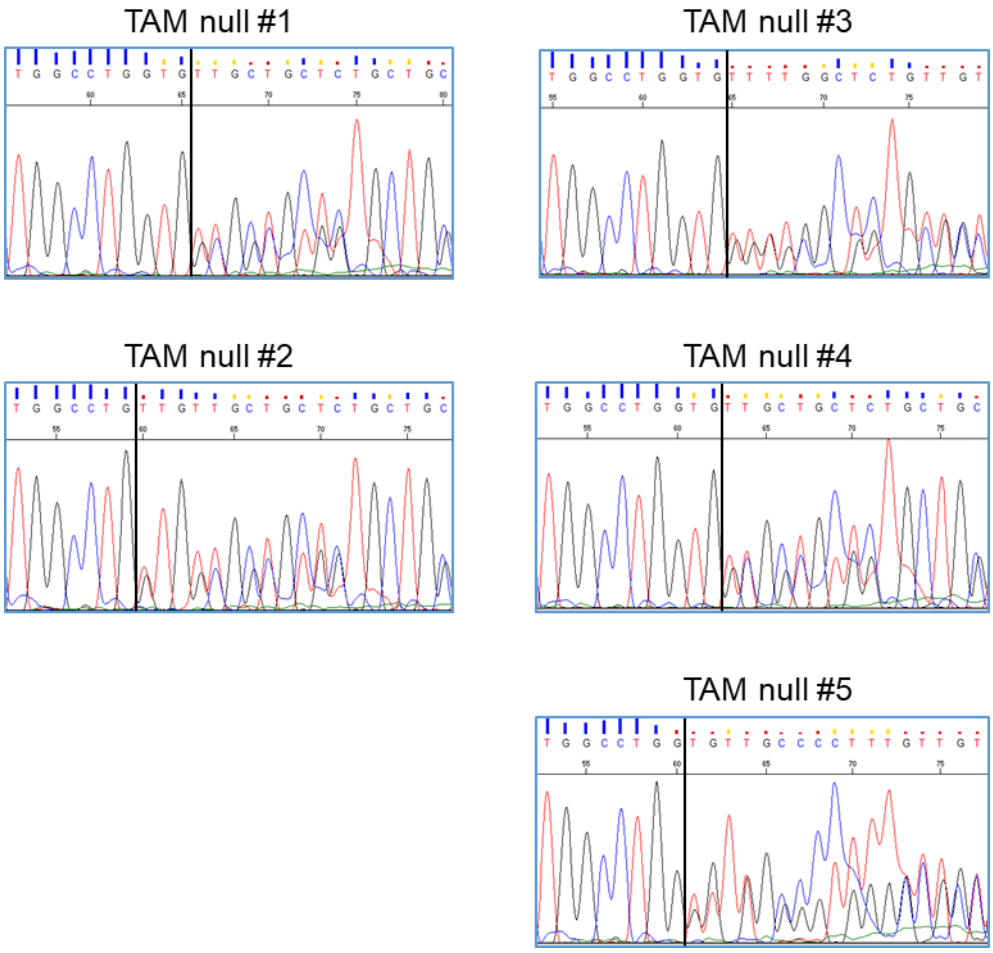

Supplementary Figure 8. Sequencing chromatograms of genomic DNA from 5TGM1 potential TAM null cell lines. Axl exon 1 PCR products amplified from genomic DNA of 5TGM1 potential TAM null clones were sequenced. Sequence chromatograms show location of insertion/deletion mutations.

TAM Null mutant allele cloning and sequencing summaries (cloned into pGEMTeasy (Promega))

Axl sequenced alleles in Thesis TAM Null Clone#3

G insertion – 4 clones; G deletion – 4 clones

All reverse complement sequencing due to hairpin avoidance:

CCCCCAGCAGCACAGCGCCAACCCACCAGGCCAGCGGGACCCTGCCCAT

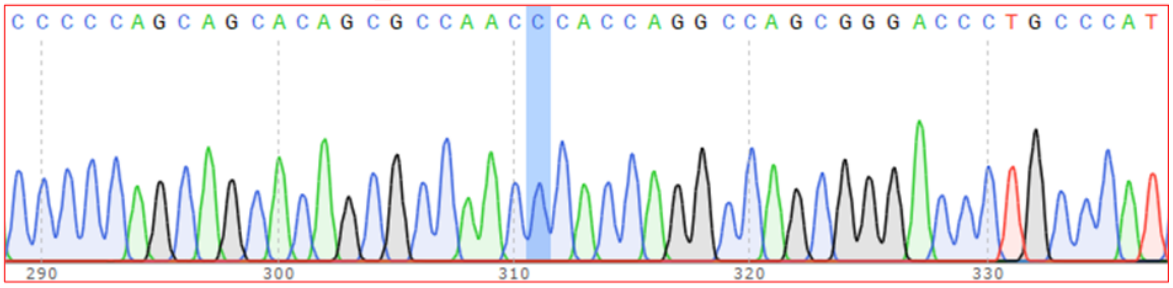

CCCCCAGCAGCACAGCGCCAAC*ACCAGGCCAGCGGGACCCTGCCCAT

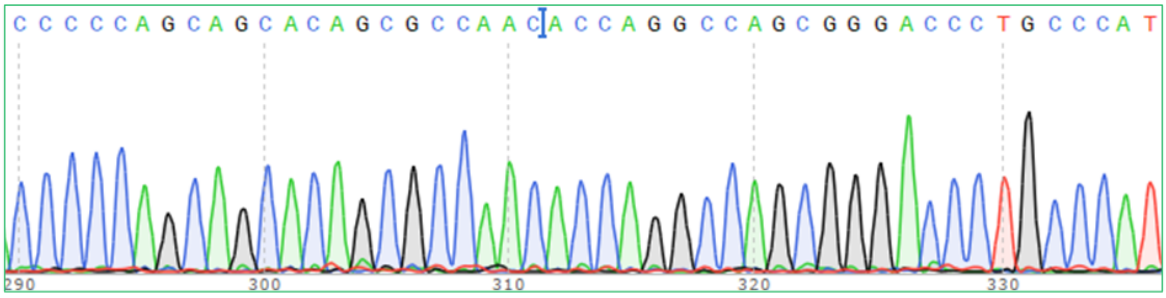

Actual sequence orientations:

ATGGGCAGGGTCCCGCTGGCCTGGTGGGTTGGCGCTGTGCTGCTGGGGG

ATGGGCAGGGTCCCGCTGGCCTGGT*GTTGGCGCTGTGCTGCTGGGGG

Axl sequenced alleles in Thesis TAM Null Clone#5

2 bp deletion – 8 clones; G deletion – 3 clones

All reverse complement sequencing due to hairpin avoidance:

CCCCCAGCAGCACAGCGCCAACC**CAGGCCAGCGGGACCCTGCCCAT

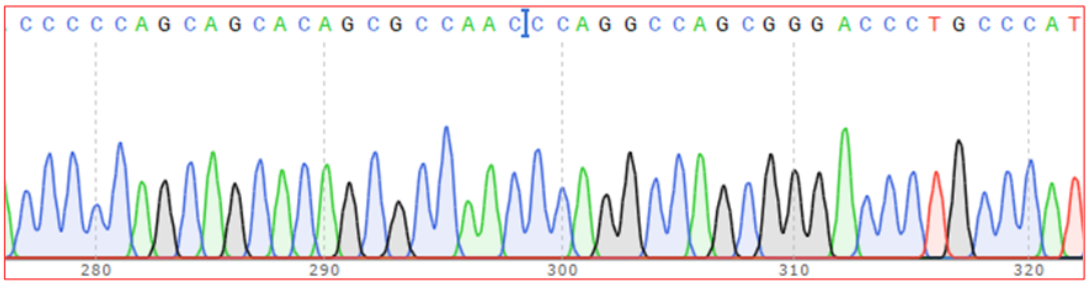

CCCCCAGCAGCACAGCGCCAAC*ACCAGGCCAGCGGGACCCTGCCCAT

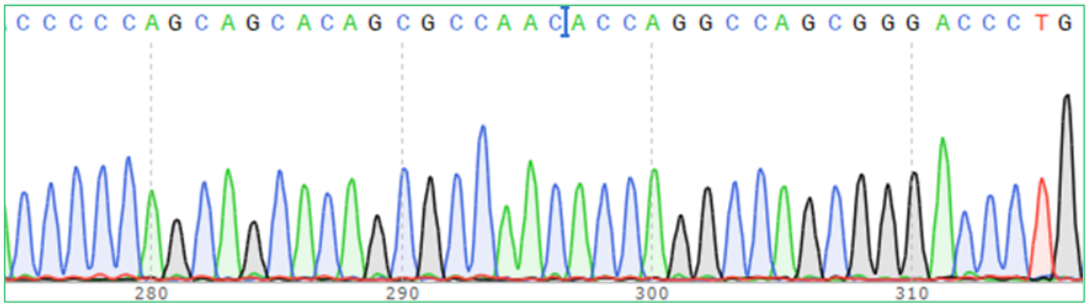

Actual sequence orientations:

ATGGGCAGGGTCCCGCTGGCCTG**GGTTGGCGCTGTGCTGCTGGGGG

ATGGGCAGGGTCCCGCTGGCCTGGT*GTTGGCGCTGTGCTGCTGGGGG

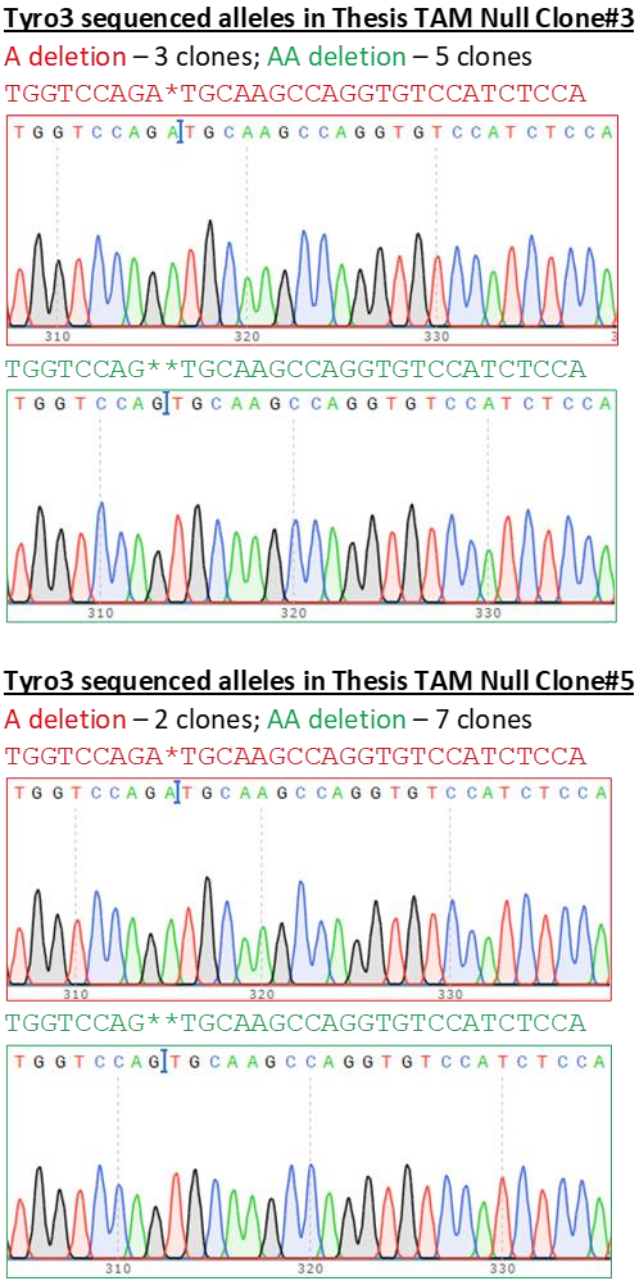

Supplementary Figure 9. Sequencing chromatograms of genomic DNA from 5TGM1 potential TAM null cell lines #3 and #5 cloned into a plasmid vector. PCR products amplified from genomic DNA of 5TGM1 potential double Axl and Tyro3 knockout clones were cloned into a plasmid vector. Sequences were obtained from the two mutant alleles inferred from the original Sanger sequences traces. Sequence chromatograms show location of insertion/deletion mutations.

Wild type Axl
888aa

MGRVPLAWWLALCCWGCAAHKDTQTEAGSPFVGNPGNITGARGLTGTLRCELQVQGEPPEVVWLRDGQILELADNTQ
TQVPLGEDWQDEWKVVSQLRISALQLSDAGEYQCMVHLEGRTFVSQPGFVGLEGLPYFLEEPEDKAVPANTPFNLSC
QAQGPPEPVTLLWLQDAVPLAPVTGHSSQHSLQTPGLNKTSSFSCEAHNAKGVTTSRTATITVLPQRPHHLHVVSRQ
PTELEVAWTPGLSGIYPLTHCNLQAVLSDDGVGIWLGKSDPPEDPLTLQVSVPPHQLRLEKLLPHTPYHIRISCSSS
QGPSPWTHWLPVETTEGVPLGPPENVSAMRNGSQVLVRWQEPRVPLQGTLLGYRLAYRGQDTPEVLMDIGLTREVTL
ELRGDRPVANLTVSVTAYTSAGDGPWSLPVPLEPWRPGQGQPLHHLVSEPPPRAFSWPWWYVLLGALVAAACVLILA
LFLVHRRKKETRYGEVFEPTVERGELVVRYRVRKSYSRRTTEATLNSLGISEELKEKLRDVMVDRHKVALGKTLGEG
EFGAVMEGQLNQDDSILKVAVKTMKIAICTRSELEDFLSEAVCMKEFDHPNVMRLIGVCFQGSDREGFPEPVVILPF
MKHGDLHSFLLYSRLGDQPVFLPTQMLVKFMADIASGMEYLSTKRFIHRDLAARNCMLNENMSVCVADFGLSKKIYN
GDYYRQGRIAKMPVKWIAIESLADRVYTSKSDVWSFGVTMWEIATRGQTPYPGVENSEIYDYLRQGNRLKQPVDCLD
GLYALMSRCWELNPRDRPSFAELREDLENTLKALPPAQEPDEILYVNMDEGGSHLEPRGAAGGADPPTQPDPKDSCS
CLTAADVHSAGRYVLCPSTAPGPTLSADRGCPAPPGQEDGA-

Double KO 1a,b 2a,b, 3a,b 4a,b, 5a,b
Prediction 1: 777aa

MVHLEGRTFVSQPGFVGLEGLPYFLEEPEDKAVPANTPFNLSCQAQGPPEPVTLLWLQDAVPLAPVTGHSSQHSLQT
PGLNKTSSFSCEAHNAKGVTTSRTATITVLPQRPHHLHVVSRQPTELEVAWTPGLSGIYPLTHCNLQAVLSDDGVGI
WLGKSDPPEDPLTLQVSVPPHQLRLEKLLPHTPYHIRISCSSSQGPSPWTHWLPVETTEGVPLGPPENVSAMRNGSQ
VLVRWQEPRVPLQGTLLGYRLAYRGQDTPEVLMDIGLTREVTLELRGDRPVANLTVSVTAYTSAGDGPWSLPVPLEP
WRPGQGQPLHHLVSEPPPRAFSWPWWYVLLGALVAAACVLILALFLVHRRKKETRYGEVFEPTVERGELVVRYRVRK
SYSRRTTEATLNSLGISEELKEKLRDVMVDRHKVALGKTLGEGEFGAVMEGQLNQDDSILKVAVKTMKIAICTRSEL
EDFLSEAVCMKEFDHPNVMRLIGVCFQGSDREGFPEPVVILPFMKHGDLHSFLLYSRLGDQPVFLPTQMLVKFMADI
ASGMEYLSTKRFIHRDLAARNCMLNENMSVCVADFGLSKKIYNGDYYRQGRIAKMPVKWIAIESLADRVYTSKSDVW
SFGVTMWEIATRGQTPYPGVENSEIYDYLRQGNRLKQPVDCLDGLYALMSRCWELNPRDRPSFAELREDLENTLKAL
PPAQEPDEILYVNMDEGGSHLEPRGAAGGADPPTQPDPKDSCSCLTAADVHSAGRYVLCPSTAPGPTLSADRGCPAP
PGQEDGA

Double KO 1a, 2a, 3b, 4a,5a
Prediction 2: 68aa

MGRVPLAWCWRCAAGGVQPIRTHRPRLAARLWGTQGISQVPEDSRGHFGVSSRFRGNPLRWCGFEMDRS

Double KO 1b,4b
Prediction 2: 67aa

MGRVPLAWWRCAAGGVQPIRTHRPRLAARLWGTQGISQVPEDSRGHFGVSSRFRGNPLRWCGFEMDRS

Double KO 2b
Prediction 2: 67aa

MGRVPLACWRCAAGGVQPIRTHRPRLAARLWGTQGISQVPEDSRGHFGVSSRFRGNPLRWCGFEMDRS

Double KO 3a
Prediction 2: 19aa

MGRVPLAWWLGAVLLGVCSP

Double KO 5b
Prediction 2: 18aa

MGRVPLAWVGAVLLGVCSP

Supplementary Figure 10. Predicted consequences of Axl mutations at the protein level in 5TGM1 potential TAM null cell lines. Sequences of 5TGM1 potential Axl knockout PCR products amplified from genomic DNA were translated into amino acids using Expasy Translate. Amino acid sequences were compared to wild type Axl, and open reading frames that code for sections of Axl are shown. For each mutation between 1-2 predictions of total amino acid (aa) length are shown. Grey highlighted sections denote wild type Axl protein sequence.

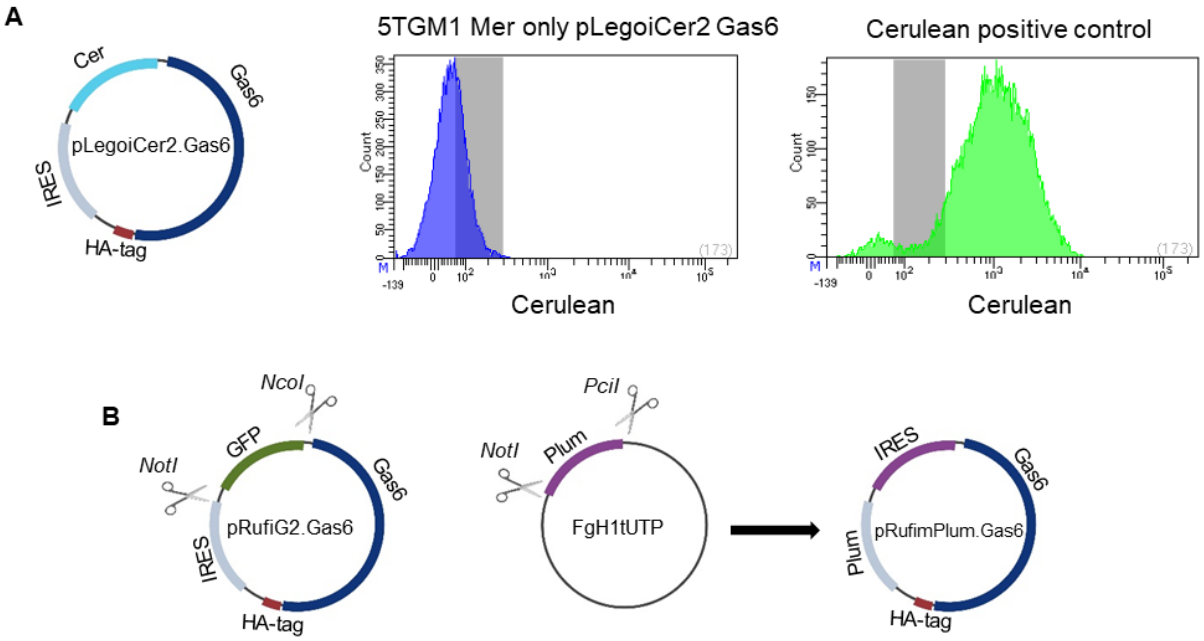

Supplementary Figure 11. Generation of a novel pRufimPlum retroviral vector. (A) Gas6 was initially cloned into the lentiviral pLegoiCer2 vector. However, when 5TGM1 cells were transfected with Gas6-encoding pLegoiCer2, cerulean reporter expression was rapidly lost (left) compared to a cerulean positive control (right). **(B)** A novel pRufiplum vector encoding Gas6, or an empty vector, were generated. The GFP insert from the pRufiG2.Gas6 was digested with *NcoI* and *NotI* and removed. The *mPlum* open reading frame was PCR amplified from the FgH1tUTP vector such that the start codon formed part of a PciI site, with a natural *NotI* site following the stop codon. Plum was digested with PciI and NotI and ligated into the pRufi vector encoding Gas6.